Dynamics of Braided River Morphology Using Advanced Geo-spatial Technology and Modeling Techniques

Thesis submitted in partial fulfilment of the requirements
for the award of the degree of

Doctor of Philosophy

in

Civil Engineering

by

Amit Kumar Dubey

Under the supervision of

Prof. Subashisa Dutta
Dr. Bimlesh Kumar

Department of Civil Engineering

Indian Institute of Technology Guwahati

Guwahati - 781039, India

DECEMBER, 2016

Dedicated to

My beloved Parents

For their love, care and support

TH-1911_10610425

Acknowledgements

It goes without saying that this journey would not have been possible without the constant support, the unconditional love and profound encouragement of my mother, my father, my sister, my brother and my love. They never questioned my intentions and whole-heartedly supported me in all my endeavours. There are no words to express my gratitude to them. Every progressive effort in this world is supported by many people. Acknowledgement for a few might be a trifle thing written on a piece of paper. Nevertheless, here I get a great opportunity to express my token of thanks to people who in a way, helped and supported me during the course of this investigation. I express my deepest sense of gratitude and veneration to my supervisor Prof. Subashisa Dutta, Head, Department of Civil Engineering and my co supervisor Dr. Bimlesh Kumar, Associate Professor, Indian Institute of Technology Guwahati (IITG), for their meticulous guidance, constructive suggestions, and sustained interest and patience throughout the present investigation. It is my sublime duty to express my deepest sense of reverence and indebtedness to the Chairman of my Doctoral Committee Prof. Arup Kumar Sarma, Professor, Department of Civil Engineering, Indian Institute of Technology Guwahati (IITG), for his constant encouragement and indelible inspiration provided during the study. I express my sincere thanks to the members of my Doctoral Committee Dr. Sreeja P., Associate Professor, Department of Civil Engineering and Prof. S. K. Dwivedy, Professor, Department of Mechanical Engineering, Indian Institute of Technology Guwahati (IITG), for their valuable suggestions, eternal encouragement, and timely help provided at various stages of the investigation and compilation of thesis. Sincere thanks are due to Dr. M. Guru Prem Prasad, Dean, Academic Affairs, Dr. S. R. M. Prasanna, Dean, Research and Development for providing necessary facilities towards successful completion of this endeavor. Thanks are due to all my colleagues, without whose support this work could not have been completed. I hereby acknowledge all the project staffs and the students of Department of Civil Engineering, Indian Institute of Technology Guwahati (IITG), for their sincere help and assistance provided during the field experiments and data collection. I am especially thankful to Mr. Binay Chembulu and Mr. A. Anjaneyulu Research Scholar of Department of Civil Engineering, IIT Guwahati, for their help to me during the compilation of the thesis. I would also like to thank Mr. Mayank Agrawal (Department of Computer Science, IITG), Mr. Mahesh Patel and Dr. Vishal Deshpande, Department of Civil Engineering, IITG for extensive help during the last phase of my PhD work, I will never forget the

TH-1911_10610425

kind and keen support provided by them. I would also like to thank Mr. Rohit Pradhan and Mr. Dharmendra Singh for their contribution in my thesis. It is often said good friends are rare to get. In this context I find myself very lucky to have friends like Mahesh, Vishal, Arpit, Mayank, Ashish, Satish, Rishi, and Shyamal. Their friendly affection, timely help, and encouragements never let me feel away from home during my stay at the institute. Words of appreciation are also due for all the Mr. Bazal Houque, lab assistant IITG Guwahati for immense help during the period of Ph. D. in the field visit and data collection. It is not possible to express in words the inspiration from my brother, sister and the noble sacrifice of my parents, whose invaluable love and support have brought me to this position. This list is obviously incomplete, but let me submit that the omissions are inadvertent and I once again record my deep felt gratitude to all those who have cooperated with me either directly or indirectly in this endeavor.

December 8, 2016 Amit Kumar Dubey

TH-1911_10610425

Declaration

I certify that

- The work contained in this thesis is original and has been done by myself and under the general supervision of my supervisor(s).
- The work reported herein has not been submitted to any other Institute for any degree or diploma.
- Whenever I have used materials (concepts, ideas, text, expressions, data, graphs, diagrams, theoretical analysis, results, etc.) from other sources, I have given due credit by citing them in the text of the thesis and giving their details in the references. Elaborate sentences used verbatim from published work have been clearly identified and quoted.
- I also affirm that no part of this thesis can be considered plagiarism to the best of my knowledge and understanding and take complete responsibility if any complaint arises.
- I am fully aware that my thesis supervisor(s) are not in a position to check for any possible instance of plagiarism within this submitted work.

December 8, 2016 Amit Kumar Dubey

TH-1911_10610425

TH-1911_10610425

Department of Civil Engineering
Indian Institute of Technology Guwahati
Guwahati - 781039, Assam, India

Dr. Subashisa Dutta
Professor
Email : subashisa@iitg.ernet.in
Phone : +91-361-258-2415

Dr. Bimlesh Kumar
Associate Professor
Email : bimlesh@iitg.ernet.in
Phone : +91-361-258-2420

Certificate

This is to certify that this thesis entitled "**Dynamics of Braided River Morphology Using Advanced Geo-spatial Technology and Modeling Techniques**" submitted by **Amit Kumar Dubey**, in partial fulfilment of the requirements for the award of the degree of Doctor of Philosophy, to the Indian Institute of Technology Guwahati, Assam, India, is a record of the bonafide research work carried out by him under my guidance and supervision at the Department of Civil Engineering, Indian Institute of Technology Guwahati, Assam, India. To the best of my knowledge, no part of the work reported in this thesis has been presented for the award of any degree at any other institution.

Date: December 8, 2016
Place: Guwahati

Prof. Subashisa Dutta

Dr. Bimlesh Kumar

TH-1911_10610425

TH-1911_10610425

Abstract

The sand bed braided rivers are morphologically dynamic rivers. The braided river morphology has intra-seasonal variability in terms of bank erosion, bar migration, bar formation and sediment mixing. These features represent the short term morphological variation during the flood waves passing over the river. These morphological features are governed by many variables such as discharge, sediment flux, river bed slope and river flow width. With many governing parameters understanding of braided river dynamics is a challenging task. The advancement in advanced geo–spatial technologies and modeling techniques have provided new insights to understand and interpret different dynamic parameters in large braided rivers.

The river stage variation is an important variable in understanding river characteristics. The satellite altimetry is used to retrieve water level variations at different reaches of the river with certain return period. The improved methodology is proposed in this study to retrieve water levels at braided reaches of the Brahmaputra river. Water level retrieval over the braided river reaches is a difficult task due to frequent channel migration and sand bar formation. The retrieved water levels over the braided reaches have shown the improved results at different locations. The performance evaluation retrieved water levels of different satellite altimeters are carried from *in–situ* gauge records. The accuracy of retrieved water level from improved methodology for Jason–2 and SARAL/Altika at different locations over braided reaches of the Brahmaputra river are found to be 55 cm and 40 cm respectively, in terms of root mean square error (RMSE). These water level informations at different locations over the Brahmaputra river are used to generate the water surface profiles. The water surface profiles are generated for the monsoon and non–monsoon season. It is found out that there is higher seasonal water difference at the downstream of the river as compared to upstream. To retrieve water levels different retracking algorithm are used for accuracy assessment. It is found out that β-5 algorithm had performed the best among four different algorithms used for evaluation such as Ice-1, Ice-2, threshold and β-5 retrackers. The retrieved water level time series are converted to discharge using rating curves for Guwahati and Tezpur gauge sites. These discharges are compared with nearby gauge stations and it is found that the discharge values are able to capture the flood-waves occurred in the Brahmaputra river. The flood waves of different interval causes river morphology to adjust itself with increased discharge and sediment flux during the monsoon season.

TH-1911_10610425

Microwave satellite images provide vital information on morphological active zones during the monsoon period. The river morphological features such as sand bar, erosion zone, deposition zone, bank erosion and sediment mixing remain active during the monsoon season. These features create different signatures in the microwave images based on the backscattering coefficient. The in–season variation is analyzed with microwave satellite images of different polarization and different time periods. In the sand bed braided rivers such as the Brahmaputra the intra-seasonal variation causes more morphological changes in the river. With the help of signature analysis it is found that morphologically active group (bank erosion zone, sand deposition zone and turbulent zone) and others such as river water, sand bar and flood–plain inundation were separable using HH polarization. However, within the morphologically active group different zones (bank erosion zone, sand deposition zone and turbulent zone) are not separable in both HH and HV polarization. The microwave satellite images of HH polarization are found to be suitable to identify the morphologically active zones within the monsoon period as compared to HV polarization. In order to separate the morphologically active features within the river, the radar backscattering coefficient is grouped into three different categories and the river reach is divided into five different zones based on morphological characteristics of the river. The microwave satellite image segmentation is done based on the different categories of backscattering coefficient representing the variation of turbulence level present within the river. These zones are then separately interpreted for each category of turbulence level associated to the morphologically active features (bank erosion zone, sand deposition zone and turbulent zone).

The hydrological modeling of the Brahmaputra river is done to estimate the spatio–temporal variations of river discharge. It is found that the simulated hydrograph could able to capture the seasonal and as well as flood pulses of different interval. The performance of simulated discharge was statistically satisfactory with R^2=0.85 and RMSE=1233 m^3/sec. The monthly discharge time series is generated using simulated data–set for different reaches of the Brahmaputra river. It is assimilated into the hydrodynamic model setup over the Brahmaputra river. The hydrodynamic modeling of the Brahmaputra river is performed from upstream of Dibrugarh to downstream of Dhubri. Manning's roughness coefficients are estimated using altimeter derived hydraulic parameters of the river at different locations as an input to the hydrodynamic model. To perform the comparative analysis, Manning's roughness coefficients are also estimated from different empirical equations using particle size distributions. The reach–wise particle size distribution is used to derive the longitudinal variations of Manning's roughness coefficient. The Manning's roughness coefficients derived using empirical equations are 2 to 3 times higher than the altimeter derived Manning's roughness coefficient. Comparison of seasonal water level difference at different locations is performed from Altimetry retrieved and model simulated water level for the

years 2014 and 2015. The simulated water levels from altimetry derived Manning's roughness coefficient were in close range with altimetry retrived water levels for years 2014 and 2015 except over the nodal reaches of the river. It is found that the simulated water surface profiles are over–predicting for all the reaches of the Brahmaputra river with Manning's roughness coefficients derived using empirical equation.

TH-1911_10610425

TH-1911_10610425

Contents

Abstract **ix**

List of Figures **xxv**

List of Tables **xxvii**

List of Symbols **xxix**

List of Abbreviations **xxxi**

1 Introduction **1**

1.1 Overview 1

1.2 Morphological dynamics of the braided rivers 2

1.3 Remote sensing of the braided rivers 3

1.3.1 Satellite altimetry over the braided rivers 5

1.3.2 Microwave satellite images of the braided rivers 5

1.4 Hydrodynamic modeling 6

1.5 Objectives of the present research 8

1.6 Organization of the Thesis 10

2 REVIEW OF LITERATURE **13**

2.1 Introduction 13

2.2 Dynamics of Braided river morphology 13

2.3 Advanced geospatial technologies 16

2.3.1 Satellite Altimetry 16

2.3.2 Microwave Remote Sensing 17

TH-1911_10610425

2.4 Numerical modeling 18
2.5 Conclusions 19

3 STUDY AREA AND DATA COLLECTION 21

3.1 Introduction 21
3.2 Study Area 21
3.3 Field Observations 23
3.3.1 Hydrographic survey 24
3.3.2 River island survey 24
3.3.3 River flood-plain survey 30
3.4 Satellite Data 32
3.4.1 Satellite altimetry data 32
3.4.2 Microwave Satellite data 34
3.4.3 Optical Satellite data 34
3.5 *In-situ* data collection 35
3.6 Conclusions 35

4 IMPROVEMENT IN SATELLITE ALTIMETRY DATA PROCESSING 37

4.1 Introduction 37
4.2 Satellite Altimetry Missions 38
4.3 Methodology for water level retrieval 40
4.3.1 Range and Geophysical Corrections 41
4.3.2 Troposphere correction (Dry and Wet) 43
4.3.3 Ionosphere correction 43
4.3.4 Solid earth and Pole Tides Correction 45
4.4 Waveform retracking 45
4.4.1 The Off Centre of Gravity (OCOG) retracker (ICE-1) 45
4.4.2 Ice-2 retracking 47
4.4.3 Beta-Parameter retracking 47
4.4.4 Threshold retracker (Sea Ice retracker) 48

TH-1911_10610425

4.5 Results and Discussion 50
4.5.1 Waveform variation and classification over the Brahmaputra river . . 50
4.5.2 Seasonal variation of Backscattering Coefficient 51
4.5.3 Improvement in water level retrieval 54
4.6 Conclusions 55

5 ACCURACY ASSESSMENT OF RETRIEVED WATER LEVEL, DISCHARGE AND WATER SURFACE SLOPES 59
5.1 Introduction 59
5.2 Methodology for water level comparisons 59
5.2.1 Pseudo stage–discharge relation 60
5.3 Seasonal water surface profiles computation 61
5.3.1 Data used 62
5.4 Results and discussion 64
5.4.1 Performance evaluation of water level derived from Jason–2 satellite 64
5.4.2 Performance evaluation of water level derived from SARAL/Altika satellite 64
5.4.3 Performance evaluation of water level derived from ENVISAT satellite 64
5.5 Discharge Estimation 71
5.5.1 Discharge estimation using Jason–2 satellite data 71
5.5.2 Discharge estimation using ENVISAT satellite data 72
5.6 Water surface profile 75
5.7 Long-term monthly discharge and annual water yield 75
5.8 Conclusions 78

6 MAPPING OF MORPHOLOGICAL FEATURES USING MICROWAVE SATELLITE IMAGES 83
6.1 Introduction 83
6.2 Braided river morphological dynamics 84
6.3 Data used 85
6.4 Methodology for river morphological features extraction 85

TH-1911_10610425

6.5 Results and Discussion 87
6.5.1 Signature analysis 89
6.5.2 River mask generation 89
6.5.3 Discharge intensity curve 94
6.5.4 Image Segmentation 94
6.5.5 Morphological dynamic interpretation 95
6.6 Conclusions 102

7 HYDROLOGICAL MODELING OF THE BRAHMAPUTRA RIVER 105
7.1 Introduction 105
7.1.1 Flood–wave characteristics of the Brahmaputra river 106
7.2 Hydrological Model description 107
7.2.1 Input data and parameters 108
7.2.2 Model calibration and performance evaluation 112
7.3 Results and Discussion 116
7.3.1 The Brahmaputra river discharge 116
7.3.2 Tributary wise discharge variation 117
7.3.3 Monthly discharge variation 119
7.4 Conclusions 123

8 HYDRODYNAMIC MODELING: SATELLITE ALTIMETRY AND DISCHARGE DATA ASSIMILATION 127
8.1 Introduction 127
8.2 Hydrodynamic model setup 128
8.3 Estimation of Manning's roughness coefficient 128
8.4 Results and Discussion 131
8.4.1 Variation of Manning's roughenss coefficient 132
8.4.2 Seasonal water depth variation 133
8.4.3 Longitudinal variations of water level 136
8.5 Conclusions 138

TH-1911_10610425

9 CONCLUSIONS AND RECOMMENDATIONS **145**

9.1 A Brief Review of the Work Done 145

9.1.1 Literature Review 146

9.1.2 Study Area and Data Collection 146

9.1.3 Improvement in Satellite Data Processing 146

9.1.4 Accuracy Assessment of Retrieved Water Level, Discharge, and Water Surface Slopes 147

9.1.5 Mapping of Morphological Features using Microwave Satellite Images 147

9.1.6 Hydrological Modeling of the Brahmaputra River 148

9.1.7 Hydrodynamic Modeling: Satellite Altimetry and Discharge Data Assimilation 149

9.2 Recommendations for Future Research 150

Publications **157**

TH-1911_10610425

TH-1911_10610425

List of Figures

1.1 Morphological dynamics of the middle reach of the Brahmaputra river (Guwahati downstream). 3

1.2 The Brahmaputra river flow width variation for different seasons with river bed elevations for the year 2013 4

1.3 Active morphological processes in the Brahmaputra river (a-b: Bank erosion, c-d: Vortex formation) during the monsoon season. 4

1.4 Yearly variation of river planform overlaid with altimeter satellite tracks. . . 6

1.5 Middle reach of the Brahmaputra river from microwave satellite image. . . . 7

1.6 Discharge and sediment flux variations in the Brahmaputra river measured at Guwahati gauge station. 8

1.7 Water level variations along the Brahmaputra river during the high flow seasons in year 2004. 9

3.1 Index map showing Brahmaputra river and its physiographic features 22

3.2 Brahmaputra river survey map 24

3.3 Photograph showing the ADCP instrument 25

3.4 The velocity distribution measured using ADCP at downstream of Guwahati 26

3.5 The velocity distribution measured using ADCP at downstream of Kalachar . 26

3.6 The velocity distribution measured using ADCP at downstream of Garimari . 27

3.7 The velocity distribution measured using ADCP at downstream of Bhagamari 27

3.8 Variation of sediment concentration near banks of active bank erosion. . . . 28

3.9 Variation of sediment concentration near sand bars with turbulent water conditions. 28

3.10 Variation of sediment concentration at nodal location (Guwahati). 29

3.11 Variation of sediment concentration near river banks at two different locations. 29

TH-1911_10610425

3.12 Photograph showing the river bed sand condition 30

3.13 Photograph showing the river islands sands formations 31

3.14 Photograph showing the flood plain near Airport 31

3.15 Photograph showing the flood plain near Narengi 32

4.1 Microwave images overlaid with Jason 2 satellite tracks crossing over the Brahmaputra River. 41

4.2 Flow-chart showing the methodology adopted for the retrieval of water level time series for braided reaches of the Brahmaputra river. 42

4.3 Optical and microwave images showing the location of virtual station for non-monsoon (February) andmonsoon (July) seasons for the satellite track 53 (a-b), 166 (c-d) and 242 (e-f), respectively over different reaches of the Brahmaputra river. 44

4.4 The Off Centre of Gravity waveform retracker. 46

4.5 The waveform retracking from the NASA 5 β parameter retracking 48

4.6 Waveform threshold retracker 49

4.7 Footrpint of Saral/Altika over the Brahmaputra river for Non-mosoon (12/04/2013) and Monsoon period (18/07/2013) for the track 438. 51

4.8 (a) Waveform variation over the Brahmaputra river for the track 438 for non–monsoon season (03/05/2013). 52

4.9 (b) Waveform classification over the Brahmaputra river for the track 438 for non–monsoon season (03/05/2013). 52

4.10 (a) Waveform variation over the Brahmaputra river for the track 438 for the monsoon season (12/07/2013). 53

4.11 (b) Waveform classification over the Brahmaputra river for the track 438 for the monsoon season (12/07/2013). 53

4.12 Variation in SARAL/Altika altimeter Backscattering coefficient passing over the Brahmaputra river at 438 track. 54

4.13 Along track backscattering coefficient variations at different locations (a) 53, (b) 166, (c) 231 and (d) 242 over the Brahmaputra River. 55

TH-1911_10610425

4.14 Performance comparison of retrieved water levels using developed methodology (a-d) and the Jason-2 derived Hydroweb water level data product (g-h) with in situ measurements at different tracks 53, 166, 231 and 242, respectively over the Brahmaputra River. 56

5.1 Sketch describing the interpolation of water level at virtual station using nearby gauge stations. 60

5.2 Generation of the rating curves for the (a) Guwahati gauge station and the (b) Virtual station (Track-166) for the year 2009. 62

5.3 Topographic map of the Brahmaputra basin on which the Jason-2 satellite tracks are superimposed. 65

5.4 Comparisons between altimetry derived and observed water levels at different satellite tracks (a) 53, (b) 166, (c) 231 and (d) 242 over the Brahmaputra river. 66

5.5 Study area showing Saral/Altika track overlaid on microwave images, passing over the Brahmaputra river 67

5.6 Correlation analysis between in situ and retrieved water level at different virtual (982, 438, 709) stations over the Brahmaputra river. 68

5.7 Correlation analysis between in situ and retrieved water level at different virtual (896,352, 266) stations over the Brahmaputra river. 69

5.8 Study area showing in situ and virtual gauging stations of ENVISAT in the Brahmaputra River. 71

5.9 Virtual gauge stations at different reaches of the Brahmaputra River (a) Dhubri, (b) Goalpara, (c) Guwahati, (d) Tezpur, (e) Nematighat, and (f) Dibrugarh. 72

5.10 Correlation analysis between the in-situ stage data and satellite altimetry derived stage (a) Dhubri (b) Goalpara (c) Guwahati (d) Tezpur (e) Nematighat, and (f) Dibrugarh. 73

5.11 (a) Correlation analysis of observed vs altimetry derived discharge for the year 2010, (b) Time series of observed and altimetry derived discharge for the year 2010. 74

5.12 Altimetry derived time series for Guwahati (Track-166) gauge station from 2008 to 2013. 75

TH-1911_10610425

5.13 Altimetry estimated and in situ discharge comparisons for non–monsoon and monsoon periods at (a)-(b) Guwahati and (c)-(d) Tezpur Gauge stations, respectively. 76

5.14 Comparison of altimetry estimated and in situ discharge hydrograph for Guwahati gauge station. 76

5.15 Comparison of altimetry estimated and in situ discharge hydrograph for Tezpur gauge station. 77

5.16 (a) Water surface profile for the Monsoon and Non-monsoon period of Brahmaputra river, (b) Water level differences between two seasons. 77

5.17 Altimetry Estimated and in situ monthly discharge hydrographs of the Brahmaputra river at (a) Guwahati and (b) Tezpur gauge station. 79

5.18 Altimetry Estimated and in situ annual water yield the of the Brahmaputra river at (a) Guwahati and (b) Tezpur gauge station. 80

6.1 Methodology to generate backscattering coefficient for microwave satellite images. 88

6.2 Backscatter variation in the microwave satellite image of HH polarization on 31 July 2011 90

6.3 Backscatter variation in the microwave satellite image of HH polarization on 3 August 2011 90

6.4 Backscatter variation in the microwave satellite image of HH polarization on 27 August 2011 91

6.5 Backscatter variation in the microwave satellite image of HV polarization on 31 July 2011 91

6.6 Backscatter variation in the microwave satellite image of HV polarization on 3 August 2011 92

6.7 Backscatter variation in the microwave satellite image of HV polarization on 27 August 2011 92

6.8 Water mask generation for the image classification for the different features present within the river 93

6.9 Sand mask generation for the image classification for the different features present within the river 93

6.10 Discharge Intensity curve for the middle reach of the Brahmaputra river during the year 2008. 96

TH-1911_10610425

6.11 Discharge Intensity curve for the middle reach of the Brahmaputra river during the year 2009. 96
6.12 Discharge Intensity curve for the middle reach of the Brahmaputra river during the year 2010. 97
6.13 Discharge Intensity curve for the middle reach of the Brahmaputra river during the year 2011. 97
6.14 Classified images of year 2008 for different morphological features present in the river. 98
6.15 Classified images of year 2009 for different morphological features present in the river. 99
6.16 Classified images of year 2010 for different morphological features present in the river. 100
6.17 Classified images of year 2011 for different morphological features present in the river. 101

7.1 Illustrative diagram showing different characteristics of flood waves in the Brahmaputra river (Karmaker and Dutta, 2010). 107
7.2 Digital elevation model of the study area 109
7.3 Sub basins of the Brahmaputra river and its tributaries 110
7.4 Cumulative topographic index of the study area. 110
7.5 Soil map of the Brahmaputra basin. 111
7.6 Major land use/ land cover classes (regrouped to hydrological similarity classes) of the study area 111
7.7 Hydrological model (RISE) simulated discharge calibration with observed discharge at Guwahati gauge station for year 1999 113
7.8 Comparison of simulated discharge vs observed discharge at Guwahati gauge station for the year 1999 113
7.9 Hydrological model (RISE) simulated discharge validation with observed discharge at Guwahati gauge station for the year 2000 114
7.10 Comparison of simulated discharge vs observed discharge at Guwahati gauge station for the year 2000 114
7.11 Performance evaluation of simulated discharge vs observed discharge at Guwahati gauge station for the period of 1999 to 2010 115

TH-1911_10610425

7.12 Simulated discharge of the Brahmaputra river for year 2004 at Jorhat 117
7.13 Simulated discharge of the Brahmaputra river for year 2004 at Tezpur . . . 118
7.14 Simulated discharge of the Brahmaputra river for year 2004 at Guwahati . . 118
7.15 Simulated discharge of the Brahmaputra river for year 2004 at Goalpara . . 119
7.16 Monthly mean and standard deviation of Kopili river for the period 1997 to 2013 120
7.17 Monthly mean and standard deviation of Subansiri river for the period 1997 to 2013 120
7.18 Monthly mean and standard deviation of Manas river for the period 1997 to 2013 121
7.19 Monthly mean and standard deviation of Lohit river for the period 1997 to 2013 121
7.20 Monthly mean and standard deviation of Siang river for the period 1997 to 2013 122
7.21 Monthly mean and standard deviation of Jia–bharali river for the period 1997 to 2013 122
7.22 Monthly mean and standard deviation of Buri–dihing river for the period 1997 to 2013 123
7.23 Monthly discharge variation of the Brahmaputra river at Guwahati for the year 2014 124
7.24 Monthly discharge variation of the Brahmaputra river at Guwahati for the year 2015 124

8.1 HEC-RAS model setup showing cross sections from 14 to 22 in the middle reach of the Brahmaputra river. 128
8.2 Cross section variations in cross sections 5 to 33. 129
8.3 Cross section variations in cross sections 40 to 59. 130
8.4 Variation of Manning's roughness coefficient (upstream to downstream) estimated using satellite altimetry derived water surface slopes. 134
8.5 Manning's roughness coefficient variation using different empirical equations. 134
8.6 The longitudinal variations of Manning's roughness coefficient with changing river depth and slopes derived from satellite altimetry for the year 2013. . . 135

TH-1911_10610425

8.7 The comparison of seasonal difference of water level in the Brahmaputra river using satellite altimetry retrieved water levels and simulated data of year 2014. 135

8.8 The comparison of seasonal difference of water level in the Brahmaputra river using satellite altimetry retrieved water levels and simulated data of year 2015. 136

8.9 The comparison of seasonal difference of water level in the Brahmaputra river using altimeter derived water level different Manning's roughness coefficient from different equations for the year 2014 137

8.10 The comparison of seasonal difference of water level in the Brahmaputra river using altimeter derived water level and different Manning's roughness coefficient from different equations for the year 2015 137

8.11 The comparison of satellite altimetry retrieved longitudinal water level variations of the Brahmaputra river (downstream to upstream) with (a) Strickler, (b) Lane and Carlson, (c) Meyer-Peter and Muller equation for the non–monsoon season of year 2014 139

8.12 The comparison of satellite altimetry retrieved longitudinal water level variations of the Brahmaputra river (downstream to upstream) with (a) Strickler, (b) Lane and Carlson, (c) Meyer-Peter and Muller equation for the monsoon season of year 2014 140

8.13 The comparison of satellite altimetry retrieved longitudinal water level variations of the Brahmaputra river (downstream to upstream) with (a) Strickler, (b) Lane and Carlson, (c) Meyer-Peter and Muller equation for the non–monsoon season of year 2015 141

8.14 The comparison of satellite altimetry retrieved longitudinal water level variations of the Brahmaputra river (downstream to upstream) with (a) Strickler, (b) Lane and Carlson, (c) Meyer-Peter and Muller equation for the monsoon season of year 2015 142

TH-1911_10610425

TH-1911_10610425

List of Tables

3.1 Brahmaputra river survey 25

5.1 Rating curve discharge coefficients for Jason–2 and ENVISAT satellites . . . 61

5.2 Statistics of virtual and *in–situ* gauge stations for SARAL/Altika satellite . . 63

5.3 Statistics of virtual and *in–situ* gauge stations for Jason–2 satellite 63

5.4 Statistics of virtual and *in–situ* gauge stations for ENVISAT satellite 63

5.5 Statistical Performance of different retracking algorithms over Brahmaputra river 70

6.1 Microwave satellite images used in morphological analysis of the Brahmaputra river 86

7.1 Country wise areas of the Brahmaputra basin. 106

7.2 Input data and model parameters. 109

7.3 Calibrated Parameters 112

7.4 Simulated peak discharge of different tributaries of the Brahmaputra river . 115

7.5 The Brahmaputra river peak discharge comparison at Guwahati 116

8.1 Reach–wise particle size distribution of the Brahmaputra river (Goswami, 1985) 132

8.2 Estimation of Manning's roughness coefficient 133

8.3 Comparison of Observed and simulated main channel velocity using different values of Manning's roughness coefficient for the monsoon season 138

TH-1911_10610425

TH-1911_10610425

List of Symbols

Symbols	Description
Alt	Satellite altitude from reference ellipsoid
dB	Backscattering coefficient
d_{50}	Median diamter of grain
DC	Thermal noise or DC level
D_{tc}	Dry Tropospheric correction
H	River stage
I_{onc}	Ionospheric correction
MSS_{ht}	Mean sea surface from the reference ellipsoid
n	Manning's roughness coefficient
n_a	Number of aliased sample
P_{tc}	Pole tide correction
P_u	Amplitude
P_n	Thermal noise level (to be removed from the waveform samples)
Q_s	Simulated discharge
Q	Discharge (m^3/sec)
R	Satellite range
S_{tc}	Solid tide
S_f	Friction slope
S_T	Slope of the logarithm of the trailing edge
T_d	Individual flood events
T_i	Arrival time of the waves
T_p	Time to peak
T_{coeff}	Threshold coefficient
T_L	Retracked gate
W_{tc}	Wet tropospheric correction
P(i)	Waveform sample value at the ith bin
β_1	Thermal noise level of the return waveform
β_2	Return signal amplitude
β_3	Mid-point on the leading edge of the waveform

TH-1911_10610425

β_4	Return waveform rise time
β_5	Slope of the trailing edge
σ^0	Mean backscatter coefficient
τ	Epoch
τ_L	Width of the leading edge

List of Abbreviations

Terms	Abbreviations
ADCP	Aquastic Doppler Current Profiler
CFD	Computational Fluid Dynamics
CTI	Cumulative Topographic Index
COG	Center of Gravity
CWC	Central Water Commission
DEM	Digital Elevation Model
DGPS	Differential Global Positioning System
DORIS	Doppler Orbitography and Radio-positioning Integrated by Satellite
ECMWF	European Centre for Medium-Range Weather Forecasts
GPS	Global Positioning System
HEC-RAS	Hydrologic Engineering Center-River Analysis System
HSC	Hydrological Similarity Classes
IMD	Indian Meteorological Department
ISRO	Indian Space Research Organization
IWAI	Inland Waterways Authority of India
LEP	Leading Edge Position
m.s.l.	Mean Sea Level
NBSS and LUP	National Bureau of Soil Survey and Land Use Planning
NCEP	U.S. National Centers for Environmental Predictions
SAR	Synthetic Aperture Radar
T/P	Topex/Poseidon
USGS	United States of Geological Survey

TH-1911_10610425

TH-1911_10610425

"You have to dream before your dreams can come true."

A.P.J. Abdul Kalam (1931 - 2015)
Indian scientist and leader

1

Introduction

1.1 Overview

The characteristic features of the large active braided river are wide and shallow channel, erodible banks and sand bar migration. The variation in discharge creates the significant effect on the river morphology within a year. The large braided rivers such as the Brahmaputra has unique flood wave characteristics, which consist of the two components namely flood waves and monsoonal (seasonal) response (Karmaker and Dutta, 2010). Noncohesive bank material, which possess less strength to hold the bank material against the river flow remains prone to rapid bank erosion (Karmaker et al., 2010; Karmaker and Dutta, 2011). Being associated with so many controlling variables (variable width, flood waves, bank erosion and bed slope) with uncertainty in measurement of input variables (discharge, sediment flux), hydrodynamic and morphodynamic processes involved in the morphological changes are always difficult to be completely understood/modeled in a large braided river. The traditional monitoring of river gauges is limited to few locations for a braided river like the Brahmaputra. Often these measurements are carried out over the nodal locations of the river, which do not have the large width of flow as compared to the floodplains of the river. River stage variations over the floodplains provide the vital information about the flood wave distribution and energy dissipation to the downstream of the nodal reaches. The water level variations at the different reaches of the river indicate the energy dissipation and the resistance offered to the river flow in terms of planform variation, variable river flow width and the bed roughness. But, non-availability of *in–situ* measurements at desired locations imposes serious constraints on river flow modeling of large rivers like the Brahmaputra. Besides this, in-situ discharge measurement is also a difficult task over the

TH-1911_10610425

large braided reaches of the river. The braided river morphology has intra-seasonal variability in terms of bank erosion, bar migration, bar formation and sediment mixing. These features represent the short term morphological variation during the flood waves passing over the river (Karmaker and Dutta, 2016). These features are identified using microwave satellite images and the river survey needs to be conducted during monsoon seasons. With the development and availability of advanced geo-spatial technologies, mapping and monitoring intra-seasonal variation in the large rivers have become possible. The unique capability of microwave remote sensing enables to capture the synoptic view of the river, even in the cloudy conditions (monsoon season). It provides useful characteristics of the river during floods, such as intra-seasonal morphological variations. These variations include active bank erosion, sediment mixing, sediment deposition around the sand bars and sand bar migration. The mapping of intra-seasonal morphological features is a new dimension in the field of microwave remote sensing over the large braided rivers. Microwave satellite images of different polarization are used to map these features for different monsoon seasons. Satellite altimetry derived the water surface elevations at different reaches of the river are used to estimate water surface slopes and discharge time series using rating curve relations developed for altimeter virtual stations. The water level information retrieved at different reaches of the river is also used to derive seasonal water level depth, water surface slopes and the roughness values at different reaches of the river. These hydrodynamic properties derived from satellite altimetry are assimilated into the river model. The river model is setup over middle reach of the Brahmaputra river. A hydrology model is used to estimate tributary level discharge contribution in the middle reach of the river as an input to the hydrodynamic model. The performance analysis is carried out with and without assimilation of reach wise roughness coefficient derived using satellite altimetry.

1.2 Morphological dynamics of the braided rivers

The river morphological dynamics is a complex process in the sand bed braided rivers (Figure 1.1). The river bed as well as river bank evolve with time as a continuous process of river adjustment to the change in river flow, sediment flux and varying plan-form. To understand the braided river dynamics in space and time, the river dynamic parameters needs to be observed and monitored in spatio-temporal domain. The advanced sensors from space platform have made it possible to monitor such phenomena in detail at different scale in space and time. To utilize these capabilities with ground based observations the morphological dynamics of the braided rivers could be characterized and could be classified for better investigation. The different morphological processes such as sand bar migration, bed erosion, bank erosion, bar formation, sediment deposition around the bars and sediment

TH-1911_10610425

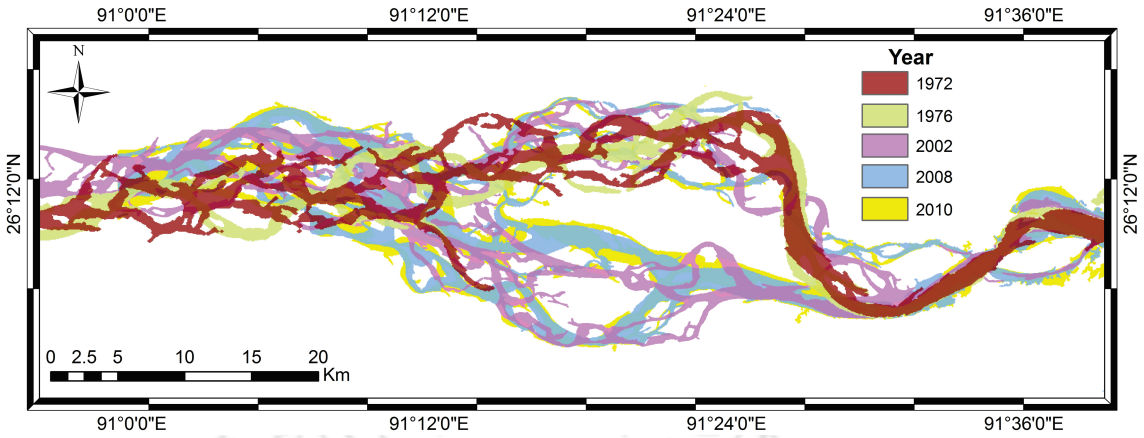

Figure 1.1: Morphological dynamics of the middle reach of the Brahmaputra river (Guwahati downstream).

mixing are the major phenomena taking place in the Brahmaputra river at different hydrodynamic conditions of the river. These morphological processes reflect the changes in the river morphology of different time and spatial scale and their effects resulting in different morphological features changing the course and the geometry of the river. There are the following factors considered to be predominant in braided river morphological dynamics such as in the Brahmaputra river.

- The Brahmaputra river is a braided river in which channel migration and bar formations cause high morphodynamics in the river.
- The discharge variations are very high in the Brahmaputra river which causes major changes in the river morphology with high influx of sediment during the monsoon season.
- The variation in river bed slope and the river flow width also plays major role causing the flow instability, which leads to river fragmentation (Figure 1.2).
- Field evidence suggest the high turbulence during the monsoon season and the bank under cutting and bank erosion occur due to high flow (Figure 1.3). The sediment mixing and bar migration also takes place during the monsoon season.

1.3 Remote sensing of the braided rivers

Satellite remote sensing techniques have been used extensively to study rivers and its morphological dynamics. The improvement in remote sensing techniques, sensor capabilities

TH-1911_10610425

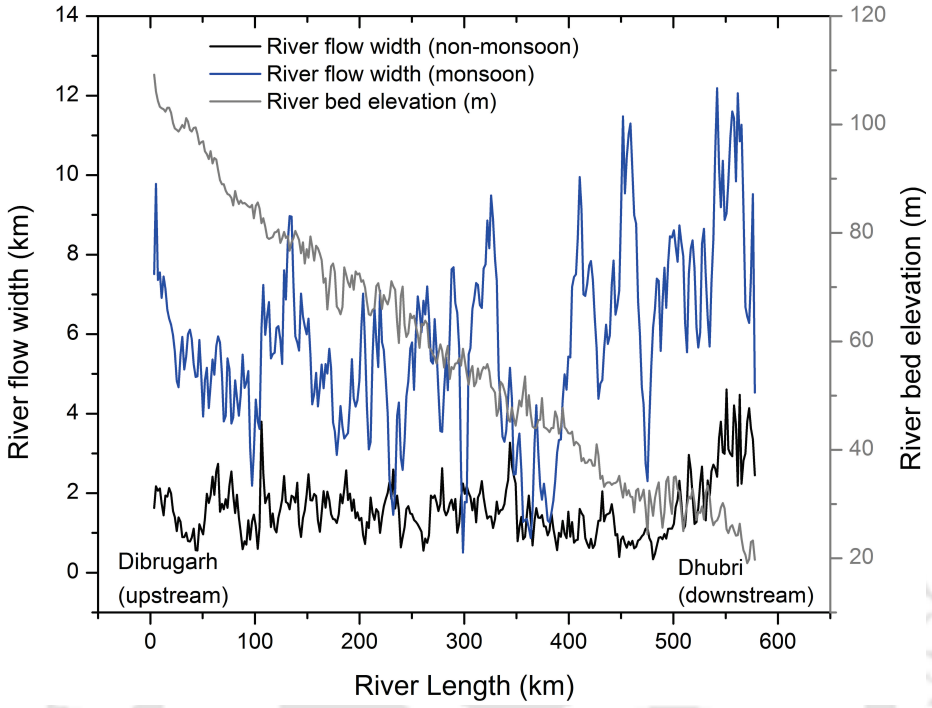

Figure 1.2: The Brahmaputra river flow width variation for different seasons with river bed elevations for the year 2013

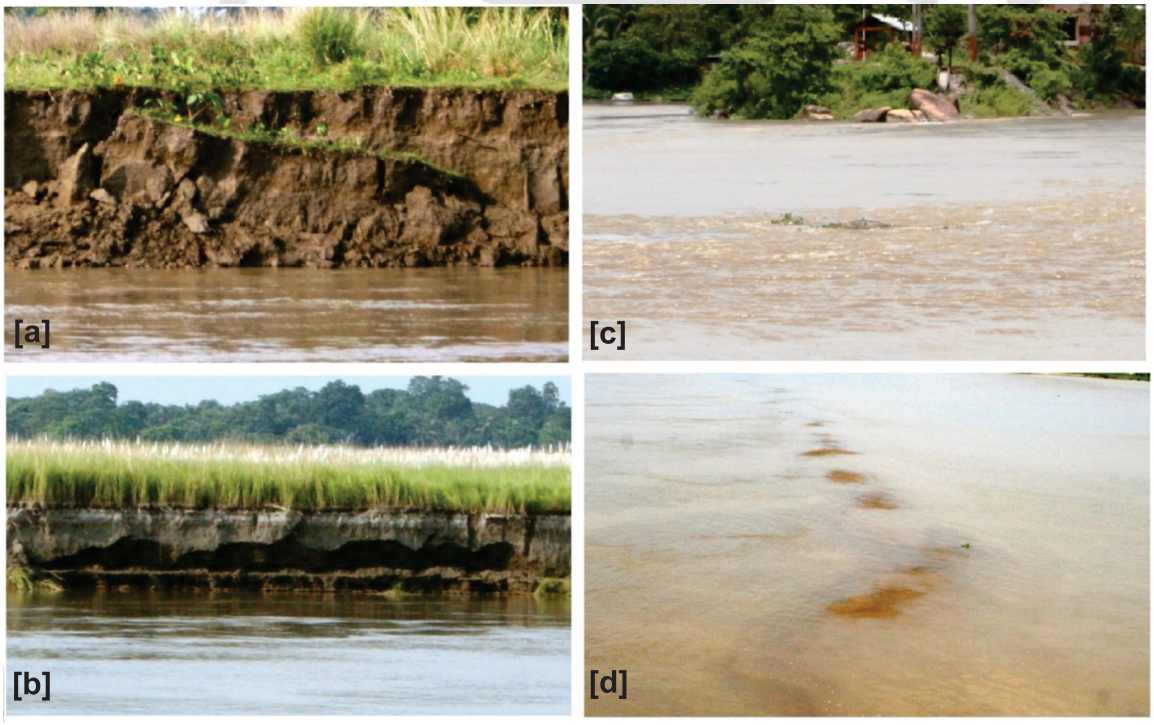

Figure 1.3: Active morphological processes in the Brahmaputra river (a-b: Bank erosion, c-d: Vortex formation) during the monsoon season.

and geo-spatial tools have greatly enhanced the capacity to investigate river systems like the Brahmaputra in different prospective. These techniques have been used to retrieve different morphological features and river dynamic parameters present within braided rivers. These parameters in different space and time scales have presented new opportunity to study these rivers with new prospectives such as satellite altimetry, it has the capacity to retrieve water level and discharge at flood-plains of the river. The microwave satellite images could observe turbulence in terms of hydrodynamic and morphologically dynamic features. With the help of remote sensing and geo-spatial techniques constant mapping and monitoring of large river systems are of vital interest in terms of river management practices. It provides consistent facility fo different hydrodynamic and morphologic regime of the river. Assimilation of these parameters in hydrological and hydrodynamic models improves the overall understanding of the sand bed braided river morphological dynamics.

1.3.1 Satellite altimetry over the braided rivers

Satellite altimetry is the recent technique used for water level retrieval in inland water applications. It is utilized to monitor inland water fluctuations for calibration and validation of hydrological and hydrodynamic models. The availability of river stage variations over the un-gauged or sparsely located gauge stations for a river basin is an useful information. The altimetry retrieved water levels are not limited to the unfeasible locations and the ground hurdles making it difficult to monitor river variations through traditional gauging stations. The river water levels over the flood-plains and at the braided reaches through satellite altimetry could be used to study river energy dissipation over the braided reaches of the river. The dense coverage of altimeters over a river basin provides an unique set of information to investigate spatial dynamics in river hydrodynamics. Altimetry applications over the braided river has been presented in this work. Detailed investigation is required to improve the accuracy of retrieved water level information for the braided reaches of the Brahmaputra river. There are a lot of challenges in retrieving water level over the braided rivers, such as presence of multiple channels, sand bar migration and formation and varying river flow width. Hence, scope of improvement is very much in the satellite altimetry for the braided rivers.

1.3.2 Microwave satellite images of the braided rivers

Microwave satellites having active synthetic aperture radars principally operates in microwave frequency. In the present study microwave images of C band (5.6 GHz) frequency are used. It has capability to capture images in all weather conditions. The microwave

TH-1911_10610425

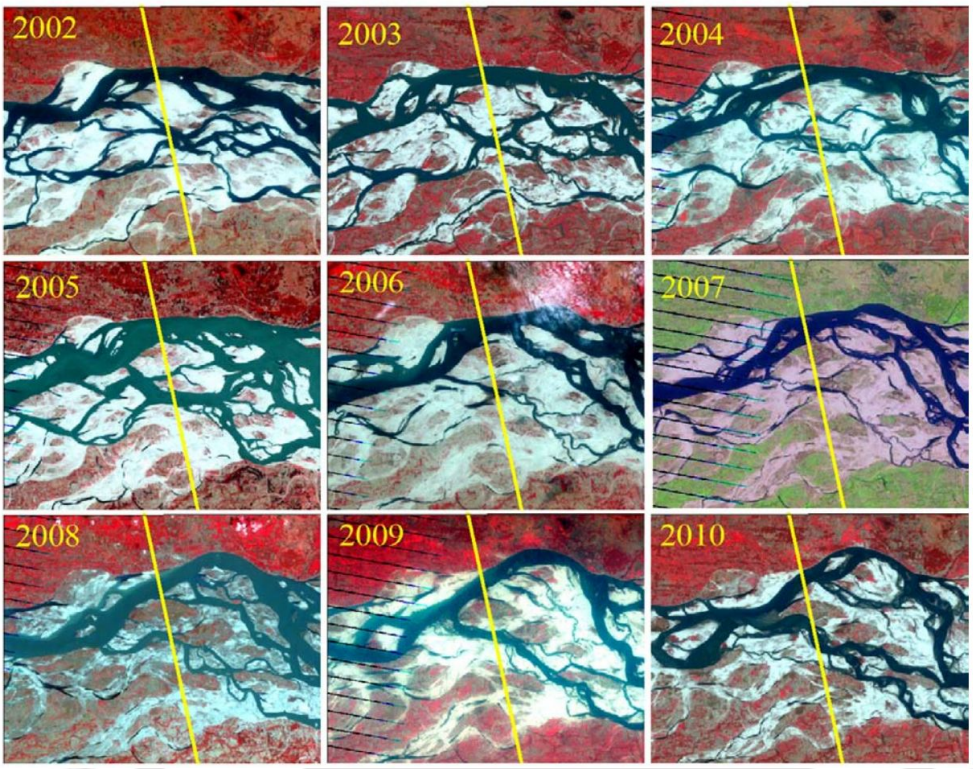

Figure 1.4: Yearly variation of river planform overlaid with altimeter satellite tracks.

images are sensitive to surface roughness and dielectric constant of the target surface. The multi-date and multi-polarized microwave images are used to study the river morphological dynamics during the monsoon season. The sand bed braided rivers such as the Brahmaputra is highly dynamic river in which various morphological processes takes place such as sand bar migration, sand bar formation, bank erosion, river bed erosion, sand deposition and sediment mixing. In microwave satellite images these features have different signatures in terms of radar back-scatter. These features could be identified and mapped using different signatures due to their unique characteristics. The mapping of morphological features with multi-date microwave images could be very useful in interpreting intra-seasonal river morphological processes.

1.4 Hydrodynamic modeling

The Brahmaputra river is a highly dynamic river with high amount of discharge and sediment flux during the monsoon season. The average annual discharge of the Brahmaputra river is 20,000 m^3/s at Pandu gauge stations located near Guwahati. The peak discharge could reach up to 50,000 m^3/s during a flood year. The sediment flux is also very much in

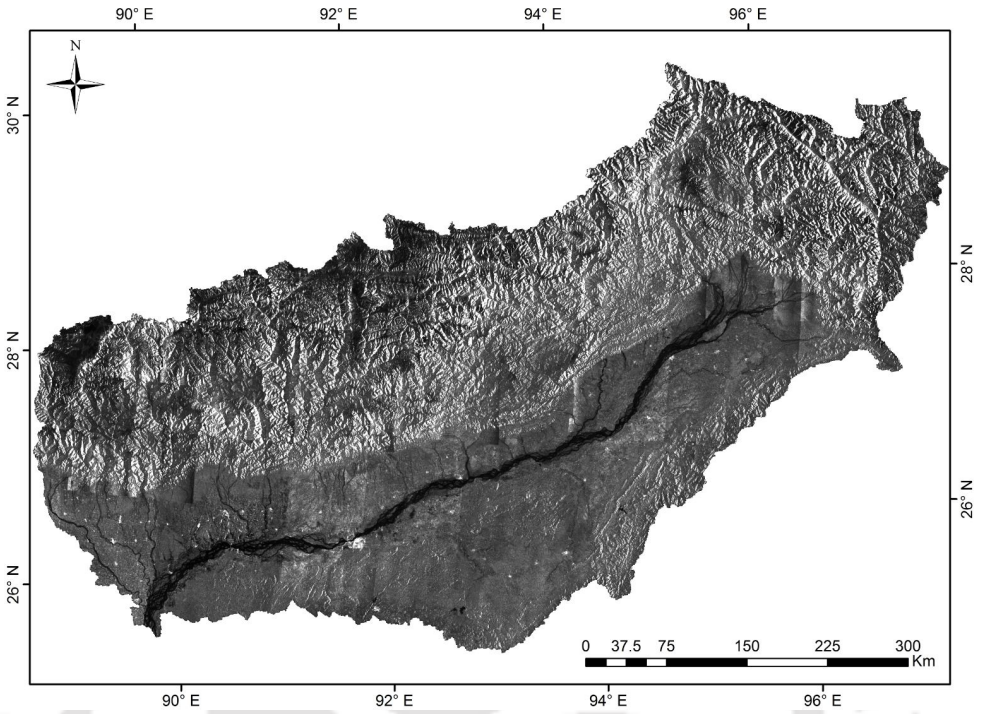

Figure 1.5: Middle reach of the Brahmaputra river from microwave satellite image.

this sand bed braided river. The mean annual suspended sediment load is about 402 million tons. The Brahmaputra river has highly dynamic bed morphology with highly erodible banks. The hydrodynamic modeling is a challenging task for this kind of river with limited amount of river bathysphere information. On the other hand different approaches are developed to study the river morphology with advanced gestational technologies and simplified hydrodynamic modeling. The one–dimensional hydrodynamic models could reflect the energy dissipation in terms of variation in river morphology and could be calibrated with geo–spatial information in terms of bed roughness (mannings roughens coefficient). The one dimension calibrated model could be used to predict river water surface profiles with acceptable accuracy. The continuous calibration of complex hydrodynamic model also poses a limitation of its applications and setup for large scale river discharge and morphological dynamics. Hence, the kind of complimentary approaches of advanced geospatial information assimilation into the simplified hydrodynamic modling framework could make it viable to understand the river flow and morphological dynamics with varying spatial and temporal scales. The flood waves of different durations occur in the Brahmaputra river. The water level variations from upstream (Dibrugarh) to downstream (Dhubri) is reported in Figure 1.7. The flood pulses of different magnitudes travel from upstream to downstream within 3-5 days. The flood pulses from upstream travel and get dispersed along the length of the river. The dispersion of flood waves disposes the high amount of shear force in

TH-1911_10610425

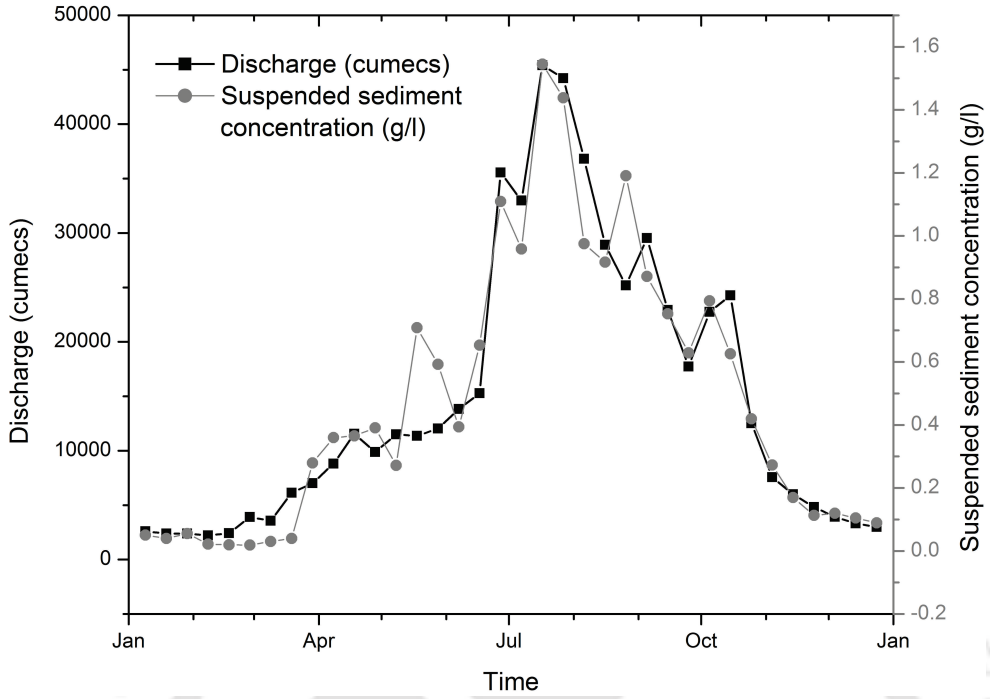

Figure 1.6: Discharge and sediment flux variations in the Brahmaputra river measured at Guwahati gauge station.

the bed and the bank of the river, which results in the sand bars formation, bed erosion, sand bar migration and river bank erosion along the length of the river. The river depth gets decreased as river width and braiding phenomena occurs, which suggest the energy dissipation by the river.

1.5 Objectives of the present research

The main objectives of the present research are:

- Improvement in the methodology to retrieve water levels over the braided reaches of the river using satellite altimetry data from different platforms (Envisat, Jason-2, SARAL/Altkia).
- To establish the relationship between satellite altimetry derived river stage and the discharge for estimation of 10 daily discharge variation and derivation of seasonal water depth and water surface slopes.
- To map intra-seasonal morphological features of the braided river using microwave satellite images of multiple polarization.

TH-1911_10610425

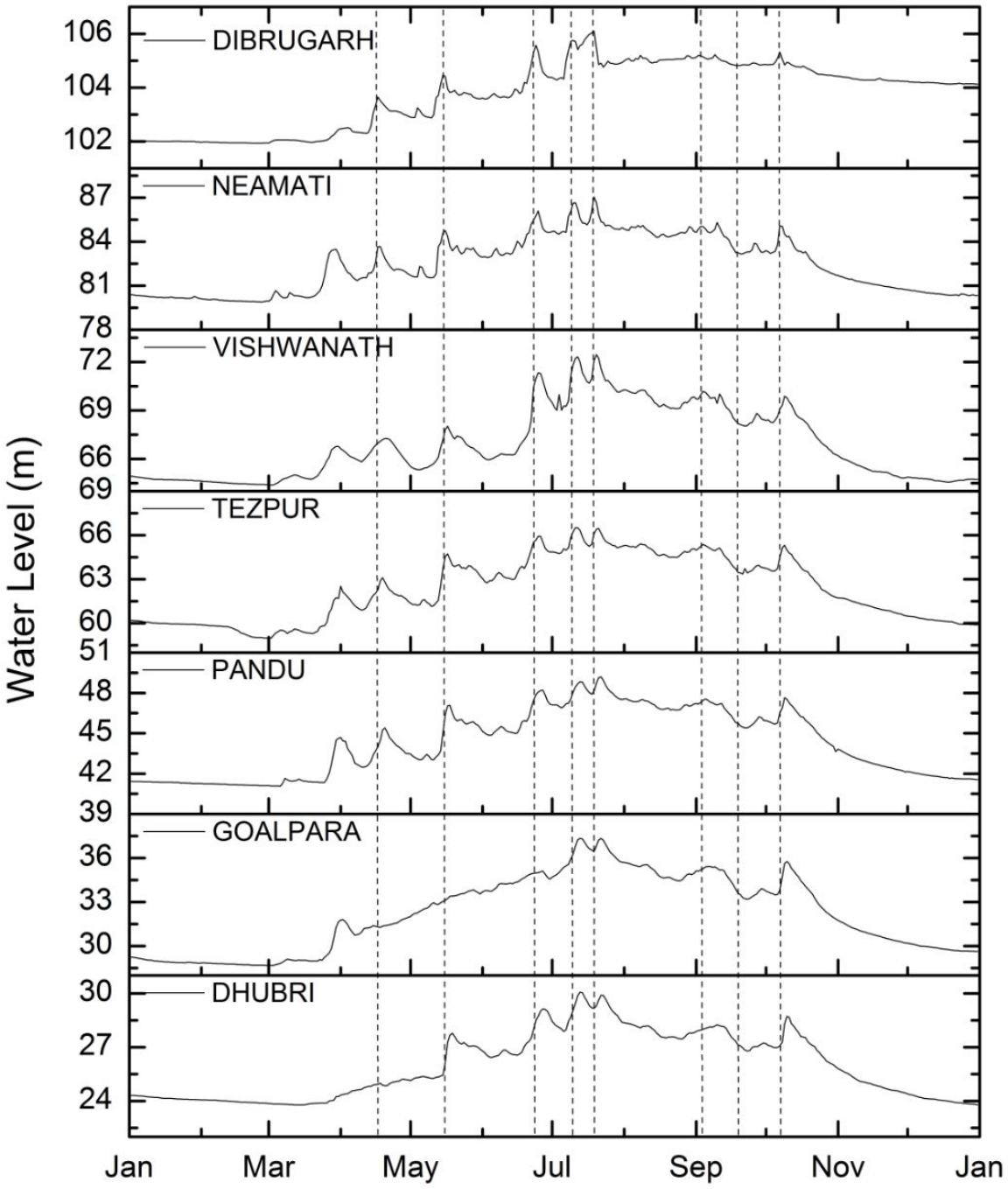

Figure 1.7: Water level variations along the Brahmaputra river during the high flow seasons in year 2004.

- Assimilation of satellite altimetry derived water surface slopes into the river model for predicting water depth variation in the different reaches of the river.

1.6 Organization of the Thesis

The present research work in the thesis is divided into the nine chapters. The research work in the thesis focuses on the morphological dynamics of the Brahmaputra river using advanced geo–spatial techniques and hydrodynamic modeling. The thesis segmentation is done in such a way that it covers the advanced remote sensing techniques such as satellite altimetery microwave satellite images. Initially, it focuses on improvement in water level retrieval over the braided reaches and to derive the hydrodynamic parameters for assimilation into the hydrodynamic modeling. The subsequent chapter covers the morphological mapping of the braided reaches of the Brahmaputra river. The later chapters include the hydrological modeling of the Brahmaputra river including the major tributaries, which contribute to the discharge in the Brahmaputra river. Finally, altimetry retrieved water levels and hydrologically simulated discharges are assimilated into the hydrodynamic modeling in the Brahmaputra river. The chapter–wise description of the thesis is given below.

Chapter 1: It provides overview measuring monitoring and modeling on large braided river morphology and short term morphological dynamics using remote sensing.

Chapter 2: In this chapter, review of literature is provided for the research work carried out.

Chapter 3: In this chapter, Details of study area, data collection and the different satellites observations are used for the research work.

Chapter 4: This chapter presents a novel technique for development of improved water level retrieval algorithm for the braided reaches of the river.

Chapter 5: This chapter describes the estimation of discharge ,water surface slopes, performance and accuracy analysis of retrieved water level over the different braided reaches of the Brahmaputra river.

Chapter 6: This chapter highlights the use of microwave satellite images for mapping morphological features in the Braided Brahmaputra river.

Chapter 7: In this chapter Hydrological modeling of the Brahmaputra river is done to estimate the spatio–temporal variation of discharge for different tributaries and the main channel of the Brahmaputra river.

Chapter 8: In this chapter assimilation of altimetry water level is performed in Hydrodynamic model using estimated manning s roughness coefficient.

Chapter 9: The final chapter highlights the conclusions arrived at and also summarizes the research work.

TH-1911_10610425

"Research is to see what everybody else has seen, and to think what nobody else has thought."

Albert Szent-Gyorgyi (1893 - 1986)
American Hungarian physiologist

2

REVIEW OF LITERATURE

2.1 Introduction

Many researchers have studied the braiding phenomena of alluvial and gravel bed rivers. High sediment load, high stream power, rapid bank erosion are very common characteristics of the braided rivers (Leopold and Wolman, 1957). Division of velocity field in to multiple core zone and associated growth of mid-channel bars are of fundamental importance to the understanding of braided rivers (Philip, 1996; Ashworth et al., 2000; Thorne et al., 1993). Historically geomorphic models have indicated the mid bar initiation and growth due to sediment deposition around and centre of it as a primary process in braiding (Philip, 1996; Ashworth et al., 2000). Geo-spatial technologies have played the great role in mapping the large rivers at various spatio-temporal scales. With the readily availability of geographic information, modeling of such large river becomes easier. Numerical modeling and Physical modeling of these large braided rivers has greatly enhanced the understanding of the processes involved at different spatial and temporal scales.

2.2 Dynamics of Braided river morphology

Braiding occurs because of instability in the flow due to topographic perturbations and the nonlinear relationship between discharge and sediment flux. Geometry of the river, discharge and sediment flux interact with each other and vary in spatial and temporal domain, which results in aggradation and degradation of river. It leads to formation of morphological features such as sand bars (Islands). Sand bar also respond to varying dis-

TH-1911_10610425

charge, sediment flux with longitudinal and transversal migration, which induce the river width variation and adjustment of the bed slope. Topographical constrain also facilitate the braiding phenomena, which makes it very complex to understand the interaction of spatio-temporal variation of discharge and sediment flux with river morphology and its effects on formation and migration of alternate bars, bed slope and bank erosion. Leopold and Wolman (1957) studied the fundamental relationships between discharge, sediment flux and flow resistance with varying velocity, depth and slope. They concluded, that the discharge controls the channel width, resistance of flow is controlled by the bed form and roughness by bed material. Discharge and sediment flux adjust the resistance of the channel, which affects the flow velocity, bed slope and depth of flow. Coleman (1969) studied the braiding patter within the channel and pointed out that braided channel converge and diverge frequently around the alluvial islands, hence causing the migration and shifting of bars from one place to another. Channel braiding can be occurred due to presence on only one island, which subsequently lead channel to become more braided with non-cohesive banks vulnerable to bank erosion. Islands are composed of both bed load and suspended sediment. Braiding is the result of steep slope, high sediment flux with easily erodible banks. Water flows in number of channels within the braided river, in which one the channel always flow as a main channel with higher width as compared to others. The daily variation in channel configuration occurs due to mid channel island and sand banks shift rapidly with fluctuating discharge and sediment flux. The river course remains highly unstable and it changes frequently. Fairbridge (1968) investigated the movement of thalweg within the river and found that its movement within the channel causes the change in channel geometry. The movement of thalweg varies with the discharge; hence its movement becomes very high during the high flow conditions (May-July). Its movement becomes low during low flow seasons (October-March). Goswami (1985) reported, that occurrence of large earthquake in 1950 with subsequent landslide provided the very high amount of sediment load that has transported from upstream to downstream. This sudden increase in sediment flux raised the river bed at various locations due to aggradation. It was observed that river bed of Brahmaputra rose by 2 m. For the different periods the rate of sediment transport was different which deposited at different reaches of the river and causes the river braiding. Bristow (1987) pointed out that in a response to spatio-temporal variation of sediment flux and discharge there is also change in bed load grain size. It remains finest during low flow and increases during peak flow. Ashworth et al. (2000) found, that central bar nucleus is behind the mechanism of sand braid-bar growth through the amalgamation of large dunes. Bar top aggradates because of dune superimposition and development of accretionary dune front. Dune migration around and onto the margins of the bar produce the later accretion, which widen the bar laterally. Richardson and Thorne (2001) stud-

ied the flow structure of the braided river from the field measurement of velocity in three dimensions with help of ADCP (Aquastic Doppler Current Profiler) in the Brahmaputra-Jamuna River. They investigated the causes leading to bifurcation of a channel and leading to braided river morphology. They found that there exist the multiple threads of velocity zones which lead to bifurcation of channel and creates multi-channel flow within a single flow width of the river. They established the empirical relationship to discriminate between channels with single and multi-thread velocity fields, based on the depth-to-width ratio and specific energy of the flow at a representative channel cross-section. Sarker and Thorne (2009) investigated the effect of earthquake of magnitude 8.6 occurred in Assam in 1950. They reported that approximately 45 x 109 m^3 of sediment were delivered to Brahmaputra river due to the landslides causes by the earthquake. He also reported that river bed rose by 3 m at Dibrugarh and 1.5 m immediately following the earthquake. The rate of aggradation reduced up to mid-1950s. Mosselman (2009) identified that bank erosion is a major problem in the Brahmaputra river. He found that non cohesive and fine grain sediment are prone to erosion and does not facilitate the strength to the bank. This causes the rapid bank erosion during the bank flow discharge. It forms the deep channel near the bank, confluences and the sharp bend on the both side of the river bank. The bank protection measures also do not provide satisfactory results due to poor understanding of morphological dynamics of large braided river like Brahmaputra (Karmaker and Dutta, 2010) flood events and their characteristics effect the flood–plain, bank erosion of alluvial rivers. High amount of rainfall during monsoon period and their clustering creates the number of flood waves. He characterizes the hydrograph in to two components, first flood waves and monsoonal (seasonal response) for larger river basin. Monsoonal response and the individual flood waves were approximate using Maxwell distribution. Karmaker et al. (2010) conducted the ADCP experiments to study the sediment transport in an active erodible channel bend of Brahmaputra river. Their study indicates the presence of multi-thread flow in the channel bed. They reported that local variation of sediment transport is controlled by active bank erosion, land spur and sand bar formation. The vertical distribution of suspended sediment concentration follows the power function with normalized depth. Zhang et al. (2011) found, that the Brahmaputra river consists primarily of fine sands and silts with little clay matrix. Therefore, river banks are highly susceptible to erosion when the flow conditions change. Frequent flood and continuous erosion have done the large scale damage in the past several decades. People living on floodplains were the worst affected by this, which made thousands of people homeless and destroyed their infrastructures.

2.3 Advanced geospatial technologies

Development of advance geospatial technologies have created the enormous opportunities to study and investigate the fluvial processes occurring in the large braided river like Brahmaputra. It provides the useful information to analyse river characteristics at different spatial and temporal scales. It was started with the initial development of remote sensing, in which satellites were able to capture the synoptic view of the earth in the optical electromagnetic spectrum, which provided the much needed information to delineate the water and land area. It provided the area of inundation after flooding and flow width of river during lean flow period. But in optical remote sensing, cloud covers were the major obstacle to capture images during monsoon season. In many times it was not possible to obtain the river characteristics during the monsoon seasons due to excessive cloud cover, until the development of Synthetic Aperture Radar (SAR) technology, which is based on active remote sensing. It allows us to capture the earth images even in cloudy conditions. The variation of water level also indicates the river condition and it is important input parameter for hydrodynamic modeling of river. Traditional gauging station observation provides water level variation only at a particular station; many times it is observed to the nodal points for the braided river like Brahmaputra. With development of satellite altimetry, it becomes possible get the water level variation at the braided reaches of the river.

2.3.1 Satellite Altimetry

Utilizing satellite radar altimetry for monitoring inland waters can play a pivotal role in enhancing our ability to monitor the cycle of surface water from the regional scale to the global scale. Although radar altimetry suffered from many drawbacks such as non-availability of retracking algorithms specialized for inland waters, discrepancies between satellite and in-situ measurements, lower temporal resolution, missing data, but recent advancements in altimetry and data processing methods have helped develop various datasets facilitating the study of inland waters effectively and efficiently (Frappart et al., 2005; Calmant and Seyler, 2006; Calmant et al., 2008). Kouraev et al. (2004) established relationships between satellite-derived water level and river discharge measurements at Salekhard gauging station near the Ob' estuary. They considered a simplified relation between the water level and river discharge without the use of detailed in situ information on hydraulic and morphological particularities of the chosen river section. They indicated that because of presence of secondary channels, the satellite time series of water level were noisy. The calculated discharge were compared with in situ discharge measurements, which showed that satellite-derived river stage data can successfully be used for hydrological studies of seasonally ice-covered

TH-1911_10610425

Arctic rivers. They suggested that the applied approach in their study has limitation to rivers that are several kilometers wide because of the present satellite altimeters resolution. Leon et al. (2006) in their study, they demonstrated, that mean reach depths can be derived from the parameters of the power law establishing the rating curve between water stages from satellite altimetry and discharges estimated by flow routing. They developed a method to extract bottom elevation, bottom and free surface slopes and roughness coefficients from a combination of altimeter and remote discharge data. Zakharova et al. (2006) used the satellite altimetry derived river stage data to estimate river discharge at three sites along the Amazon River. They established empirical relationships between satellite-derived water levels and daily estimations of river discharges based on rating curves and in situ level measurements at gauging stations. In their study, they found a decrease in accuracy of satellite derived water level measurements over the Amazon during the low water season. These observations were resulted from the contamination of vegetated areas, sand beaches and dry land reflections in the reflected radar signal. Other errors were due to uncertainty in the water level-discharge relationship. Papa et al. (2010) evaluated the altimetry derived river stage records for Ganga and Brahmaputra rivers to estimate the monthly discharge at different virtual stations. They found that seasonal variation of discharge was clearly indicated by the satellite-derived discharges. However, they have found that increased daily relative errors are obtained during the low discharge periods. During these periods, the river is narrower; the spatial length of the altimeter-river crossing is thus smaller than during the period of high water flow. The radar signal also can be contaminated by the presence of dry land resulting in noisier and less accurate estimates of the river height. The comparison of in situ and satellite-derived discharge estimates shows that the satellites reproduce the seasonal timing of the various stages of the hydrological regime (seasonal low/high water flow) as well as the inter-annual variations.

2.3.2 Microwave Remote Sensing

Remote sensing of the earth in optical region of electromagnetic spectrum has provided useful scientific operational data for various earth resources applications. Optical sensor essentially records the reflectance of sunlight from the earth's surface. However, under cloud cover conditions, operational capabilities of optical sensors become limited. In contrast cloud cover is considerably more transparent at microwave wavelengths, hence microwave sensors plays important role in data collection, which is independent of weather and sun light conditions. Besides this, there are specific applications where microwave sensors have shown their proven capabilities which otherwise could not be possible. The all-weather capability of microwaves is one of the major factors for many applications. The radar energy

TH-1911_10610425

has the ability to penetrate clouds, haze and even light rain. Further, radar sensors use their own source of energy to illuminate the terrain and as a result data can be acquired during night and need not be restricted to day light hours. Microwaves have greater surface penetration capabilities than the optical and thermal sensors. The depth to which radar penetrates into soil and vegetation surface depends on the wavelength of the radiation and dielectric properties of surface materials. In the microwave region, penetration of wave increases, with the wavelength. Microwave's unique sensitivity to water content of surface material allows a number of applications related to vegetation and soil moisture and snow wetness. Coherence properties of radar are able to provide new tool is called interferometry. Smith et al. (1996) derived the relationship between effective width and measured discharge for three braided rivers from the images of synthetic aperture radar and also related the morphologic and hydraulic field measurements from two of the rivers to the SAR data. They found that power law relationship between effective width and measured discharge. Synthetic values of effective width and discharge generated by a cellular model of stream braiding also show a smooth power law correlation. They have suggested that discharge prediction can be made more accurate by successful parameterization of morphologic controls such as total sinuosity, slope, vegetation cover, and distribution of braid channel widths. Smith (1997) investigated the utilization of microwave satellite images to acquire estimates of inundation area over very large rivers. Spaceborne synthetic aperture radars (SARs) are not limited by weather conditions or darkness. Single polarization, C-band SARs are effective for mapping smooth, open water bodies. However, emergent vegetation, trees, wind or flow turbulence can all increase radar back-scatter returns, making interpretation of microwave image more problematic. Nykanen et al. (1998) investigated the presence of spatial scaling relationships in natural braided river patterns using Synthetic Aperture Radar (SAR) imagery, which has opened a door of opportunity in the area of quantitative studies of braided rivers. They also explored how this scaling might be affected by flow rate, braiding index, and large-scale topographic controls, such as mountains.They found, that self-affine spatial scaling for braided rivers was held over at different flow rates and instants of time when the river was free of topographic controls (e.g., mountains). They found it poor for the places where development of braid plan was morphological constrained by topographic features and also for braided pattern with a predominant flow path.

2.4 Numerical modeling

The application of numerical models to understand and predict river characteristics have increased in recent period. However, unavailability of reliable field measurements is ma-

TH-1911_10610425

jor hindrance in understanding the complex system of braided river. Numerical modeling has a potential to solve this complex problems with the development of high speed computing, commercially available computational fluid dynamics (CFD) softwares, but they do not consider the bed movement. Development of two dimensional and three dimensional morphological models can be used to understand the braiding mechanism with changing flow and sediment regime. Attempt has been made to understand aspects of braided rivers with the help of physically-based numerical models in simulation of alternate bar formation at shallow channels for depth, flow, width variations and bank erosion in alluvial river (Bernini et al. (2009); Bertoldi et al. (2009); Karmaker et al. (2010)). Despite this progress, numerical modeling remains challenging task with limited availability of data sets such as river bathymetry to used as the tool for understanding flow and sediment interactions in the braided rivers. Nicholas (2003) applied the two-dimensional model to a braided reach to investigate the depth, velocity and shear stress frequency distributions over a range of discharges. The simulated results from model indicate the similarity between the observed depth and velocity in the field. However field measurements show the more variability at all sections as compared to model simulated results. Field measurement errors could also attribute to the differences between observed and simulated results. Model grid scale may also be responsible for the differences between the flow parameters, because the processes occur in field are at smaller scales as compared to individual model grid cells. The cell based simplified models (Cellular automata) are also used to study the river morphological processes for the longer time period (Murray and Paola (1994); Thomas and Nicholas (2002); Coulthard et al. (2006);Murray and Paola (2003)). However to simulate reach specific hydrodynamic variations remains complex for these kinds of model too.

2.5 Conclusions

The literature review revealed that previous studies focused on braided river dynamics using traditional methodologies. With advancement in space based platforms with different capabilities opens up the new dimension to study braided rivers with different perspective. In this study advanced geo–spatial techniques were used to investigate braided rivers such as satellite altimetry, microwave and optical remote sensing. The assimilation of these advanced techniques into the hydrodynamic modeling has enhanced the overall understanding on morphological dynamics of these large sand bed braided rivers.

TH-1911_10610425

"Any sufficiently advanced technology is indistinguishable from magic."

Arthur C. Clarke (1917 – 2008)
English naturalist

3

STUDY AREA AND DATA COLLECTION

3.1 Introduction

This chapter describes about the study area and its hydro–morphological characteristics. The different field campaigns were conducted during this research work. To understand the braided river morphology, field measurements are utmost important hence sufficient *in–situ* data to be collected for this study, combined with field survey of the Brahmaputra river during the monsoon and non-monsoon phases of the river. The river island survey was conducted to understand the morphological characteristics of the sand bar. The flood plain data has been also collected during the monsoon season. Apart from field survey, satellite data of different platforms were also acquired from various sources such as microwave satellite images for intra-seasonal morphology variations. The altimetry satellite data for water level retrieval and optical satellite images for analysis of non-monsoon period were acquired. To validate the results archived *in–situ* data was also collected. The water level, sediment flux and discharge data was obtained from Central Water Commission of India (CWC) for the period of 2000 to 2010 for Guwahati and Tezpur gauge station at 10 daily interval. Historical water level records were also obtained from the Inland Water Authority of India (IWAI) from the period of 1997 to 2015.

3.2 Study Area

The Brahmaputra river is one of the major trans-boundary river of Asia, being the fourth largest in the world in terms of average flow discharge of 19,830 m^3 $s^{-}1$ (Goswami, 1985).

TH-1911_10610425

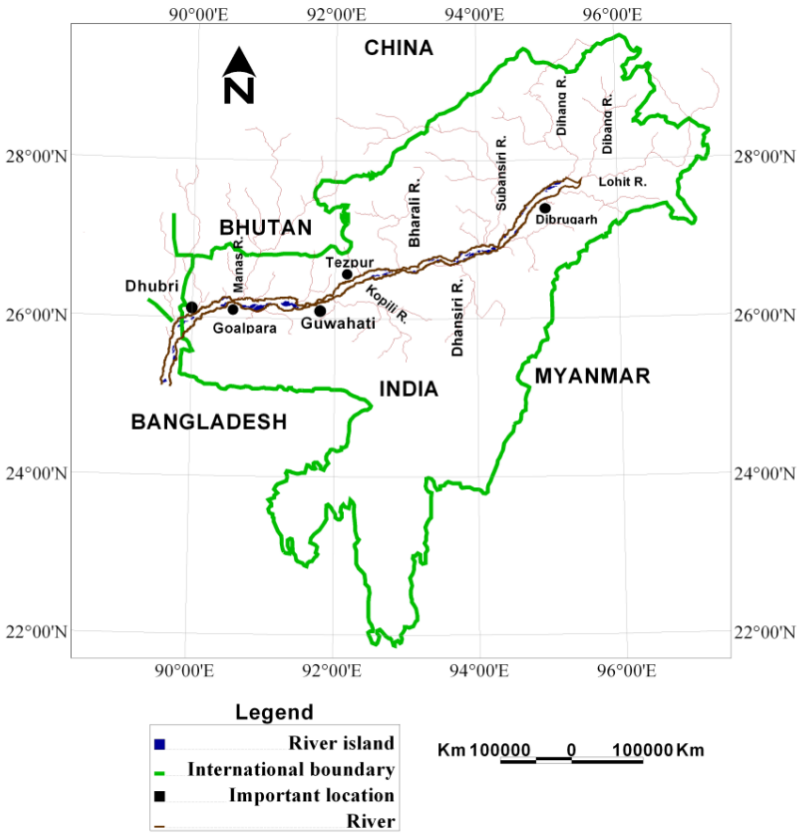

Figure 3.1: Index map showing Brahmaputra river and its physiographic features

It ranks 22nd in terms of catchment area which is around 380,000 km^2 from Tibet plateau to the Bay of Bengal (Bristow, 1987). The river is 2880 km long, out of which it traverses in an easterly course of 1,625 km in Tibet, a south and westerly course of 918 km in North-eastern India and a southerly course of 337 km in Bangladesh. The longitudinal slope of the river varies at different reaches, being 0.27 m/km from Kobo to Dibrugarh, 0.17 m/km from Dibrugarh to Nematighat (near Bessamora), 0.15 m/km from Nematighat to Tezpur, 0.14 m/km from Tezpur to Guwahati (near Guwahati), 0.11 m/km from Guwahati to Jogighopa 0.094 m/km from Jogighopa to Dhubri and 0.079 m/km from Dhubri to the mouth. The river exhibits a sudden decrease in slope in front of Himalayas near Pasighat; resulting in increased sediment deposition and giving rise to prominent braiding pattern (Sarma, 2005). The middle reach of the river valley has width varying from 64 to 90 km and spreads about 640 km long in India. It consists of flood plain area, hilly terrain and the river along with its tributaries. The river is a highly dynamic fluvial environment, with widely varying discharge, sediment load and easily eroded bank soils. The bed material is composed of medium to fine sand and silt (d_{50}=0.16 mm) (Karmaker and Dutta, 2010, 2011). Because of very fine bed materials, the river bed becomes highly mobile causing significant order of

TH-1911_10610425

morphological change by responding any change in the fluvial processes. River shifting is quite frequent in its braid belt, which results in flow division and growth of mid-channel bar and formation of different level of braiding (Richardson and Thorne, 2001). The flow regimes of the Brahmaputra river is largely dominated by runoff generated by monsoon, with high flows occurring between July and September and low flows from January to March. The river generally peaks during the period of July and August and the mean annual flood discharge at Pandu gauging station is about 51,156 m^3/s. The catchment of the Brahmaputra surrounded by an almost continuous chain of high hills and plateaus on the north, east, and south, the Brahmaputra valley in Assam represents a tectono-sedimentary province 720 km long and 80-90 km wide, with elevations ranging from 120 m at Kobo in the extreme east through 50.5 m at Guwahati to 28.45 m at Dhubri in the extreme west. The channel of the river itself, with an average width of 8 km, occupies about one tenth of the valley (Goswami, 1985). The Brahmaputra river is characterized by fine sedimentary environment with highly mobile beds and banks (Karmaker and Dutta, 2011). They found that sediment is uniformly graded and has very low strength and transport resistance. Mean sediment sizes of the river vary from 220um to 165um, showing insignificant changes from the upstream to the downstream. The river is braided with meta-stable islands and nodal reaches, mobile sandbars, shifting anabranches and severe bank erosion (Thorne et al., 1993). The mean annual suspended sediment load is 402 million tons and average monthly sediment discharge is the highest in June (19.05 %) and lowest in January (1.02). The bed load at Pandu was found to be 5-15 of the total load of the river (Sarma, 2005).

3.3 Field Observations

To understand the river hydrodynamic and morphological characteristics, field campaign were conducted. During the field visits various measurements were taken to validate the results. These survey were conducted during the monsoon period at time when most of the morphological processes within the river remains active. Different river survey equipments such as Acoustic Doppler Current Profiler (ADCP), Eco-sounder and suspended sediment probe were carried in the survey vessel to measure the river hydrodynamic and morphological parameters. These instruments measure river velocity, discharge, river depth and suspended sediment concentration. Frequent and multiple measurements were taken at different active zones of the river in transverse as well as in longitudinal directions.

TH-1911_10610425

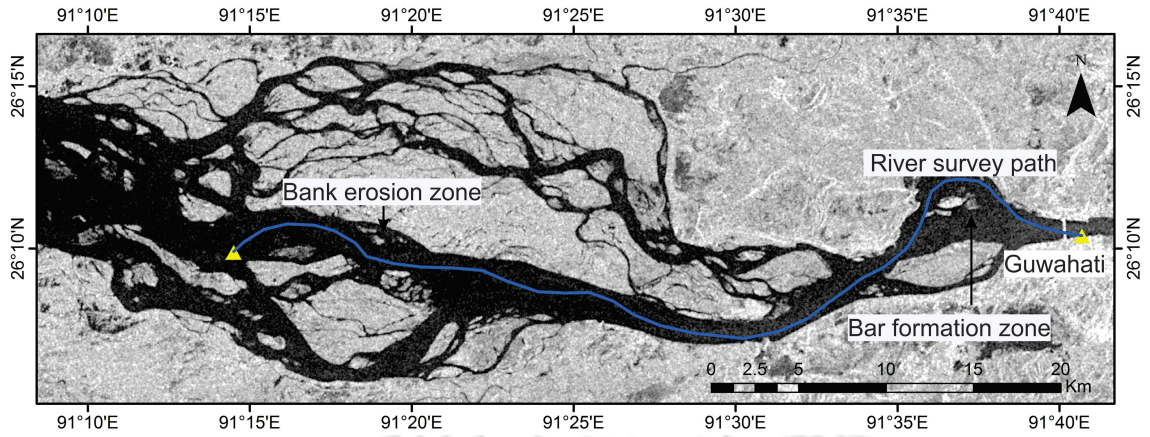

Figure 3.2: Brahmaputra river survey map

3.3.1 Hydrographic survey

At downstream of Guwahati detailed hydrographic survey was conducted thrice during the flood condition (Figure 3.2). The survey includes detailed data collection like bathymetry using GPS aided Echo-sounder, velocity profile through ADCP, sediment concentration from sediment probe. The measuring devices were mounted on an engine propelled vessel. The advance river survey instrument like ADCP (Figure 3.3) provides the three dimensional velocity profiles on a continuous moving boat facility. The cross section profiling was done at different locations using ADCP instruments. The velocity profiles were plotted for downstream of Guwahati (Figure 3.4), Kalachar (Figure 3.5), Gariamari (Figure 3.6) and Bhagmari (Figure 3.7). The velocity profiles indicate velocity distribution within the main channel of the river during the monsoon seasons. The suspended sediment concentration was also recorded for different locations in the river. The suspended sediment concentration vary at different reaches of the river, the sediment concentration was many times higher at active bank erosion (Figure 3.8) and the near sand bar (Figure 3.9) as compared to the nodal reach (Guwahati, Figure 3.10) of the river. At some reaches of the river sediment concentration was found to be high with higher turbulent zone. Sediment concentration was higher at the confluences of the river, at active sediment deposition around the sand bar (Figure 3.9), at active bank erosion zones and near thalweg line.

3.3.2 River island survey

The river island survey was done to understand the sand bar characteristics and the sand bar grain size distribution. The topography survey was conducted during the lean flow season. Over the sand bar situated downstream of Guwahati (Figure 3.12, Figure 3.13),to-

TH-1911_10610425

Table 3.1: Brahmaputra river survey

Date of River Survey	Instrument Used	Measurements
11th June 2011	Eco-sounder	Depth
	ADCP	Depth, Velocity, Discharge
	Suspended Sediment Probe	Suspended Sediment Concentration
	GPS	Positioning
7th July 2011	Eco-sounder	Depth
	ADCP	Depth, Velocity, Discharge
	Suspended Sediment Probe	Suspended Sediment Concentration
	GPS	Positioning
14th Sep. 2011	Eco-sounder	Depth
	Sub-bottom profiler	Depth Below the river bed
	Suspended Sediment Probe	Suspended Sediment Concentration
	GPS	Positioning



Figure 3.3: Photograph showing the ADCP instrument

TH-1911_10610425

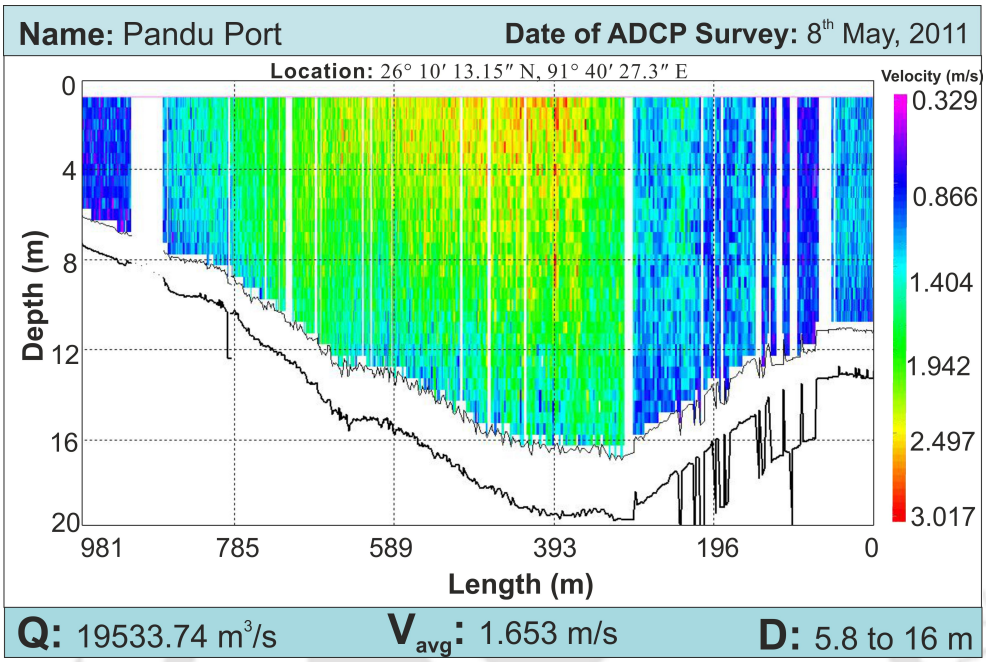

Figure 3.4: The velocity distribution measured using ADCP at downstream of Guwahati

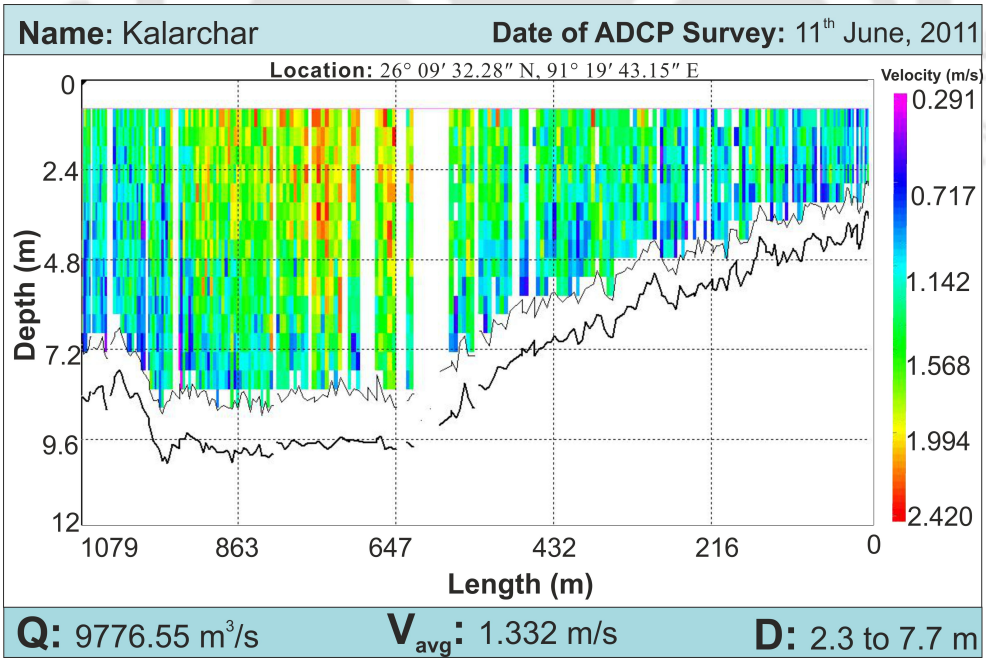

Figure 3.5: The velocity distribution measured using ADCP at downstream of Kalachar

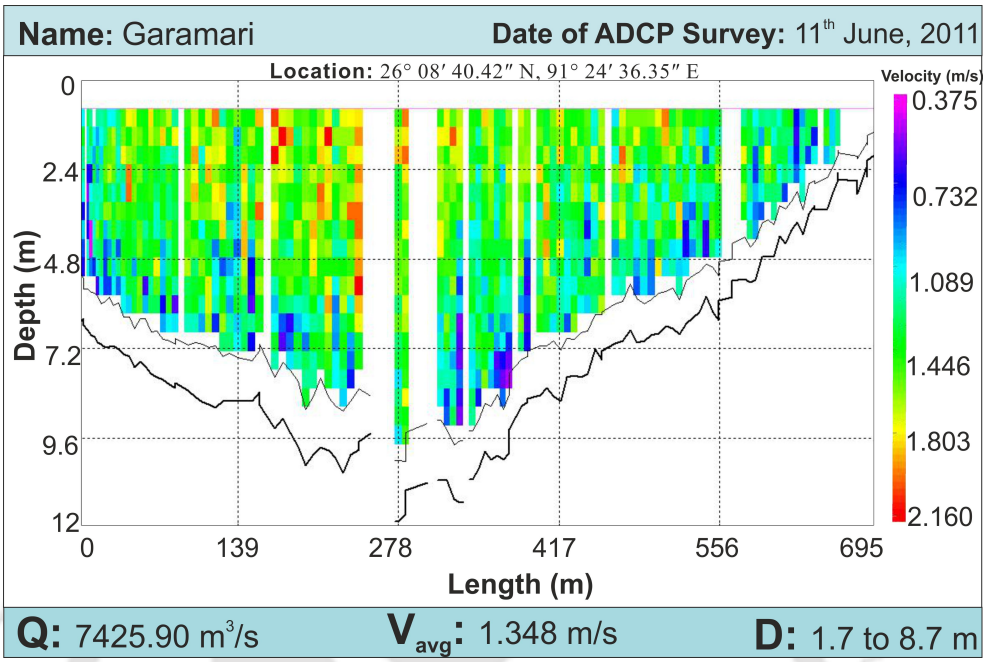

Figure 3.6: The velocity distribution measured using ADCP at downstream of Garimari

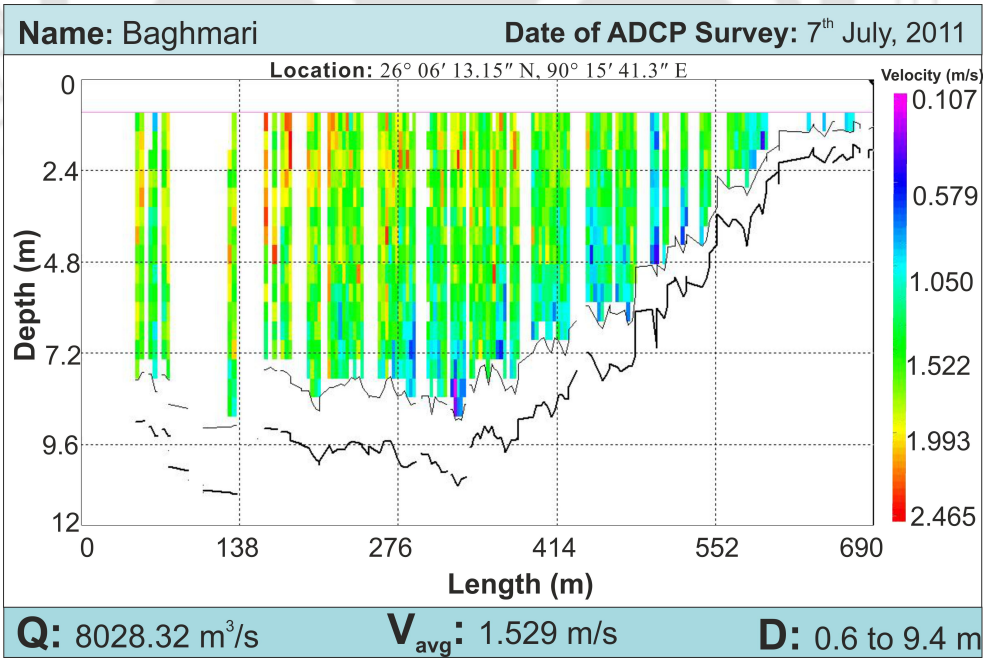

Figure 3.7: The velocity distribution measured using ADCP at downstream of Bhagamari

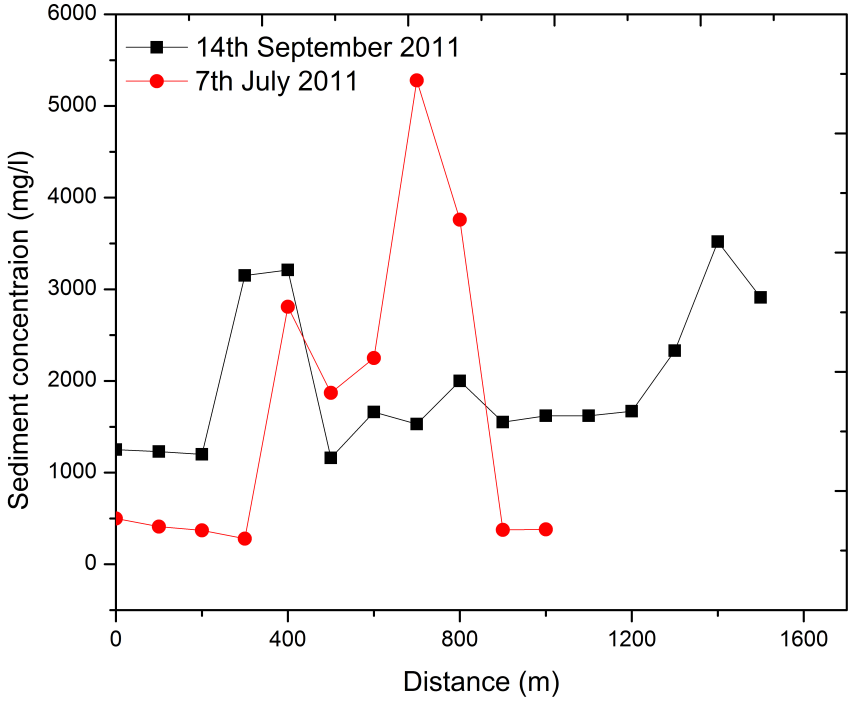

Figure 3.8: Variation of sediment concentration near banks of active bank erosion.

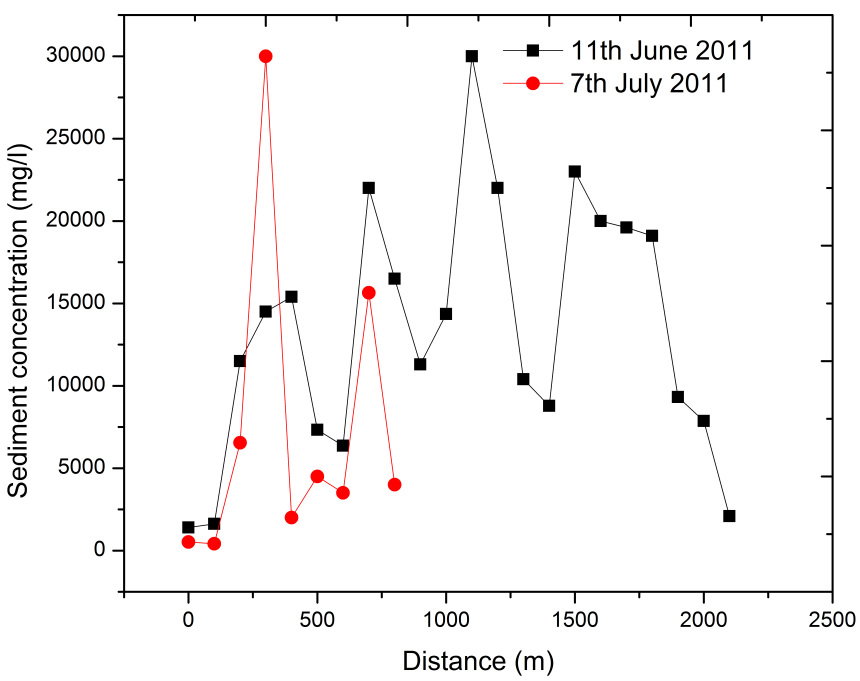

Figure 3.9: Variation of sediment concentration near sand bars with turbulent water conditions.

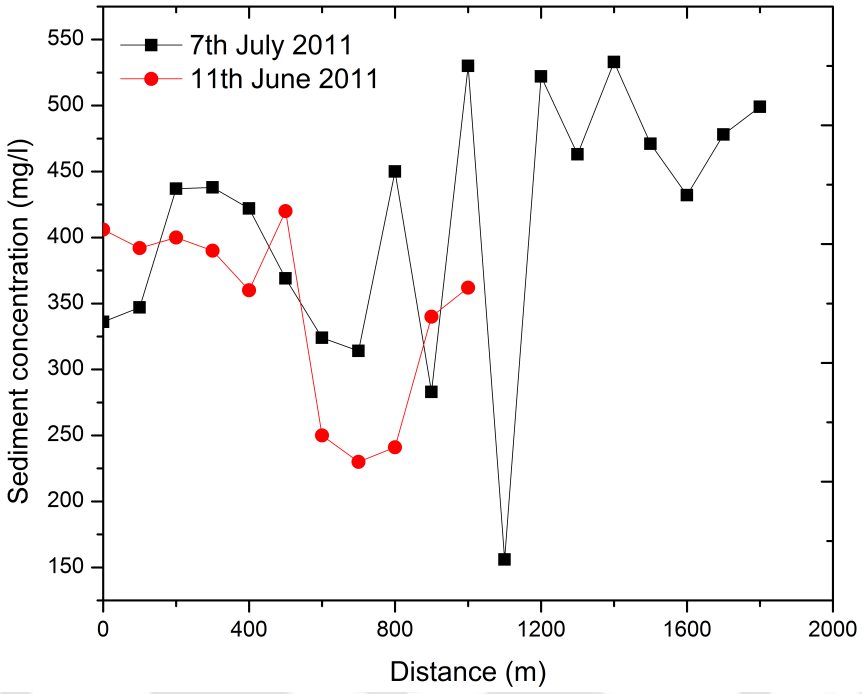

Figure 3.10: Variation of sediment concentration at nodal location (Guwahati).

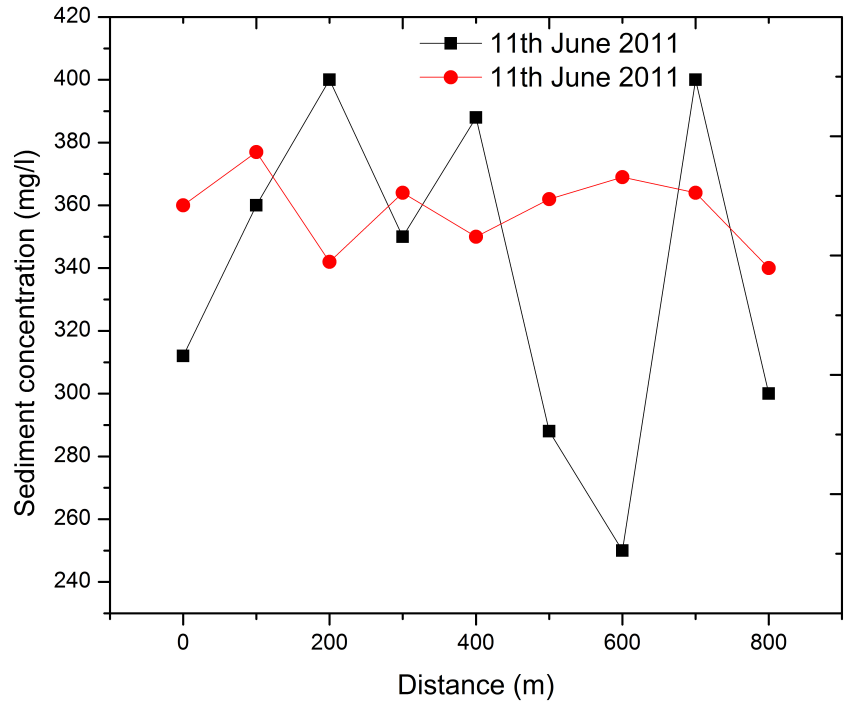

Figure 3.11: Variation of sediment concentration near river banks at two different locations.



Figure 3.12: Photograph showing the river bed sand condition

pography survey was performed using Differential Global positioning system (DGPS). The post processing was done to obtain the corrected elevation with respect to base station. The sand samples were collected for sieve analysis and the sand profile was observed by taking 3 feet deep sand profile over the sand bar. The sand profile was homogeneous with fine grain of d_{50} 0.02 mm diameter. In some portion vegetation growth was also observed during the field survey.

3.3.3 River flood-plain survey

The Brahmaputra river flood–plain survey was conducted to identify the different features during the monsoon season synchronized with microwave satellite pass to collect the signature and as the ground truth for the interpretation of microwave satellite images of different polarization and time period. The flood–plain survey was conducted at the downstream of Guwahati (Figure 3.14, Figure 3.15) during the survey different features were identified and geo–locations and field photographs were collected.

TH-1911_10610425



Source: Field Photograph **Name:** Mukalmua
Date: 24th December, 2010 **Location:** 26°15'43.74"N, 91°21'8.54"E

Figure 3.13: Photograph showing the river islands sands formations



Source: Field Photograph **Name:** Guwahati Airport
Date: 25th June, 2011 **Location:** 26° 7'39.95"N, 91°35'19.05"E

Figure 3.14: Photograph showing the flood plain near Airport



Source: Field Photograph **Name:** Narengi
Date: 25th June, 2011 **Location:** 26°12'57.60"N, 91°48'46.70"E

Figure 3.15: Photograph showing the flood plain near Narengi

3.4 Satellite Data

Satellite data of different sensors were collected to study the braider river dynamics of the Brahmaputra river. The advanced satellites such as SARAL/altika, Jason-2 and ENVISAT satellite data were used as altimetery data. Microwave satellite data such as RADARSAT-2 and RISAT-2 images of monsoon seasons were used in this study.

3.4.1 Satellite altimetry data

SARAL stands for SAtellite for ARgos and ALtiKa, it was launched on 25 February 2013. It is a joint-mission of CNES-ISRO to provide continuous monitoring of ocean and continental water surface. The SARAK/Altika is part of operational satellite altimetry mission with Jason–2 satellite. It was launched into a Sun synchronous polar orbit at an altitude of 790 km with 35 days of orbit repetition and 501 pass following same ground track as ENVISAT satellite. It has 98.55 deg of inclination with 80 km of equatorial cross track separation. It has Ka-band (35.75 GHz) radar altimeter with enhanced bandwidth (500 MHz). The primary objective of the SARAL/Altika mission to provide vital information to the oceanographic, climate and coastal research studies. The secondary objective of the mission to monitor the cryosphere and continental water bodies, such as river, wetland and reservoirs. Satellite altimetry missions started with major focus on monitoring the ocean

TH-1911_10610425

circulation, sea surface topography and ice sheet thickness. Advancement on altimetry missions have enabled the monitoring of continental waters. Jason-1 satellite was launched on December 2001 with the same orbit as Topex/Posidon (T/P) satellite with 10 day of orbit repetition. The major drawback of Jason-1 satellite was frequent loses of tracking over the land surfaces and lose of data even for the larger rivers (Santos et al. 2010). In combination of the T/P and Jason–1 satellite altimetry missions, Jason–2 was launched on 10th June 2008 with same orbit repetition and widely-spaced ground tracks (approximately 315 km near the equator). The tracking system was improved in Jason-2 satellite with on board Digital Elevation Model information. This made it possible to dynamically change the tracking window over steep slopes and undulating terrain, hence it enables the availability of waveform data over continental surface. The Jason–2 satellite orbits on the same ground-track as Jason–1 and the T/P satellite with 254 passes and 10-day repeat cycle. It has an inclination of 66.07 degree with satellite altitude (equatorial) of 1336 km from reference ellipsoid. The 20 Hz waveform data provides the measurements at interval of 350 m approximately. It has a repeat period of 10 days with 127 revolutions within a cycle. The HydroWeb data base, one of the sources for satellite altimetry dataset, provides time series over water levels of large rivers, lakes and wetlands around the world, derived from altimetry data from Topex/Poseidon, ERS–1 and ERS–2, Envisat, Jason–1 and GFO satellite missions. The dataset can be accessed through the LEGOS website (http://www.legos.obs-mip.fr/en/soa/hydrologie/hydroweb/). This dataset has a temporal resolution of 35 days, i.e. a measurement at the same location is available every 35 days. Crétaux et al. (2011) and Calmant et al. (2008) have described in detail about the satellites, atmospheric corrections, retracking algorithms and methodologies used to construct water level time series over rivers and lakes. For the Brahmaputra river, the ENVISAT derived water level time series for the period of year 2002 to 2008 was downloaded from (www.legos.obs-mip.fr/en/soa/hydrologie/hydroweb/). The River and Lake product obtained from the processing of ERS and ENVISAT data at De Montfort University, UK, on behalf of ESA (Berry (2006) and Calmant et al. (2008)).The data have a temporal resolution of 35 days, owing to the ERS and ENVISAT satellites having a 35-day repeat cycle. The ENVISAT derived water level time series for the period of year 2002 to 2010. Each data set contains date, water level height from the mean, latitude, longitude, and standard deviation. Note that the water level heights have been referenced to EGM96 geoid. There are six locations in the middle reach of the Brahmaputra where satellite altimetry data are available for the period of 2002-2010.

3.4.2 Microwave Satellite data

In case of monsoon season presence of clouds obstructs the optical satellite to map the ground conditions. Hence, during this period microwave remote sensing satellite data is used (C-band SAR), which can penetrate through clouds and sense the ground conditions. The water reflects most of the radar signal to the opposite direction, so it appears black in the image. The microwave satellite images of RADARSAT-2 and RISAT-1 satellites were used to classify different morphological features present within the river. RADARSAT-2 satellite was launched on 14th December 2007 for the Canadian Space Agency. It is a follow-on mission to RADARSAT-1, which, was terminated in April 2013. It has a sun-synchronous orbit with orbit altitude of 798 km. It has 6 p.m. ascending node and 6 a.m. descending node with 14.29 orbits per day. It has different data acquisition modes with multiple polarization (HH, HV, VV and VH). In this study, standard dual pole 25 m resolution data was used to classify the images. RISAT-1 is made by Indian space research organization (ISRO) and launched on 26th April 2012. It used C–band (5.35 Ghz) synthetic aperture radar to acquire images in different modes with multiple polarization. The satellite has orbit altitude of 536 km with orbital inclination of 97 degrees. It is a polar sun-synchronous orbit with 25 days of repetition. The medium resolution ScanSAR mode (MRS) acquired images of 25 m resolution were used to identify the different morphological features within the river.

3.4.3 Optical Satellite data

The optical and microwave images are utilized to identify the river flow channels within the Brahmaputra river. The optical images from landsat-7 and landsat-8 satellites are used in this study. Landsat-7 satellite was launched on 15 April, 1999 and Landsat-8 satellite was launched on 11 February 2013. The objectives of Landsat–7 and Landsat–8 satellites are to provide continuous images of earth surface for various earth sciences applications. The Landsat program is managed by the United States of Geological Survey (USGS) and data from Landsat series is distributed through Glovis (http://glovis.usgs.gov/) and Earth Explorer (http://earthexplorer.usgs.gov/) websites. The panchromatic band (0.5 – 0.68 um) data is used in this study to set up the virtual stations during the non-monsoon season. The optical remote sensing satellite data provides river morphological condition during the non-monsoon season, when the cloud cover is not the limitation to map the ground features.

TH-1911_10610425

3.5 *In-situ* data collection

The Brahmaputra river stage records at six different reaches, Dibrugarh, Nematighat, Tezpur, Guwahati, Goalpara and Dhubri were collected for the period of year 2000 to 2015 from Inland Water Authority of India. The 10 daily discharge and sediment flux data were obtained for the period of year 2000 to 2010 for the Guwahati and Tezpur gauge site from Central Water Commission of India. The river cross sections of 58 locations at 10 km interval from Dibrugarh to Dhubri was collected from the Brahmaputra Board, Water Resources Ministry.

3.6 Conclusions

To study the dynamics of the Brahmaputra river all the necessary data was collected from different sources to address such a difficult problem. The available data in time and space were collected for the middle reach of the Brahmaputra river. The satellite data has capability to observe surface characteristics in the large scale and time series of such data reveal the large scale changes with change in time. Historical *in-situ* records area also at–most important to validate the hypothesis, have more than 15 years of in situ record of water level were collected at 6 different locations of the Brahmaputra river. The various parameters such as discharge, sediment flux, rainfall were also collected for minimum period of a decade for this study. Field campaigns have also provided insight in–to the complex problem undertaken. Hence field samples and ground truth have provided much evidence to the support of this research work.

TH-1911_10610425

TH-1911_10610425

"Nature holds the key to our aesthetic, intellectual, cognitive and even spiritual satisfaction."

Edward Osborne Wilson (1929)
American biologist

4

IMPROVEMENT IN SATELLITE ALTIMETRY DATA PROCESSING

4.1 Introduction

River stage monitoring is a fundamental observation in the watershed hydrology to understand the spatio-temporal response of the river basin in terms of stage hydrograph. It is a very crucial parameter for calibration and validation of the surface hydrological models, which performs the runoff estimation over the river basins. River stage measurements are also used to broadcast the flood forecast for the downstream regions of the river. Traditionally these measurements are carried out over the nodal locations of the river, which do not have the large width of flow as compared to the floodplains of the river. River stage variations over the floodplains provide the vital information about the flood wave distribution and energy dissipation to the downstream of the nodal reaches. Satellite altimetry has an advantage of measuring river level fluctuations over the sites, where installation and monitoring of traditional river gauge stations are not possible. Utilizing satellite altimetry for monitoring river stage fluctuations can play a vital role in enhancing our ability to monitor the cycle of surface water from the regional scale to the global scale (Berry, 2006). Although satellite altimetry suffered from many drawbacks such as non-availability of retracking algorithms specialized for inland waters, discrepancies between satellite and *in–situ* measurements, lower temporal resolution, missing data, but recent advancements in altimetry and methods for waveform data processing have helped to develop various datasets facilitating the study of inland waters effectively and efficiently (Frappart et al., 2005; Calmant and Seyler, 2006; Calmant et al., 2008). A radar altimeter is an active microwave instrument,

TH-1911_10610425

which principally works by transmitting a short microwave pulse in the nadir direction. It transmits signals at high frequencies (1800 Hz, Jason-2) towards the Earth surface and record the reflected echo in the range window. The range is estimated by two-way travel time taken by the pulse between satellite and target. The river elevations are calculated by taking the difference between satellite orbit altitude from a reference datum and range estimated by the altimeter. The precise orbit determination is done with the navigation devices like Doppler Orbitography and Radio-positioning Integrated by Satellite (DORIS) and global positioning system (GPS) receiver with reference to the world geodetic system (WGS 84). In the Braided river system, presence of sand bars/islands and varying river flow width frequently contaminate the altimeter footprint. Altimeter footprint contamination is caused due to undulating terrain present within the river. It produces the complex waveforms with multiple peaks, which are difficult to be retracked. Hence, many methodologies have been developed for selection of waveform over inland water bodies, i.e. defining the virtual station (Berry et al., 2005; Leon et al., 2006; Kouraev et al., 2004; Zakharova et al., 2006; Roux et al., 2010). In many of the research studies over large rivers, virtual stations are defined using the satellite information of river flow characteristics. (Kouraev et al., 2004), considered only the main channel for data selection due to presence of multiple channels with vast flood plain which caused noise in satellite time series of water level and created quit different hydrologic regime that differ from main channel of the Ob' river. (Zakharova et al., 2006) have used radar images from JERS satellite to define virtual stations over the intersection of satellite track and the river. They have extracted the dataset over the defined virtual station over the main channel of the river to minimize the contamination from the surroundings such as islands and vegetation. Since, braided rivers change their flow frequently with multiple channels splitting and rejoining creating a challenging task to define the virtual stations over the river. However, a proper investigation is needed to devise a suitable methodology to define the virtual stations before applying any retracking algorithms to waveform data. Therefore, in this study, an effort has been made to develop a methodology to select the data points over a virtual station in the braided rivers such as Brahmaputra river and retrieve the water levels. The improved methodology has focused on the selection of the waveforms over the dynamic braided river network and to retrieve the water level at different morphological conditions of the Brahmaputra river.

4.2 Satellite Altimetry Missions

Satellite altimetry missions were started with major focus on monitoring the ocean circulation, sea surface topography and ice sheet dynamics over the Polar Regions. Apart from the traditional application of satellite altimetry in oceanography studies, it was also used

TH-1911_10610425

to monitor the continental waters. Topex/Poseidon's satellite was launched in the orbit of 1336 km on 10 August 1992 with orbit period of 10 days. Topex/Poseidon main objective was to measure the sea surface height; it was also used to retrieve the water level fluctuations in the large rivers around the world. It was a joint mission between NASA, the US space agency, and CNES the French space agency. Topex/Poseidon was shifted to new orbit on 15 September 2002. ESA, the European Space Agency, sent the ENVISAT as follow on mission after ERS–1 and ERS–2. It carries the dual altimeter (RA2) of S (3.2 GHz) and Ku (13.6 GHz) band. Its orbit period was 35 days and 501 orbits per cycle with finer ground track spacing (90 kilometers at the equator). On October 22, 2010 it was shifted to new orbit with 30 days and 431 orbits per cycle. Jason–1 satellite was launched on December 2001 with the same orbit of T/P satellite with 10 day of orbit repetition. The major drawback of Jason 1 satellite was frequent loses of tracking over the land surfaces and lose of data even for the larger rivers (Da Silva et al., 2010). In continuation of the T/P and Jason–1 satellite altimetry missions Jason–2 was launched on 10th June 2008 with same orbit repetition and widely-spaced ground tracks (315 kilometers at the equator). The tracking system was improved in Jason 2 satellite with on board Digital Elevation Model information. This made it possible to dynamically change the tracking window over steep slopes and undulating terrain, hence made the availability of waveform data over continental surfaces. ENVISAT satellite was launched on 1st March 2002 into a Sun synchronous polar orbit at an altitude of 790 km with 35 day of orbit repetition. In continuation of the ENVISAT satellite altimetry missions SARAL/Altika was launched on 23rd February 2013 with same orbit repetition with densely spaced ground tracks (175 km at the equator). Use of DORIS on board navigator 'DIODE' gives the altitude of the satellite with respect to the geoid with an accuracy of 10 cm. DEM information stored in Altika for better onboard tracking and to keep lock on inland water bodies. Open loop tracking and acquisition with advanced DIODE/DEM mode in Altika made it possible to track more number of waveforms. SARAL/AltiKa is a new mission with Ka band altimeter with 35.7 GHz frequency, previously all altimeters were launched with Ku band (13.6 GHz) frequency coupled with S or C band for correcting ionosphere delay. The higher bandwidth of 500 MHz at Ka band provides shorter pulse duration; hence increase the vertical range resolution (0.3 m) as well as spatial resolution. The advantage of Ka band is that it reduces footprint as compared to Ku band altimeters. The decrease in time decorrelation between successive echoes has increased the pulse repetition frequency to 4000 Hz as compared to 2000 Hz with Ku band altimeters. The limitation of higher frequency is that attenuation, due to rainfall is higher as the rainfall intensity becomes more than 2 mm/hr.

4.3 Methodology for water level retrieval

Over the rivers altimeter gets very complex and multi-peaked waveforms due to complex terrain and rapidly varying slopes. Given the fact that the radar altimeter footprint varies in terms of few squares of kilometer, presence of vegetation and sand bars (Figure 4.1) in a braided river system distort the return power of the waveform. The return power from the water surface remains higher as compared to the other surface features present within the footprint of the altimeter due to its dielectric property and surface characteristics. Step-wise procedure has been described in the flow chart (Figure 4.2) to generate the reliable time series of river stage variations, different filtering procedures have been adopted to exclude the noisy waveform affected by the presence of vegetation and sand bars/islands. In order to minimize potential contamination of Jason–2 signal by land reflections and at the same time to retain sufficiently large number of altimeter measurements on the water surface. The Landsat-7 and Landsat-8 panchromatic images of 15 m pixel resolution, downloaded from the Earth Explorer portal was used to select the satellite track and river intersections during the lean flow. Since, the river width in this reach changes from 1.7 to 18 km depending on the phase of the hydrologic regime. Microwave images of RADARSAT–2 satellite with 25 m pixel resolution were used during the monsoon season to identify the main channel location within the river. The virtual stations were set-up around the main channel of the river with two domains (inner and outer). The initial information of these domains was given from the satellite images of non-monsoon and monsoon periods (Figure 4.3). Once the retracking process initiated over a virtual station the subsequent position of the virtual station for the next cycle of altimeter pass, defined using the backscattering coefficients calculated from previous cycle. The outer domain with 4.5 km length and 3.5 km width was selected to extract the waveform data for further processing. Then the inner domain with 3.15 km in length and 1.75 km width was setup as a dynamic window, which could move within the outer domain over the main channel of the river. The Center point of the altimeter footprint within the inner domain was considered as a seed point. As the braided rivers change their course regularly, the main channel may also shift within the river. To keep track of main channel the backscattering coefficients were calculated for the inner domain and seed point was moved corresponding to higher backscattering coefficient within the outer domain. Finally, a set of waveforms within the inner domain was selected to retrack the water level information. The final water level was selected based on the highest backscattering coefficient within the inner domain. The standard deviations were calculated from the retrieved water level of inner domain for different satellite tracks (Figure 4.3).

TH-1911_10610425

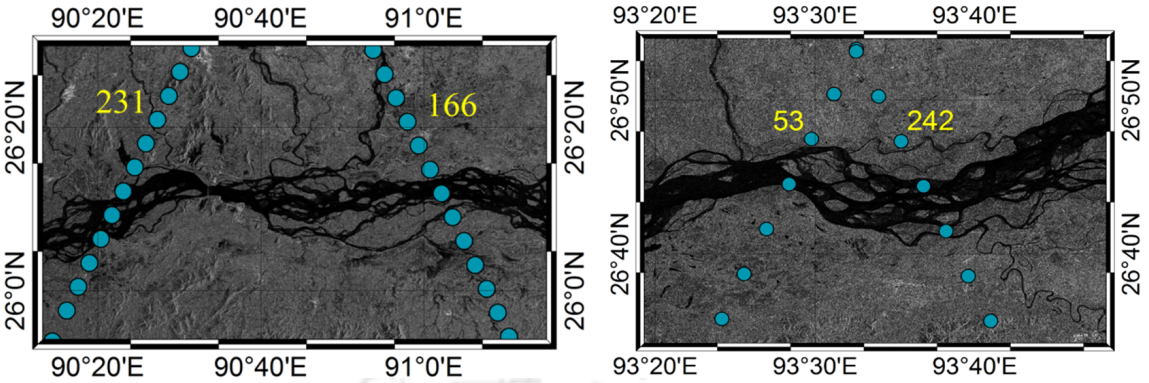

Figure 4.1: Microwave images overlaid with Jason 2 satellite tracks crossing over the Brahmaputra River.

4.3.1 Range and Geophysical Corrections

Presence of dry gases and water vapor in the troposphere and free electrons in the ionosphere reduce the velocity of microwave pulses in the atmosphere. Microwave pulse is attenuated by the oxygen and water vapor molecules, since the droplets are much smaller than Ku and C band microwave wavelength (Ku 2 cm and C 6 cm). Attenuation in these wavelengths by cloud liquid water is governed by Rayleigh scattering. Microwave wavelengths are much sensitive to precipitation rather than dry gases, water vapor and clouds (Chelton et al., 2001). The water level elevations are determined by the satellite orbit altitude, Alt and the altimeter range, R measurement. Prior to obtaining the water surface elevation, atmospheric and geophysical corrections are applied on retracked range values. The various corrections are applied to account the time delay of microwave pulses such as dry tropospheric correction, wet tropospheric correction, ionospheric correction and correction for pole and solid tidal effects on the Earth (Chelton et al., 2001). The dry and wet tropospheric corrections were provided by the European Center for Medium Range Weather Forecasting (ECWMRF). Whereas the earth tide was calculated using (Cartwright and Edden, 1973) tables and pole tide was calculated based on deformation of the Earth induced by polar motion as described by (Wahr, 1985). Finally, orthometric height H is obtained by subtracting mean sea level from elevation values with reference to ellipsoid (Equation 4.1).

$$H = Alt - R - [D_{tc} + W_{tc} + I_{onc} + S_{tc} + P_{tc}] - MSS_{ht} \tag{4.1}$$

Where, H is the corrected orthometric height, Alt is the satellite altitude from reference ellipsoid, R is the satellite range, D_{tc} is the Dry Tropospheric correction, W_{tc} the Wet tro-

TH-1911_10610425

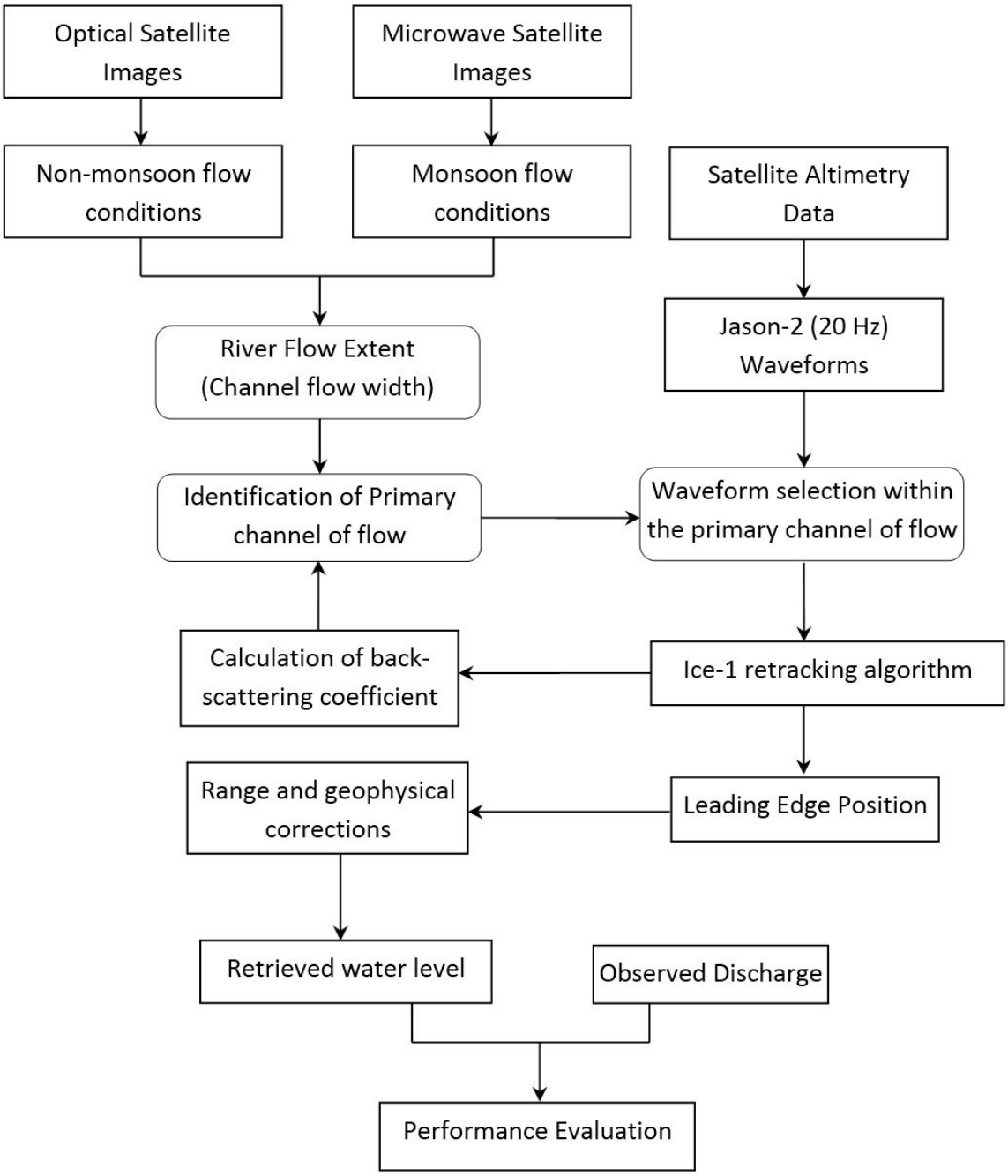

Figure 4.2: Flow-chart showing the methodology adopted for the retrieval of water level time series for braided reaches of the Brahmaputra river.

pospheric correction, I_{onc} the Ionospheric correction, S_{tc} the solid earth tide and P_{tc} the pole tide correction and MSS_{ht} is the mean sea surface height from the reference ellipsoid. The elevation values are obtained by the equation 4.1, H is considered with respect to the mean sea surface. The wet troposphere correction varies from 0.20 m to 0.43 m and the dry troposphere correction ranges from 2.26 m to 2.275 m for the study area.

4.3.2 Troposphere correction (Dry and Wet)

The microwave pulses are slowed by the dry gases present in the atmosphere. It contributes the largest values of correction as compared to others. The delay causes by the dry gases could be as large as -2.3 m. The air density is closely related to the pressure; hence the approximated dry troposphere correction is calculated by pressure at sea level, where refractivity constant is 0.2277 cm^3/g (Vignudelli et al., 2011). The water vapor and cloud liquid water droplet in troposphere cause the delay of microwave pulses. The water vapor is dynamic variable in the troposphere and it can make error in range estimation of -6 cm to -40 cm. The on–board satellite downward looking microwave channels with the brightness temperatures in the nadir path at 18.7, 23.8 and 34.0 GHz can be used to measure the water vapor. Both the dry and wet troposphere corrections can also be generated with the ground based observations assimilated into gridded model like European Centre for Medium-Range Weather Forecasts (ECMWF) and U.S. National Centers for Environmental Predictions (NCEP).

4.3.3 Ionosphere correction

Presence of free electrons in the earth's ionosphere reduces the propagation velocity of microwave pulses. The density and amount of free electrons in the ionosphere is known as total electron content (TEC) and it may up to 1016 electrons/m^2. Hence, total delay is calculated from the presence of electrons per unit area in a vertical column between earth and the altimeter. The time delay between two frequencies is used to calculate the ionospheric correction by dual frequency microwave channels present in on–board satellite. The GPS derived ionosphere maps (GIM) generated by Jet Propulsion Laboratory and University of Berne on 6 hourly basis can be used to interpolate TEC values for the altimeter ground track.

TH-1911_10610425

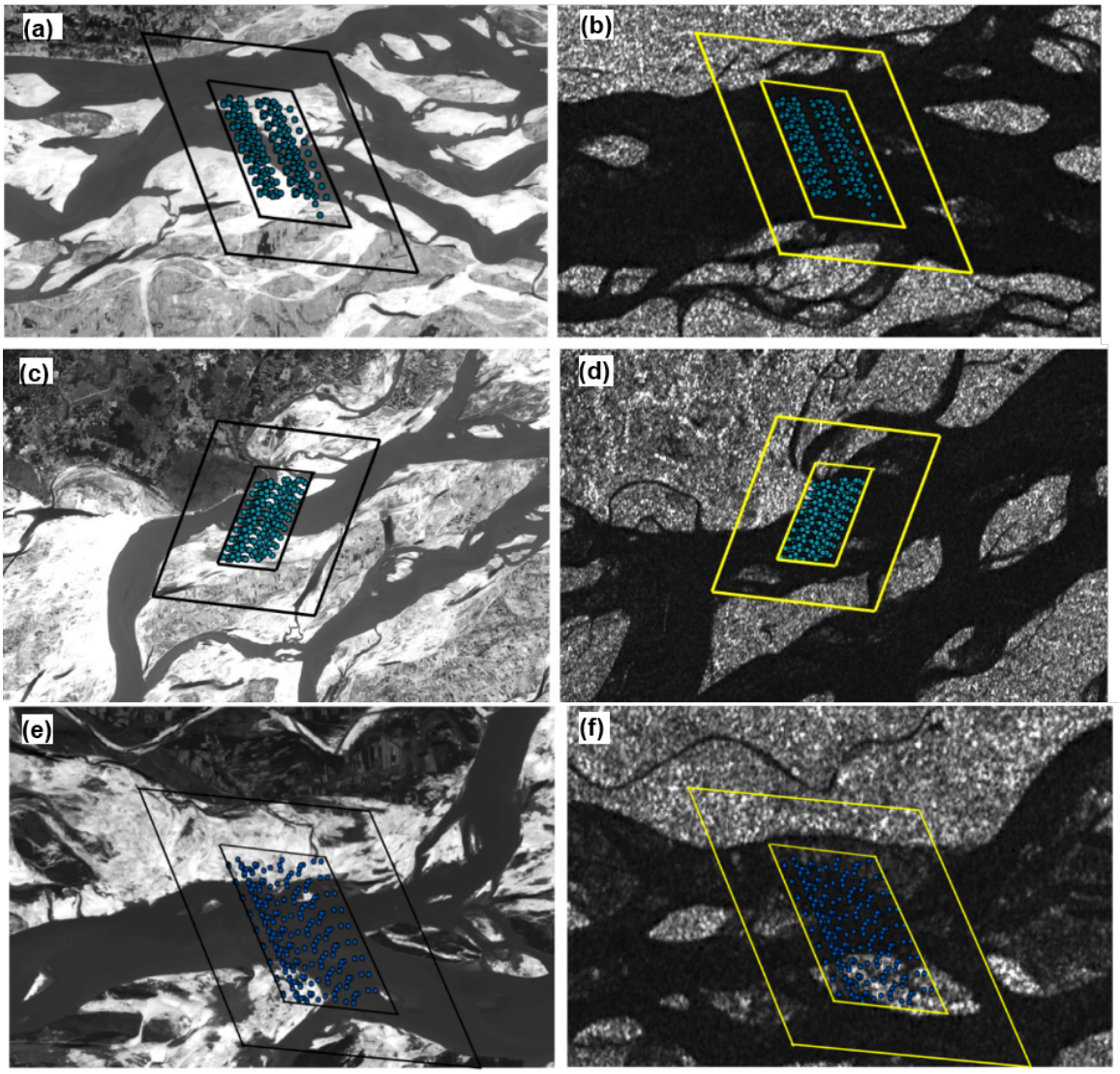

Figure 4.3: Optical and microwave images showing the location of virtual station for non-monsoon (February) andmonsoon (July) seasons for the satellite track 53 (a-b), 166 (c-d) and 242 (e-f), respectively over different reaches of the Brahmaputra river.

4.3.4 Solid earth and Pole Tides Correction

The external gravitational forces from Sun and Moon cause ocean like tide on solid earth. The response of earth surface to these external forces cause the solid earth tide. This correction is determined from the proportionality constants, which is called Love numbers (Cartwright and Tayler, 1971). Earth's rotational axis creates the centrifugal potential due to small perturbations in it. In the response of this centrifugal potential solid Earth and ocean causes the tide like motion in the ocean that is called pole tide (Wahr, 1985).

4.4 Waveform retracking

Waveform retracking is the post-processing procedure to correct the estimated range by on–board tracker. The on–board tracker has the initial information of satellite orbit to target range, where it built the tracking window to record the return echo (power). Hence, different retracking algorithms have been developed to estimate the offset between the tracker range and the leading edge of the waveform to the corresponding target. In this study different retracking algorithm are used to find out the best retracking technique for the Braided Brahmaputra river.

There are the following algorithms were used to retrieve water level

1. The Off Centre of Gravity retracker (Ice-1)
2. Ice-2 retracker
3. β-parameter retracker
4. Threshold retracker

4.4.1 The Off Centre of Gravity (OCOG) retracker (ICE-1)

The aim of this retracking algorithm is to calculate the center of gravity (COG) of each waveform (Figure 4.4). Estimation of leading edge of the waveform is done by subtracting the half width of the waveform from the centre of gravity point (Wingham et al., 1986). The advantage of this algorithm is that if the return power of leading and trailing edge is in the analysis window, it can compute the midpoint of the leading edge for every waveform. The amplitude, COG and width of COG are given by equation 4.3, equation 4.4 and equation 4.2, respectively.

TH-1911_10610425

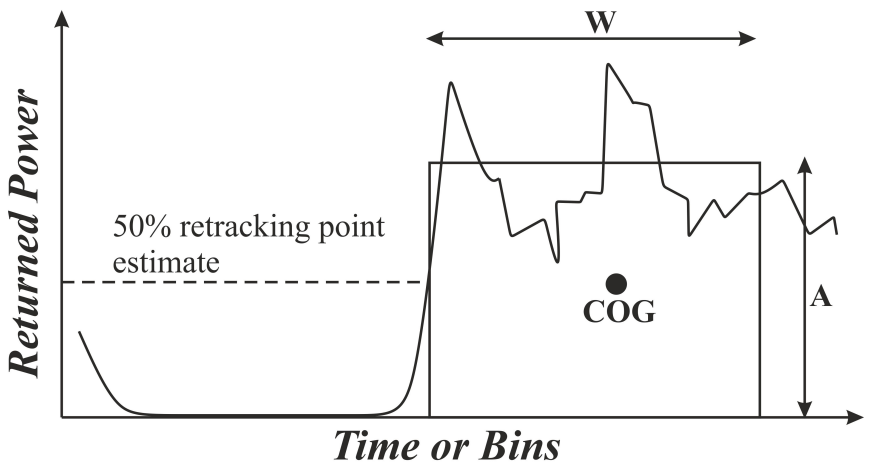

Figure 4.4: The Off Centre of Gravity waveform retracker.

$$COG = \sum_{i-1+n_a}^{104-n_a} ip^2(i) / \sum_{i=1+n_a}^{104-n_a} p^2(i) \tag{4.2}$$

$$A = \sqrt{\sum_{i-1+n_a}^{104-n_a} p^4(i) / \sum_{i=1+n_a}^{104-n_a} p^2(i)} \tag{4.3}$$

$$W = \left(\sum_{i-1+n_a}^{104-n_a} p^4(i) \right)^2 / \sum_{i=1+n_a}^{104-n_a} p^4(i) \tag{4.4}$$

Where *P(i)* is the waveform sample value at the ith bin, and na is the number of aliased sample (Lee, 2008). The mid-point Leading Edge Position (LEP) is given by:

$$LEP = COG - \frac{W}{2} \tag{4.5}$$

This algorithm is simple and robust to implement due to statistical in nature. It is sensitive to the waveform shape as it considers all the points in it and only treat it mathematically, hence it should be used cautiously.

4.4.2 Ice-2 retracking

The Ice-2 retracking algorithm was developed to retrack the altimeter waveforms over the non-ocean surfaces, primarily for the ice cap studies. The Ice-2 algorithm was used in ENVISAT RA-2 altimeter to retrack the waveforms. It detects the leading edge position, amplitude, slope of the trailing edge by fitting an error and exponential decay function (Legresy and Remy, 1997).

$$Vm\left(t\right)=\frac{P_u}{2}\left[1+erf\left(\frac{t-\tau}{\sigma_L}\right)\right]\exp\left[S_T\left(t-\tau\right)\right]+P_n \tag{4.6}$$

Where, the parameters to be estimated are:

- τ : the epoch
- σ_L : the width of the leading edge
- P_u : the amplitude
- S_T : the slope of the logarithm of the trailing edge
- P_n : the thermal noise level (to be removed from the waveform samples)

4.4.3 Beta-Parameter retracking

This algorithm is developed by the (Martin et al., 1983); they first used this method to retrack all SEASAT radar waveforms to estimate the surface elevations. This algorithm can be used for single or double-ramped waveforms with 5 or 9 parameters function respectively. In this study 5 parameter retracker is used to fit the specular reflection of waveforms from the water surface (Figure 4.5). Basically with 5 parameters fitting is done over the waveform to retrieve the geophysical parameters from the fitted function using equations 4.7, 4.8 and 4.9.

$$y\left(t\right)=\beta_1+\beta_2\exp\left(-\beta_5 Q_i\right)P\left(\frac{t-\beta_{3i}}{\beta_{4i}}\right) \tag{4.7}$$

$$Q_i=\begin{cases}0,\ t<\beta_3-2\beta_4\\ t-\left(\beta_3+0.5\beta_4\right),\ t\geq\beta_3-2\beta_4\end{cases} \tag{4.8}$$

TH-1911_10610425

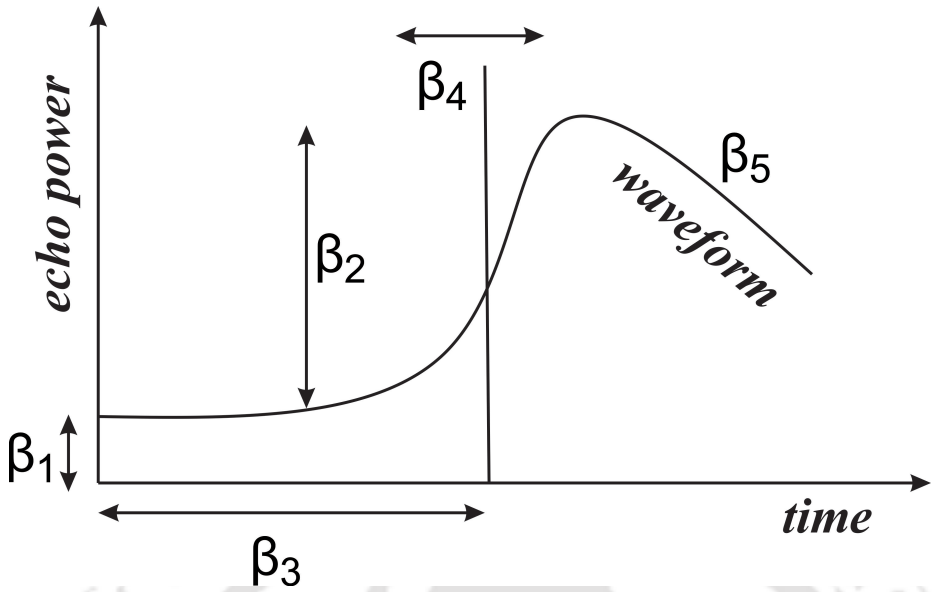

Figure 4.5: The waveform retracking from the NASA 5 β parameter retracking

$$P(x) = \int_{-\infty}^{x} \frac{1}{\sqrt{2\pi}} \exp\left(\frac{-q}{2}\right) dq \tag{4.9}$$

Where, n is taken 1 for single ramp waveform in Equation 4.7. The 5 unknown parameters are as follows:

- β_1: The thermal noise level of the return waveform
- β_2: Return signal amplitude
- β_3: The mid-point on the leading edge of the waveform.
- β_4: The return waveform rise time
- β_5: The slope of the trailing edge

4.4.4 Threshold retracker (Sea Ice retracker)

An improved threshold retracking method was developed by ESA and used it in ERS satellite mission (Davis, 1995). In this method the leading edge position is determined by identifying the gate value exceeding the threshold amplitude (Figure 4.6). The amplitude value is determined using OCOG (Ice-1) retracker in improved threshold method (Bamber, 1994) or the maximum return power of waveform (Davis, 1997). To exclude the thermal noise (DC bias) on the maximum amplitude the first three bins are averaged. The DC bias may

TH-1911_10610425

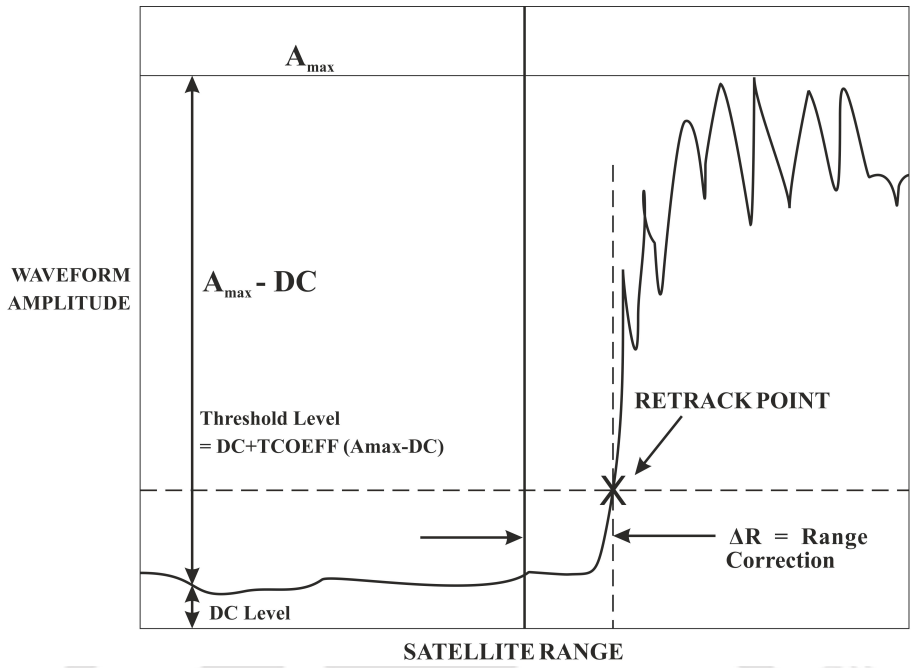

Figure 4.6: Waveform threshold retracker

have different value for the two satellites. Different threshold value can be taken to see the performance of this retracker. Here, 50% threshold to identify the leading edge position, which is dominated by surface scattering (Davis, 1997). The following equations 4.10, 4.11 and 4.12 are used to estimate the mid point of the leading edge position.

$$A_{\max} = \max\left(P\left(i\right)\right) \tag{4.10}$$

$$DC = \frac{1}{3}\sum_{i=5}^{7}\left(p\left(i\right)\right) \tag{4.11}$$

$$TL = DC + T_{coff}\left(A_{\max} - DC\right) \tag{4.12}$$

Where,

A_{max}: Maximum waveform amplitude

DC: Thermal noise or DC level

$T_(coeff)$: Threshold

T_L: Retracked gate

Each retracking algorithm has its own limitation; Ice-1 is simple retracking algorithms, which mathematically form a rectangle whose area equals the total area under the waveform. Then it uses the centre of gravity of the rectangle to compute the leading edge of the waveform. Whereas, the Ice-2 algorithm utilize the fitting functions to derive different retracking parameters, such as the epoch, width of the leading edge, the slope of the trailing edge and the thermal noise. The least square method is used to minimize the error between the actual waveform and the fitting function, which utilize the error and exponential decay function. The threshold method is also a simple and robust method to retrack the complex waveforms over the inland water bodies, it uses the percentage of maximum power as a threshold value, the retrack gate or bin is defined when the return power reach the threshold level. The threshold percentage is usually taken 50 (Davis, 1997) for the inland water surface waveforms. The β parameter algorithm is relatively complex as compared to others retracking algorithms, It tries to use the fitting functions to derive the retracking parameters. It uses the five β parameters to fit the function, after the error minimization using least square method, the coefficients provide information such as β_1 thermal noise, β_2 the waveform amplitude, β_3 the mid-point of the leading edge, β_4 waveform rise time and β_5 the slope of the trailing edge. The advantage of the β parameter algorithm is that it applies exponential decay to fit the trailing edge, which is typical to the waveforms present within the river.

4.5 Results and Discussion

The water level retrieval was done using waveform retracking for the Jason–2 and SARAL/Altika satellite data. The different retacking algorithms were used to retrieve water level at different reaches of the braided Brahmaputra river. The new methodology proposed in this study performed well over the braided reaches of the river. The nested window approach was adopted in this study to select the waveforms over the main channel of the river. Further, waveform classification and radar backscattering coefficient was analyzed to exclude the noisy waveforms present in the study area. With the help of improved methodology water levels retrieval could be done with more accurately

4.5.1 Waveform variation and classification over the Brahmaputra river

Waveform classification was done using k-means clustering technique to eliminate the noisy waveforms over the Brahmaputra river. Waveforms were classified in to 6 different groups, which represent the heterogeneity present between them due to altimeter echo contamina-

TH-1911_10610425

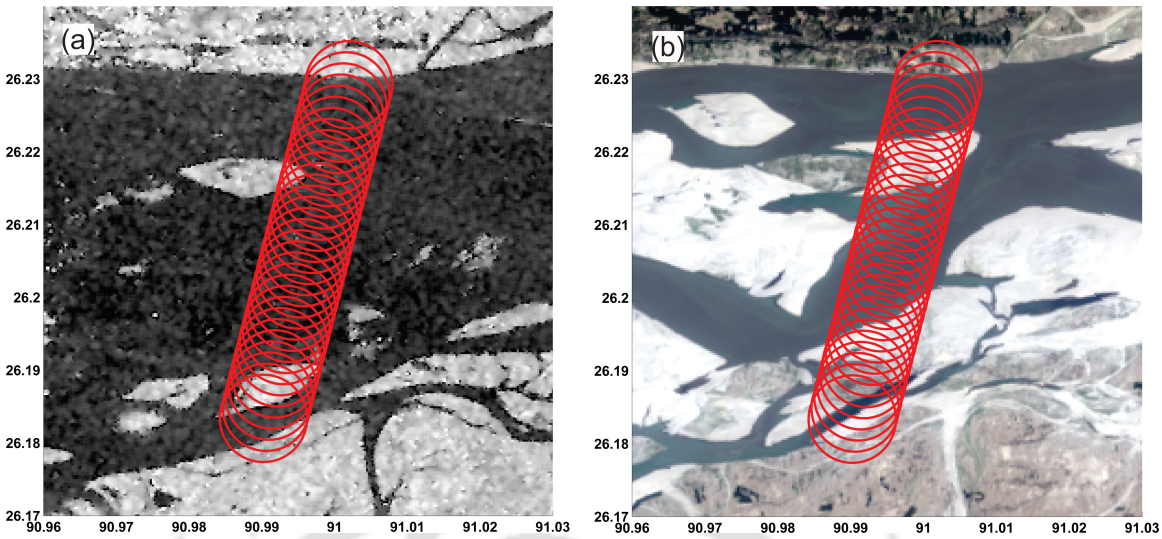

Figure 4.7: Footrpint of Saral/Altika over the Brahmaputra river for Non-mosoon (12/04/2013) and Monsoon period (18/07/2013) for the track 438.

tion. The altimeter footprint crossing the Brahmaputra river is shown for the monsoon and non-monsoon periods in Figure 4.7, which clearly indicate echo contamination because of different features present within the river. The heterogeneity present within the altimeter footprint reflect the mix response of backscattered energy, which was recorded by the satellite sensor. Hence, multi–peak waveforms are quite evident during the lean flow period (Figure 4.8 and Figure 4.9). During the monsoon season the return echo has less contamination, due to large river flow width (Figure 4.11). Figure 4.10 shows the single peak waveforms, which represent the signature of water surface dominance within the altimeter footprint. The use of Ka band SARAL/Altika has reduced altimeter footprint size of 1.39 km diameter as compared to Jason-2 (2.39 km diameter). The reduction of footprint size has also increased the accuracy of altimeter to precisely measure the water level fluctuations over the braided river system, such as the Brahmaputra river.

4.5.2 Seasonal variation of Backscattering Coefficient

Backscattering coefficient represents the physical characteristics of scattering surface present within the altimeter footprint. The effects of river level variations in the backscattering coefficients were investigated. It was found that backscattering coefficients were distinctly different from non-monsoon to monsoon period for all the altimeter tracks used in this study (Figure 4.12). Figure 4.13 indicates the along track variation of backscattering coefficients over the main channel width of the river. The mean backscatter coefficient, σ^0 was 48 dB during monsoon, which decreases to 35 dB during non-monsoon period. Higher values

TH-1911_10610425

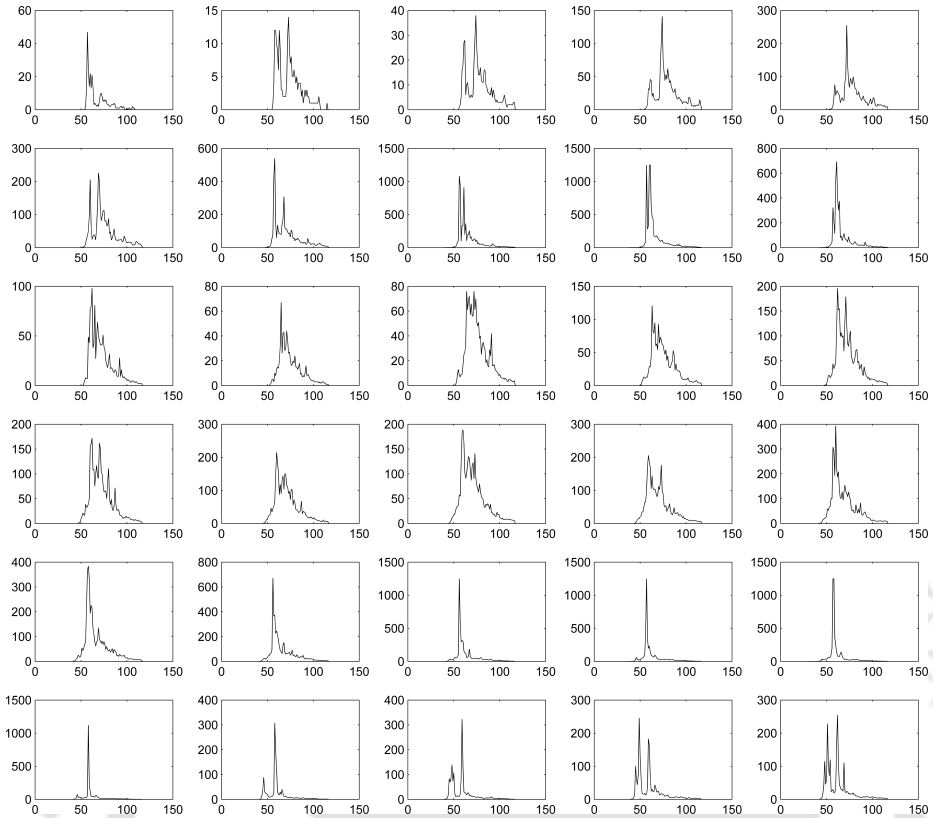

Figure 4.8: (a) Waveform variation over the Brahmaputra river for the track 438 for non–monsoon season (03/05/2013).

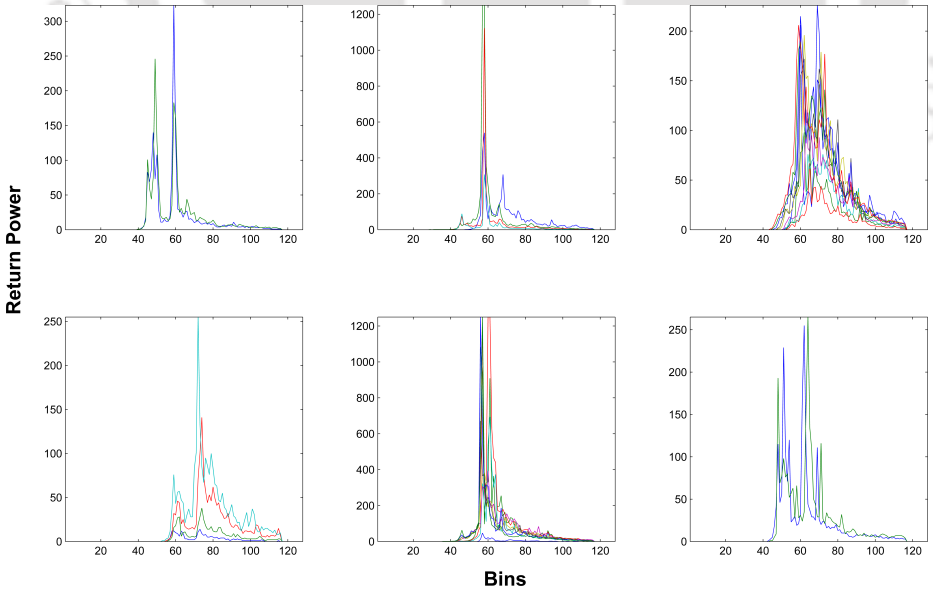

Figure 4.9: (b) Waveform classification over the Brahmaputra river for the track 438 for non–monsoon season (03/05/2013).

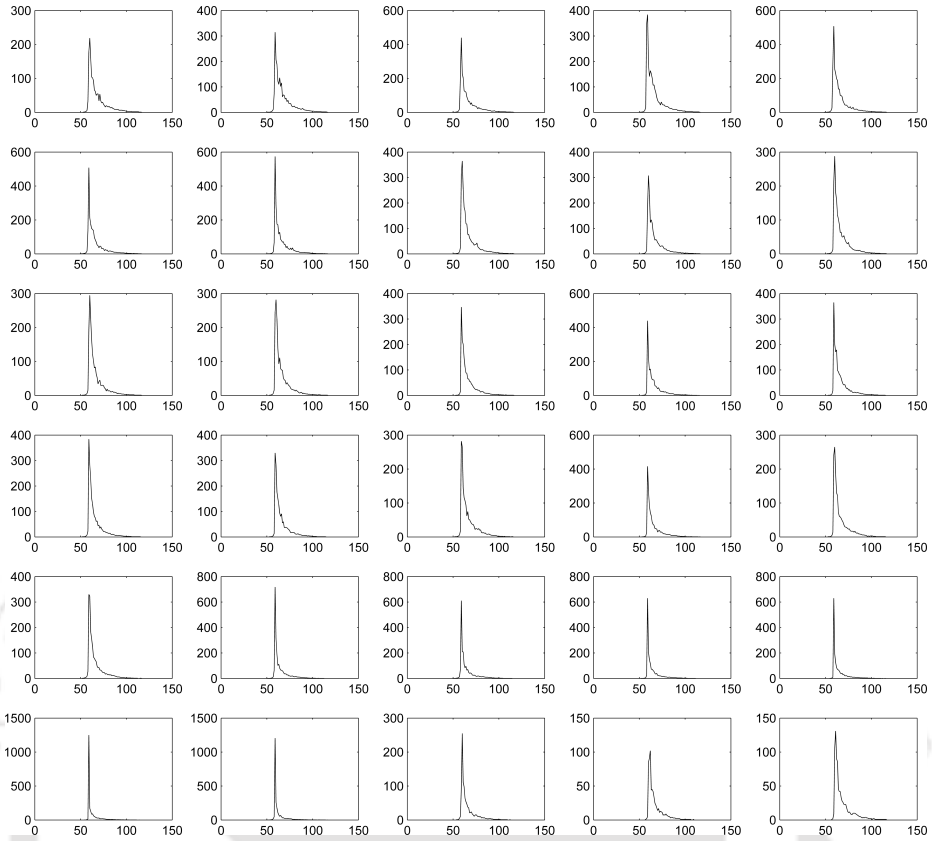

Figure 4.10: (a) Waveform variation over the Brahmaputra river for the track 438 for the monsoon season (12/07/2013).

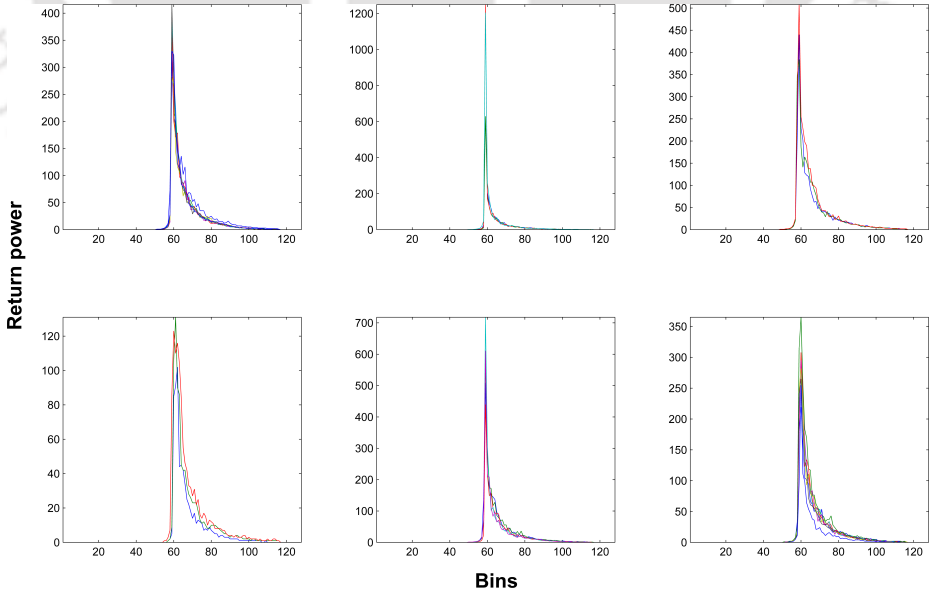

Figure 4.11: (b) Waveform classification over the Brahmaputra river for the track 438 for the monsoon season (12/07/2013).

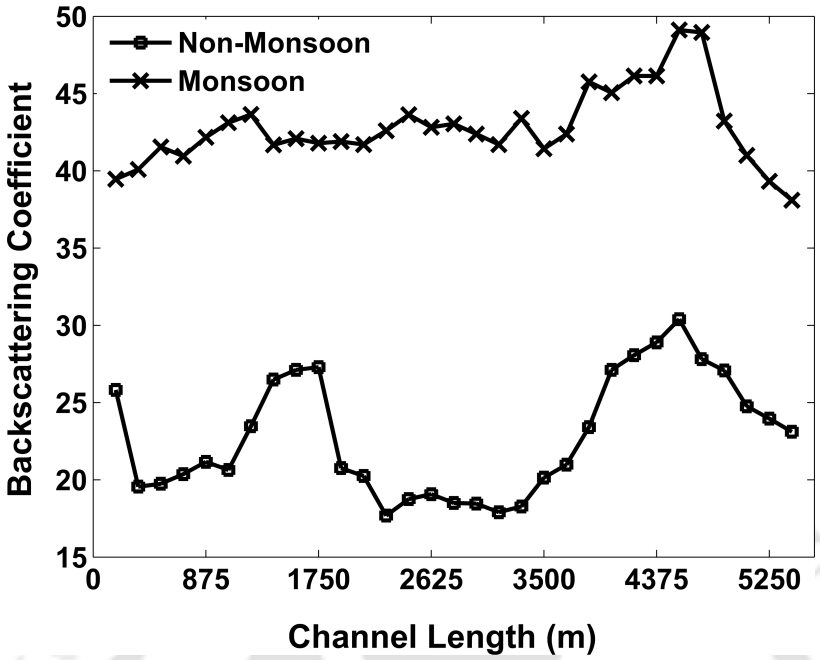

Figure 4.12: Variation in SARAL/Altika altimeter Backscattering coefficient passing over the Brahmaputra river at 438 track.

of backscatter coefficient coincide with rise in water level as well as the river flow extent. The seasonal variability in backscatter coefficient indicates the morphological dynamics of braided river.

4.5.3 Improvement in water level retrieval

To evaluate the performance of retrieved water level over braided rivers, correlation analysis was done between retrieved water levels using proposed methodology and the global Hydroweb dataset available for the Brahmaputra river. The retrieved water levels from the proposed methodology using Jason-2 data and from Hydroweb were compared with the in situ river stage records. It was found that proposed methodology has statistically (R^2, RMSE and Nash-Scutliffe coefficient) improved the retrieved water level accuracy as compared to Hydroweb dataset for the braided Brahmaputra river for all the satellite tracks used in this study (Figure 4.14). The most statistically significant result was found for the track 231, in which new methodology has retrieved water level with accuracy of 0.56 m RMSE and R^2=0.92. Hydroweb data–set for the same track could not capture the water level variations and perform poorly with 1.07 m RMSE and R^2=0.07. The significant disparity for the track number 231 was due to braiding pattern with presence of multiple channels which caused the poor results from the method adopted by Hydroweb product

TH-1911_10610425

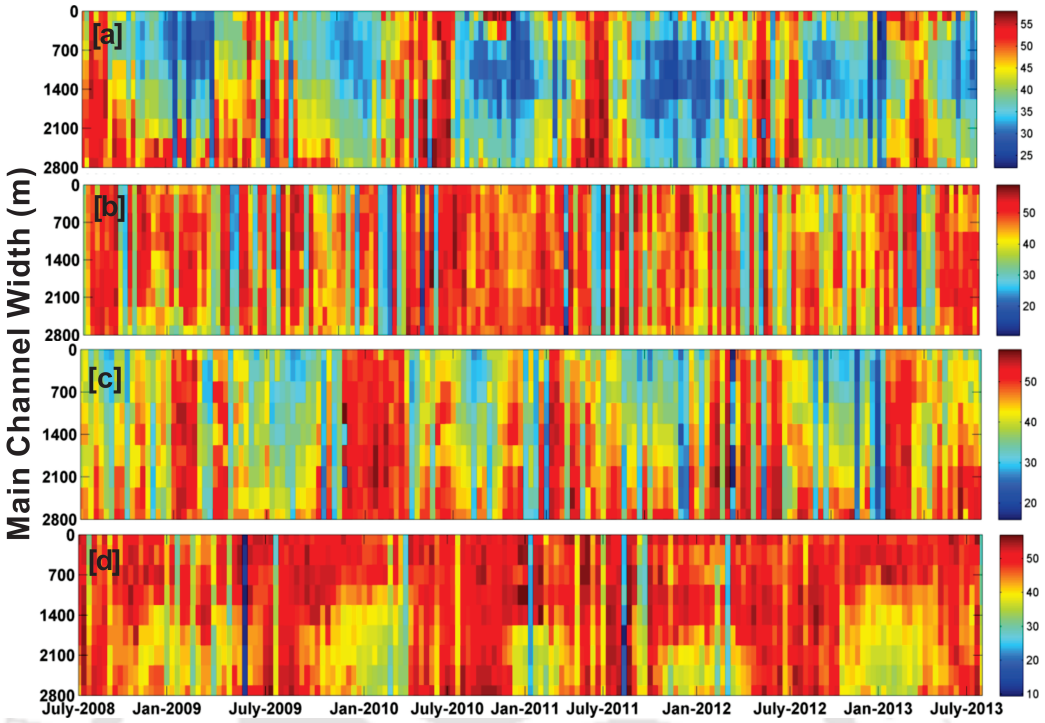

Figure 4.13: Along track backscattering coefficient variations at different locations (a) 53, (b) 166, (c) 231 and (d) 242 over the Brahmaputra River.

generation. The accuracy of water level retrieved from new methodology has shown good performance (0.50–0.56 m) as compared to Hydroweb data-set (0.55–1.07 m). Hence, proposed methodology has an advantage to identify the main channel and to retrieve the accurate water levels in the braided river systems as compared to other methods. The accuracy of retrieved water levels was within the range of 50 to 56 cm in terms of root mean square error, which is quite consistent and may be acceptable for this kind of rivers. The accuracy of Hydroweb product was varying from 55 to 107 cm, indicating the difficulties in water level retrieval over braided reaches of the Brahmaputra river.

4.6 Conclusions

Water level retrieval over the braided river reaches is a difficult task due to frequent channel migration and sand bar formation. The morphological dynamics in this type of river causes the noise in altimeter return signal. The altimetry return signal make noisy waveforms due to presence of sand bars and vegetation within its footprint. To overcome these challenges a proper methodology needs to be adopted to filter out these noisy waveforms due to change in river morphology. Hence, an dynamic window selection techniques is

TH-1911_10610425

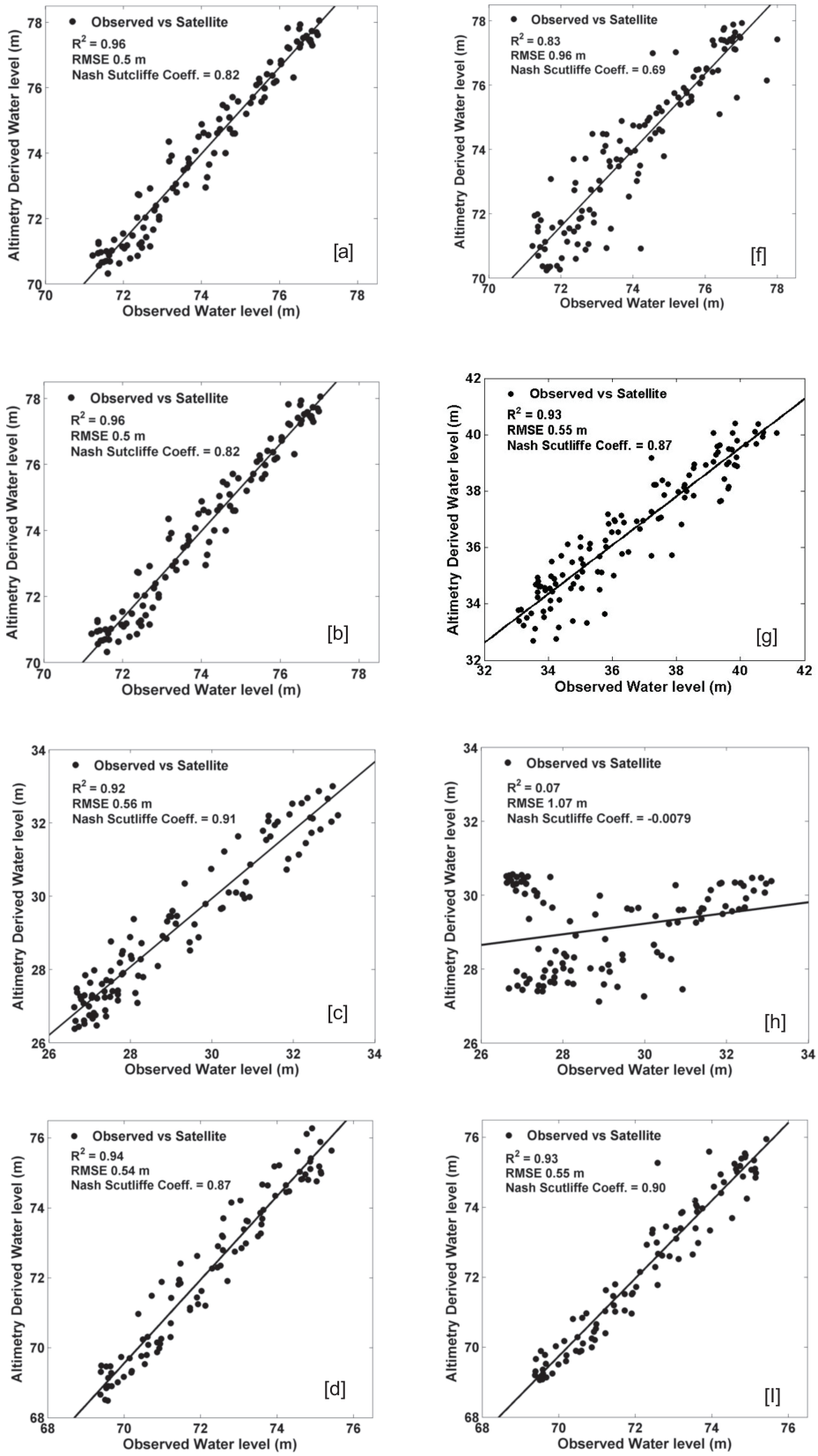

Figure 4.14: Performance comparison of retrieved water levels using developed methodology (a-d) and the Jason-2 derived Hydroweb water level data product (g-h) with in situ measurements at different tracks 53, 166, 231 and 242, respectively over the Brahmaputra River.

TH-1911_10610425

adopted to retain the waveforms from the main channel of the river and which could adjust according to changes in the course of the river main channel. The nested window approach is a new method to filter out the noisy waveforms within the braided reaches of the river and it could enable the selection of waveforms from the main channel. This dynamic nested window approach has produced better results as compared to river mask based approaches. The retrieved water levels are compared to various data sets available for the Brahmaputra river. It was found out that with this proposed methodology water level retrieval has improved form 1.07 to 0.55 m of uncertainty in terms of RMSE, when evaluated at four different Jason-2 satellite tracks passing over the Brahmaputra river. The waveforms were classified after the selection and they were divided in different groups. The group of higher backscattering coefficient was selected for water level retrieval. The different classes represents how the waveforms are contaminated due to presence of various features within the altimeter footprint. Different retracking methods were used to derive water level information. To evaluate the performance of this algorithm the similar retracking algorithm (Ice-1) was used to compared the available data–sets (Hydroweb) for the Brahmaputra river.

TH-1911_10610425

TH-1911_10610425

"Everything that depends on the action of nature is by nature as good as it can be."

Aristotle (384 BC – 322 BC)
Greek philosopher and scientist

5

ACCURACY ASSESSMENT OF RETRIEVED WATER LEVEL, DISCHARGE AND WATER SURFACE SLOPES

5.1 Introduction

In this chapter assessment of retrieved water level was done using different satellite altimeters such as Jason-2, SARAL/Altika and ENVISAT. The water level comparisons of different sensors were done for the different time period and different reaches of the Brahmaputra river. The SARAL/Altika 40 Hz waveform data was used for waveform retracking using different retracking algorithms such as Ice-1, Ice-2, threshold and β parameter for comparative analysis. The pseudo stage–discharge realtions were developed for the altimetery retrived water levels and the discharge data of *in–situ* gauge stations to estimate the discharge time series from altimetry data set. The discharge time series of Guwahati and Tezpur gauge stations was produced from altimetry derived water levels from Jason–2 and ENVISAT satellite. The seasonal water surface profiles were generated using SARAL/Altika satellite derived water levels at 10 different locations for monsoon and non-monsoon periods.

5.2 Methodology for water level comparisons

To compare the water level derived from altimeter satellites the *in–situ* river stage records of the same period were obtained for co-relation and error analysis. The differences of water

TH-1911_10610425

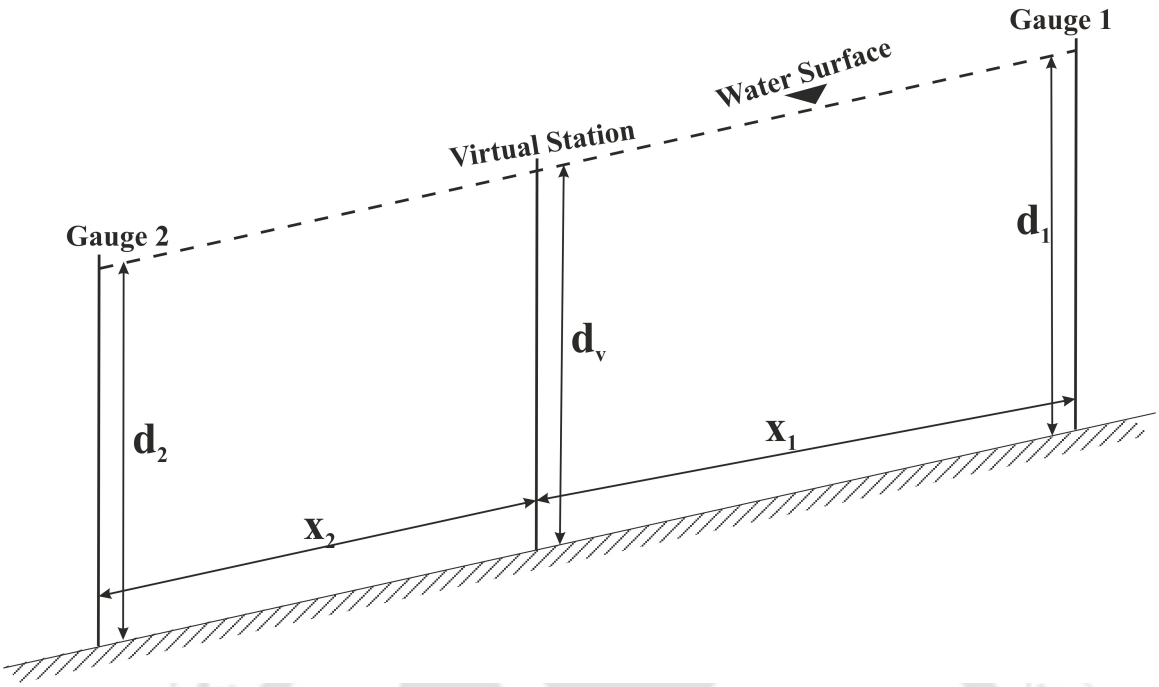

Figure 5.1: Sketch describing the interpolation of water level at virtual station using nearby gauge stations.

level between these two records were due to the spatial and datum variations. In order to nullify the differences we first applied the spatial interpolation of in situ measurements to obtain observed water level at the virtual gauging station. Second, we applied the datum correction on the observed interpolated stage records. In the datum correction approach, it is assumed that the local deviation of the river stage records due to datum difference between in situ and the altimetry derived stage records are the deviation between their average values. The locations of virtual and their distance from *in–situ* gauge stations were presented respectively for different satellite altimeters in Table 5.2 for SARAL/Altika, Table 5.3 for Jason–2 and Table 5.4 for ENVISAT. The linear interpolation (Equation 5.1) of observed water level between the two nearby in situ gauging stations has been carried out to estimate the actual water level at the virtual station (Figure 5.1).The interpolation is based on the Euclidean distance between the gauging stations.

$$d_v = d_2 + \frac{(d_1 - d_2)\, x_2}{x_1 + x_2} \tag{5.1}$$

5.2.1 Pseudo stage–discharge relation

The variation of river stage is strongly related with the river discharge, if the geometry of the particular station remains unchanged. The functional relationship between river stage

Table 5.1: Rating curve discharge coefficients for Jason–2 and ENVISAT satellites

Coefficients	Jason–2	ENVISAT	
	Guwahati	Guwahati	Tezpur
a	6 x 10^{-13}	8 x 10^{-21}	1 x 10^{-41}
b	10.68	15.24	25.20
R^2	0.80	0.91	0.97

and discharge is termed as rating curve.

$$Q = a\ H^b \tag{5.2}$$

Where Q is the discharge (m^3/sec), H is the river stage (m) and a, b are coefficients. These coefficients for Guwahati and Tezpur are derived using altimetry retrieved river stage and observed discharge (Table 5.1).

In this study, there was no discharge measurement available over the virtual stations. Hence, the rating curve relations were developed using the near-by gauge discharge values. Literature on discharge estimation have also supported the fact that, many researchers have used retrieved water level over a virtual station and near-by gauging station to develop the pseudo rating curve (Kouraev et al., 2004; Zakharova et al., 2006; Papa et al., 2010). Ample, study on discharge estimation over rivers have shown the capability of satellite altimetry retrieved water level to produce discharge time series such as over Ob river (Kouraev et al., 2004), different sites along the Amazon river (Zakharova et al., 2006) and Ganga and Brahmaputra river (Papa et al., 2010) using nearby gauging stations to calibrate the retrieved water levels. Pseudo rating curve relation for a virtual stations were developed for Guwahati (track-166) gauge records near to respective virtual stations of Jason–2 satellite (Figure 5.2). It may be noted that year 2009 data were used to develop the relationship. The performance analysis of altimetry estimated discharge was done for the year 2010. In case of ENVISAT satellite pseudo rating curve relations were developed fro Guwahati and Tezpur gauge site.

5.3 Seasonal water surface profiles computation

The water surface profiles were generated using SARAL/Altika satellite data for 10 different locations for the monsoon and non-monsoon flow periods (Table 5.2). The retrieved water level during the month of January and February was considered for the non–monsoon water

TH-1911_10610425

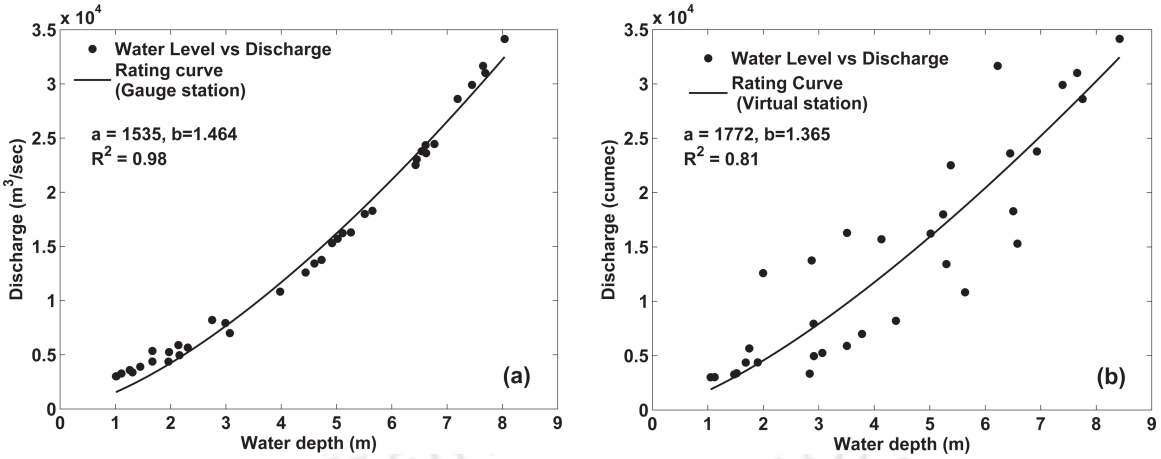

Figure 5.2: Generation of the rating curves for the (a) Guwahati gauge station and the (b) Virtual station (Track-166) for the year 2009.

surface profiles and the water level retrieved for the months of July and August was used for monsoon water surface profile. The water surface profile is an important indicator of energy dissipation over a reach by the river. Since, SARAL/Altika have dense track across the Brahmaputra river the variation on surface water profile of the river could be well captured. It is also an important parameter for Hydraulic and sediment transport models.

5.3.1 Data used

F The different altimeter satellite data was used for water level comparisons with *in–situ* gauge records. Here, water retrieved at different locations of the river using satellite altimetry are termed as virtual stations (V.S.), which were compared with near–by gauge stations (G.S.). The Jason–2 retrieved water levels were compared with the *in–situ* river stage records for different locations (Table 5.3). The Jason–2 altimeter data was used for the period of 2008 to 2013 at the four different reaches (Figure 5.3) and the SARAL/Altika altimeter for the period of 2013 to 2015 for the 10 different locations (Table 5.2) of the Brahmaputra river. The ENVISAT water level was available for the period of 2008 to 2010, which was analyzed for 6 different locations (Table 5.4) over the Brahmaputra river. The SARAL/Altika satellite has highly dense track over the Brahmaputra river, which provide a unique opportunity to study the dynamics of Brahmaputra river at finer scale as compared to in situ gauge stations. The study covers the middle reach of the Brahmaputra river, in which 10 satellite tracks (Figure 5.5) were selected. These tracks well represent the spatio-temporal variability in river flow regime. To retrieve water level over the braided river reaches, the virtual stations were set up over the main channel of the river.

TH-1911_10610425

Table 5.2: Statistics of virtual and *in–situ* gauge stations for SARAL/Altika satellite

Satellite Track (V.S.)	Nearest in situ gauge Station	Location of V. S. (Lat/Lon, degree)	River bed elevation (m.s.l.)	Virtual stations w.r.t., nearest Gauge Stations	Distance between V.S. and G.S. (km)	River High / Low flow width at V.S.(km)
982	Dhubri	90°14′47.9″E 26°6′49.4″N	23	U/S	30.2	13.2/5.94
438	Goalpara	90°59′27.6″E 26°13′6.8″N	28.5	D/S	42	5.53/4.11
709	Goalpara	91°5′26.2″E 26°11′51.4″N	28.5	D/S	52.1	7.34/5.25
896	Guwahati	91°42′23.6″E 26°10′45.3″N	40.35	U/S	6.8	3.3/1.6
623	Tezpur	92°26′16.1″E 26°32′46.3″N	58	D/S	40	8.7/3.23
352	Tezpur	92°31′37″E 26°36′23.3″N	58	D/S	30.15	7.28/3.57
810	Tezpur	93°7′47.2″E 26°38′35.4″N	58	U/S	47.85	7.10/5.76
537	Nematighat	93°47′43.8″E 26°49′7.6″N	80.4	D/S	28.42	11.72/2.42
266	Nematighat	94°2′30.8″E 26°52′25.8″N	80.4	D/S	3.24	9.6/3.46
995	Nematighat	94°28′18.2″E 27°2′29.6″N	80.4	U/S	46.08	10.5/2.6

Table 5.3: Statistics of virtual and *in–situ* gauge stations for Jason–2 satellite

In Situ gauge stations (V.S. track)	Location of V. S. (Lat/Lon) (degree)	River bed elevation (m.s.l.)	Virtual Stations w.r.t., nearest Gauge Stations	Distance between V.S. and,G.S. (km)	Datum Correction (m)	River High flow / Lean flow width at V.S.(km)
Tezpur (53)	26°45′33.74″N 93°28′49.47″E	58	U/S	71.5	7.77	5.3/1.4
Goalpara (166)	26°12′46.82″N 91° 1′46.61″E	28.5	U/S	41	3.06	8.5/2.8
Dhubri (231)	26° 9′18.43″N 90°21′31.23″E	23	U/S	39	2.3	13.6/10.5
Nematighat (242)	26°43′41.09″N 93°36′31.61″E	80.4	D/S	62.5	-3.64	7.9/1.5

Table 5.4: Statistics of virtual and *in–situ* gauge stations for ENVISAT satellite

In Situ gauge stations	River bed elevation (m.s.l.)	Virtual Stations w.r.t., nearest Gauge Stations	Distance between V.S. and, G.S. (km)	Datum Correction (m)
Dhubri	23	D/S	40	0.28
Goalpara	28.55	U/S	45	2.14
Guwahati	40.35	U/S	12	3.09
Tezpur	58	U/S	33	3.22

TH-1911_10610425

5.4 Results and discussion

The retrieved water levels capture the seasonal variability in river stage variations. The flood waves of different time period were also well picked up by the retrieved water levels. The large variations were evident during the lean flow period with higher values of standard deviation as compared to high river flow period (Figure 5.4). It further established the fact that altimeter provide better water level estimation during the monsoon season, when the width of flow remains large as compared to non-monsoon season.

5.4.1 Performance evaluation of water level derived from Jason–2 satellite

A correlation and error analysis between in-situ and satellite Jason-2 altimeter derived river levels were carried out at different virtual stations. The large variations were evident during the lean flow period with higher values of standard deviation as compared to high flow period (Figure 5.4). It has further established the fact that altimeter provide better water level estimation during the monsoon season, when the river width of flow remains large as compared to non-monsoon season. The accuracy of retrieved water levels was within the range of 50 to 60 cm in terms of root mean square error.

5.4.2 Performance evaluation of water level derived from SARAL/Altika satellite

To evaluate the performance of SARAL/Altika retrieved water level over braided rivers, correlation analysis was done at 10 satellite tracks intersecting the rivers at different locations. It was found that retrieved water levels showing good agreement with observed water levels (Figure 5.6 and Figure 5.7). Different retracking algorithms (Ice-1, Ice-2, Threshold and β parameter) were used to retrieve water level at different reaches of the river. It was found that out of 10 tracks, Beta parameter algorithm has performed the best over 7 tracks at different locations. Whereas Ice-1, threshold and Beta have performed the best over 438, 982 and 352 satellite tracks respectively. Using β parameter algorithm water level retrieval could be done within 40 cm of root mean square error in most of the cases except for the track 982, 623 and 995 (Table 5.5).

5.4.3 Performance evaluation of water level derived from ENVISAT satellite

The observed river stages at six in situ gauge stations have been compared with the ENVISAT water levels. These co-relation scatter plots are given in Figure 5.10. The scatter plots show

TH-1911_10610425

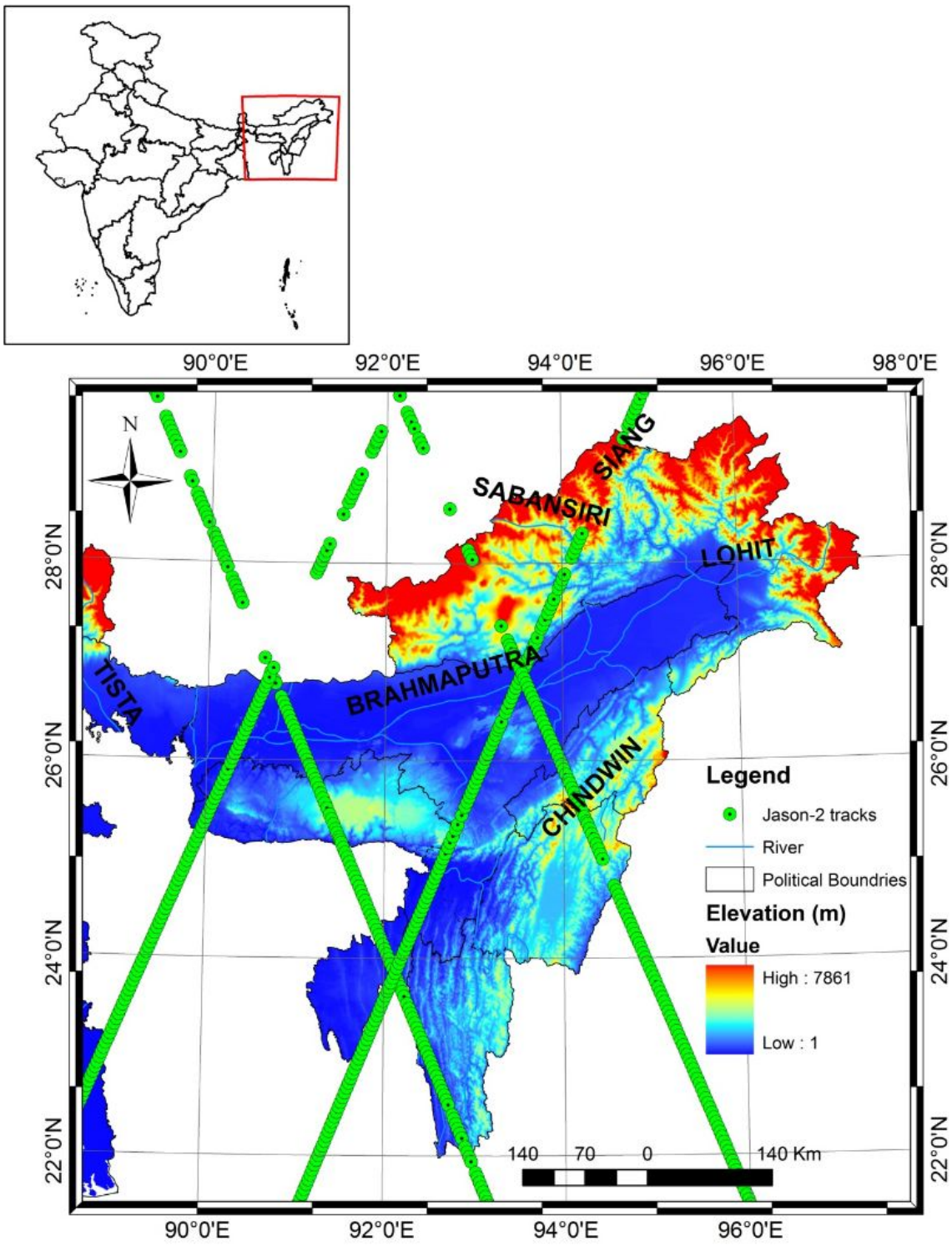

Figure 5.3: Topographic map of the Brahmaputra basin on which the Jason-2 satellite tracks are superimposed.

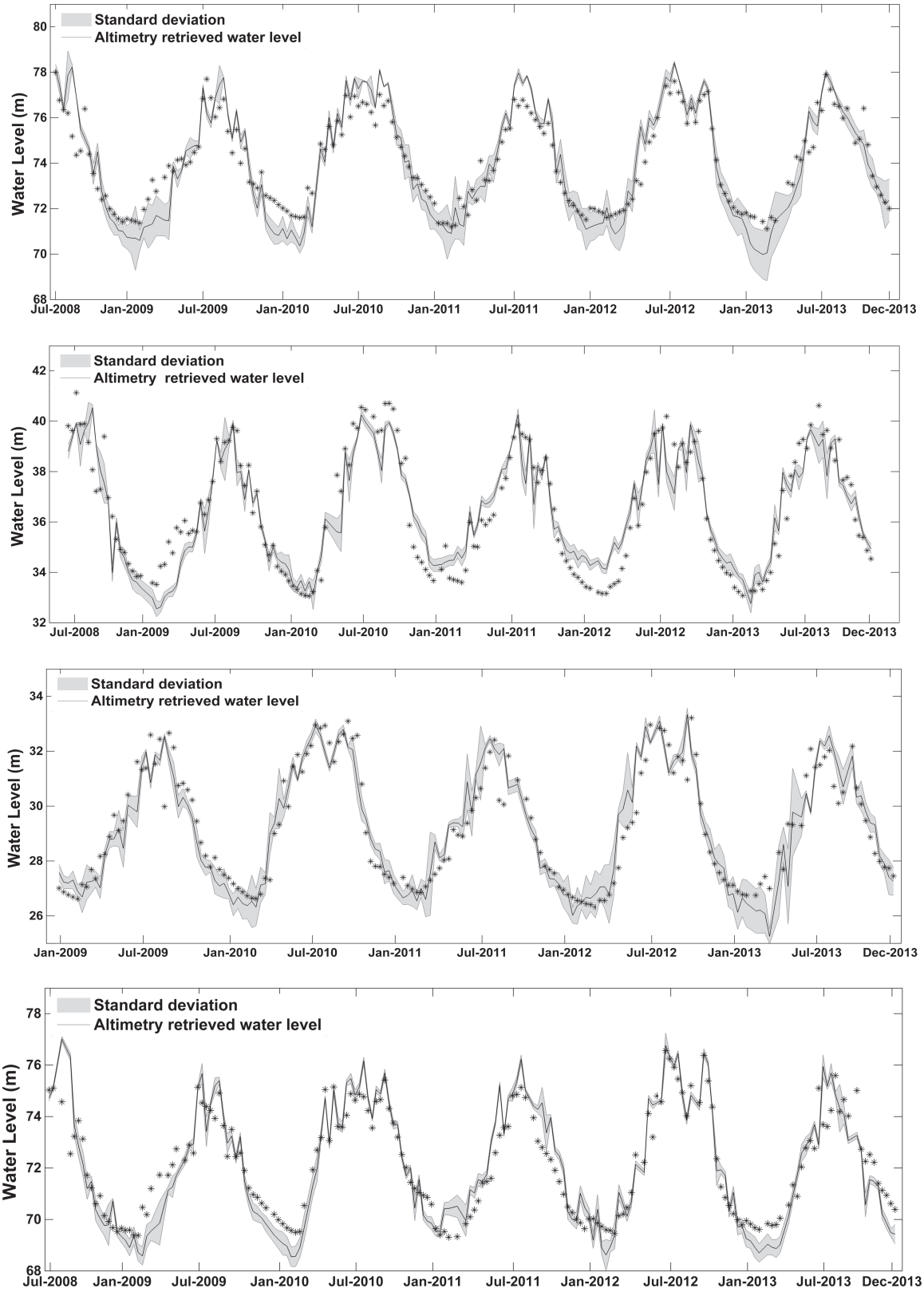

Figure 5.4: Comparisons between altimetry derived and observed water levels at different satellite tracks (a) 53, (b) 166, (c) 231 and (d) 242 over the Brahmaputra river.

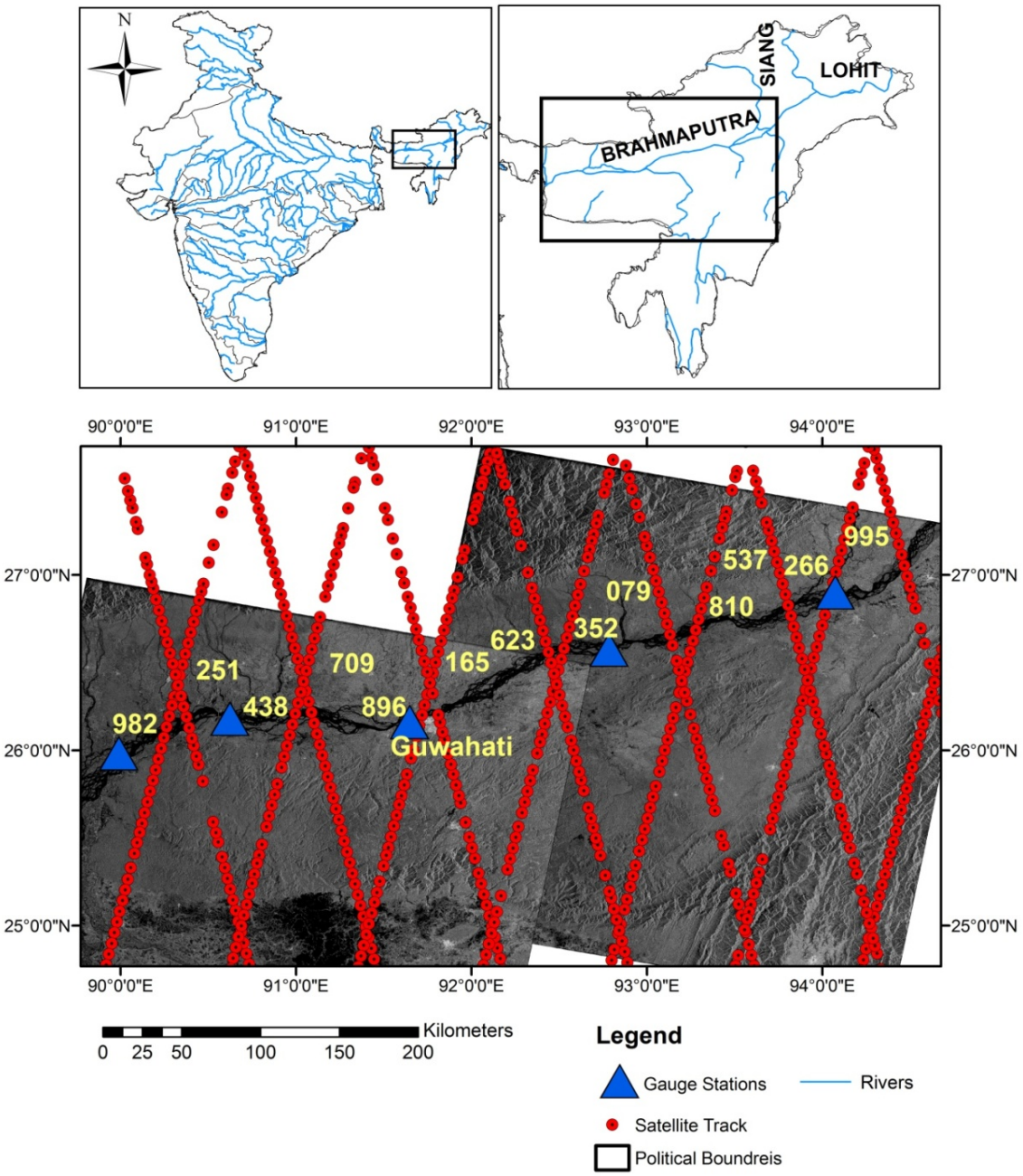

Figure 5.5: Study area showing Saral/Altika track overlaid on microwave images, passing over the Brahmaputra river

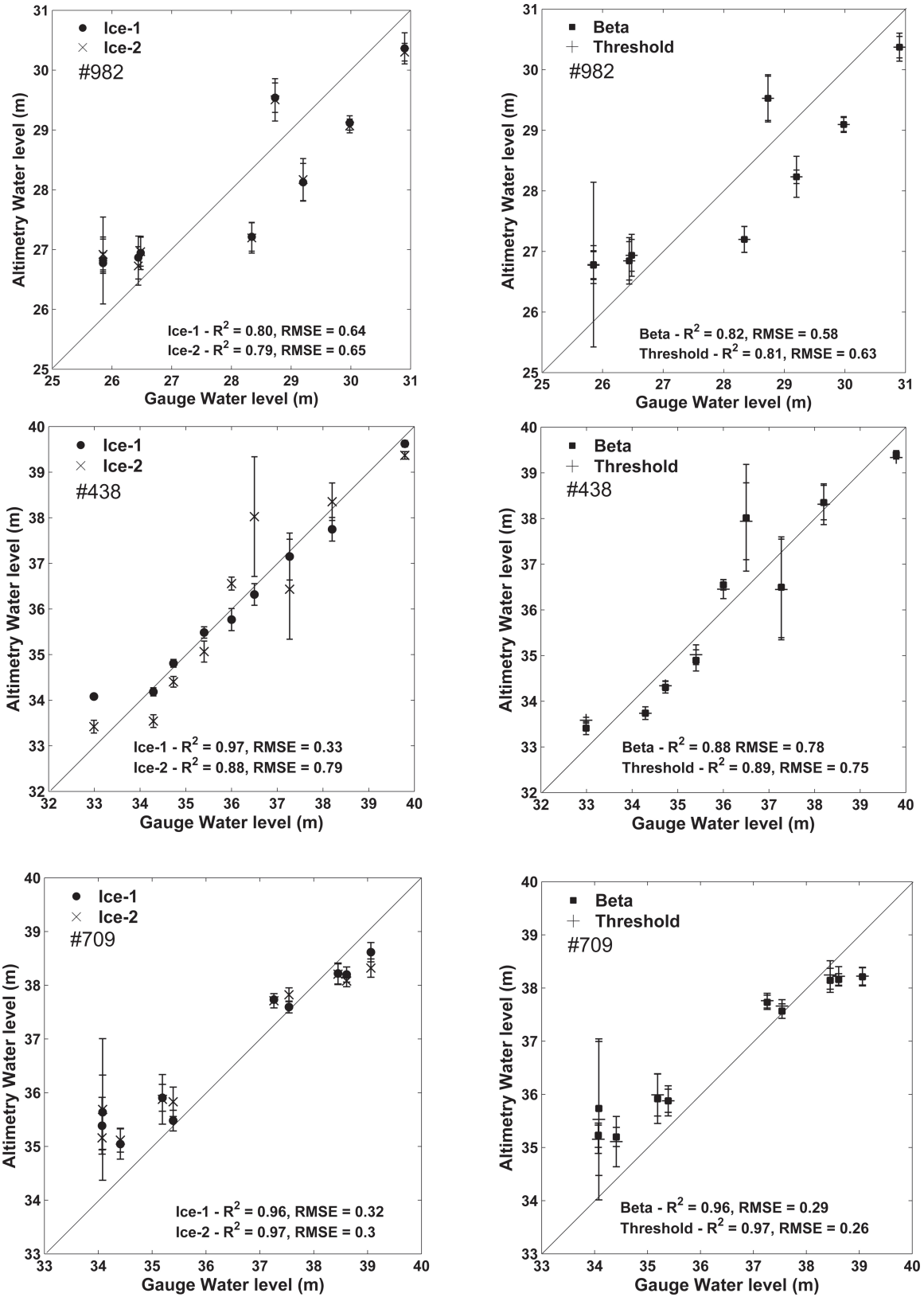

Figure 5.6: Correlation analysis between in situ and retrieved water level at different virtual (982, 438, 709) stations over the Brahmaputra river.

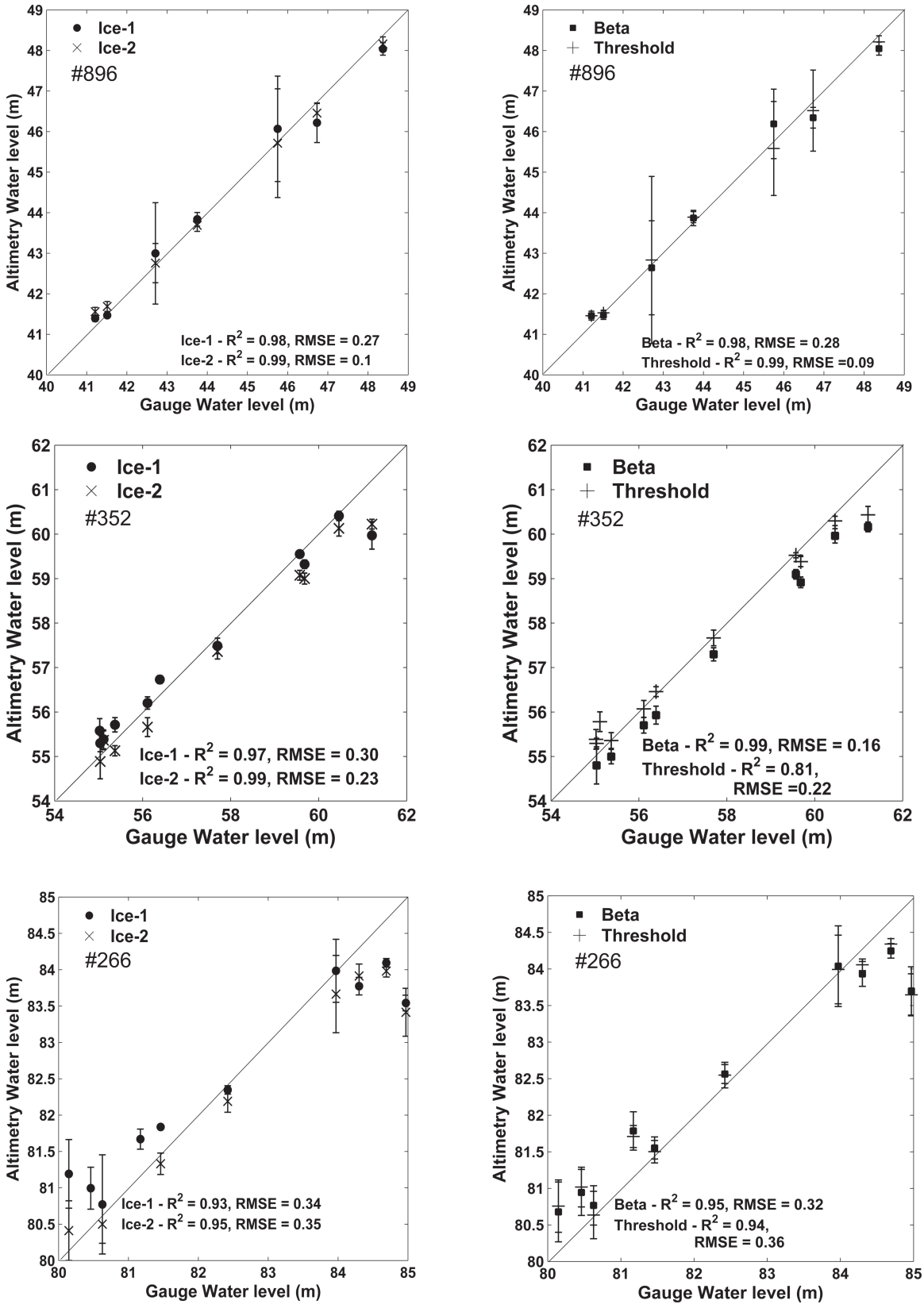

Figure 5.7: Correlation analysis between in situ and retrieved water level at different virtual (896,352, 266) stations over the Brahmaputra river.

Table 5.5: Statistical Performance of different retracking algorithms over Brahmaputra river

Track No.	Retrackers	R2	RMSE (m)	Nash Sutcliffe coefficient
982	Ice-1	0.8	0.64	0.78
	Ice-2	0.79	0.65	0.76
	Beta	0.82	0.58	0.77
	Threshold	0.81	0.63	0.79
438	Ice-1	0.97	0.34	0.95
	Ice-2	0.88	0.79	0.87
	Beta	0.89	0.78	0.88
	Threshold	0.88	0.76	0.88
709	Ice-1	0.96	0.32	0.88
	Ice-2	0.97	0.3	0.89
	Beta	0.96	0.29	0.87
	Threshold	0.97	0.26	0.9
896	Ice-1	0.98	0.27	0.98
	Ice-2	0.99	0.08	0.99
	Beta	0.98	0.28	0.97
	Threshold	0.98	0.09	0.98
623	Ice-1	0.81	0.74	0.8
	Ice-2	0.88	0.6	0.88
	Beta	0.9	0.62	0.87
	Threshold	0.89	0.61	0.87
352	Ice-1	0.97	0.30	0.96
	Ice-2	0.99	0.23	0.98
	Beta	0.99	0.16	0.99
	Threshold	0.81	0.23	0.97
810	Ice-1	0.82	0.96	0.75
	Ice-2	0.99	0.23	0.98
	Beta	0.98	0.26	0.97
	Threshold	0.96	0.42	0.95
537	Ice-1	0.95	0.44	0.95
	Ice-2	0.97	0.37	0.97
	Beta	0.96	0.37	0.97
	Threshold	0.95	0.47	0.94
266	Ice-1	0.93	0.34	0.86
	Ice-2	0.95	0.35	0.93
	Beta	0.95	0.32	0.91
	Threshold	0.94	0.36	0.9
995	Ice-1	0.88	0.81	0.5
	Ice-2	0.9	0.8	0.4
	Beta	0.89	0.8	0.45
	Threshold	0.9	0.78	0.5

TH-1911_10610425

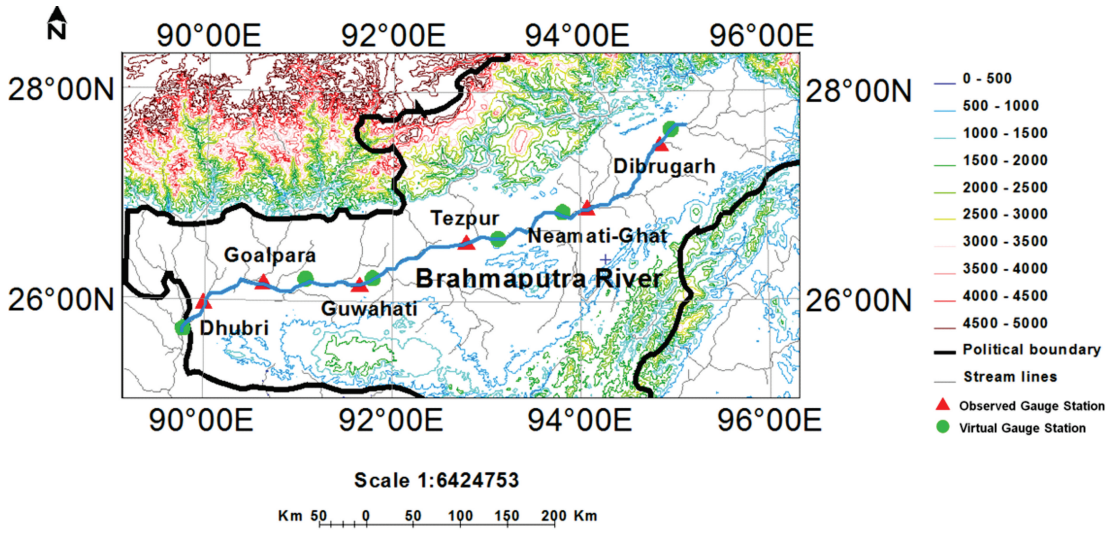

Figure 5.8: Study area showing in situ and virtual gauging stations of ENVISAT in the Brahmaputra River.

that out of six virtual gauging stations, five gauging stations have statistical significance co-relation with coefficient of determination (R^2) greater than 0.75. Gauging station at Dibrugarh shows very low co-relation with wide scatter data. It may be noted that water level variation at the five gauging stations ranges from 6 to 10 m, whereas this variation at Dibrugarh station is about 2 to 5 m. This low co-relation between altimeter and in situ measurement may be attributed to aggradation phase of the shallow depth reach. It may be concluded that for the braided reaches with transversal aggradation/degradation phases altimetry data may have poor performance in water level and its related measurements.

5.5 Discharge Estimation

The Brahmaputra river discharge estimation was done using Jason–2 and ENISAT river stage records. To derive discharge rating curve relations were developed for the nearby gauge stations for both the satellite data sets. The discharge at Guwahati was estimated using Jason–2 stage records for the period of year 2008 to 2013. The discharge at Guwahati and Tezpur was estimated using ENVISAT stage records for the period of year 2000 to 2010.

5.5.1 Discharge estimation using Jason–2 satellite data

The altimetry derived stage time series from Jason-2 satellite has been converted into the discharge time series through rating curve relation (Equation 5.2). In Figure 5.11, perfor-

TH-1911_10610425

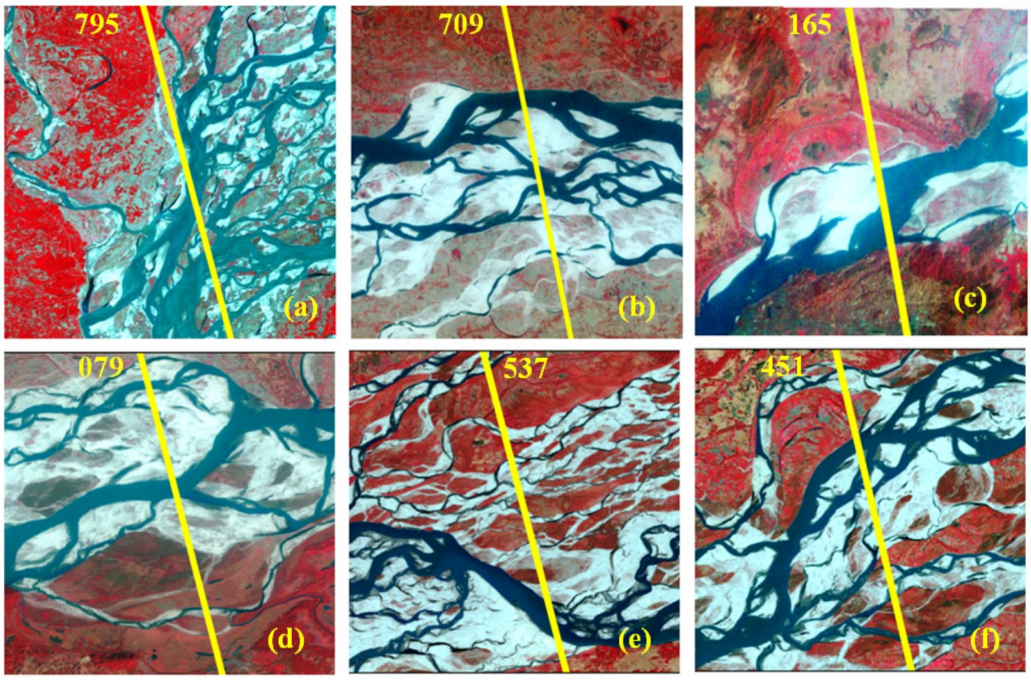

Figure 5.9: Virtual gauge stations at different reaches of the Brahmaputra River (a) Dhubri, (b) Goalpara, (c) Guwahati, (d) Tezpur, (e) Nematighat, and (f) Dibrugarh.

mance analysis of the estimated discharge with the nearby in situ (observed) gauge station is presented for Guwahati. It can be seen that the altimetry estimated discharge have well captured the flow variations as compared to observed discharges for Guwahati (Figure 5.12) gauging station. Statistical analysis has been done to check the performance of altimetry estimated discharge values. Altimetry estimated and observed discharges found to be in good agreement with high correlation coefficient of 0.94 Guwahati. To assess the discharge estimation accuracy Nash Scutliffe coefficient (N.S.) was calculated for the virtual station for the year 2010. It represents how model prediction is close to the observed mean; the N.S. coefficient values were high (Guwahati- 0.88).

5.5.2 Discharge estimation using ENVISAT satellite data

The ENVISAT satellite river stage time series has been converted into the discharge time series through rating curve relation (Equation 5.2). In Figure 5.14 and 5.15, a visual comparison of the estimated discharge with the nearby in situ (observed) gauge station is presented for Guwahati and Tezpur, respectively. It can be seen that the altimetry estimated discharge have captured the flow variations very well as compared to observed discharge dataset. Statistical analysis has been done to check the performance of altimetry estimated discharge values for monsoon and non-monsoon periods. It was found that altimetry es-

TH-1911_10610425

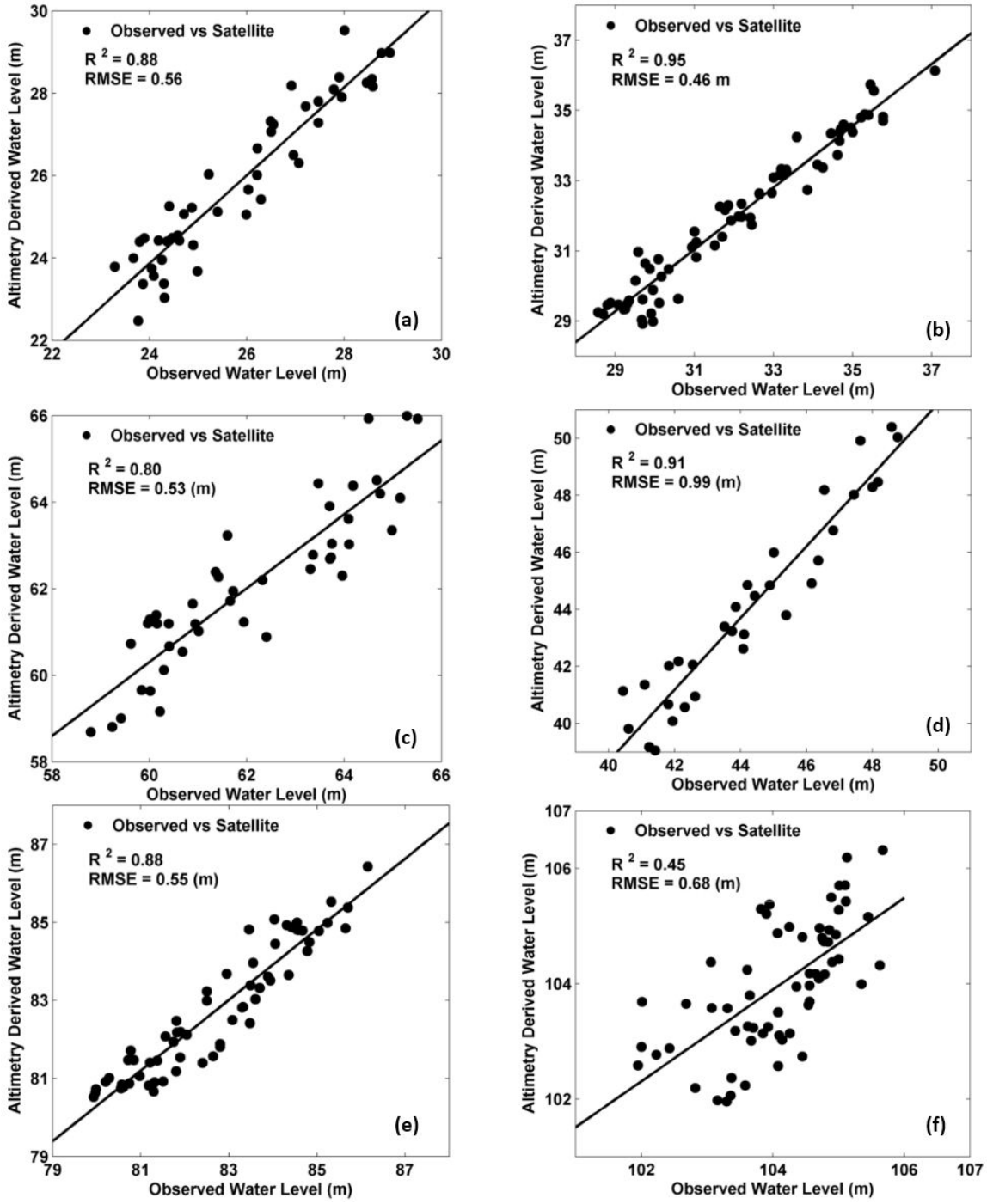

Figure 5.10: Correlation analysis between the in-situ stage data and satellite altimetry derived stage (a) Dhubri (b) Goalpara (c) Guwahati (d) Tezpur (e) Nematighat, and (f) Dibrugarh.

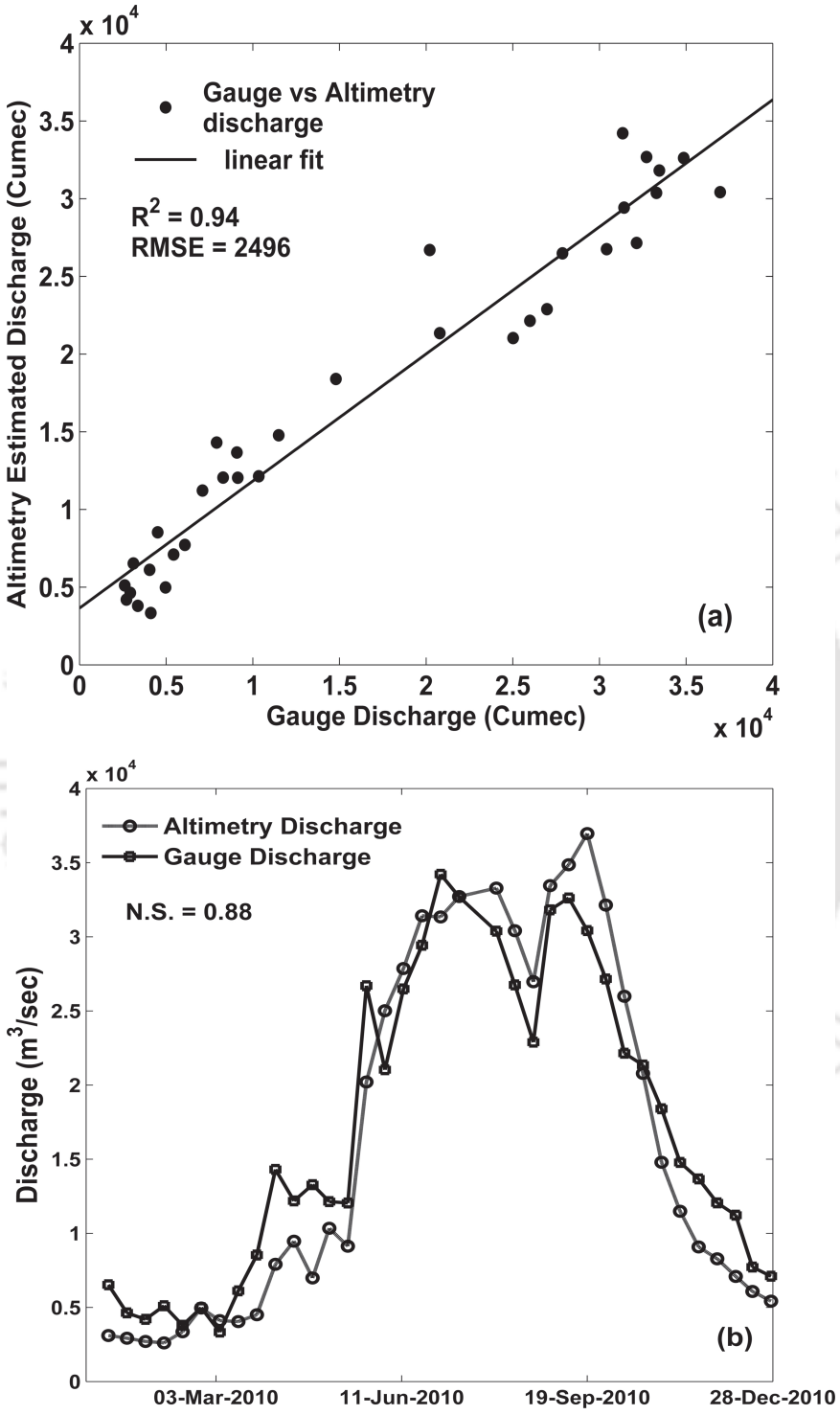

Figure 5.11: (a) Correlation analysis of observed vs altimetry derived discharge for the year 2010, (b) Time series of observed and altimetry derived discharge for the year 2010.

TH-1911_10610425

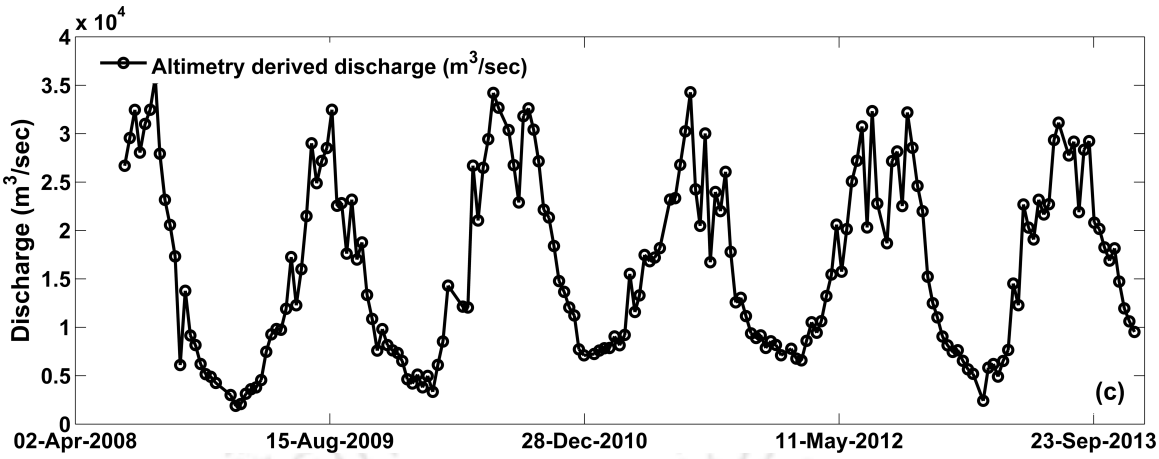

Figure 5.12: Altimetry derived time series for Guwahati (Track-166) gauge station from 2008 to 2013.

timated discharge have well captured the flow variations during the monsoon period as compared to non monsoon (Figure 5.13). There was low correlation coefficient (R^2 = 0.44) found between in situ and altimetry derived discharges during non-monsoon period for Guwahati gauge station. However, altimetry estimated and observed discharges for the monsoon season found to be in good agreement with high correlation coefficient R^2 = 0.85 and R^2 = 0.84 for Guwahati and Tezpur, respectively (Figure 5.13).

5.6 Water surface profile

The water surface profiles generated using SARAL/Altika satellite data indicate the seasonal water depth variations from upstream to downstream. The seasonal water depth variations were found to be higher for the downstream reaches of the river (6–7 m) as compared to the upstream reaches (4–5 m). The monsoon and Non-monsoon water level difference vary for station to station Figure 5.16(b), it also has decreasing trend form the downstream to upstream. The highest water level difference was 6.9 m at track 982, downstream of the river. Whereas the lowest difference 3.75 m was found at track 266 upstream of the river. Water surface profile of Brahmaputra river also indicates the bed slope variation of the river from the upstream point of Neematighat to downstream point of Dhubri (Figure 5.16(a)).

5.7 Long-term monthly discharge and annual water yield

Monthly average discharge has been calculated from the daily observed dataset for the period 2002 to 2010 using ENVISAT satellite data. The long term monthly average variation of

TH-1911_10610425

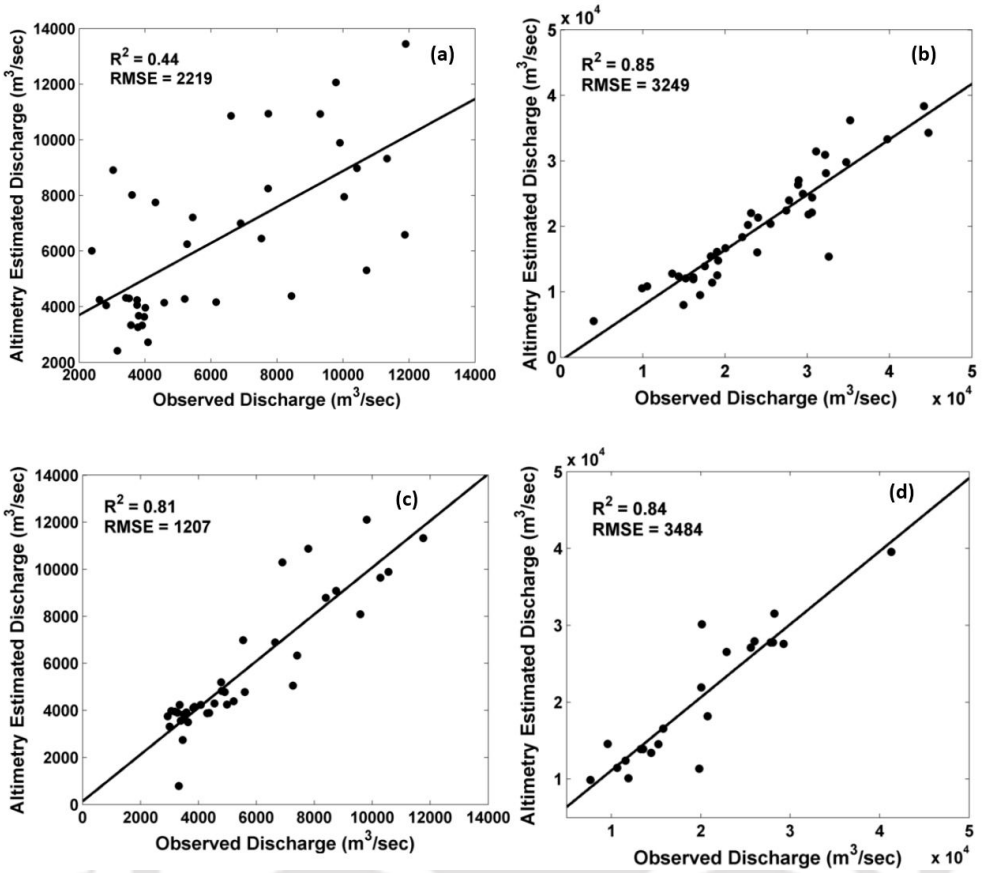

Figure 5.13: Altimetry estimated and in situ discharge comparisons for non–monsoon and monsoon periods at (a)-(b) Guwahati and (c)-(d) Tezpur Gauge stations, respectively.

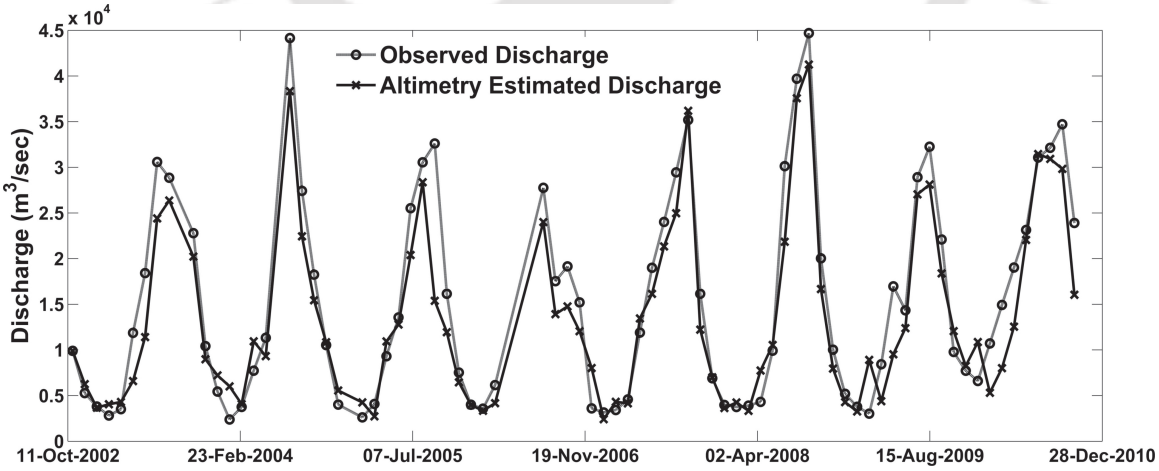

Figure 5.14: Comparison of altimetry estimated and in situ discharge hydrograph for Guwahati gauge station.

TH-1911_10610425

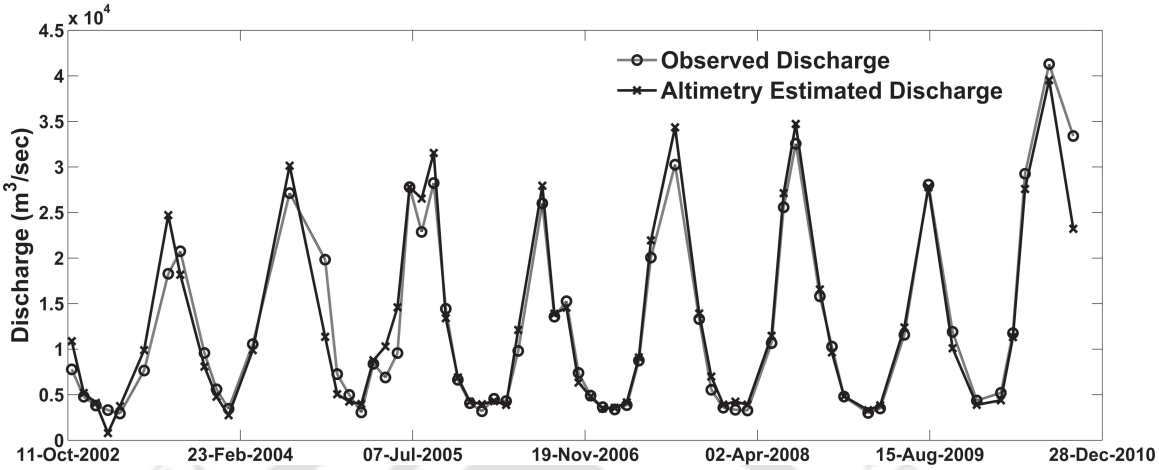

Figure 5.15: Comparison of altimetry estimated and in situ discharge hydrograph for Tezpur gauge station.

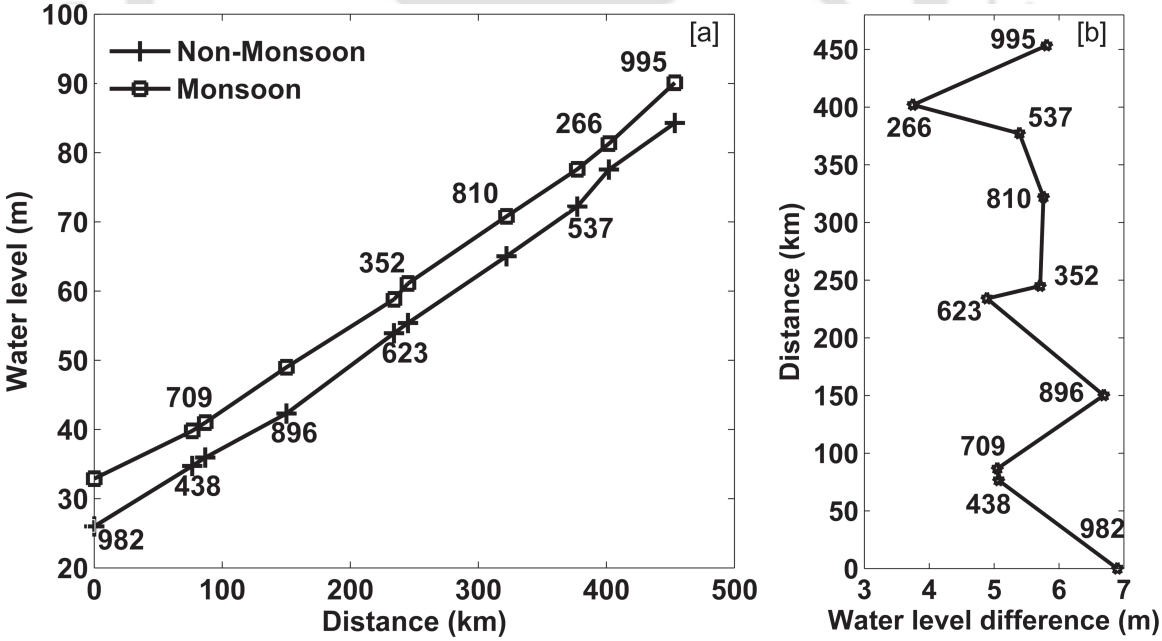

Figure 5.16: (a) Water surface profile for the Monsoon and Non-monsoon period of Brahmaputra river, (b) Water level differences between two seasons.

TH-1911_10610425

discharge at Guwahati and Tezpur is represented by the hydrographs (Figure 5.17), which is compared with that of altimetry data series. The figure indicates that its accuracy in estimating non monsoon month (November-May) flow is high as compared to the monsoon season (June-October) flow. During the monsoon flow (June-October) the error in the discharge estimation was higher than 10 % from the observed discharge but for the non monsoon flow the error in prediction was lower than 10 % for both the gauge stations (Guwahati and Tezpur). It could be because of the fact that altimetry measurements provides only 35 days of receptivity, which may not be able to capture high flood waves during the monsoon season. Flow variation during the monsoon period is high in Brahmaputra river as compared to non monsoon flow. This could be seen by the higher standard deviation for the monsoon months as compared to non-monsoon months. Hence, monthly comparison during the monsoon season is lesser accurate as compared to non-monsoon season. Similarly, the annual water yield has been calculated for Guwahati and Tezpur gauge stations (Figure 5.18) from the in situ and virtual gauge discharges for the period of year 2002 to 2010. The approximate error in average water yield by altimetry estimated discharge for Guwahati and Tezpur were about 10 % and 6 % respectively. Altimetry annual water yield has been predicted very well for the year 2006, 2007 and 2009 at Guwahati gauge stations; whereas, it has predicted well for the year 2007 at Tezpur gauge station.

5.8 Conclusions

Water level retrieval was done from Jason-2 satellite and SARAL/Altika satellite altimeters. The retrieved water levels from Jason-2, SARAL/Altka and ENVISAT altimeter retrieved water level product (Hydroweb) were compared for accuracy assessment from nearby gauging stations. The accuracy of retrieved water level from improved methodology for Jason-2 at 4 locations over the Brahmaputra river was found to be 55 cm in terms of root mean square error (RMSE). The SARAL/Altika has more dense tracks and Ka (36.7 Ghz) band altimeter as compared to Jason-2 with Ku band (16 Ghz) frequency. It has produced better accuracy with improved algorithm with 40 cm of RMSE when compared for 10 different locations over the Brahmaputra river. These water level informations at different locations over the Brahmaputra river were used to generate the water surface profiles. The water surface profiles were generated for the monsoon and non-monsoon season. It was found out that there is higher seasonal water difference at the downstream of the river as compared to upstream.

To retrieve water levels different retracking algorithm were used for accuracy assessment. It was found β-5 algorithm had performed best among four different algorithms used for

TH-1911_10610425

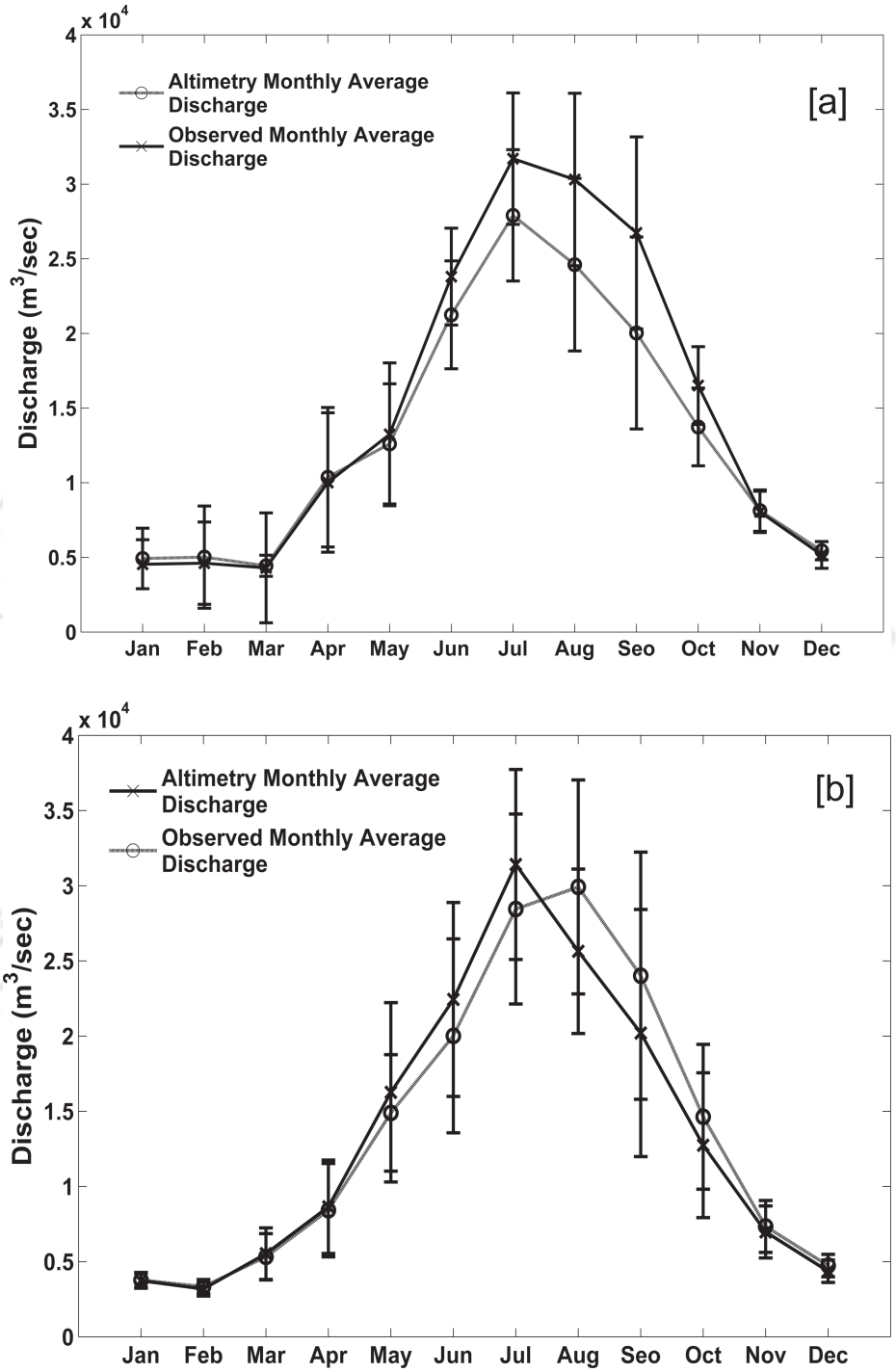

Figure 5.17: Altimetry Estimated and in situ monthly discharge hydrographs of the Brahmaputra river at (a) Guwahati and (b) Tezpur gauge station.

TH-1911_10610425

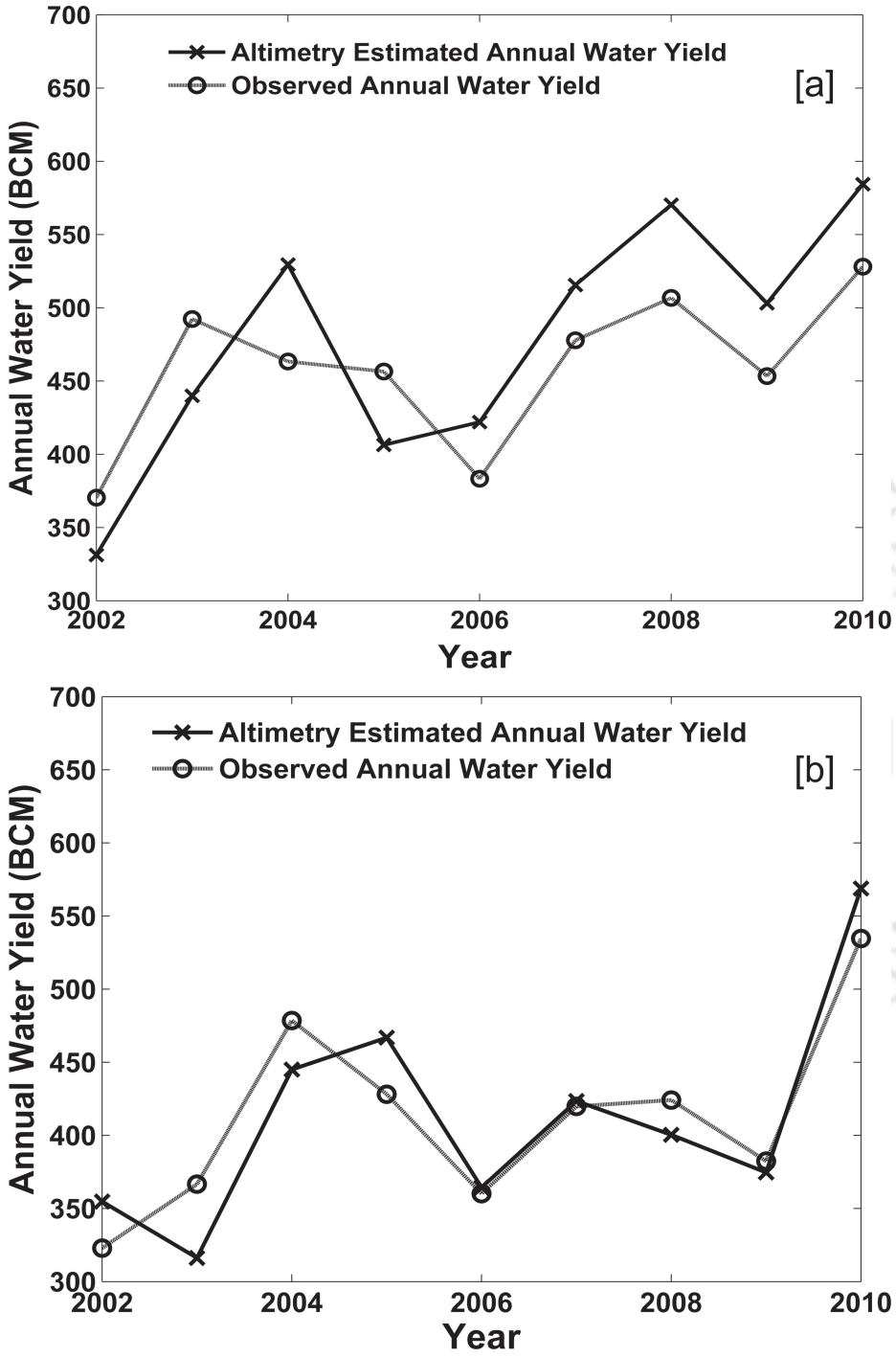

Figure 5.18: Altimetry Estimated and in situ annual water yield the of the Brahmaputra river at (a) Guwahati and (b) Tezpur gauge station.

evaluation such as Ice-1, Ice-2, threshold and β-5 retrackers. The retrieved water levels were converted into the discharge time series based on the rating curve developed over the virtual stations. These discharges were compared with nearby gauge stations and it was found out that the discharge values were able to capture the flood-waves occurred in the Brahmaputra river. The discharge comparisons were done for the Guwahati and Tezpur gauge stations. The discharge values were also used to estimate annual water yield at Guwahati and Tezpur gauge stations.



TH-1911_10610425

"Two things are infinite: the universe and human stupidity; and I'm not sure about the universe."

Albert Einstein (1879 – 1955)
German–born Theoretical physicist

6

MAPPING OF MORPHOLOGICAL FEATURES USING MICROWAVE SATELLITE IMAGES

6.1 Introduction

Remote sensing of the earth in optical region of electromagnetic spectrum has provided useful scientific operational data for various earth resources applications. Optical sensor essentially records the reflectance of sunlight from the earth's surface. However, under cloud cover conditions, operational capabilities of optical sensors become limited. In contrast cloud cover is considerably more transparent at microwave wavelengths, hence microwave sensors plays important role in data collection, which is independent of weather and sun light conditions. Besides this, there are specific applications where microwave sensors have shown their proven capabilities which otherwise could not had been possible. The all-weather capability of microwaves is one of the major factors for many applications. The radar energy has the ability to penetrate clouds, haze and even light rain. Further, radar sensors use their own source of energy to illuminate the terrain and as a result data can be acquired during night and need not be restricted to day light hours. Microwaves have greater surface penetration capabilities than the optical and thermal sensors. The depth to which radar penetrates into soil and vegetation surface depends on the wavelength of the radiation and dielectric properties of surface materials. In the microwave region, penetration of wave increases, with the wavelength. Microwave's unique sensitivity to water content of surface material allows a number of applications related to vegetation and soil moisture and snow wetness.

The Brahmaputra river is highly morphological dynamic river in which seasonal and intra-

TH-1911_10610425

seasonal variations are evident frequently. The morphological features such as sand bar formation, sand bar migration, bank erosion, sand deposition and river bed dynamics have different spatio-temporal scale. The yearly and long term morphological variations has been reported by the many researchers for the sand bed braided rivers but intra-seasonal variations which occur in the period of shorter duration has not been studied in detail. The availability of frequent microwave images has made it possible to investigate dynamic morphological phenomena in higher temporal and spatial scale which occur within a season or between occurrence of different flood waves. The flood waves passes through the Brahmaputra river causes huge morphological changes each year with high amount of water and sediment flux. The river discharge and sediment flux are the driving factor in morphological dynamics in the middle reach of the Brahmaputra river. Each flood wave during the monsoon season causes the sand bars migration, sand deposition, river bed and bank erosion. These intra-seasonal morphological features are studied with the help of microwave satellite images with synchronized river survey during the month of June, August and September 2011, which represents the different hydrological regime of the river. The microwave satellite images are sensitive to surface roughness and the dielectric constant of the object. In the Brahmaputra river high turbulence persist during the monsoon seasons, which is reflected in higher back-scattering coefficient in the microwave satellite images. The higher turbulence with high velocity of flow causes sediment migration and bank erosion. The bar migration and sand deposition around the bars also reflect different signature in the microwave images. In this study, we have collected the backscattering signature from the different morphological events occurred at different locations based on the field campaign. The microwave images were also used to generate the river mask as it clearly distinguish water and non water surface. Hence, different masks and the signature collected for different features are used for morphological mapping for different years of microwave images. The mapping of morphological feature in the sand bed braided river has its own importance. It provides vital information of river dynamics within the monsoon season for better river navigation and bank protection measures to avoid the losses of property and human lives.

6.2 Braided river morphological dynamics

Sand bed braided rivers such as the Brahmaputra are highly dynamic in nature. They change their course of flow frequently, which causes huge bank erosion and sand bar migration. During the monsoon season the braided river has higher sediment carrying capacity and the erosion power. The huge amount of energy dissipation takes place in terms of river fragmentation and sand bar migration and bar erosion. These are the common charac-

TH-1911_10610425

teristics of the sand bed braided rivers morphological dynamics. The suspended sediment concentration was varying at different reaches of the river, the sediment concentration was many times higher at active bank erosion and the near sand bar (Figure 3.8 and Figure 3.9) as compared to the nodal reaches of the river (Figure 3.10). At the river reaches where surface water roughness was high the sediment concentration was also found higher. Sediment concentration was higher at the confluences of tributaries with the river at places of active sediment deposition around the sand bar, at places of active bank erosion zones and near thalweg line (Figure 3.8 and Figure 3.9).

6.3 Data used

Microwave images were acquired during the flood period of year 2009 to 2011. The dual polarization (HH, HV) data of satellite with synthetic aperture radar (SAR) instrument aboard, an active radar operating at a wavelength of 5.66 cm and a 5.3 GHz frequency (C band) was used. The data was multi-look (noise-reduced), ground range, system-corrected digital image of C-band microwave data. The data was converted from slant range to ground range (Figure 6.1). The brightness values of beta naught were converted to estimates of the backscattering coefficient. All backscattering coefficients were expressed in decibels. Differences in incident angle occurring across a swath were included in this conversion. No correction was applied for topographic effects: a flat terrain was assumed for all river flood–plain. This was justified, as slopes were generally low. An average value of the backscattering coefficient was calculated for every pixel in each image, using a moving window of 5 by 5 pixels (corresponding to 125 by 125 m in the field). The radar images were selected such that they matched previous field campaigns in the year 2011. In situ data were obtained from field campaigns in 2011-13. During the 2011-13 campaigns sediment concentration and bathymetry data were collected along the Brahmaputra river. The cross sectional transects data were also collected at certain locations. The field campaigns were done for the both high and lean flow period. A Global Positioning System (GPS), with an accuracy of about 5 m was used for positioning and keeping the longitudinal track of the river survey.

6.4 Methodology for river morphological features extraction

To map different morphological features within the sand bed braided river from microwave satellite images signature analysis was performed. The signature of different features were collected in terms of backscattering coefficient (dB) variation based on synchronized river

TH-1911_10610425

Table 6.1: Microwave satellite images used in morphological analysis of the Brahmaputra river

Year	Date of Image acquisition	Discharge (m^3/sec)
2008	10-Jul-08	34485.28
	3-Aug-08	37600.9
	27-Aug-08	43367
2009	5-Jul-09	31660.07
	29-Jul-09	23788.96
	22-Aug-09	34149.09
2010	5-Jul-10	31341.3
	5-Aug-10	30411.2
	29-Aug-10	33454.91
2011	31-Jul-11	29807.37
	24-Aug-11	28071.47
	17-Sep-11	22601.07

survey for the year 2011. The backscattering signature of different morphological features such as sand bar, sand deposition zone, bank erosion zone, turbulent zone and river water were collected from the microwave satellite images. The signatures of bank erosion zone, sand deposition zone and turbulent zone were in close range for both the polarizations (HH and HV). However, these zones (morphologically active group) were distinct in HH polarization from river water as compared to the HV polarization. In HV polarization signature of these morphological active zones were close to river water. The back-scatter variation was found to be more in HH polarization as compared to HV polarization hence, HH polarization images were used to map different features within the river. The microwave satellite images backscatter coefficient variation in HH polarization is largely govern by the turbulence in the river, which generate the rough water surface. The morphological feature in the river are associated with different levels of turbulence presence withing the river due to bed roughness or/and plan–form roughness. The microwave satellite images were categorized in to different classes (i) the groups which could be easily separated based on the radar backscatter or based on the river flow mask. (ii) The morphological active groups represents in terms of turbulent features (Rough water surface). The second group which could not be well separated, were further grouped into different category of turbulence. The higher the backscattering coefficient more would be the water surface roughness (turbulence), hence higher the category.

The morphological active group was sub-divided into three categories, Category-I, Category-

TH-1911_10610425

II and Category-III.

- Category-I – -20 dB to -22 dB
- Category-II – -17.5 dB to -20 dB
- Category-III – -15 dB to -17.5 dB

To interpret different morphologically active zones present within the river, the river reach was divided in two 5 different zones.

- Zone-I - The nodal reach of the river.
- Zone II - The river reach with presence of middle and side sand bar.
- Zone-III - An active main channel of the river.
- Zone IV - Presence of multiple bars, multiple channels.
- Zone V - The river reach with highly dynamic morphology with sand bars migration and deposition.

These different categories were then interpreted with their association with different zones in which different morphological processes were active. The image segmentation was done based on the different turbulence categories. The interpretation of different categories into morphologically active group was done based on their association to the different zones in the river.

6.5 Results and Discussion

The microwave satellite images of year 2008 to 2011 were used to identify different morphological features. The field campaign were conducted during the year 2011 to collect the ground samples and as the ground truth for identification of different morphological features. The signature analysis has provided the radar back-scatter variation for different months for the year 2011 indicating the different hydrodynamic conditions of the river. The satellite images were classified in 6 morphological features such as sand bar, sand deposition, bank erosion, turbulent zone, river water and flood-plain inundation. The morphological features clearly indicate the formation and migration of sand bars during the monsoon season. The high bank erosion zones were also picked up with higher back-scattering coefficient. The sediment concentration were also found out to very high at near erodible banks

TH-1911_10610425

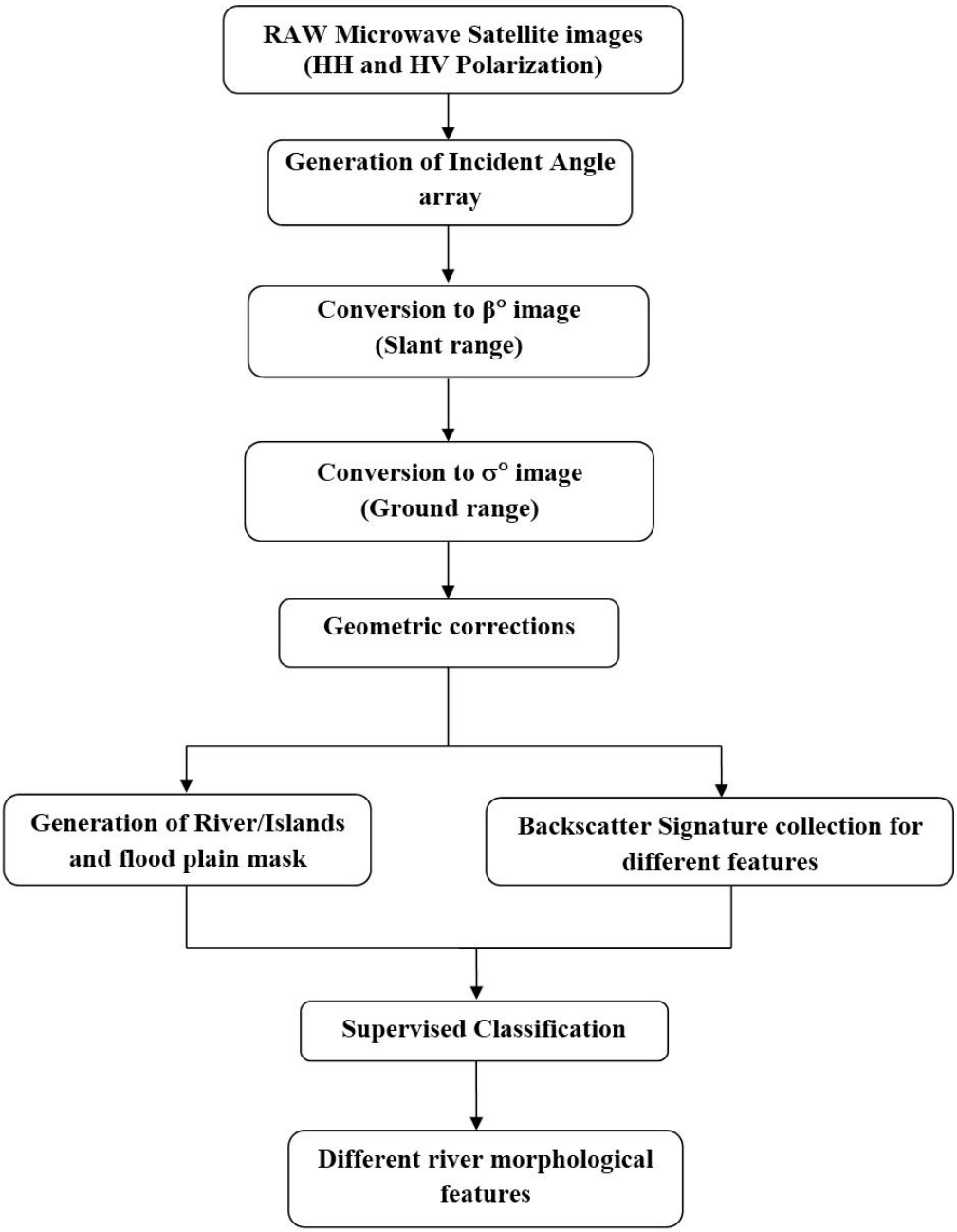

Figure 6.1: Methodology to generate backscattering coefficient for microwave satellite images.

TH-1911_10610425

with high flow velocity. The sediment concentration was also high near the sand bars. indicating higher sediment near sand bars. It is an indication of sand bar migration and sand deposition around sand bars and increase their size. The classified microwave images resent the synoptic view of different morphological processes happening at different time and scale.

6.5.1 Signature analysis

The signature analysis was performed to identify the different morphological processes present within the river. It was found out that turbulent zones varies from -18 dB to -21 dB in the month of July, -17 dB to -20 dB in the month of August and -17.5 dB to -21.5 dB in the month of September, 2011. The sand bars reflected higher back-scattering coefficient with the range of -7 dB to -14 dB. Signature analysis was performed to derive the morphological features within the river from the microwave data of different polarization and incident angle. The morphological features within the river were considered as sand bars, sand deposition, bank erosion, turbulent zone, river water and floodplain inundation. The signatures were collected from the microwave satellite images of HH and HV polarization. The HH polarization was found to be sensitive to surface water roughness as compared to HV polarization. The turbulence variations were distinctly visible in HH polarization as compared to non–turbulent zone. These turbulent zones were found to be present in different morphological active zones such as bank erosion zone, sand deposition zone and the turbulent zone in main channel. These zones were identified as the morphologically active group, which could be separable to other groups but could not be separated within each other in HH polarization. In HH polarization variation in backscattering coefficient was found to be higher between river water and morphologically active group (Figure 6.2, Figure 6.3 and Figure 6.4) as compared to HV polarization for all the months presented in Figure 6.5, Figure 6.6 and Figure 6.7. In the HV polarization turbulent zones could not be separated from non-turbulent zones.

6.5.2 River mask generation

Different river masks (Figure 6.8 and Figure 6.9) were generated to classify the microwave images to different river morphological features such as turbulent zone, erosion zone, sand deposition zone, sand bars, flood–plain inundation and river water. The HV polarization was used to generate river and island masks due to sharp contrast between water and non–water features in the river. The river flow mask was generated to identify the flood–plain inundation separately.

TH-1911_10610425

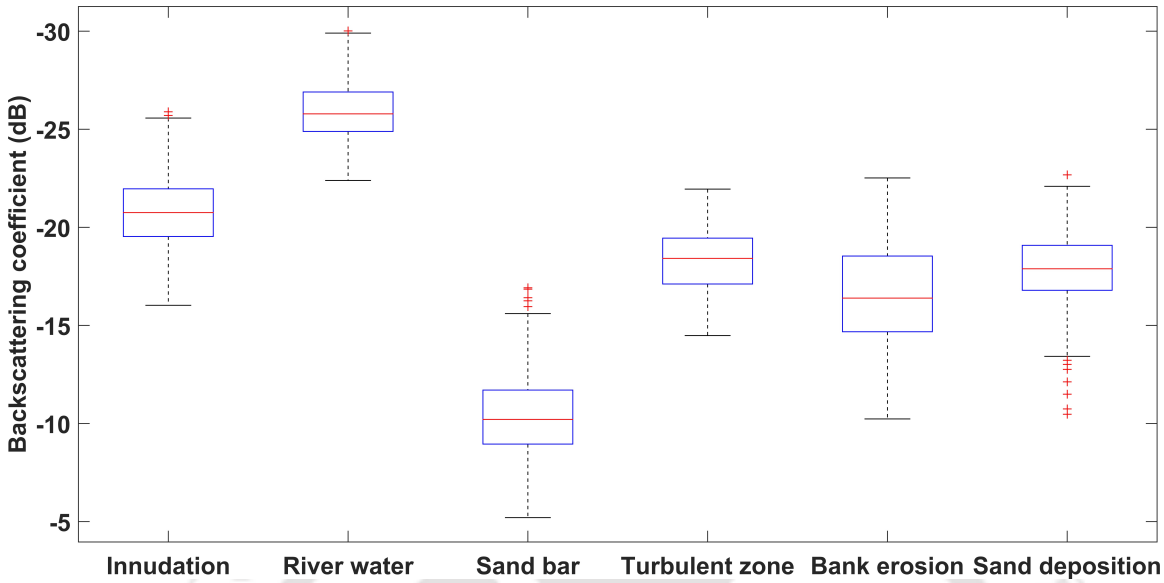

Figure 6.2: Backscatter variation in the microwave satellite image of HH polarization on 31 July 2011

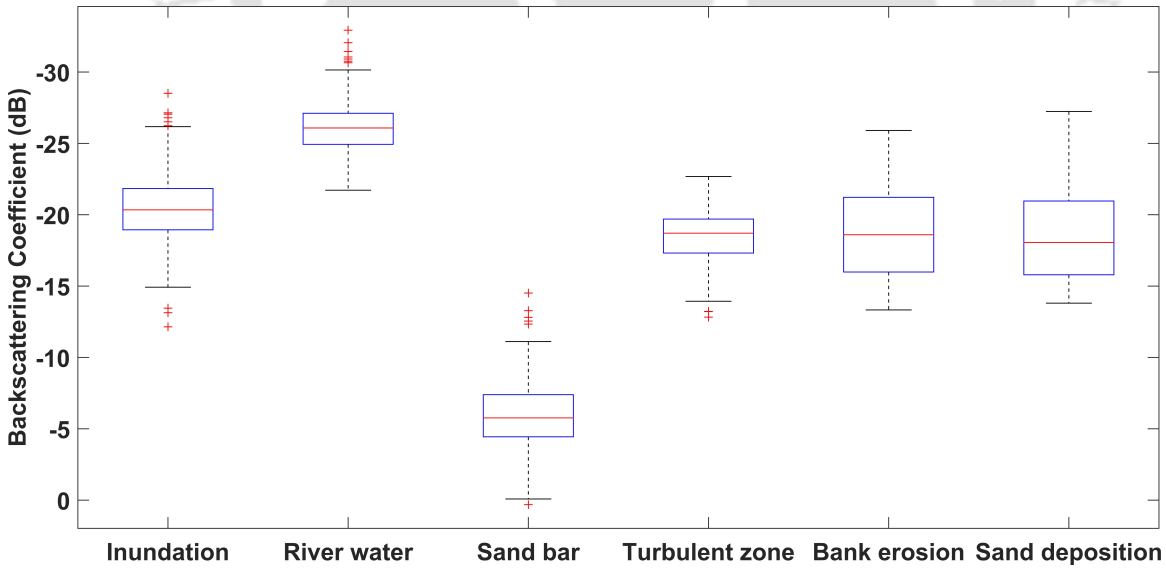

Figure 6.3: Backscatter variation in the microwave satellite image of HH polarization on 3 August 2011

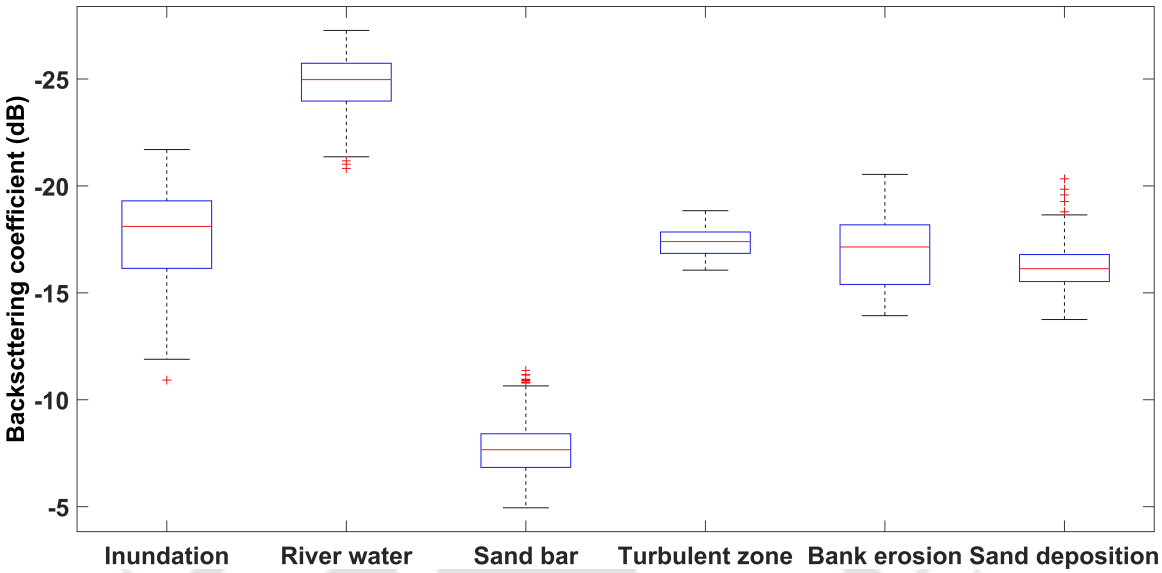

Figure 6.4: Backscatter variation in the microwave satellite image of HH polarization on 27 August 2011

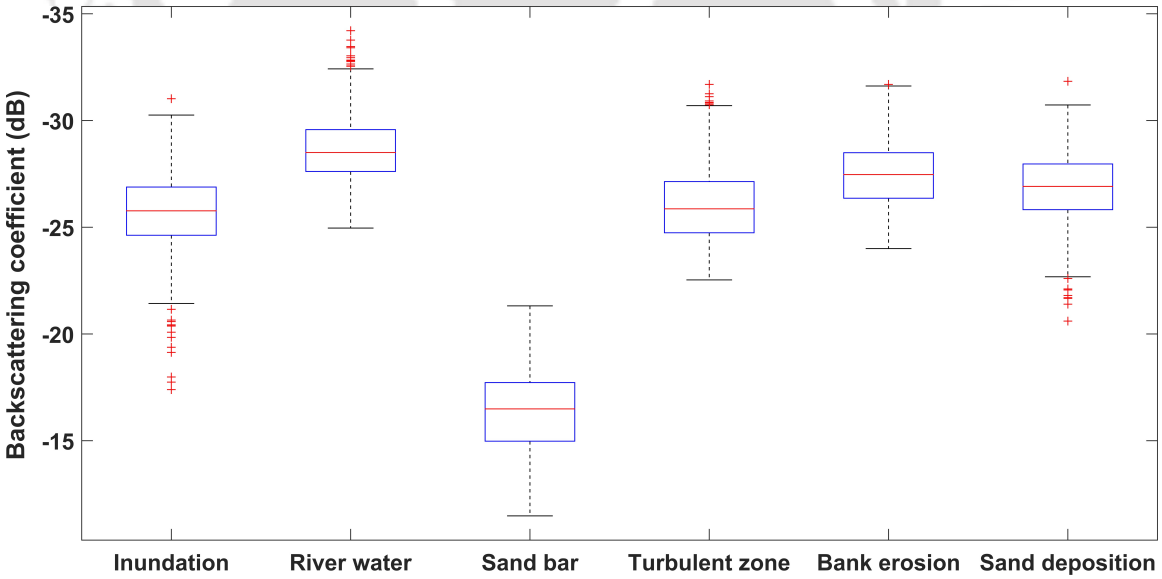

Figure 6.5: Backscatter variation in the microwave satellite image of HV polarization on 31 July 2011

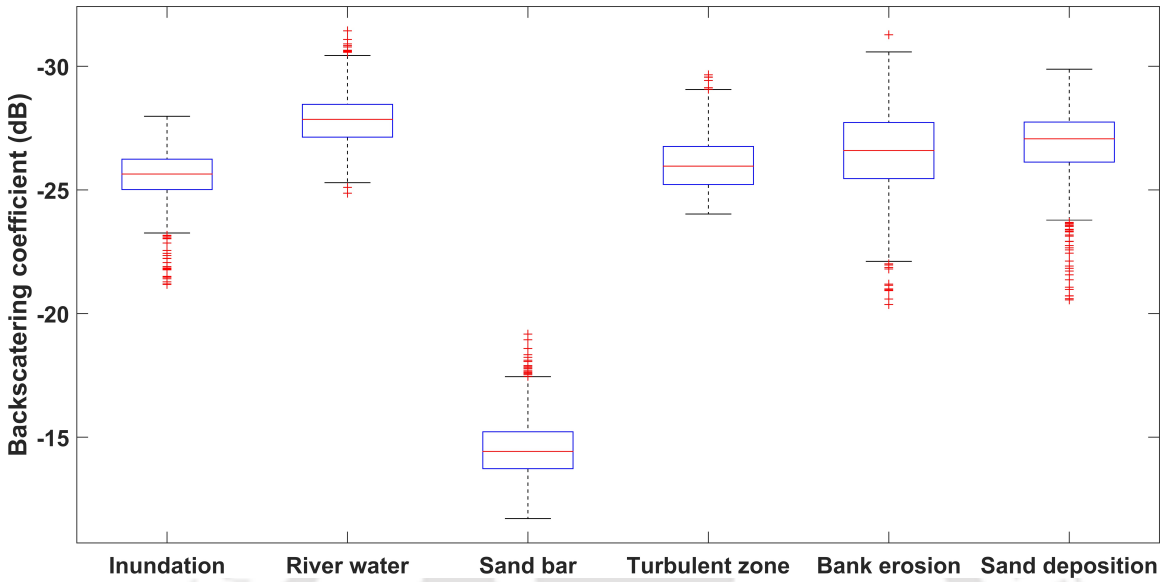

Figure 6.6: Backscatter variation in the microwave satellite image of HV polarization on 3 August 2011

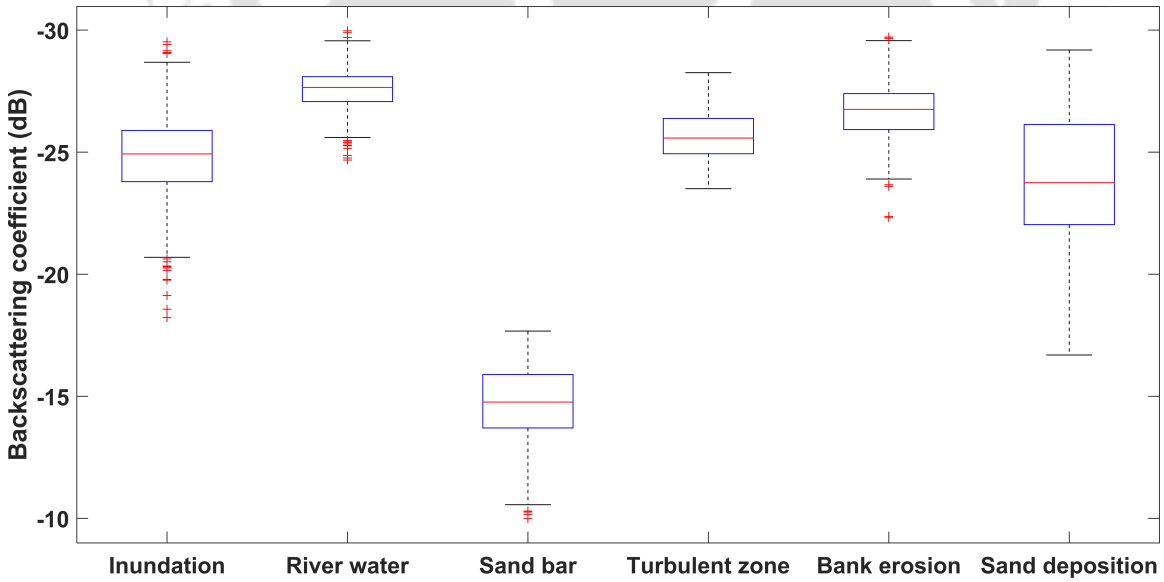

Figure 6.7: Backscatter variation in the microwave satellite image of HV polarization on 27 August 2011

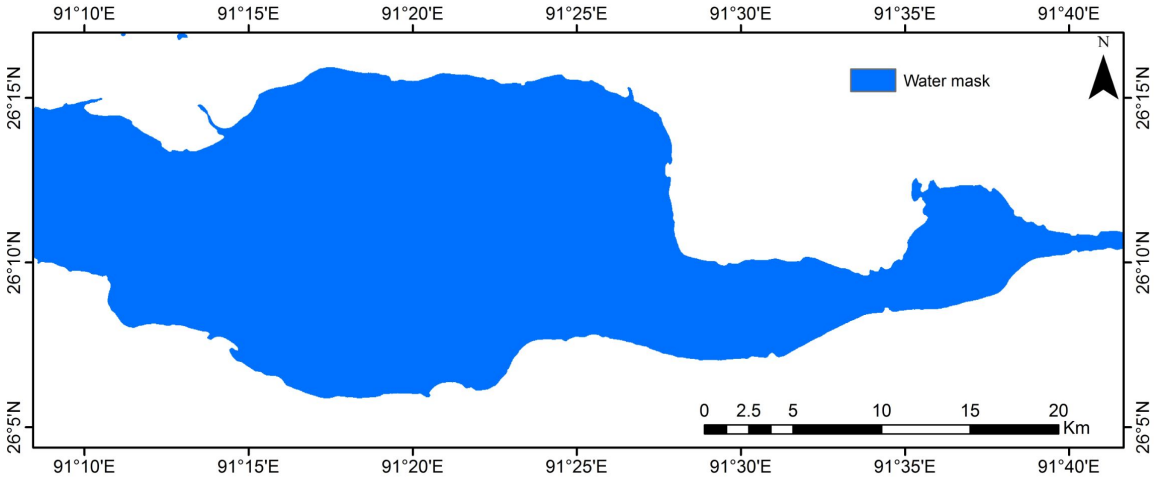

Figure 6.8: Water mask generation for the image classification for the different features present within the river

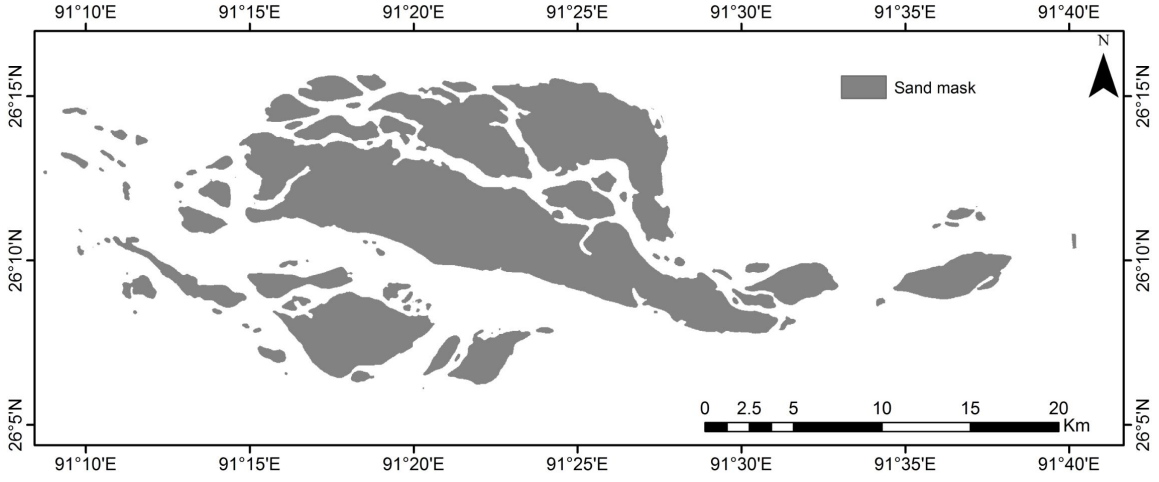

Figure 6.9: Sand mask generation for the image classification for the different features present within the river

6.5.3 Discharge intensity curve

The discharge intensity curve is the ratio of discharge to the effective river flow width. To interpret the morphological dynamic features present within the river discharge intensity curve has been produced for the middle reach of the Brahmaputra river. The discharge intensity curve for different zones of the middle reach of the Brahmaputra river reflects the flow intensity, which causes the local scale morphological processes. The variation of discharge intensity at different zones could be used to interpret the local morphological dynamics of the river such as bar formation, bar migration, river bank and river bed erosion. The discharge intensity was higher at Zone–I for all the time period (Figure 6.10, Figure 6.11, Figure 6.12 and Figure 6.13) as compared to other Zones, due to lower river flow width. The discharge intensity gradually decreased from Zone–II to Zone–IV and then slightly increased in Zone–V. The trend was found to be similar for different month's and the years of flow. The highest discharge intensity was in the year 2008 (Figure 6.10) as compared to other years.

6.5.4 Image Segmentation

The image segmentation was done in 6 different groups based on the signature analysis. The morphological active groups such as erosion, deposition and turbulent zones were closely associated based on the backscattering coefficient. The separability of these morphological active groups were difficult based on the backscattering values for the entire river reach. Hence, the microwave satellite images of the middle reach of the Brahmaputra river were divided in five different zones based on different characteristics of the reach.

Segmentation of morphologically active zones for the year 2008 and 2009

The microwave satellite images of year 2008 to 2011 were classified in to different groups. The morphological active groups which could not be separated was interpreted for each zone and year separately. The satellite images of year 2008 (Figure 6.14), which was the flood year represented the higher turbulence in Zone-I for the images of 10 July 2008, 3 August 2008 due to higher discharge intensity as compared to 27 Aug 2008, in–spite the fact that discharge intensity was higher on 27 Aug 2008. It could be the fact that river was much turbulent when it flows to the bank full discharge during the rising period in the monsoon. The Bank full discharge in the Brahmaputra river varies from 30,000 m^3/sec to 35,000 m^3/sec at Guwahati in which the river produced lot of turbulence and morphological changes. The turbulence in Zone–I represent the rough water surface. In the Zone-II turbulence of Category–I and Category–II could be associated with formation of

TH-1911_10610425

side bar largely due to sand deposition for the period of 10 July 2008 to 3 August 2008. In Zone-III, turbulence level of Category–I and Category–II indicated the main channel flow as the depth of river would be higher. Whereas, Category–II turbulence is associated with bar erosion at side and tip of the bar. In Zone–IV the Category–II turbulence near the banks reflect the active bank erosion. In Zone–V the discharge intensity remains the lower and the Category–I turbulence is present largely, which reflect the deposition of sand and formation of shallow river depth. In year 2009 the discharge intensity is lower as compared to year 2008. The microwave satellite images of 5 July 2009, 29 July 2009 and 22 August 2009 (Figure 6.15) were classified. Zone–I in each images represented Category–II and Category–III turbulence, which were caused due to higher discharge intensity, whereas in the Zone–II side bar formation remain continuous process. In Zone–II for each satellite images turbulence Category–I represent main channel of flow. In the Zone–IV on 5 July 2009 the turbulence Category–II represent the active bank erosion process. In the Zone–V on 29 July and 22 August 2009. It was dominated by Category–I turbulence, which represent sand deposition phenomena.

Segmentation of morphologically active zones for the year 2010 and 2011

In year 2010 for Zone–I turbulence Category–II and Category–III represent water surface roughness due to higher discharge intensity. The Zone–II has Category–I turbulence associated to bar formation, Zone–II has Category–II and Category–II turbulence level which represent the main channel of flow. In Zone–IV on 5 August 2010 (Figure 6.16) turbulence level of Category–II and Category–II were associated to the river bank and bar erosion processes and Zone–V on the same images were dominated by Category–II turbulence which reflect the higher bar migration and sand deposition. In the year 2011 all the microwave satellite images on Zone–I with Category–II and Category–III turbulence level were due to higher discharge intensity. The Zone–II has Category–I and Category–II level of turbulence on 17 September 2011 (Figure 6.17) which represent the side bar formation and mid bar erosion processes. Zone–II has Category–I turbulence in all the images due to lower discharge intensity. Zone–IV on 17 September 2011 has Category–II and Category–III turbulence level which represent the bar formation and bank erosion Zone–V with turbulence level of Category–II largely represent the sand deposition.

6.5.5 Morphological dynamic interpretation

Zone–I in the nodal location (Guwahati) was dominated with Category–II and Category–III level of turbulence for all the years due to high discharge intensity. The Zone–II with

TH-1911_10610425

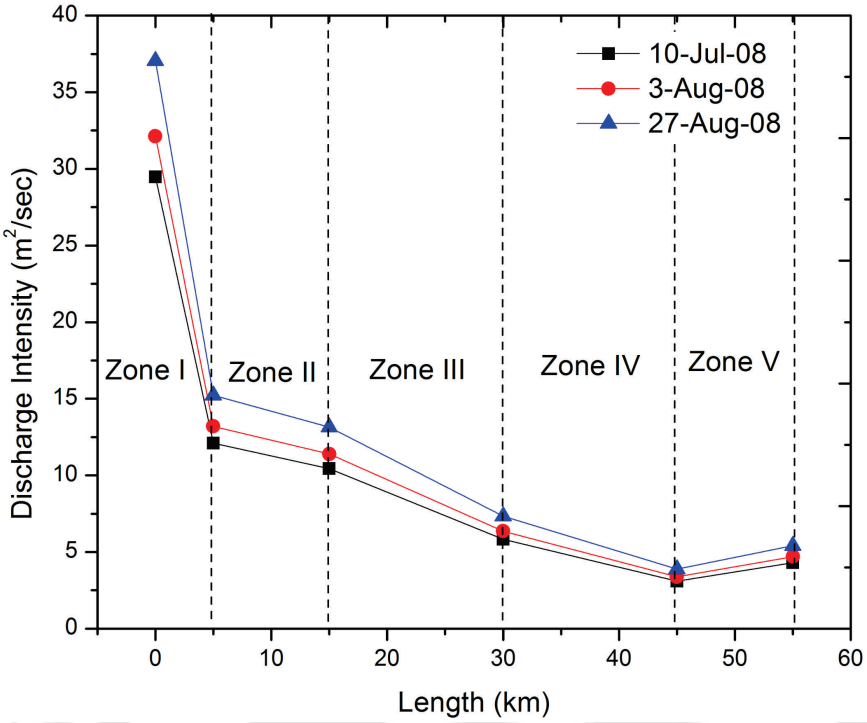

Figure 6.10: Discharge Intensity curve for the middle reach of the Brahmaputra river during the year 2008.

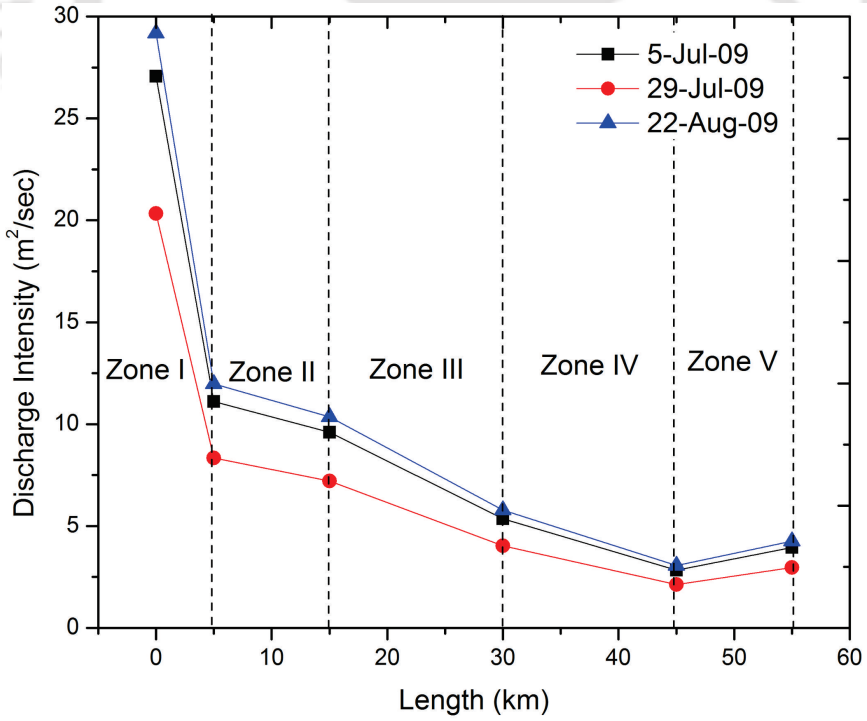

Figure 6.11: Discharge Intensity curve for the middle reach of the Brahmaputra river during the year 2009.

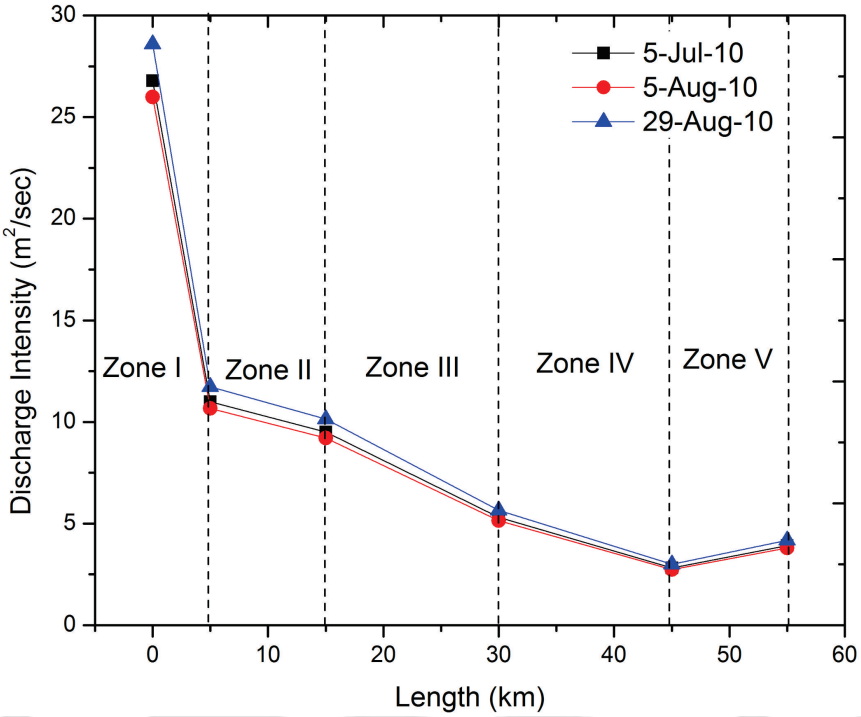

Figure 6.12: Discharge Intensity curve for the middle reach of the Brahmaputra river during the year 2010.

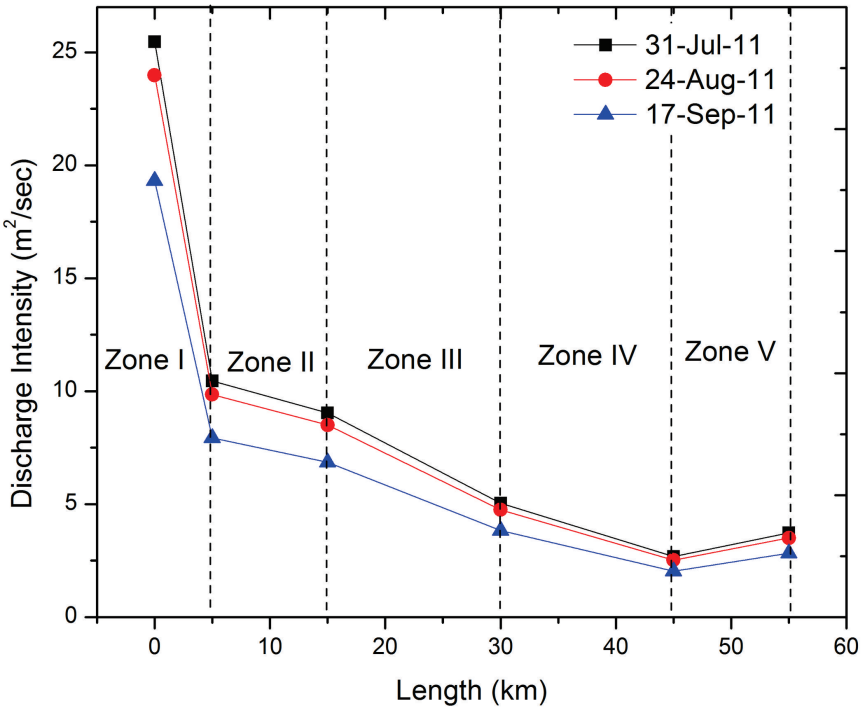

Figure 6.13: Discharge Intensity curve for the middle reach of the Brahmaputra river during the year 2011.

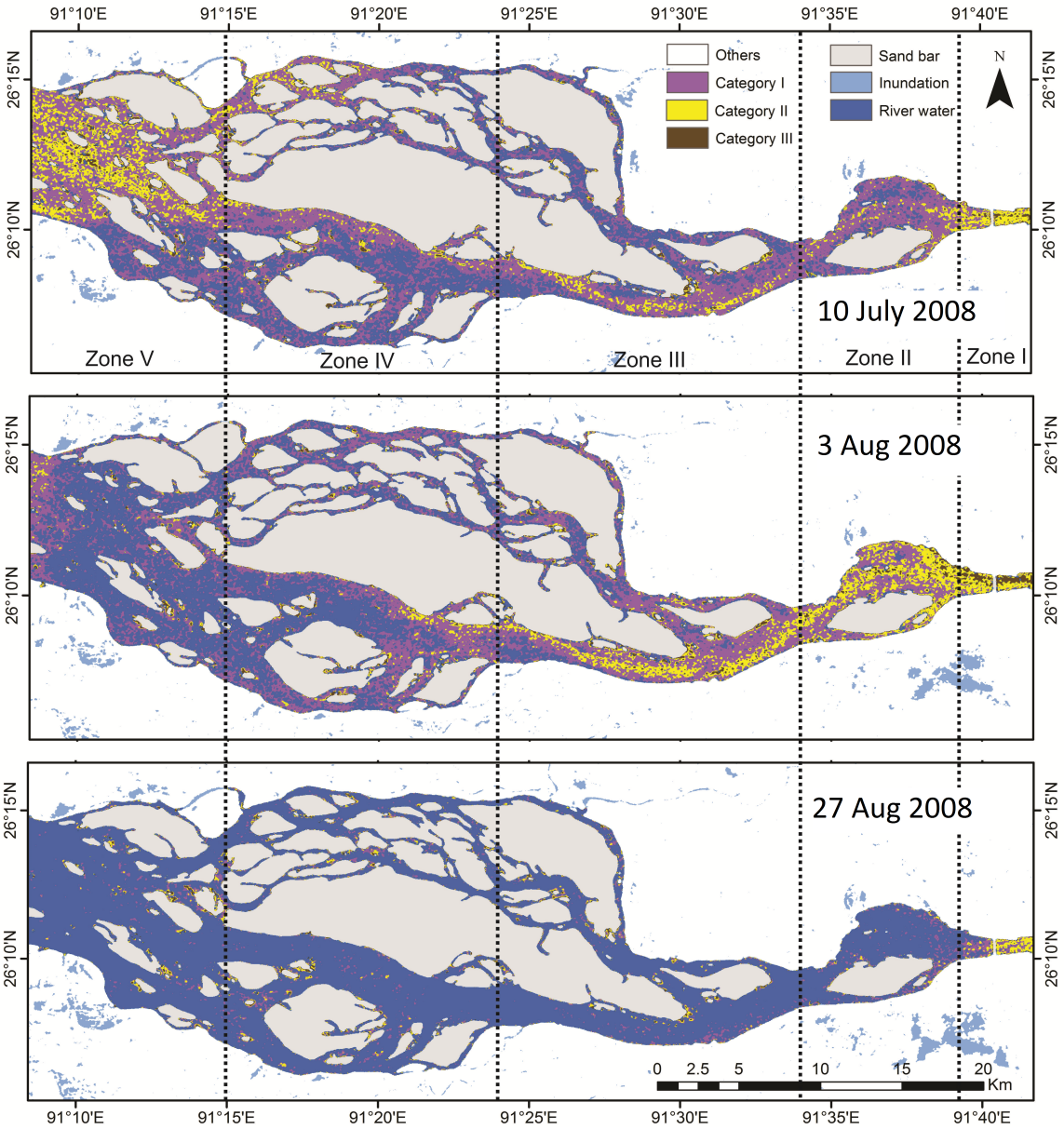

Figure 6.14: Classified images of year 2008 for different morphological features present in the river.

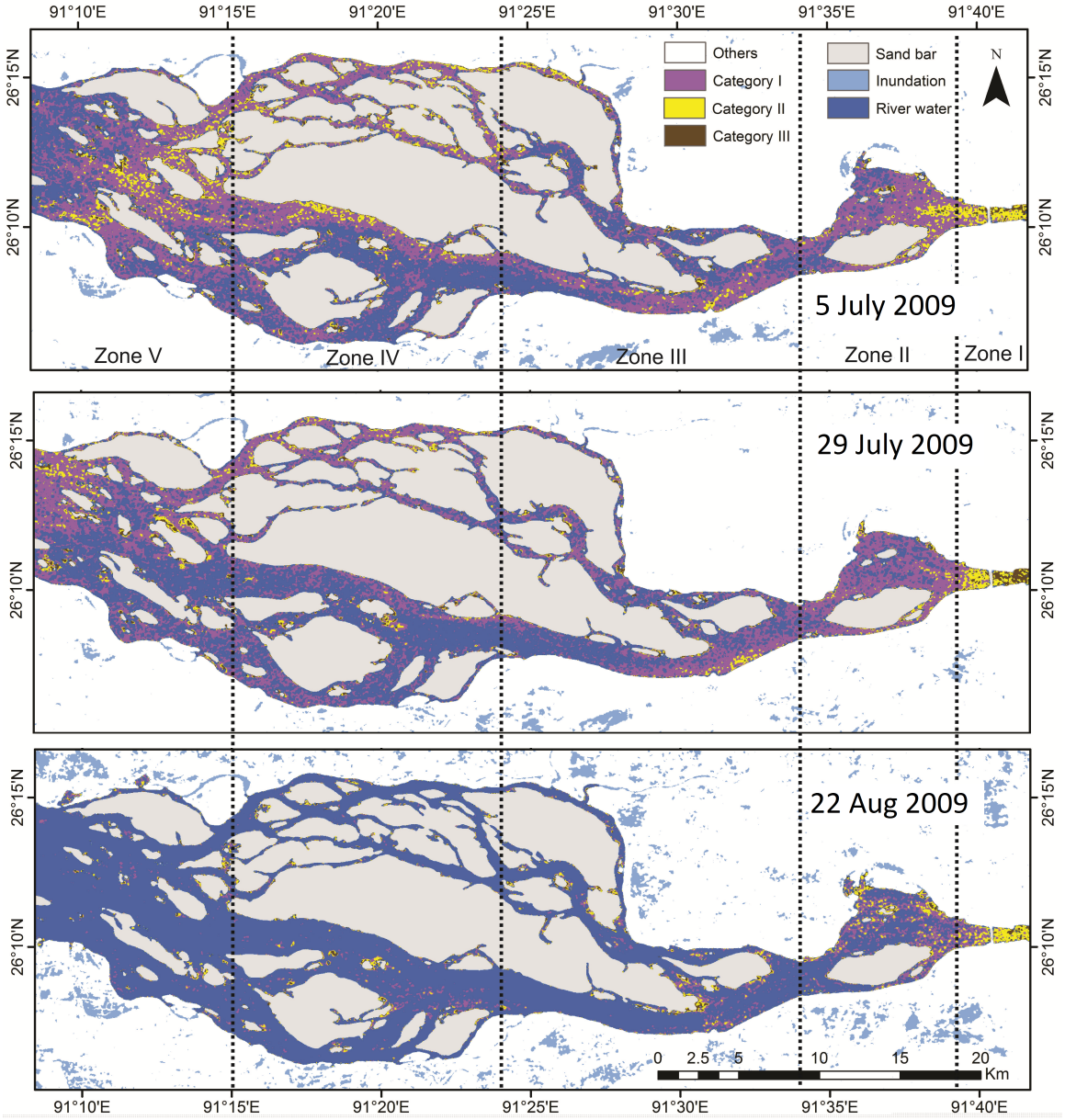

Figure 6.15: Classified images of year 2009 for different morphological features present in the river.

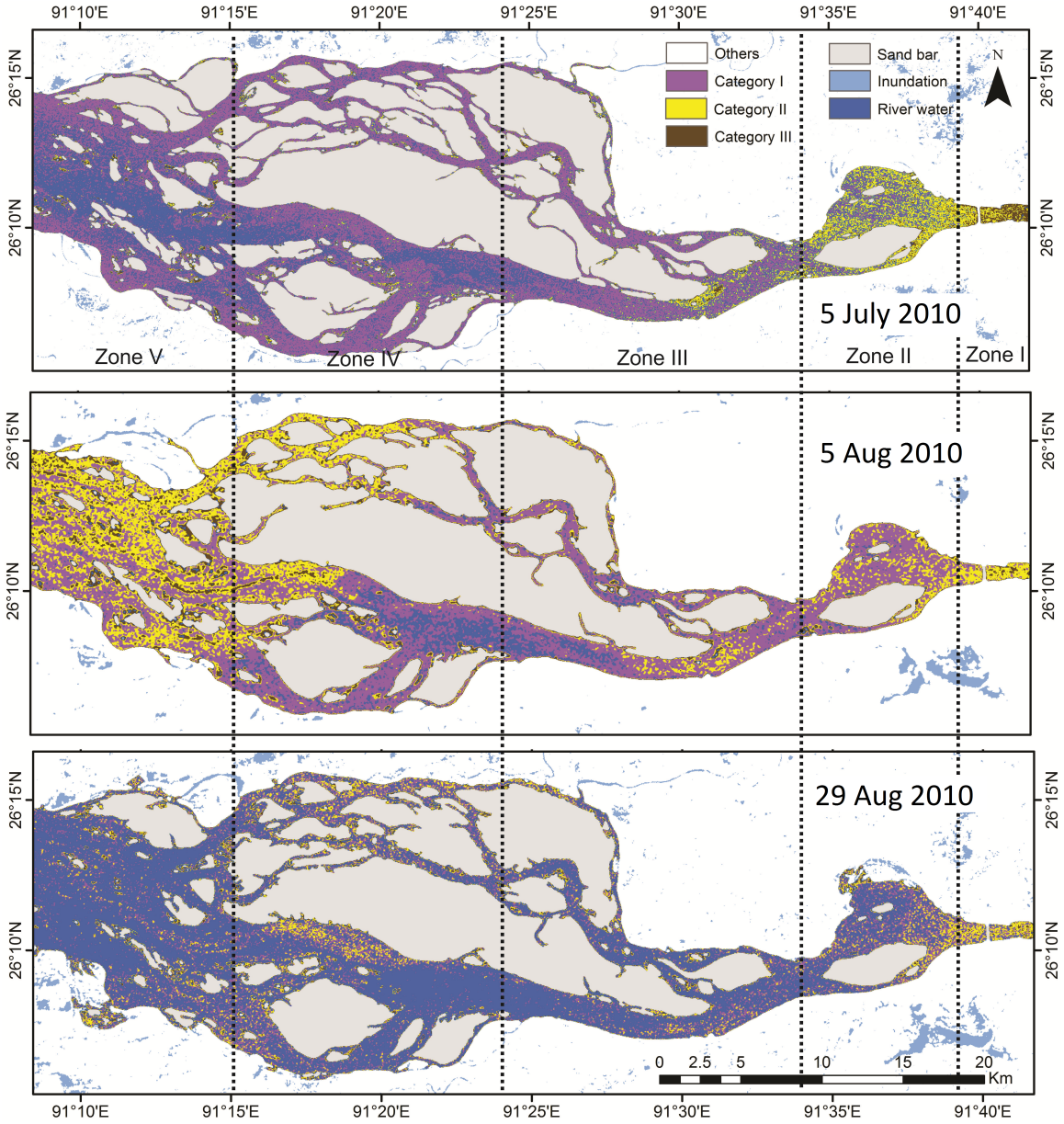

Figure 6.16: Classified images of year 2010 for different morphological features present in the river.

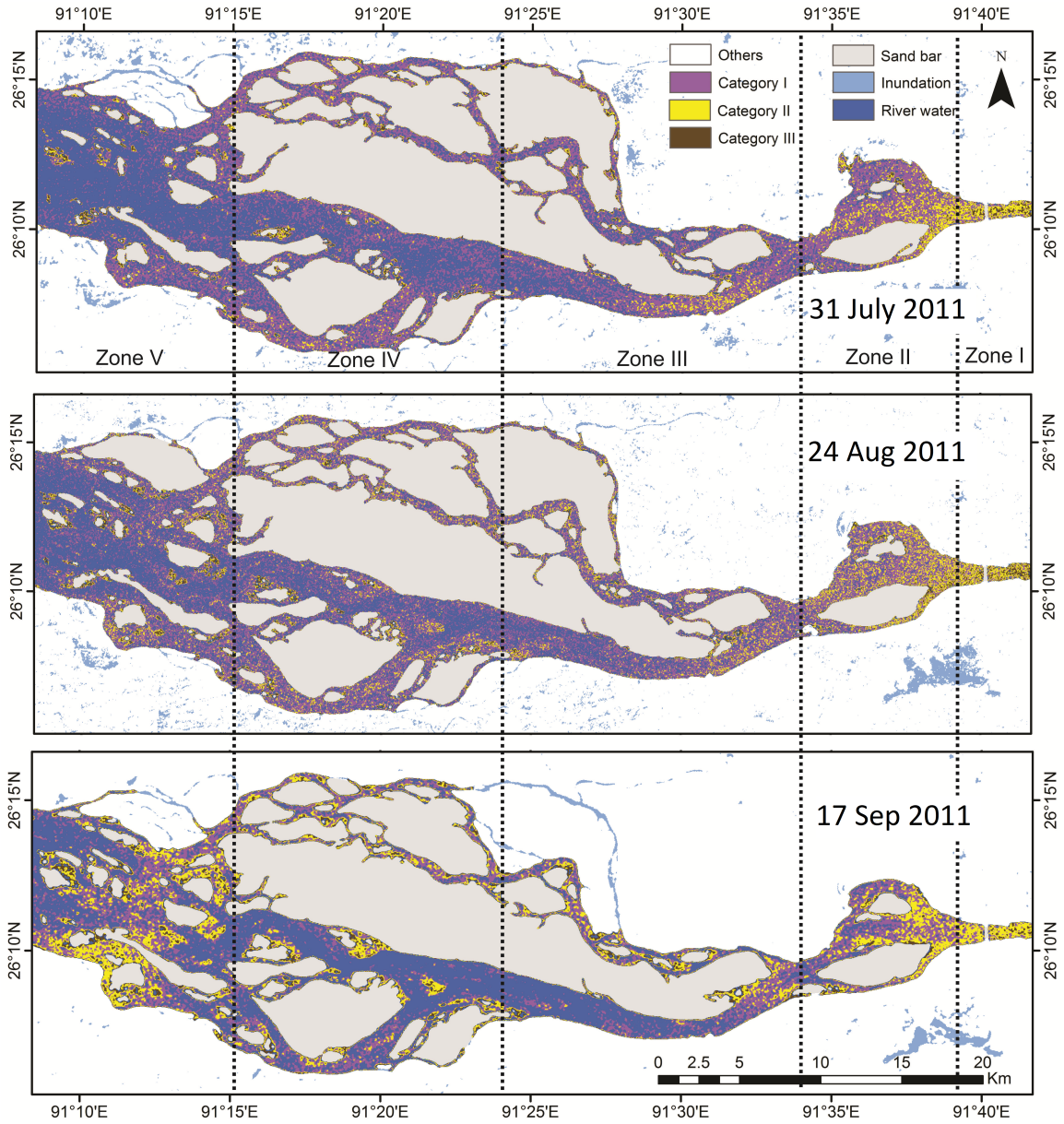

Figure 6.17: Classified images of year 2011 for different morphological features present in the river.

braided loop formation was morphologically active zone during the rising phase of monsoon discharge. The process of side bar formation could be observed from year 2008 to 2011. In Zone–III the river bend with a 2.5 km width shows its thalweg line formations in the initial phase. The thalweg line was near the outer bend, in the month of August. In the month of September morphologically active zones were not observed. The Zone–IV which was the braided loop with divergence of channels at the bar tip and presence of fragmented bars. Rising phase of the monsoon discharge clearly indicate the bank erosion process at the northern side of the bar and bar depositions. Scouring and depositions were happening at bar periphery. In the Zone–V there were fragmented bars in which effective flow width decreased and discharge intensity increased. Morphological active features were present in the river during this period. The fragmented bar zones were found to be an active morphological processes in narrow and shallow channels present in this zone.

6.6 Conclusions

Microwave satellite images provide vital information on morphological active zones during the monsoon period. The in-season variation was analyzed with microwave satellite images of different polarization and different time periods. In the sand bed braided rivers such as the Brahmaputra the intra-seasonal variation causes more morphological changes in the river. The flood waves of different interval causes the morphology to adjust itself with increased discharge and sediment flux during the monsoon season (Figure 1.6). Microwave images sensitive to surface roughness were able to capture the different morphological active features present within the river. The river morphological features such as sand bar, erosion zone, deposition zone, bank erosion and sediment mixing remain active during the monsoon season. These features create different signatures in the microwave images based on the backscattering coefficient. The signature analysis of different morphological features were performed based on the river survey with synchronized satellite passes over the middle reach of the Brahmaputra river. With the help of signature analysis it was found that morphologically active group (bank erosion zone, sand deposition zone and turbulent zone) and others such as river water, sand bar and flood–plain inundation were separable using HH polarization. However, within the morphologically active group different zones (bank erosion zone, sand deposition zone and turbulent zone) were not separable in both HH and HV polarization. The microwave satellite images of HH polarization were found to be suitable to identify the morphologically active zones within the monsoon period as compared to HV polarization. In order to separate the morphologically active features within the river, the radar backscattering coefficient was divided into three different categories and the river reach was divided into five different zones based on morphological characteristics

TH-1911_10610425

of the river. The microwave satellite image segmentation was done based on the different categories of backscattering coefficient representing the variation of turbulence level present within the river. These zones were then separately interpreted for each category of turbulence level associated to the morphologically active features (bank erosion zone, sand deposition zone and turbulent zone).

TH-1911_10610425

"Science without religion is lame, religion without science is blind."

Albert Einstein (1879 – 1955)
German–born Theoretical physicist

7

HYDROLOGICAL MODELING OF THE BRAHMAPUTRA RIVER

7.1 Introduction

The hydrological modeling is performed over the Brahmaputra river basin to estimate the spatio–temporal variations of discharge. In the Brahmaputra river basin hill–slope runoff generation is the dominant runoff generation process, which includes macropore characteristics of different land use/ land cover of the catchment (Zade and Dutta (2003); Sarkar et al. (2008a); Sarkar et al. (2008b); Beven and Kirkby (1979); Rajyalakshmi and Dutta (2006)). The semi-distributed hydrological model was used to perform hydrological modeling from the period of 1997 to 2015. The model calibration is done from the year 1999 and validation was done for the year 2000 with observed discharge at Guwahati, Pandu gauging station. The model calibration is done for the monsoon and non-monsoon flow periods of the river to capture the flood peaks of different interval. Parameters include relative permeability, rice bund height, macropore capacity and topographic parameters are used for different seasons. The Brahmaputra river has many tributaries joining it at different locations from upstream to downstream. The major tributaries of the Brahmaputra river are Subanshri, Manas, Lohit, Kosi, Dibang, Siang, Jia-bhrali and Dihing. These tributaries contribute majority of Brahmaputra discharge and their response in different time interval, which reflects in discharge of the Brahmaputra river. The flood pulses in the Brahmaputra river are caused due to flashy response of the tributaries, which provides large amount of discharge at different locations of the Brahmaputra river. To perform any hydrodynamic modeling in the Brahmaputra river accurate knowledge of tributary level contribution is

TH-1911_10610425

Table 7.1: Country wise areas of the Brahmaputra basin.

Country	Drainage area (km^2)
1. Tibet	29300
2. Bhutan	45000
3. India	194413
(I) Assam	81424
(II) Arunachal pradesh	70634
(III) Nagaland	10803
(IV) Meghalaya	11667
(V) Sikkim	7300
(VI) West Bengol	12585
4. Banglaesh	4700

utmost important. To understand morphological variation in the Brahmaputra river the hydrodynamic variation needs to be understood and estimated accurately. The RISE model (Zade and Dutta (2003); Mishra et al. (2008); Ghosh and Dutta (2012); Dutta and Ghosh (2012); Sarkar et al. (2008a)) is used to estimate flood wave response of the Brahmaputra river. The simulated discharge has very well captured the flood waves as compared to the observed discharge for the period of year 2000 to 2010. It should be noted that discharge simulations were performed at daily time step and observed discharge was available for the 10 day interval. The simulated discharge were used in the hydrodynamic modeling for the Brahmaputra river as the tributary level discharges are well captured through hydrology model.

7.1.1 Flood–wave characteristics of the Brahmaputra river

The intense monsoonal rainfall spells frequently occur over the basin during the pre–monsoon and monsoonal seasons. These intense spells of rainfall cause fast hydrological response in the form of flood waves. Due to its large contributing area with dense drainage network the flood wave prevails for a longer duration with significant flood lift. Typical stage hydrograph of the river the Brahmaputra river at Guwahati gauge station during a monsoon period is presented in the Figure 7.1. In this hydrograph seven distinct flood waves can be noticed. The hydrograph characteristics are found to be similar over the observed years and can be separated into two components, namely flood waves and monsoonal response. The flood waves are found to be the fast hydrological response caused by the clustered rainfall spells in the river basin. The other component is the average response of the monsoonal rainfall distribution. From such a typical hydrograph, flood wave characteristics such as duration of the individual flood events (T_d), arrival time of the waves (T_i), time to peak (T_p) and maximum flood lift can be estimated using the time series of discharge

TH-1911_10610425

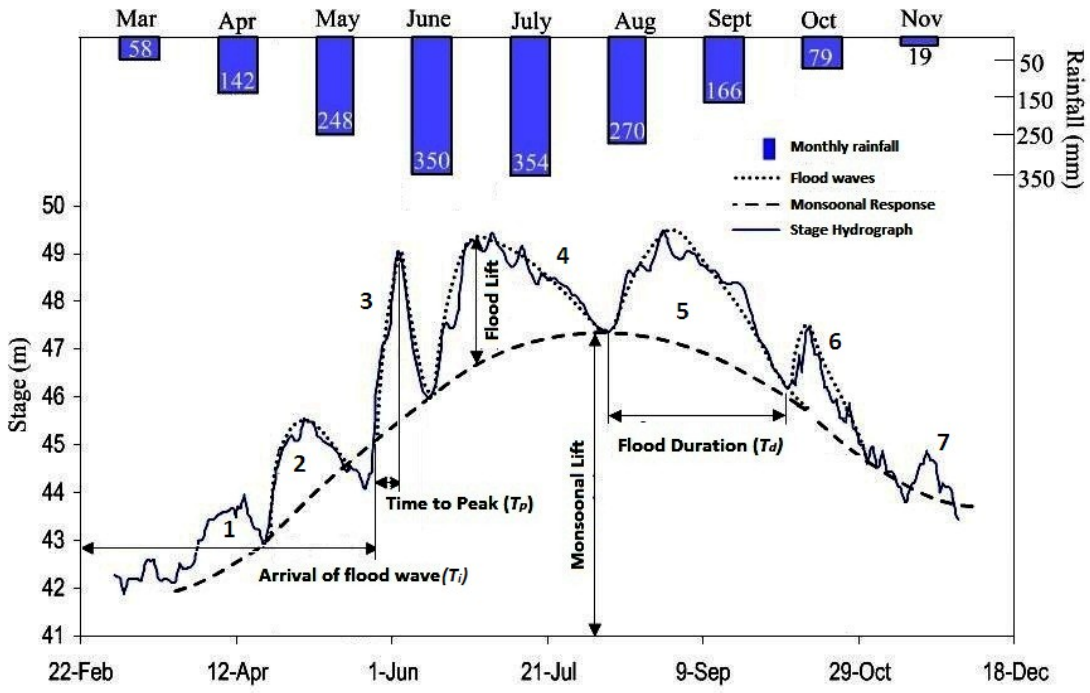

Figure 7.1: Illustrative diagram showing different characteristics of flood waves in the Brahmaputra river (Karmaker and Dutta, 2010).

data. On average the river Brahmaputra experiences 4 to 5 major flood waves, in addition to the normal monsoonal response, annually during the monsoon months (Karmaker and Dutta (2010)).

7.2 Hydrological Model description

RISE, Rice Irrigation System Evaluation, a physically based semi distributed rainfall-runoff and sediment transport model, describes all the physically-based processes involved in a rice-agriculture and/or vegetated hillsope dominated watershed. It works on different hydrological similarity classes (HSC). The delineation of the HSC's are based on soil type distribution and land use/land cover type. For each HSC class, runoff generation processes have been conceptualized. Various hydrological processes such as infiltration, overland flow, surface water budgeting, sub-surface water budgeting, and channel flow are described with physically based equations. A detailed formulation of each hydrological process used in the model is described in Mishra et al. (2008) (given in Appendix-A).

The model requires three different types of input dataset:

TH-1911_10610425

1. Spatial data
2. Time series data
3. Parameters

The spatial input data includes digital elevation model (DEM)(Figure 7.2) , flow direction, flow accumulation, land use/ land cover distribution, rainfall distribution, soil distribution (Figure 7.5) and cumulative topographic index (CTI) (Figure 7.4) of the watershed. While, the precipitation and temperature data are to be given as time series data. Apart from that the model has to be provided with a number of input and calibration parameters defining rainfall-runoff processes. The input rainfall data was used from Indian Meteorological Department (IMD) 0.25 degree grid data product for entire India. The IMD rainfall from 1997 to 2013 were used for model simulations and the TRMM Gsmap data was used for the period of 2014 to 2015. There are the following simulation categories.

- Average budgeting components at the outlet of the basin.
- Budgeting components at any computational cell location, and thus the spatial distribution can be obtained.
- Budgeting components for all the computational cell location at any time step, and thus the spatio-temporal distribution can also be obtained.

7.2.1 Input data and parameters

There are a number of input data and model parameters that have been used in the model. Details of those are tabulated in the Table 7.2. The topographic information was obtained from Hydro1K data set for Asia provided by USGS. The elevation data (Figure 7.2) is used to estimate compound topographic index (CTI) (Figure 7.4), slope, aspect, flow-direction, flow accumulation, drainage basins and stream network with spatial spatial resolution of 1 km. In order to define the physical processes occurring in various parts of the basin hydrological similarity classes (HSC) was generated (Figure 7.6). Global land use/land cover data of 300 meters from "European Space Agency- Ionia Glob Cover Portal" (http://ionia1.esrin.esa.int/) was used for this purpose. The land cover types were regrouped into seven land use / land cover classes which have been spatially overlapped with the soil and topography data to delineate four hydrological similarity classes (HSC). The classes were resampled to the grid size of 1000 m used in the simulation. Though, any convenient grid size can be adopted for the model simulations, finer grid sizes increases the computational time considerably. Soil maps (Figure 7.5) of 1:500,000 scale obtained from

TH-1911_10610425

Table 7.2: Input data and model parameters.

Parameter	Name	Source
Static	Topography and Basin Characteristics	Hydro1k database, USGS
	Soil type distribution	NBSS&LUP, India
	Soil parameters	NBSS&LUP, India
	Land use classes	Ionia glob cover portal, ESA
	Average surface storage in paddy field (h)	Calibration parameter
	Degree of impermeability of hardpan formation (r)	Calibration parameter
	Minimum storing depth in macropores (Smax)	Calibration parameter
Dynamic	Exponential transmissivity decay function (m)	Calibration parameter
	Natural logarithm of transmissivity of just saturated soil profile (lnT0)	Calibration parameter
	Initial saturated topographic index (TI)	Hydro1k database, USGS
	Variable advection, diffusion constants (a, b, α ,β)	Computed model parameters
Time Series	Daily observed stage data	CWC, Shillong
	Rainfall distribution	IMD, Pune, India
	Future rainfall and temperature data	IITM, Pune, India

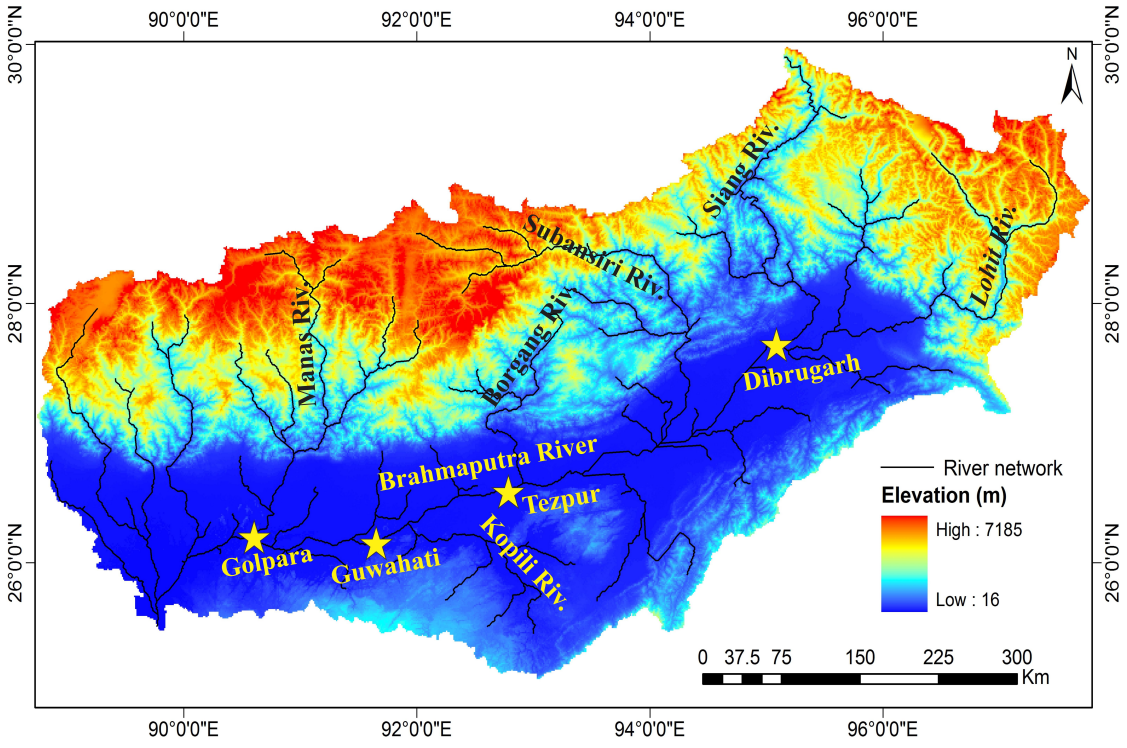

Figure 7.2: Digital elevation model of the study area

TH-1911_10610425

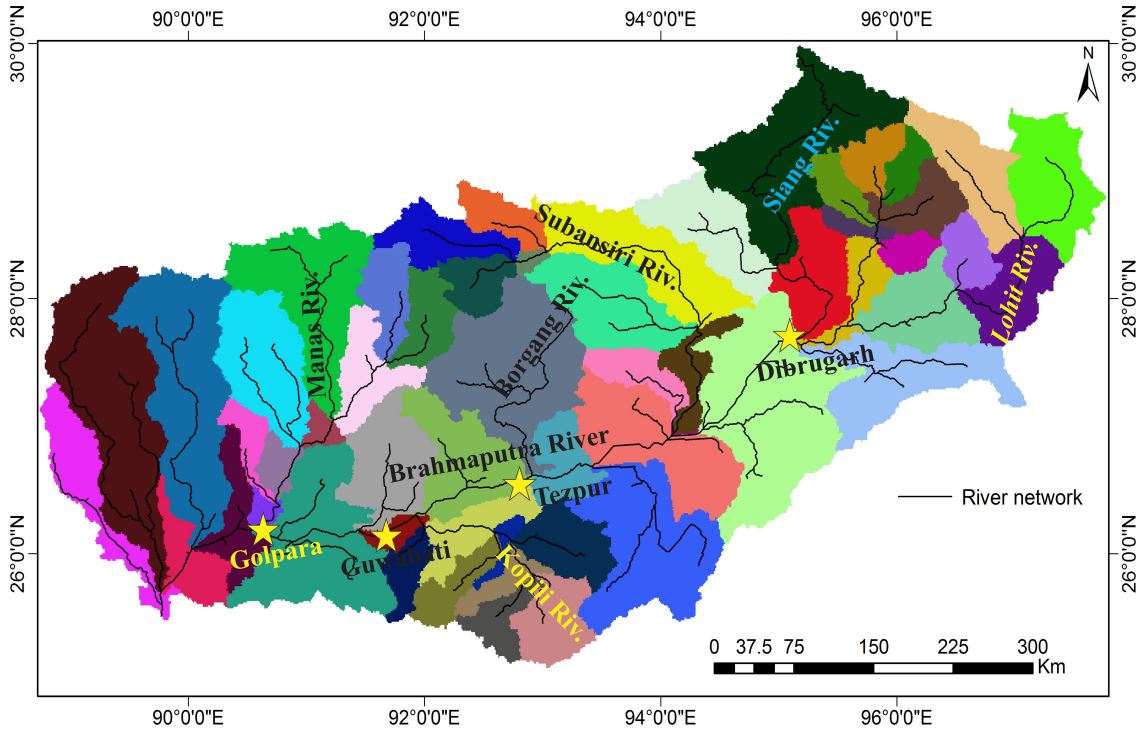

Figure 7.3: Sub basins of the Brahmaputra river and its tributaries

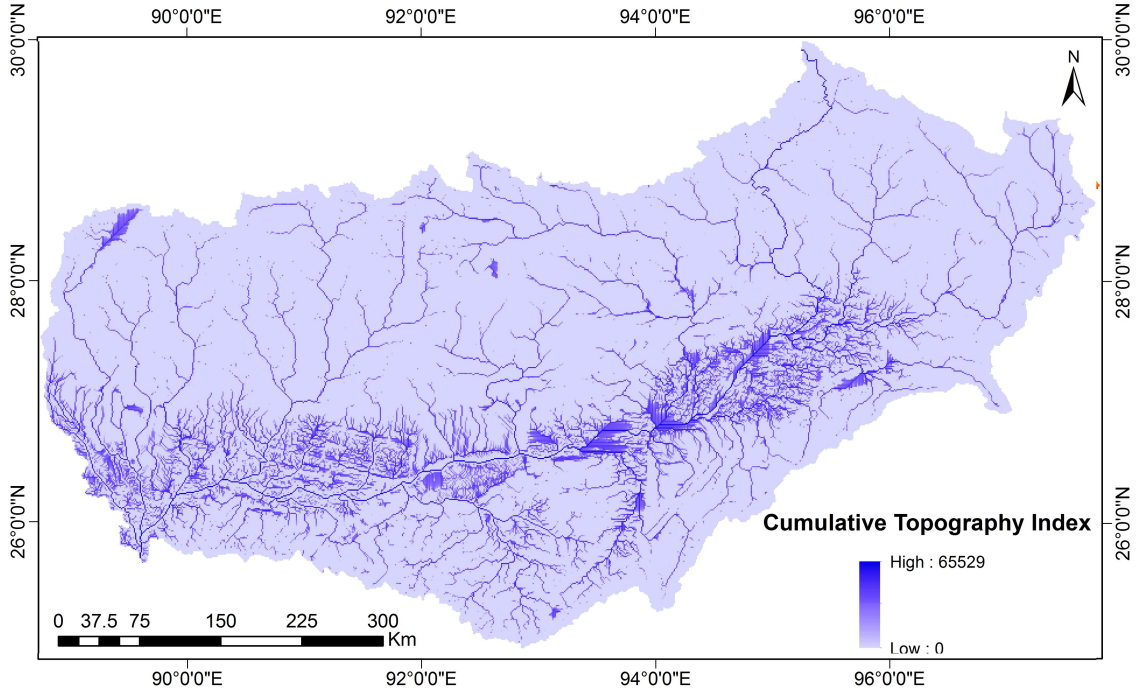

Figure 7.4: Cumulative topographic index of the study area.

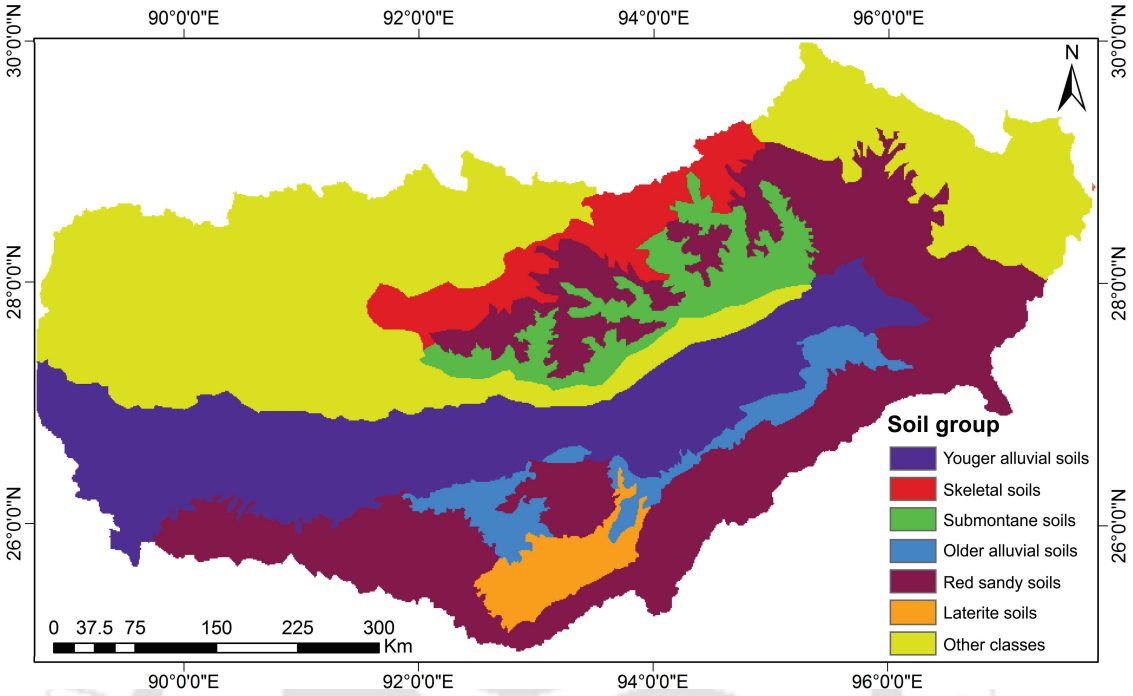

Figure 7.5: Soil map of the Brahmaputra basin.

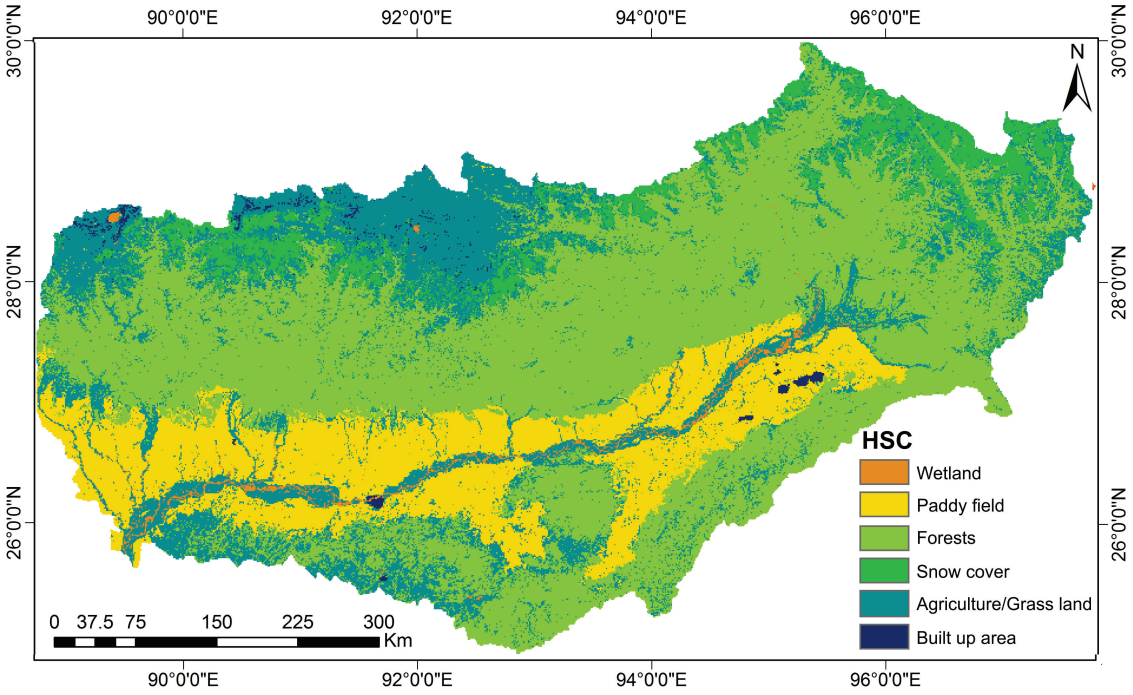

Figure 7.6: Major land use/ land cover classes (regrouped to hydrological similarity classes) of the study area

Table 7.3: Calibrated Parameters

Calibration parameters	Calibrated value (monsoon)	Calibrated value (non-monsoon)	Range
Average surface storage in paddy field (hret)	0.2 m	0.2 m	0-0.5 m
Degree of impermeability of hardpan formation (r)	1200	4000	700-5000
Maximum storing depth in macropores (Smax)	0.1 m	0.1 m	0.03-0.9 m
Exponential transmissivity decay function (m)	0.1	0.035	0.002-0.4
Natural logarithm of transmissivity of just saturated soil (lnT0)	0.001	0.01	0-1.6

National Bureau of Soil Survey and Land Use Planning, India (NBSS and LUP) was used to generate the soil distribution zones within the watersheds. The daily rainfall data of 0.25 x 0.25 degree resolution from Indian Meteorological Department (IMD) was used in this study. The simulations with uniform grid size of 1 km and a simulation time step of 24 hour was adopted. The time step of 24 hour was found to be sufficient for capturing time scales of important flood characteristics, such as time of peak flow (average 7 days), duration of the flood waves (average 15 days) etc. In order to eliminate the possible deviations due to the initial conditions, the simulation was started well before the pre–monsoonal season.

7.2.2 Model calibration and performance evaluation

Different model calibration parameters were adjusted manually for the river basin. The monsoon and non–monsoon seasons of the year 1999 was considered as the calibration period. The available discharge data in Guwahati of the Brahmaputra reach was used for the model calibration. A number of different sets of simulations and comparison with observed data were performed to estimate the calibration coefficients. The calibration parameters, their range and calibrated values are given in the Table 7.3. The Figure 7.7 represent the observed stage hydrograph at Guwahati gauging station compared with simulated discharge (Q_s) hydrograph. It can be observed that the flood waves have been predicted accurately in terms of arrival of the wave, flood duration and time to peak. The multiple peak of flood waves during the monsoon were reflected in the simulation result Figure 7.7 and Figure 7.9. Comparison between the simulated discharge and observed discharge are presented in the Figure 7.9 and Figure 7.10. It could found that the peak discharges during the highest flood lifts closely matched with the observed discharge of greater than 35,000 m^3/s.

TH-1911_10610425

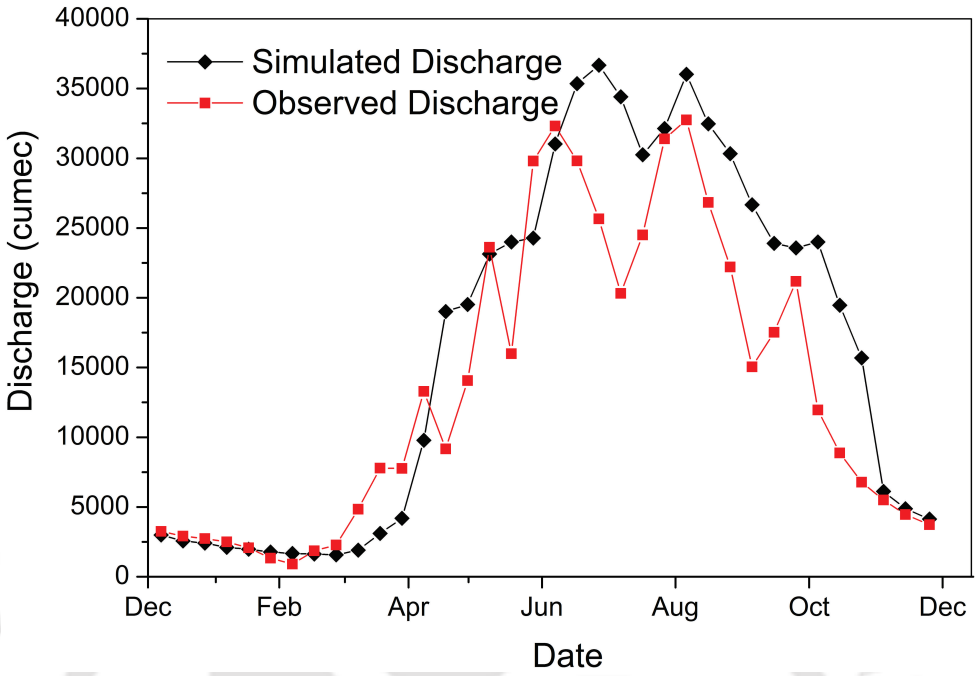

Figure 7.7: Hydrological model (RISE) simulated discharge calibration with observed discharge at Guwahati gauge station for year 1999

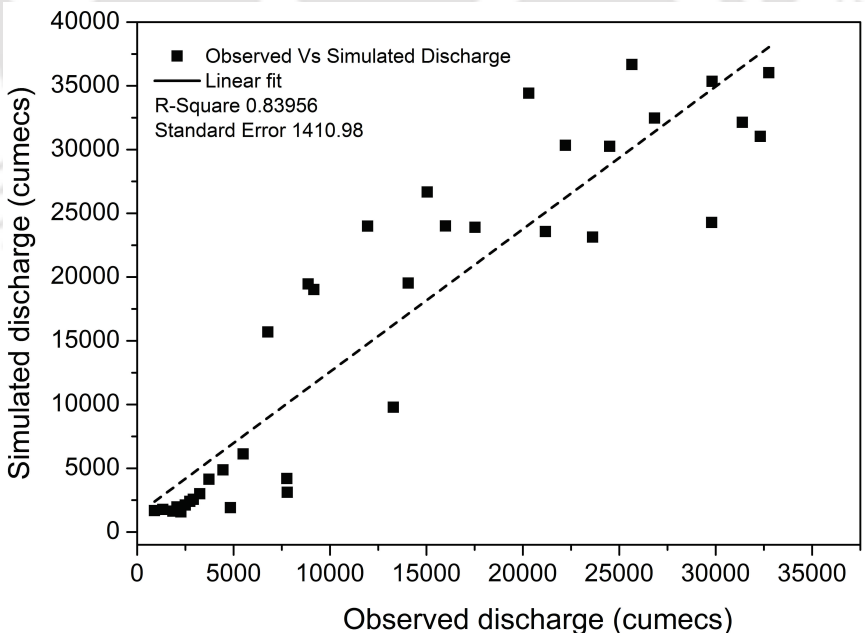

Figure 7.8: Comparison of simulated discharge vs observed discharge at Guwahati gauge station for the year 1999

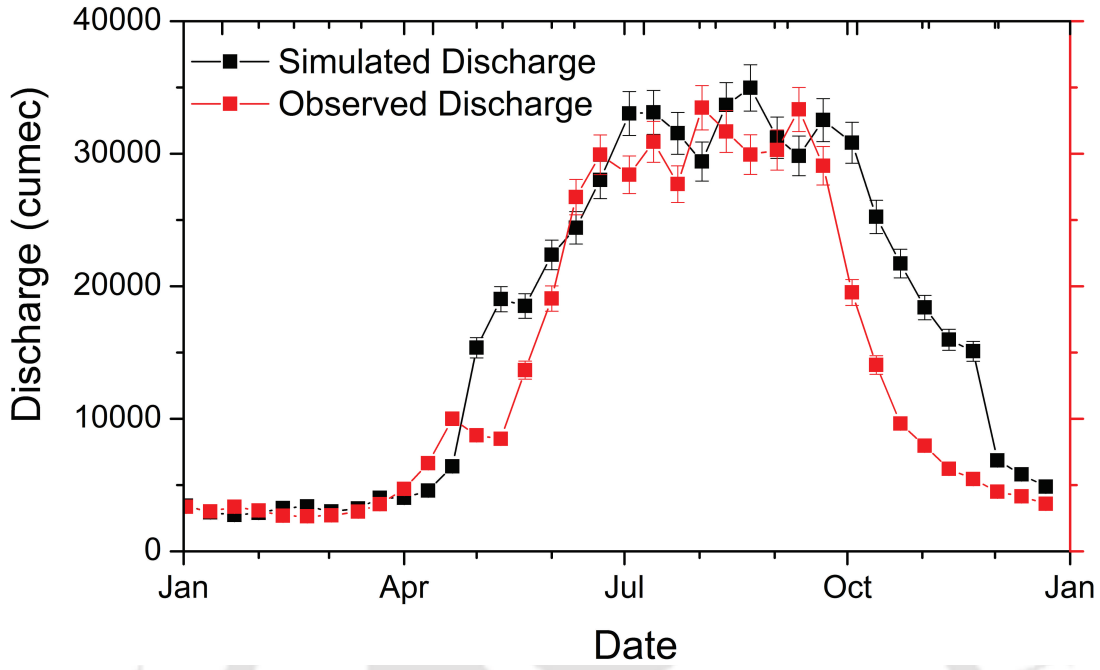

Figure 7.9: Hydrological model (RISE) simulated discharge validation with observed discharge at Guwahati gauge station for the year 2000

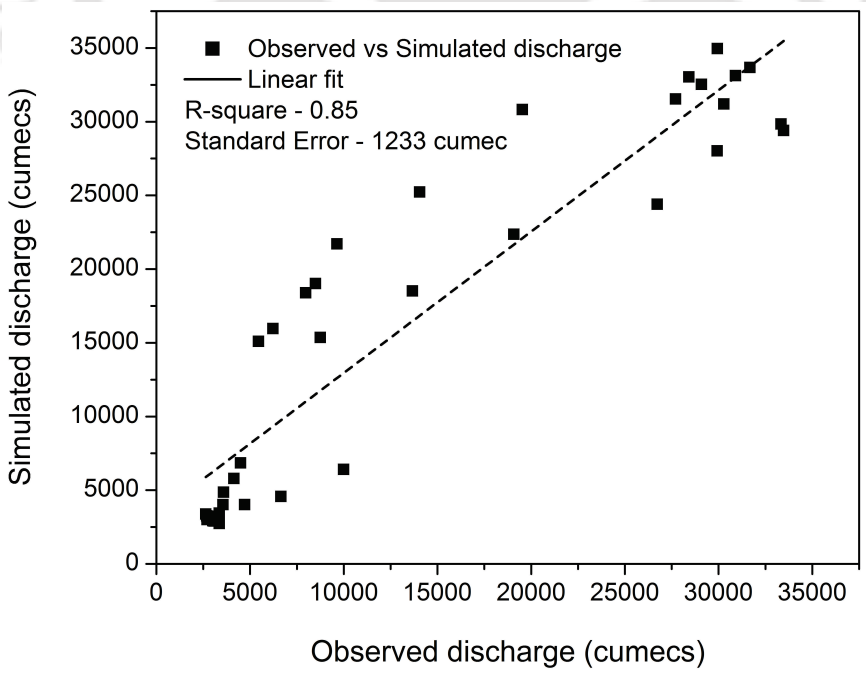

Figure 7.10: Comparison of simulated discharge vs observed discharge at Guwahati gauge station for the year 2000

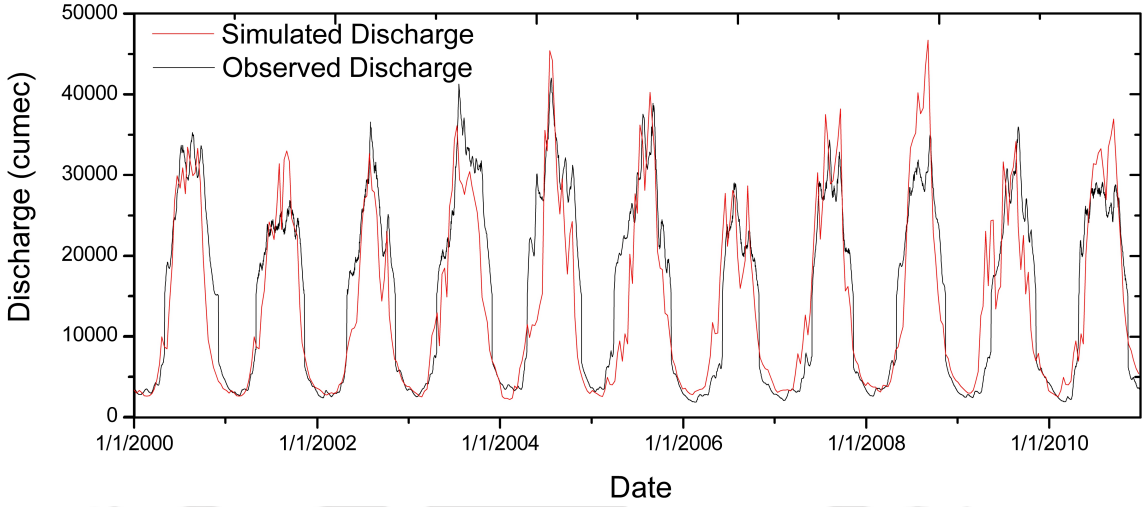

Figure 7.11: Performance evaluation of simulated discharge vs observed discharge at Guwahati gauge station for the period of 1999 to 2010

Table 7.4: Simulated peak discharge of different tributaries of the Brahmaputra river

River (reach)	Simulated peak discharge for the monsoonal season (m^3/sec)							Average discharge (m^3/sec)
	2000	**2002**	**2004**	**2006**	**2008**	**2010**	**2012**	
Subansiri	4969	4988	5813	4102	4926	4136	4985	4963
Jia–bharali	3989	4677	5993	3033	4087	3970	6404	4567
Manas	4841	5004	6692	3619	4904	4409	5213	4938
Kopili	6542	6343	7902	4655	6106	5008	6170	6157
Buri–dehing	3713	3796	4359	4798	4291	3350	3879	4057
Lohit	4102	3926	4880	3719	4065	3558	3982	4070
Siang	3837	4084	4738	3797	4242	3513	3927	4013
Tezpur	28780	29637	34054	24672	28832	24580	28267	28453
Guwahati	35287	36560	42050	32013	35050	29145	34310	34555

TH-1911_10610425

Table 7.5: The Brahmaputra river peak discharge comparison at Guwahati

Year	Peak discharge (m^3/sec)		Difference
	Guwahati (Simulated)	Guwahati (Observed)	
1999	38093	32755	5338
2000	35287	33473	1814
2001	26825	32976	-6151
2002	36560	32648	3912
2003	41266	36124	5142
2004	42050	45405	-3355
2005	38920	40235	-1315
2006	29013	28657	356
2007	34359	38199	-3840
2008	35050	46707	-11657
2009	35971	34149	1822
2010	29145	36965	-7820

7.3 Results and Discussion

The hydrological simulations were performed for the period of 1997 to 2013. The model calibration was done for the year 1999 and validation for the year 2000. The model validation proved that its performance was good in capturing the discharge hydrograph at Guwahati location with R^2=0.85 and RMSE=1233 cumecs. The long term discharge comparison with observed data reflected that the model could predict the long term hydrological variations for the Brahmaputra river. The tributary wise discharge was also analyzed for 17 years. The Brahmaputra river has many tributaries such as Subansiri, Jia–bharali, Manas, Kopili, Buri–dihing, and Siang. The peak discharge at Guwahati was also compared with observed data. It was observed that peak discharge could be estimated with deviation of 5,000 cumes in most of the cases.

7.3.1 The Brahmaputra river discharge

The discharge hydrogrphs of the main channel of the Brahmaputra river represent the flood waves of different interval occurring during the period of 2004. The simulated discharge was found to be highest during the year of 2004 and 2008, which considered to be high flood years. The flood hydrographs of year 2004 was shown to highlight the flood waves generation in the Brahmaputra river. The Brahmaputra river hydrograph of Jorhat (Figure 7.12), Tezpur (Figure 7.13), Guwahati (Figure 7.14) and Goalpara (Figure 7.15) represent the flood wave propagation from upstream to the downstream of the river. The flood peaks

TH-1911_10610425

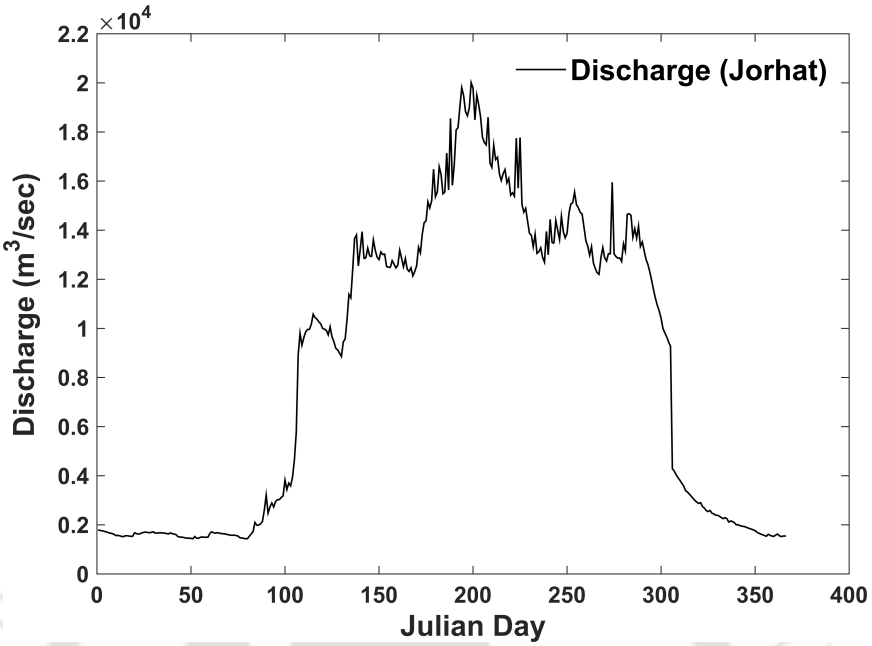

Figure 7.12: Simulated discharge of the Brahmaputra river for year 2004 at Jorhat

were clearly visible during the month of July with flood discharge values vary from 30,000 m^3/sec to 45,000 m^3/sec.

7.3.2 Tributary wise discharge variation

The tributary wise statistics of 17 years (1997 to 2013) of simulated discharge presented the mean and standard deviation of river flow in different tributaries of the Brahmaputra river. The Kopili river contribution was the highest (17.9%) in the Brahmaputra river for the year 2004 as compared to the peak discharge at the Guwahati gauge station. The mean discharge of Kopili river (Figure 7.16) reach up to 5000 m^3/sec with 1000 m^3/sec of standard deviation. The Subansiri river contribute 13.28% to the peak flow and the mean discharge (Figure 7.17) reach up to 4500 m^3/sec with 900 m^3/sec of deviation. The contribution of Manas river was 13.05% to the peak discharge of Guwahati for the year 2004. The mean discharge of Manas (Figure 7.18) remain up to 4000 m^3/sec with 700 m^3/sec of deviation. The contribution of Lohit river to the peak discharge was about 10.68% to the peak flow. The mean discharge of Lohit (Figure 7.19) reach up to 3250 m^3/sec with 500 m^3/sec of deviation in the river flow. The Siang river contribution to the peak discharge at Guwahati was about 10.22% with 17 years mean of 3100 m^3/sec (Figure 7.20) with 450 m^3/sec of deviation from the mean discharge. The Jia–bharali river peak discharge contribution to the Brahmaputra river at Guwahati was about 9.89%. The mean discharge

TH-1911_10610425

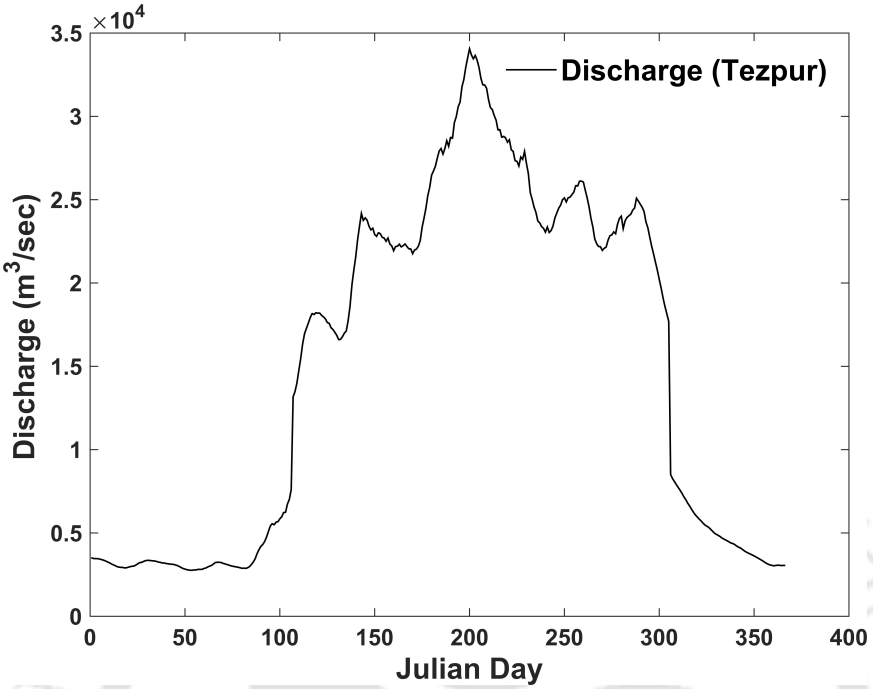

Figure 7.13: Simulated discharge of the Brahmaputra river for year 2004 at Tezpur

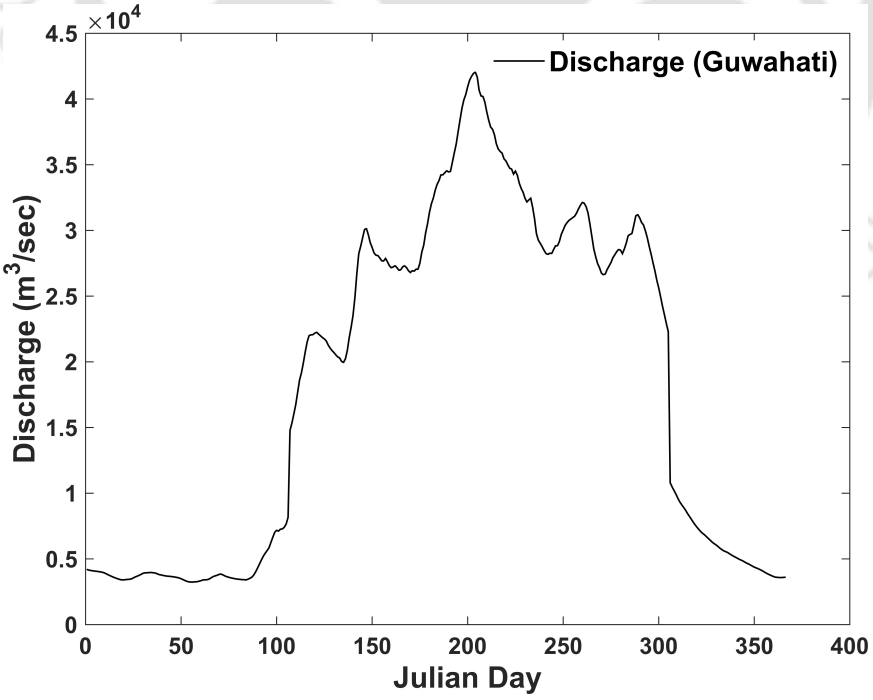

Figure 7.14: Simulated discharge of the Brahmaputra river for year 2004 at Guwahati

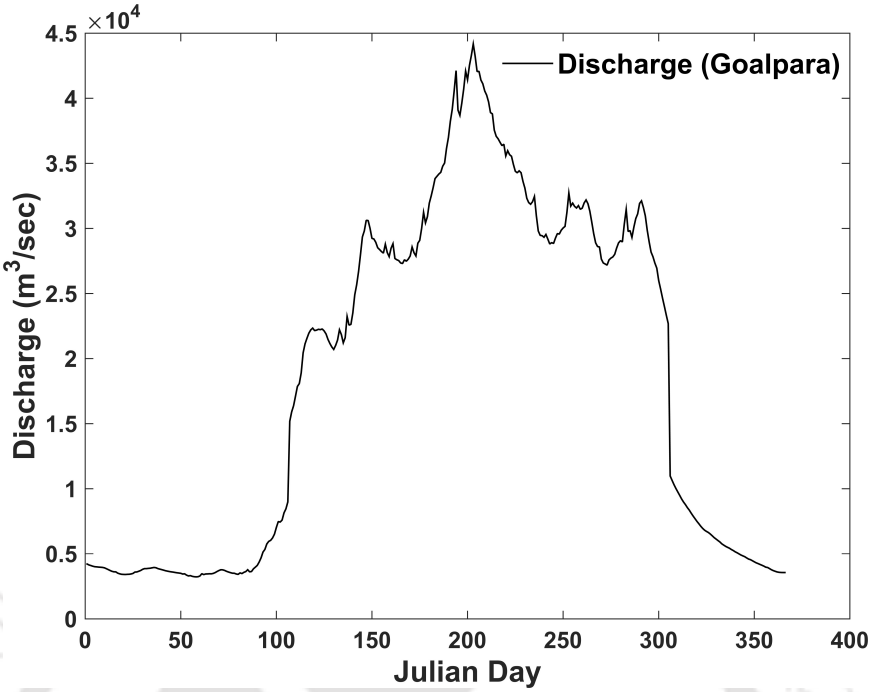

Figure 7.15: Simulated discharge of the Brahmaputra river for year 2004 at Goalpara

has the peak value of 2750 m^3/sec (Figure 7.21) with 850 m^3/sec of deviation from the mean discharge. The peak discharge contribution of Buri dihing river to the main channel discharge at Guwahati was about 9.15%. The Buri–dihing mean discharge (Figure 7.22) of 17 years reaches up to peak value of 2700 m^3/sec with deviation of 700 m^3/sec from mean discharge. These tributaries in combine contribution to the Brahmaputra river about 84.2% of the peak discharge at the Guwahati gauge station.

7.3.3 Monthly discharge variation

The simulated discharge values were averaged at monthly time period. The monthly scale averaging was done to study the river hydrodynamic variations at monthly level, since the altimetry derived hydraulic variables were available at monthly scale. To evaluate the model performance all the variables were brought to monthly scale, discharge hydrograph at different locations of the river were averaged at monthly scale to provide the spatio–temporal discharge variability in the hydrodynamic modeling. The monthly discharge hydrograph shown in the (Figure 7.23 and 7.24) indicate the seasonal variation in the flow hydrograph at Guwahati gauge station for the year 2014 and 2015. The monthly discharge peaks vary from 30,000 m^3/sec to 37,000 m^3/sec during the months of June to September. These monthly values indicate change in the water depth of the river at different reaches. The

TH-1911_10610425

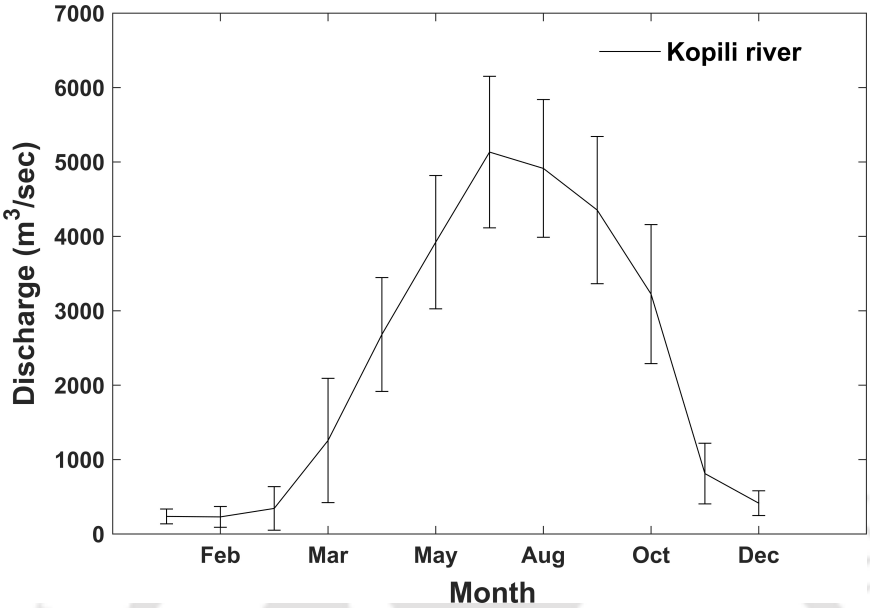

Figure 7.16: Monthly mean and standard deviation of Kopili river for the period 1997 to 2013

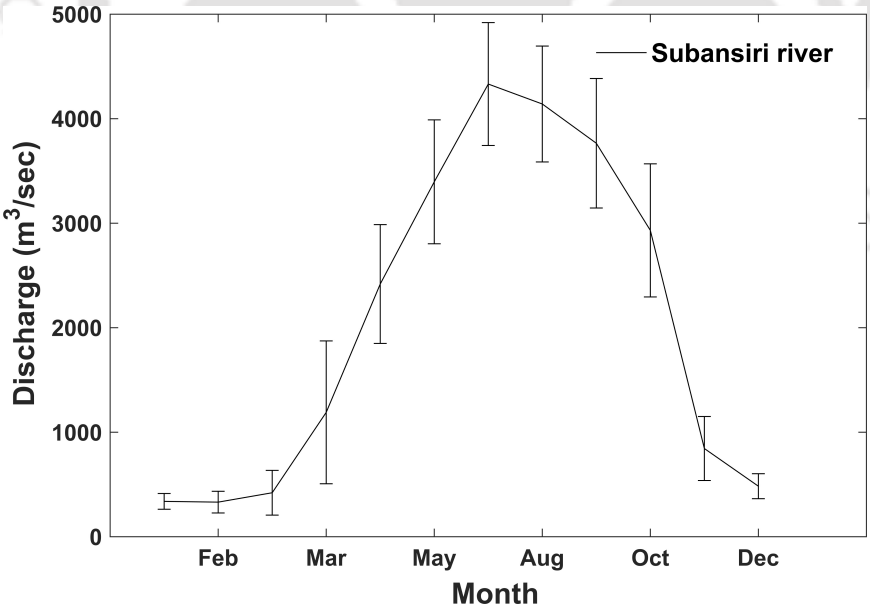

Figure 7.17: Monthly mean and standard deviation of Subansiri river for the period 1997 to 2013

TH-1911_10610425

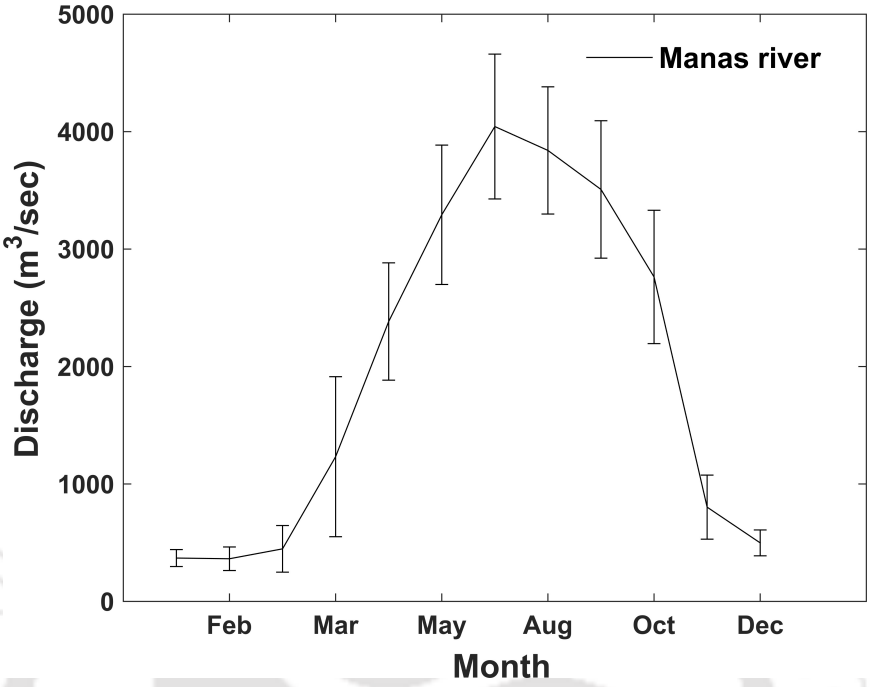

Figure 7.18: Monthly mean and standard deviation of Manas river for the period 1997 to 2013

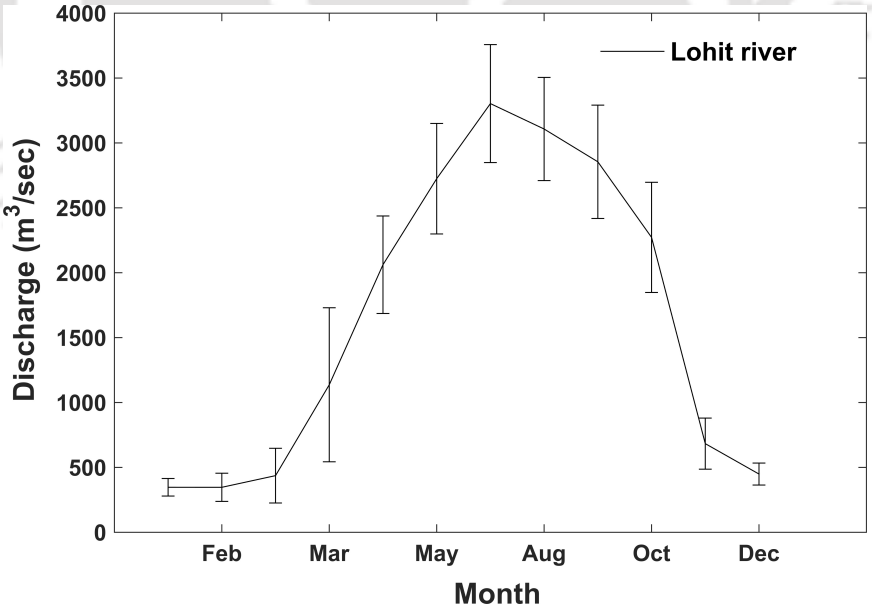

Figure 7.19: Monthly mean and standard deviation of Lohit river for the period 1997 to 2013

TH-1911_10610425

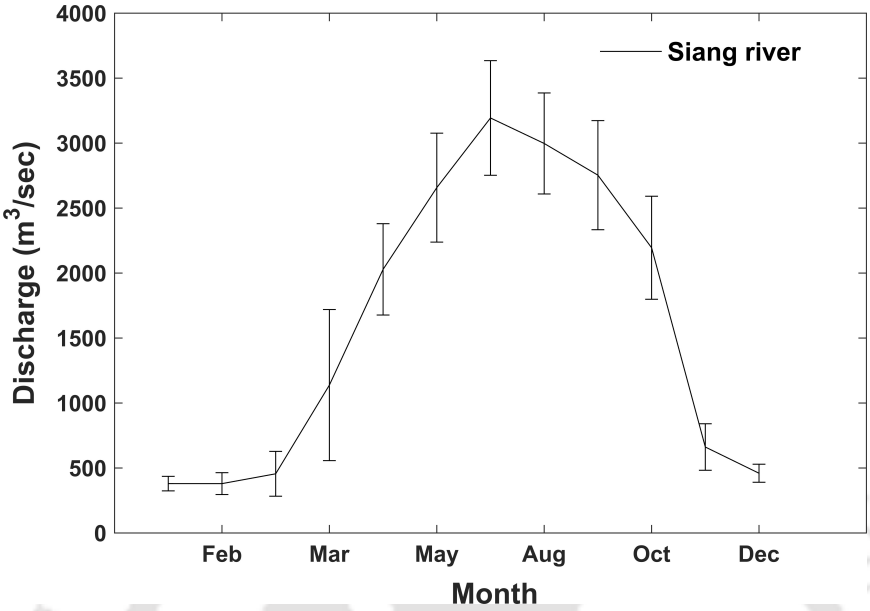

Figure 7.20: Monthly mean and standard deviation of Siang river for the period 1997 to 2013

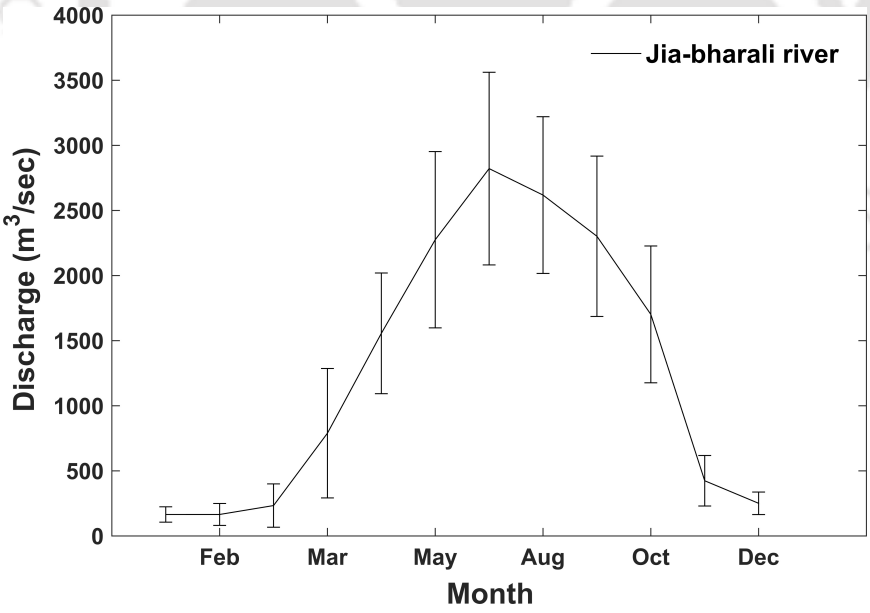

Figure 7.21: Monthly mean and standard deviation of Jia–bharali river for the period 1997 to 2013

TH-1911_10610425

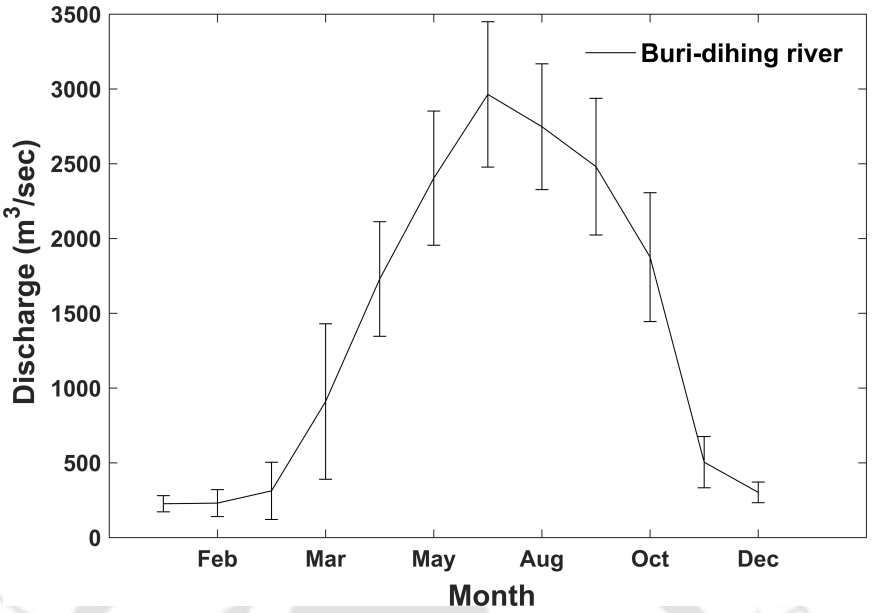

Figure 7.22: Monthly mean and standard deviation of Buri–dihing river for the period 1997 to 2013

lean flow was 2,500 m^3/sec to 5,000 m^3/sec during the month of January to March and November to December.

7.4 Conclusions

The hydrological modeling of the Brahmaputra river was done to estimate the spatio–temporal variations of river discharge. The model simulations were preformed for the period of 1997 to 2015. To setup the hydrological model different input parameters were used such as DEM, soil type, land use land cover, temperature and rainfall. The model calibration was done for the year 1999. The calibration of simulated discharge was performed with the Guwahati gauge observed discharge data. The model calibration was done for the Brahmaputra river. The unavailability of tributary discharge could not make it possible to calibrate the model at tributary scale. The different calibration parameters were used in the model. The model was calibrated for monsoon and non–monsoon seasons separately. The model validation was performed for the year 2000. It was found that the simulated hydrographs could be able to capture the seasonal and as well as flood pulses of different interval. However, the rising and receding phases of the simulated discharge was gradual as compared to observed discharges at the Guwahati. The performance of simulated discharge was statistically satisfactory with R^2=0.85 and RMSE=1233 m^3/sec. The discharge hydrograph of the main channel of the Brahmaputra river was analyzed and it was found that

TH-1911_10610425

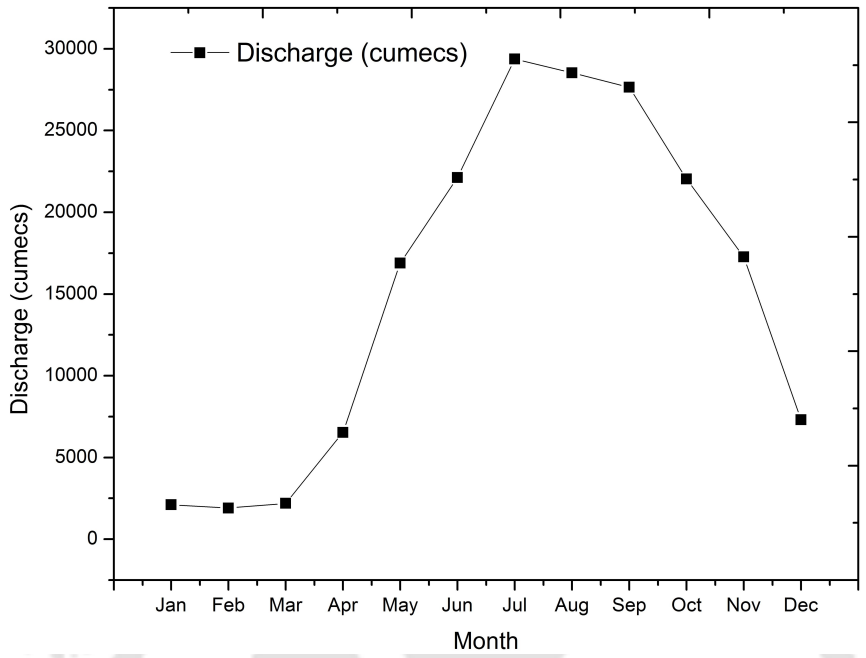

Figure 7.23: Monthly discharge variation of the Brahmaputra river at Guwahati for the year 2014

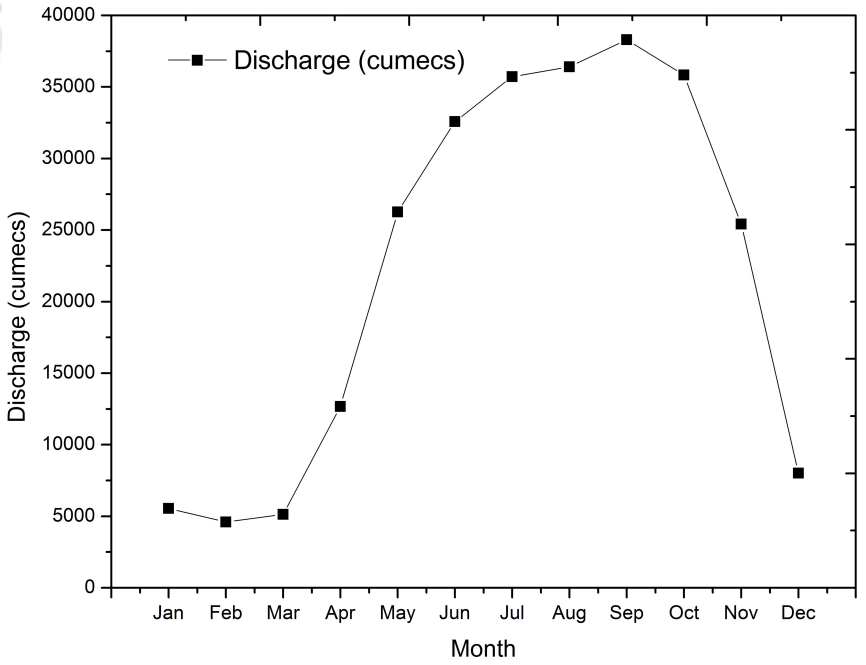

Figure 7.24: Monthly discharge variation of the Brahmaputra river at Guwahati for the year 2015

flood pulses at different locations from upstream to downstream were simulated with their occurrence at different time interval. The tributary wise discharges were also analyzed for the period of 1999 to 2015. It was found that the different tributaries in the Brahmaputra river contribute approximately 9% to 15% of annual flow in the Brahmaputra river. The peak discharge contribution of each tributary was estimated for the year 2004. The mean discharge and its deviation was estimated for each tributary for the period of 17 years. The peak values for mean discharge vary from 2,700 m^3/sec to 5,000 m^3/sec during the monsoon month. The monthly scale discharge will be used in the hydrodynamic modeling of the Brahmaputra river to generate the monthly water surface profiles for the period of 2013 to 2015.

TH-1911_10610425

TH-1911_10610425

"An expert is a person who has made all the mistakes that can be made in a very narrow field."

Niels Bohr (1885 – 1962)
Danish Physicist

8

HYDRODYNAMIC MODELING: SATELLITE ALTIMETRY AND DISCHARGE DATA ASSIMILATION

8.1 Introduction

To understand the basin level river characteristics hydrological simulations were performed using a hydrological model. The hydrological model used was a physically based semi distributed rainfall-runoff model, describes all the physically-based processes involved in a rice-agriculture and vegetated hillsope dominated watershed Mishra et al. (2008). It was simulated from 1997 to 2015. The spatio–temporal discharge variation at different reaches were averaged at monthly level. The monthly averaged discharge of 2013 was used for one dimensional flow routing from Dibrugarh to Dhrubri using HEC-RAS. The satellite altimetry derived monthly water surface profiles were used to estimate reach wise roughness variation. The water level retrieval was done over 10 different locations of the river, with return period of 35 days, hence monthly water levels were available at different locations. These water levels were used to estimate seasonal water level difference and water surface slopes for the different reaches of the river. The seasonal difference in water level depths and the slopes at different reaches of the river were used to estimate seasonal Manning's roughness coefficient. The Manning's roughness coefficients were assimilated in to the HEC-RAS model and the steady flow simulations were carried out for the middle reach of the Brahmaputra river.

TH-1911_10610425

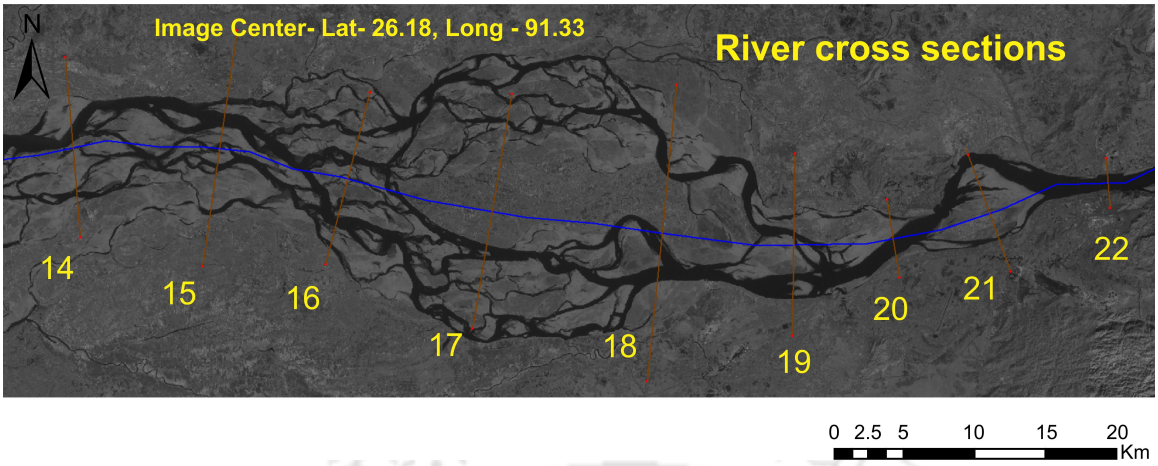

Figure 8.1: HEC-RAS model setup showing cross sections from 14 to 22 in the middle reach of the Brahmaputra river.

8.2 Hydrodynamic model setup

Hydrodynamic modeling was done in the middle reach of the Brahmaputra river. To perform the hydrodynamic simulations, HEC–RAS model was used. It is a one–dimensional model frequently used for steady and unsteady flow simulations. The spatio–temporal simulations of discharge was used in the model for steady flow simulations. The tributary and main river simulated discharge was given as an input to the model. The observed water level at Dibrugarh and Dhubri were given as the upstream and downstream boundary conditions. The 58 cross sections (Figure 8.2 and Figure 8.3) at about 10 km interval were used for geometry data setup (8.1). The total river reach of about 560 km was considered for model simulations. The Manning's roughness coefficient were also estimated using altimetry derived hydraulic properties of the river and from different empirical equations. The model simulations were performed for monthly averaged discharge to predict the monthly water surface profiles.

8.3 Estimation of Manning's roughness coefficient

To perform hydrodynamic simulations of the Brahmaputra river, reach–wise Manning's roughness coefficient (n) estimation was done. The Manning's roughness coefficient was estimated using hydraulic properties derive from satellite altimetry for different reaches of the river. The hydraulic parameters of the river include water levels, seasonal water level difference and water surface slopes at different reaches of the river. These parameters were used in Equation 8.1 given by Jarrett and Petsch (1985), for Manning's roughness coefficient

TH-1911_10610425

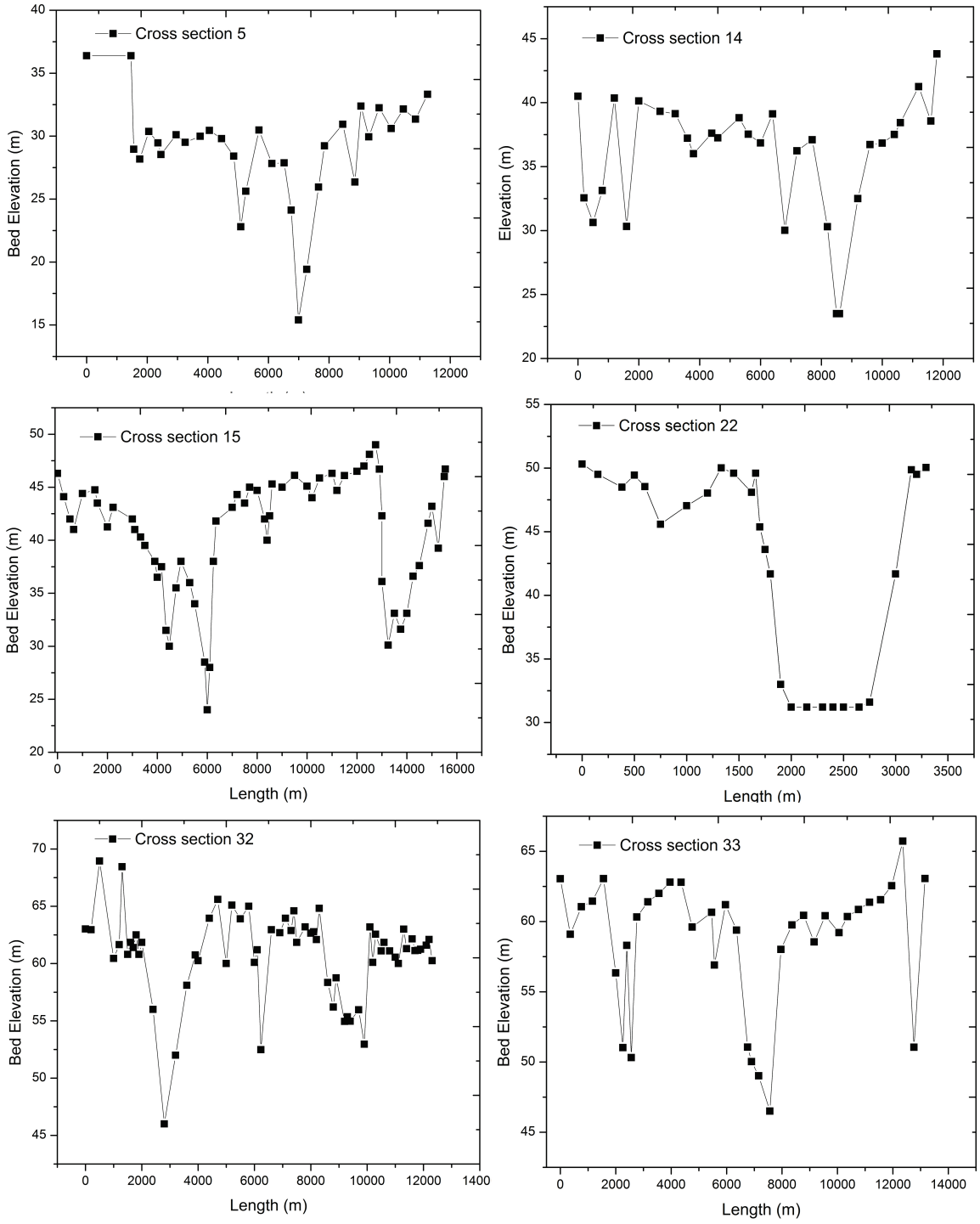

Figure 8.2: Cross section variations in cross sections 5 to 33.

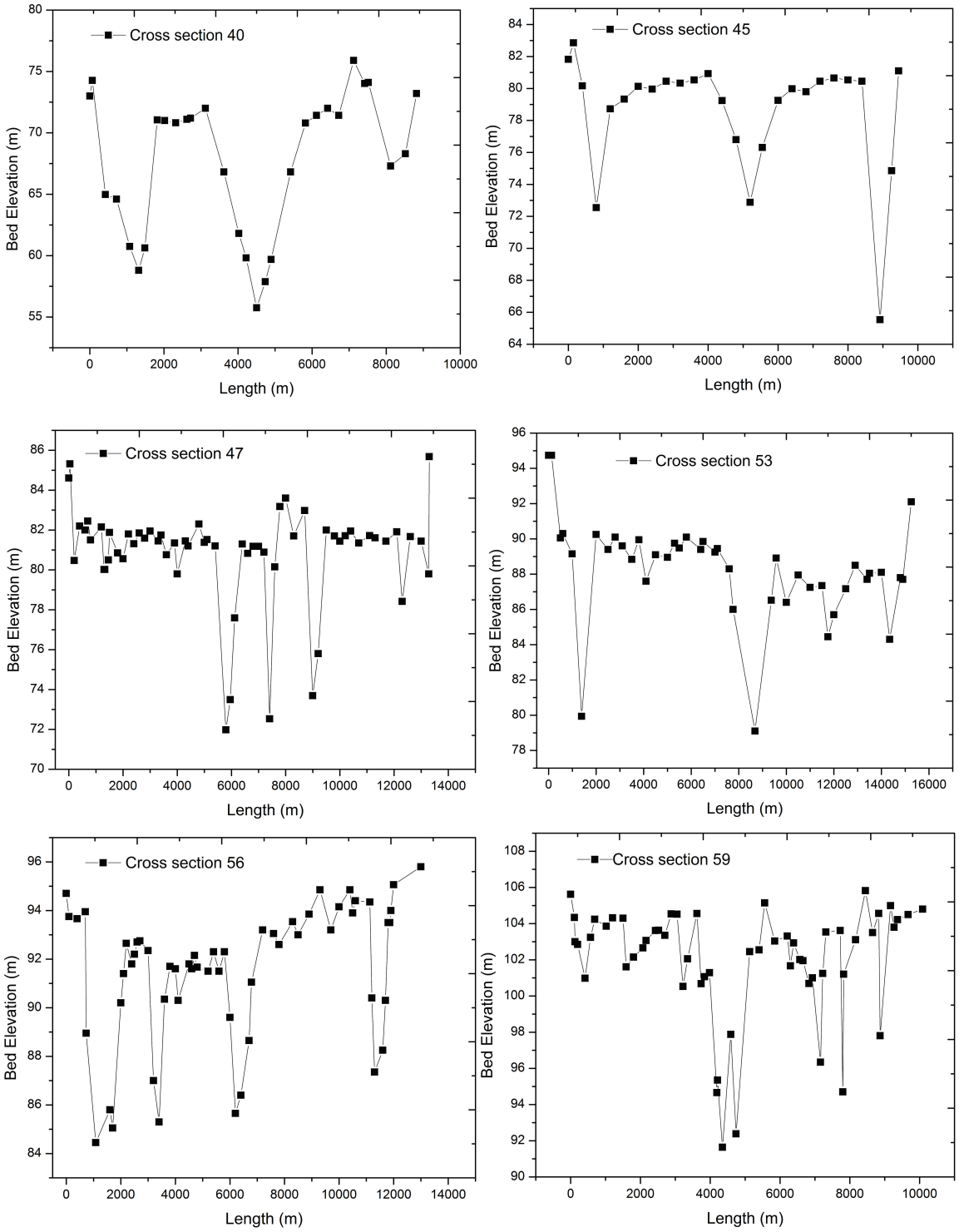

Figure 8.3: Cross section variations in cross sections 40 to 59.

estimation. The lean flow depth of 2 m was assumed for estimation of hydraulic radius R of different locations. The water surface slopes derived using satellite altimetry were assumed equal to the friction slope S_f of the river. Many researchers have proposed the empirical equations to estimate the Manning's roughness coefficient such as Strickler (1923), has proposed Equation 8.2, Meyer-Peter and Muller (1948) Equation 8.3 and Lane and Carlson (1953) Equation 8.4. These different equations use bed particle size distribution to estimate the Manning's roughness coefficient values. The Brahmaputra river reach–wise particle size distribution (Table 8.1) was used in different empirical equations to estimate the Manning's roughness coefficients variations at different reaches of the river (Table 8.2).

$$n = 0.39{S_f}^{0.38}R^{-0.16} \tag{8.1}$$

$$n = \frac{1}{21.1}d_{50}^{1/6} \tag{8.2}$$

$$n = \frac{1}{26}d_{90}^{1/6} \tag{8.3}$$

$$n = \frac{1}{21.14}d_{75}^{1/6} \tag{8.4}$$

The particle size distribution provided by (Goswami, 1985) for the middle reach of the Brahmaputra river was used in this study (Table 8.1). The particle sizes of d_{50}, d_{75} and d_{90} represents the variation in grain size from upstream (Dibrugarh) to downstream (Guwahati). The d_{50} in Dibrugarh reported as 0.034 mm and for Goalpara 0.085 mm. Similarly, these variations in the particle sizes were used in estimating Manning's roughens coefficient for the different reaches of the Brahmaputra river. Different empirical equation derived by various researchers were used the particle seize distribution to estimate the Manning's roughness coefficient. Hence, using these equations reach–wise roughness variations are generated for hydrodynamic model simulation.

8.4 Results and Discussion

HEC–RAS one dimensional model setup was setup to perform different hydrodynamic simulations. The river cross sections (Figure 8.2 and Figure 8.3) was used for model set up. The discharge distribution of Brahmaputra river was used for steady flow simulations for the period of 2013 to 2015. The water level information were given as the boundary con-

TH-1911_10610425

Table 8.1: Reach–wise particle size distribution of the Brahmaputra river (Goswami, 1985)

Station Name	Particle Sizes (mm)		
	d_{50}	d_{75}	d_{90}
Dibrugarh	0.034	0.07	0.1125
Salmara	0.117	0.24	0.3
Hatimura	0.04	0.055	0.09
Pandu	0.34	0.43	0.48
Goalpara	0.085	0.12	0.195

ditions for model simulations. Reach–wise distribution of Manning's roughness coefficient were used for model simulations. The different sets of Manning's roughness coefficient were used to generate water surface profiles of the river. To evaluate the model performance for different sets of Manning's roughness coefficients, seasonal difference of water level (monsoon and non-monsoon) were estimated. The differences in seasonal water surface profiles provided the reach wise water depth variations for different sets of Manning's roughness coefficients. These water depths for different reaches were compared with altimeter derived water depth variations for monsoon and non–monsoon season. The seasonal water depth at different river reaches were used to evaluate the performance of the model simulations. Since, altimeter derived water level were the only source of information in terms of reach wise seasonal water depth variation for the braided river like the Brahmaputra. The Manning's roughness coefficients were estimated for the year 2013 and performance evaluation was done for the year 2014 and 2015.

8.4.1 Variation of Manning's roughenss coefficient

The Manning's roughness coefficient estimated from particle size distribution using different empirical equations given in the Table 8.2. The estimated Manning's roughness coefficient represent the reach wise variations in river bed roughness. The Manning's roughness coefficients vary differently from Dibrugarh to Goalpara with different equations. The values of Manning's roughness coefficients were higher using Lane and Carlson (1953) method as compared to Strickler (1923) and Meyer–Peter Muller (1948) for all the reaches of the Brahmaputra river (Figure 8.5). The Manning's roughness coefficient was estimated for monsoon and non–monsoon seasons using satellite altimeter derived hydraulic properties of different reaches of the Brahmaputra river (Figure 8.4). The seasonal variation in water depths and water surface slopes of the main channel was used in the Equation 8.1 to derive the Manning's roughness coefficient. The variation in Manning's roughness coefficient clearly indicate the seasonal difference at all the reaches of the Brahmaputra river. The non–monsoon Manning's roughness coefficients values were higher as compared to the

TH-1911_10610425

Table 8.2: Estimation of Manning's roughness coefficient

Station Name	Manning's Roughness Coefficient (n)		
	Strickler (1923)	Lane & Carlson (1953)	Meyer-Peter & Muller (1948)
Dibrugarh	0.0270	0.0304	0.0267
Salmara	0.0331	0.0373	0.0315
Hatimura	0.0277	0.0292	0.0257
Pandu	0.0396	0.0411	0.0340
Guma	0.0353	0.0359	0.0305
Goalpara	0.0314	0.0332	0.0293

monsoon season (Figure 8.4), which was evident due to higher plan–form roughness during non–monsoon season. During the monsoon season river morphology stabilizes after the rising period of flow, hence channel morphology offers lesser resistance as compared to the non–monsoon season. The peak values of Manning's roughness coefficients were evident for the nodal locations and the river bends, where the river flow width remain narrow. The higher values of Manning's roughness coefficient at the cross sections 45, 32 and 22 correspond to the narrow river flow width. The Brahmaputra river at cross section 45 (downstream of Jorhat city) had river bend with main channel flow width of about 2 km. The river at cross section 32 (near Tezpur) has 1.5 km of average main channel flow width. The average river flow width at cross section 22 (near Guwahati) was 1.7 km. The variation of Manning's roughness coefficient was analyzed with monsoonal water surface slopes and the seasonal difference in water levels derived from satellite altimetry for the year 2013. The Manning's roughness coefficient vary from upstream to downstream. The Manning's roughness coefficient was higher for the cross sections 45, 32 and 22, which were the narrow river reaches (Figure 8.6). The seasonal water depth was higher for these narrow river reaches, which varied from 4 m to 8 m. The water surface slopes was decreasing from upstream 1/5,000 to the downstream 1/10,000.

8.4.2 Seasonal water depth variation

Comparison of seasonal water level difference was done from Altimetry retrieved and model simulated values for the year 2014 and 2015. From the Figure 8.7 and 8.8 it was evident that the model could not predict the water level variations over the narrow river reaches (cross sections, 22, 45 and 32) or near to the nodal locations. The different reaches of the river except nodal locations model prediction performed well and matched closely with altimetry retrieved water level differences. The water level differences of monsoon and non–monsoon were also generated using different empirical equations of Manning's roughness coefficient. The model simulations results of year 2014 and 2015 were compared with altimetry retrieved water level differences. It was found that the simulated values were

TH-1911_10610425

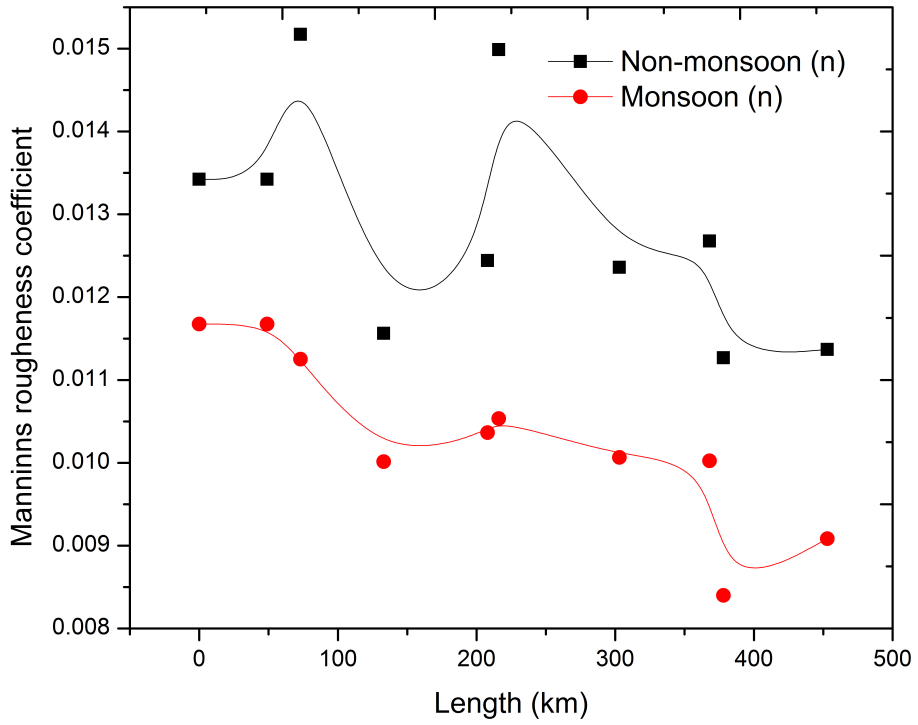

Figure 8.4: Variation of Manning's roughness coefficient (upstream to downstream) estimated using satellite altimetry derived water surface slopes.

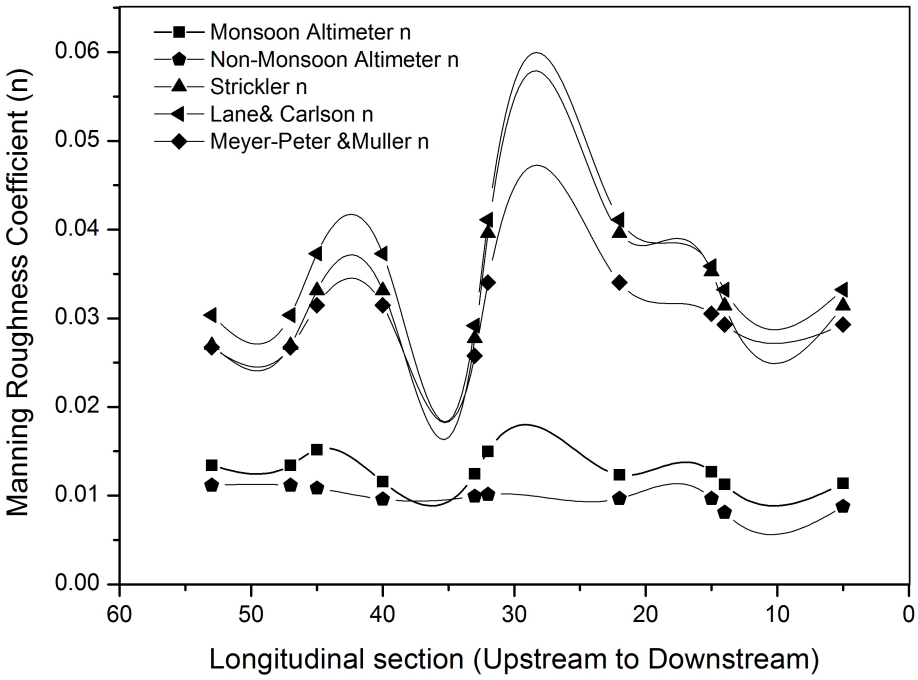

Figure 8.5: Manning's roughness coefficient variation using different empirical equations.

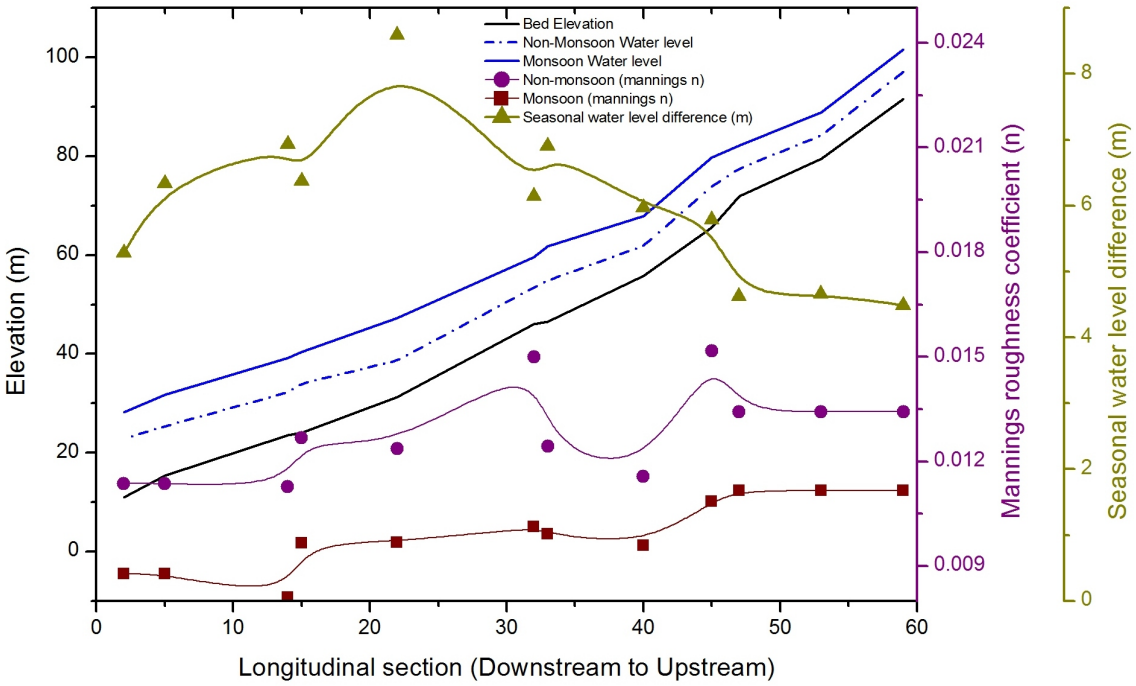

Figure 8.6: The longitudinal variations of Manning's roughness coefficient with changing river depth and slopes derived from satellite altimetry for the year 2013.

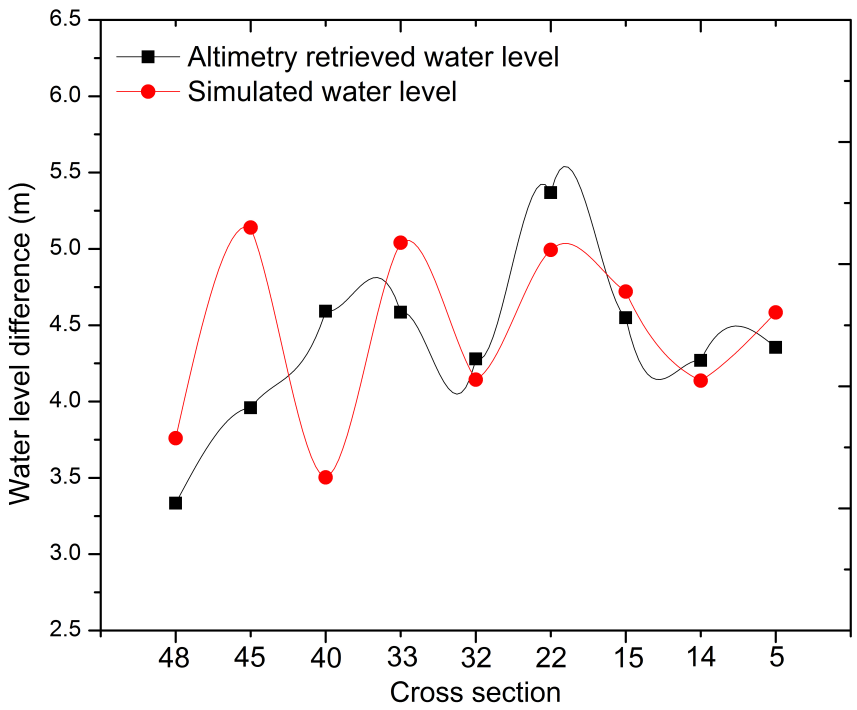

Figure 8.7: The comparison of seasonal difference of water level in the Brahmaputra river using satellite altimetry retrieved water levels and simulated data of year 2014.

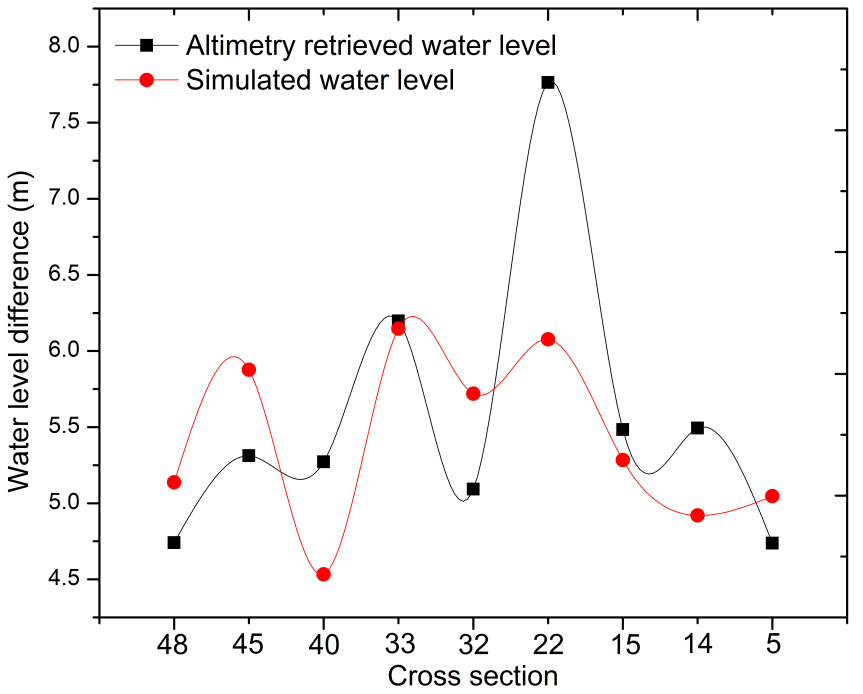

Figure 8.8: The comparison of seasonal difference of water level in the Brahmaputra river using satellite altimetry retrieved water levels and simulated data of year 2015.

over–predicting for all the reaches of the Brahmaputra river (Figure 8.9 and Figure 8.10). However, the reach wise water level variation trend was captured by the simulated water depths. The over prediction of water depth was mainly due to higher values of Manning's roughness coefficient derived using empirical equations. The higher values of Manning's roughness coefficient reduced the velocity of river flow, which resulted in higher depth of flow. The observed velocities were also compared with simulated velocities for downstream reach of the Guwahati during the monsoon season (Table 8.3).

8.4.3 Longitudinal variations of water level

The simulated longitudinal water surface profiles estimated using different Manning's roughness coefficient were compared with water surface profile generated from altimetery derived Manning's roughness coefficient. The difference in water depths at different reaches of the river were higher during the monsoon period as compared to non–monsoon for the year 2014 (Figure 8.11 and Figure 8.12) and 2015 (Figure 8.13 and Figure 8.14). It was found in all the cases that the simulated water surface profiles estimated using empirical equations were overestimating as compared to water surface profiles estimated using altimetry derived Manning's roughness coefficient. The comparison was done for the non–

TH-1911_10610425

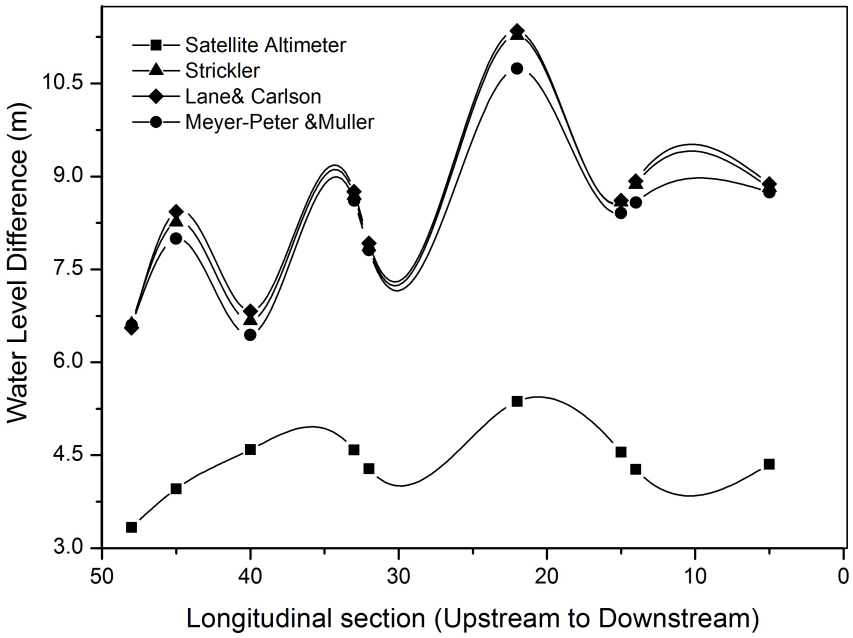

Figure 8.9: The comparison of seasonal difference of water level in the Brahmaputra river using altimeter derived water level different Manning's roughness coefficient from different equations for the year 2014

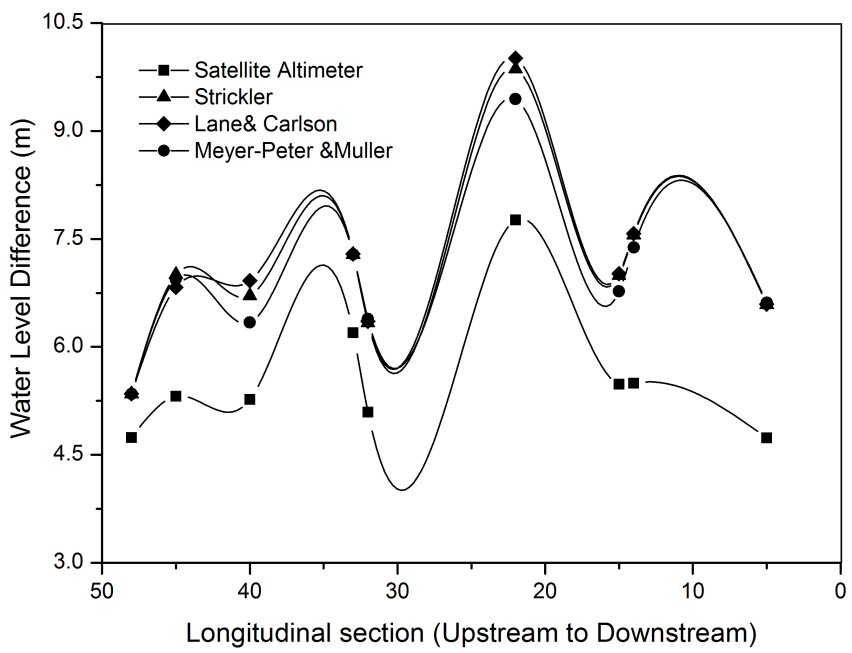

Figure 8.10: The comparison of seasonal difference of water level in the Brahmaputra river using altimeter derived water level and different Manning's roughness coefficient from different equations for the year 2015

TH-1911_10610425

Table 8.3: Comparison of Observed and simulated main channel velocity using different values of Manning's roughness coefficient for the monsoon season

Cross sections	Average Observed velocity (m/sec)	Avg. simulated velocity (m/sec) (Altimeter , n)	Avg. simulated velocity (m/sec) (Strickler, n)	Avg. simulated velocity (m/sec) (LC, n)	Avg. simulated velocity (m/sec) (MPM, n)
22	2.73	2.81	1.19	1.33	1.28
18	2.12	1.98	1.13	0.37	0.66
17	1.9	1.83	1.13	0.47	0.75
16	2.21	2.25	0.89	0.57	0.85

monsoon (January) and monsoon (August) period of years 2014 and 2015. The average monsoon velocities observed during the river survey were close to the hydrodynamic model simulations using altimetry derived Manning's roughness coefficients. The average main channel velocity during the monsoon season was found to be about 1.33 to 1.65 m/sec (Figure 3.4, Figure 3.5, Figure 3.6 and Figure 3.7). The under prediction of velocity values by empirical equations were due to higher values of Manning's roughness coefficients at different reaches of the river.

8.5 Conclusions

The hydrodynamic modeling of the Brahmaputra river was performed from upstream of Dibrugarh to downstream of Dhubri. The one–dimensional model was setup for the river reach of about 560 km with 58 cross sections. The input parameters such as discharge variations at different cross sections were provided from hydrological model simulations. The boundary condition was given as water level elevations at upstream and downstream of the river. The estimation of Manning's roughness coefficient was done using altimeter derived hydraulic parameters of the river at different locations. To perform the comparative analysis Manning's roughness coefficients were also estimated using different empirical equations, which use the particle size distributions. The reach–wise particle size distribution was used to derive the longitudinal variations of Manning's roughness coefficient. The model was setup to predict monthly water surface profiles of the river. The hydrodynamic simulations were performed for steady flow at monthly time scale. The Manning's roughness coefficient was found to be higher using empirical equations as compared to altimeter derived Manning's roughness coefficient values. The Manning's roughness coefficient derived using empirical equations was in the range of about 0.027 to 0.04. The range of altimeter derived Manning's roughness coefficient was varying from 0.009 to 0.015 for both the monsoon and non–monsoons seasons. The Manning's roughness coefficients derived using empirical equation were 2 to 3 times higher than the altimeter derived Manning's roughness coefficient. The velocity variations were also compared for the downstream of the Guwahati.

TH-1911_10610425

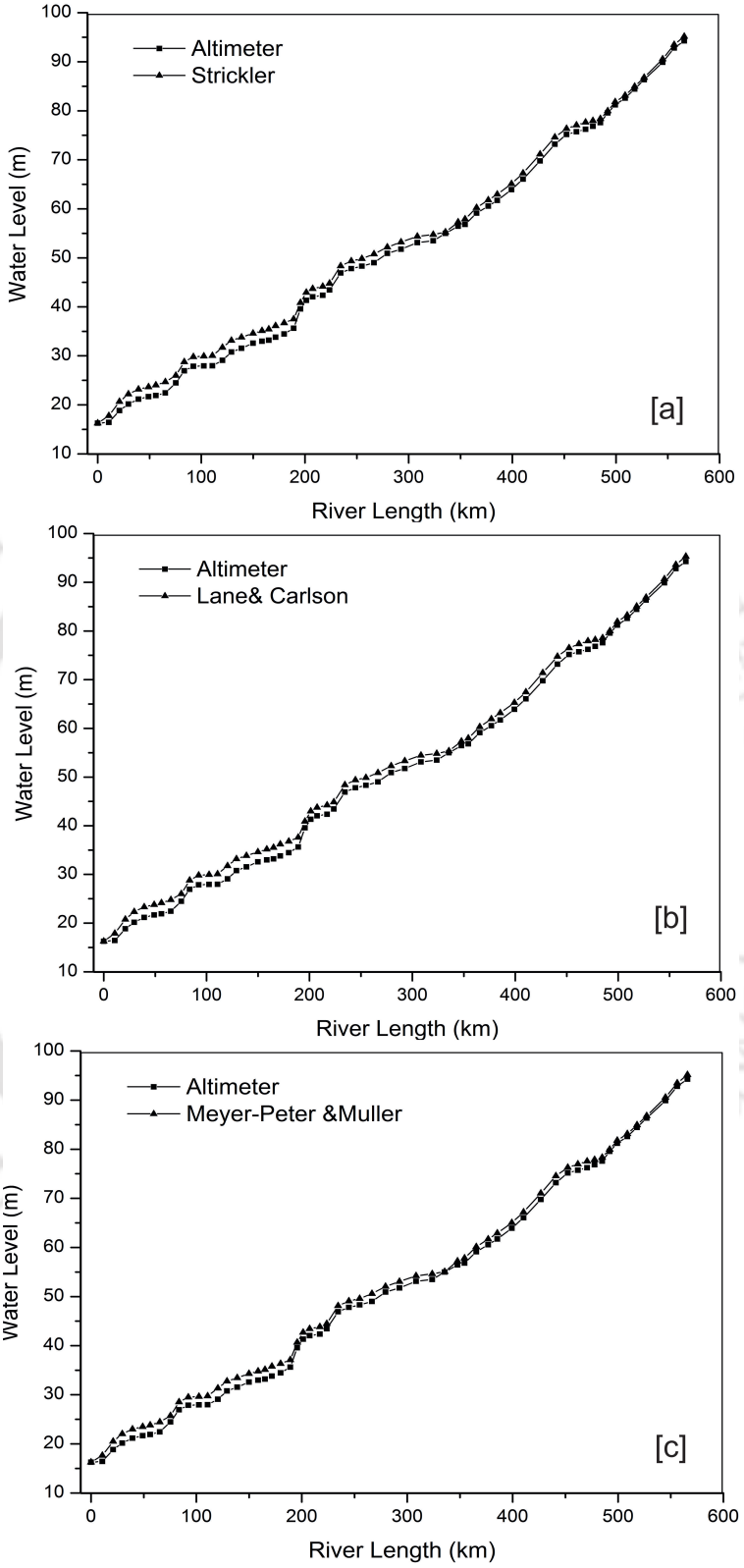

Figure 8.11: The comparison of satellite altimetry retrieved longitudinal water level variations of the Brahmaputra river (downstream to upstream) with (a) Strickler, (b) Lane and Carlson, (c) Meyer-Peter and Muller equation for the non–monsoon season of year 2014

TH-1911_10610425

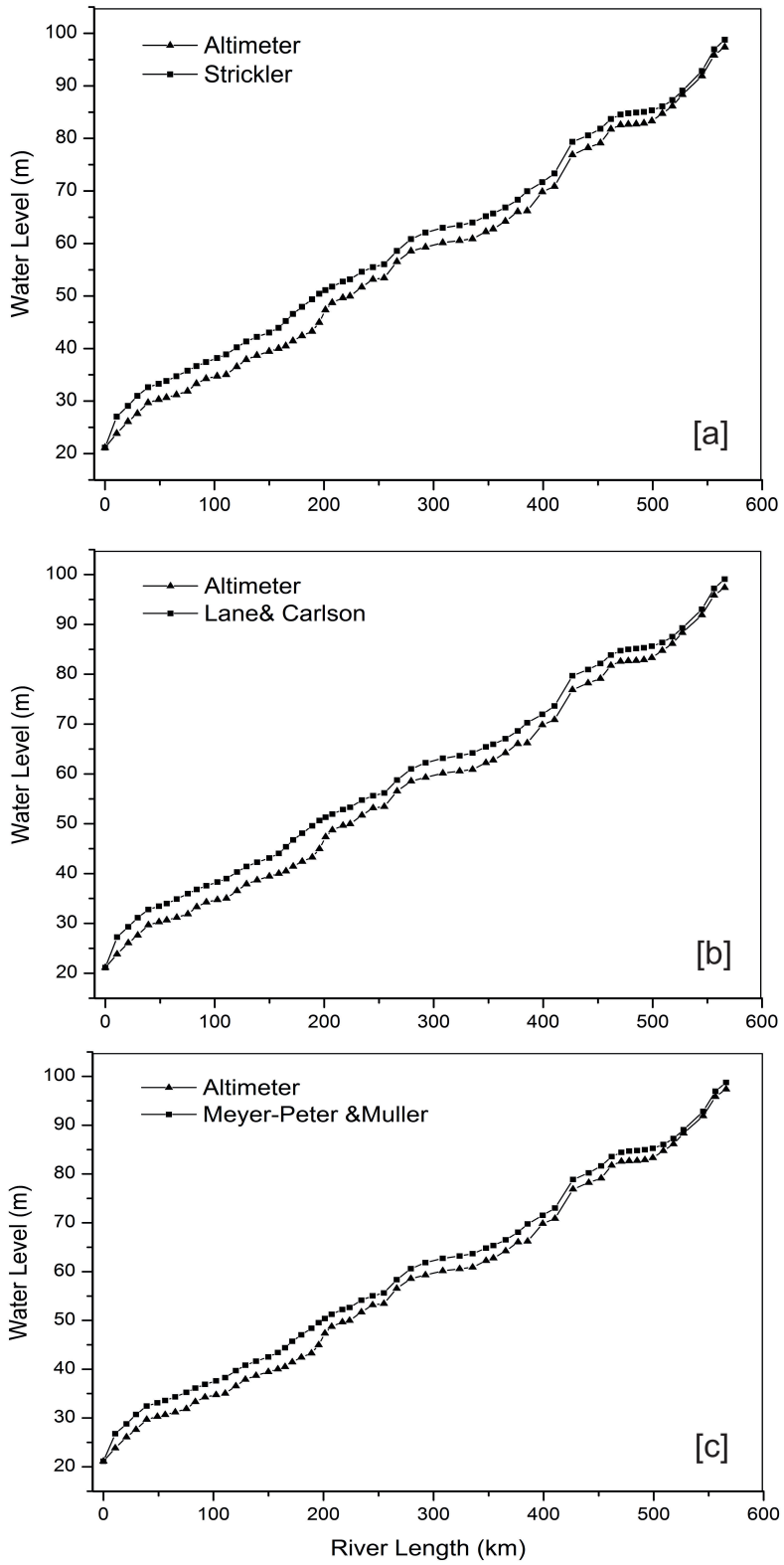

Figure 8.12: The comparison of satellite altimetry retrieved longitudinal water level variations of the Brahmaputra river (downstream to upstream) with (a) Strickler, (b) Lane and Carlson, (c) Meyer-Peter and Muller equation for the monsoon season of year 2014

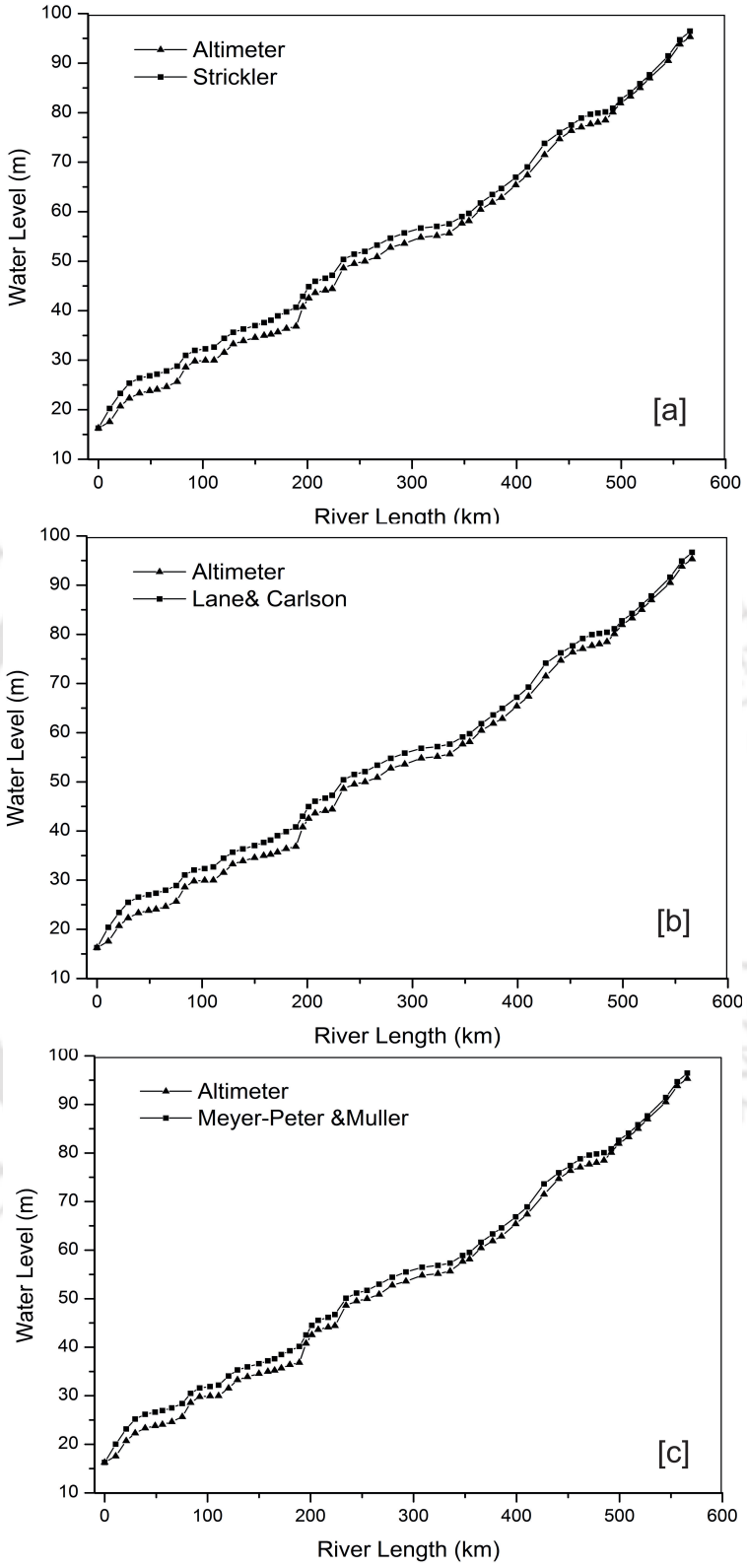

Figure 8.13: The comparison of satellite altimetry retrieved longitudinal water level variations of the Brahmaputra river (downstream to upstream) with (a) Strickler, (b) Lane and Carlson, (c) Meyer-Peter and Muller equation for the non–monsoon season of year 2015

TH-1911_10610425

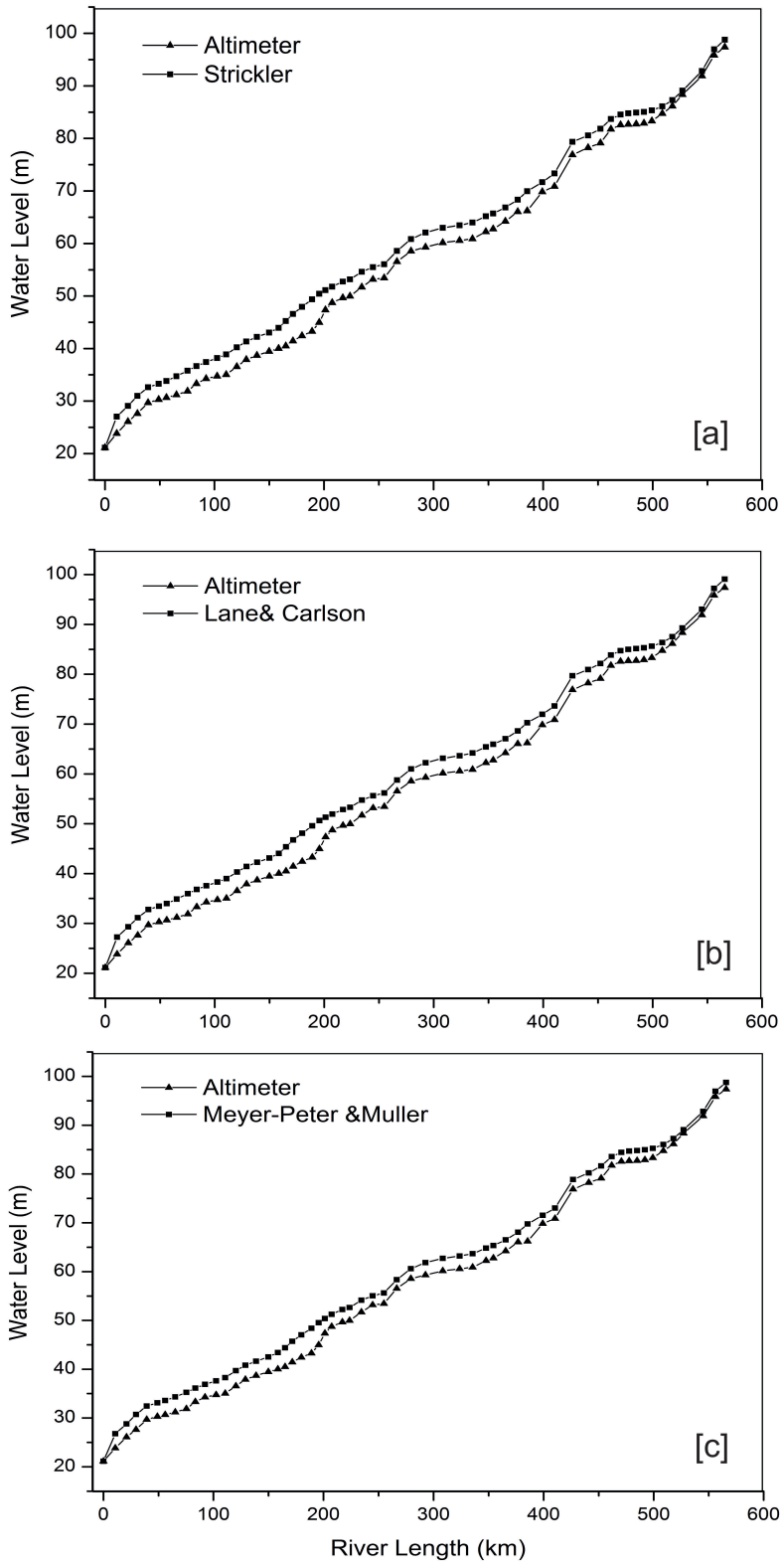

Figure 8.14: The comparison of satellite altimetry retrieved longitudinal water level variations of the Brahmaputra river (downstream to upstream) with (a) Strickler, (b) Lane and Carlson, (c) Meyer-Peter and Muller equation for the monsoon season of year 2015

TH-1911_10610425

The observed velocities were close to simulated velocity using altimeter derived Manning's roughness coefficient. Whereas the velocities were under predicted using empirical equations for all the cases. The longitudinal water surface profiles simulated using different empirical equations were compared with water surface profiles simulated using altimeter derived Manning's roughness coefficient for monsoon and non–monsoon seasons.

TH-1911_10610425

TH-1911_10610425

"The woods are lovely, dark and deep. But I have promises to keep, and miles to go before I sleep."

Robert Frost (1874 – 1963)
American Poet

9

CONCLUSIONS AND RECOMMENDATIONS

9.1 A Brief Review of the Work Done

Water level retrieval from satellite altimetry over the braided rivers was a difficult task due to dynamic river morphology. Frequent channel shifting and bar migration were the major hurdle to accurately retrack and retrieve the water level information. The improvement of altimetry retrieved water levels have shown good agreement with observed water levels of nearby gauging stations. Performance and accuracy analysis has established that water level can be retrieved with less than 40 cm RMSE for most of the braided reaches of the Brahmaputra river. The water surface profile has been generated from retrieved water levels at different locations. The seasonal water level difference from model simulation and the altimetry derived water level were compared. It was found out that assimilation of Manning's roughness coefficient into the HEC-RAS model has improved the prediction of water surface elevation at the different reaches of the Brahmaputra river. Different values of Manning's roughness coefficients using different empirical equations were ingested into the model to analyze the water level variations at different reaches of the river. It was found out that seasonal and reach wise variation in Manning's roughness coefficient derived using altimetry retrieved hydrodynamic parameters have improved the estimation of water surface profiles for the middle reach of the Brahmaputra river. The microwave satellite images were able to capture the intra-seasonal monsoonal morphological features causing short term morphological changes within the river.

TH-1911_10610425

9.1.1 Literature Review

The literature review carried out on sand bed braided rivers with advanced remote sensing techniques was discussed in chapter 2. The Brahmaputra river is a sand bed braided river and it has a highly dynamic morphology as discussed by many researchers. The understanding of morphological dynamics of braided rivers consists sand bar migration and formation studies in combination with field measurements. The advanced technologies have provided insight into the different processes going on this complicated system.

9.1.2 Study Area and Data Collection

The study area consists of middle reach of the Brahmaputra river as discussed in chapter 3. The Brahmaputra river flows from Tibet to Bay of Bengal travel through India, in which it forms got highly braided patterns. The field campaigns were conducted to study the various morphological processes within the river. The *in-situ* data was collected to study the historical behavior of the river.

9.1.3 Improvement in Satellite Data Processing

The satellite altimetry provides the vital information of river state at different locations over a period of time. The altimetry derived heights were used to study the hydrodynamic conditions of the Brahmaputra river. Water level retrieval over the braided river reaches is a difficult task due to frequent channel migration and sand bar formation. The morphological dynamics in this type of river causes the noise in altimeter return signal. The altimetry return signal make noisy waveforms due to presence of sand bars and vegetation within its footprint. To overcome these challenges a proper methodology needs to be adopted to filter out these noisy waveforms due to change in river morphology. The nested window approach is a new method to filter out the noisy waveforms within the braided reaches of the river and it could enable the selection of waveforms from the main channel. This dynamic nested window approach has produced better results as compared to river mask based approaches. The retrieved water levels were compared to various data sets available for the Brahmaputra river. It was found out that with this proposed methodology water level retrieval has improved form 1 m uncertainty in RMSE to 0.55 m. of in–accuracy in terms of RMSE, when evaluated at four different Jason-2 satellite tracks passing over the Brahmaputra river. The waveforms were classified after the selection and they were divided in different groups. The group of higher backscattering coefficient was selected for water level retrieval. The different classes represents how the waveforms are contaminated due to presence of various features within the altimeter footprint. Different retracking

TH-1911_10610425

methods were used to derive water level information. To evaluate the performance of this algorithm the similar retracking algorithm (Ice-1) was used to compared the available data–sets (Hydroweb) for the Brahmaputra river. Improvement in satellite altimetry data processing was discussed in chapter 4, which describes the algorithm developed to process the altimeter waveforms to retrieve water levels more accurately over the braided reaches of river.

9.1.4 Accuracy Assessment of Retrieved Water Level, Discharge, and Water Surface Slopes

In this chapter 5, accuracy assessment of retrieved water level was carried out to quantify the statistical accuracy of the method. The accuracy of retrieved water level from improved methodology for Jason-2 at 4 locations over the Brahmaputra river was found to be 55 cm in terms of root mean square error (RMSE). The SARAL/Altika has more dense tracks and Ka (36.7 Ghz) band altimeter as compared to Jason-2 with Ku band (16 Ghz) frequency. It has produced better accuracy with improved algorithm with 40 cm of RMSE when compared for 10 different locations over the Brahmaputra river. These water level informations at different locations over the Brahmaputra river were used to generate the water surface profiles. The water surface profiles were generated for the monsoon and non-monsoon season. It was found that there is higher seasonal water difference at the downstream of the river as compared to upstream. To retrieve water levels different retracking algorithm were used for accuracy assessment. It was found β-5 algorithm had performed the best among four different algorithms used for evaluation such as Ice-1, Ice-2, threshold and β-5 retrackers. The retrieved water levels were converted into the discharge time series based on the rating curve developed over the virtual stations. These discharges were compared with nearby gauge stations and it was found that the discharge values were able to capture the flood-waves occurred in the Brahmaputra river. The discharge comparisons were done for the Guwahati and Tezpur gauge stations. The discharge values were also used to estimate annual water yield at Guwahati and Tezpur gauge stations.

9.1.5 Mapping of Morphological Features using Microwave Satellite Images

Microwave satellite images were used to understand the intra-seasonal variations within the Brahmaputra river during the monsoon season. Different morphological processes takes place during the high flow period as discussed in chapter 6. Mapping of these morphological processes provides more insight in to the braided river morphology and its dynamics. The in-season variation was analyzed with microwave satellite images of different polariza-

TH-1911_10610425

tion and different time periods. In the sand bed braided rivers such as the Brahmaputra the intra-seasonal variation causes more morphological changes in the river. The flood waves of different interval causes the morphology to adjust itself with increased discharge and sediment flux during the monsoon season. Microwave images sensitive to surface roughness were able to capture the different morphological active features present within the river. The river morphological features such as sand bar, erosion zone, deposition zone, bank erosion and sediment mixing remain active during the monsoon season. These features create different signatures in the microwave images based on the backscattering coefficient. The signature analysis of different morphological features were performed based on the river survey with synchronized satellite passes over the middle reach of the Brahmaputra river. With the help of signature analysis it was found that morphologically active group (bank erosion zone, sand deposition zone and turbulent zone) and others such as river water, sand bar and flood–plain inundation were separable using HH polarization. However, within the morphologically active group different zones (bank erosion zone, sand deposition zone and turbulent zone) were not separable in both HH and HV polarization. The microwave satellite images of HH polarization were found to be suitable to identify the morphologically active zones within the monsoon period as compared to HV polarization. In order to separate the morphologically active features within the river, the radar backscattering coefficient was divided into three different categories and the river reach was divided into five different zones based on morphological characteristics of the river. The image segmentation was done based on the different categories of backscattering coefficient representing the variation of turbulence level present within the river. These zones were then separately interpreted for each category of turbulence level associated to the morphologically active features (bank erosion zone, sand deposition zone and turbulent zone).

9.1.6 Hydrological Modeling of the Brahmaputra River

Hydrological modeling of the Brahmaputra river was done using semi-distributed hydrological model. The model performs rainfall runoff modeling and estimates tributary level discharge variations over the Brahmaputra basin. The spatio–temporal hydrological variations were utmost importance to study the hydro–dynamic and morphological changes within the river. The model simulations were preformed for the period of 1997 to 2015. To setup the hydrological model different input parameters were used such as DEM, soil type, land use land cover, temperature and rainfall. The model calibration was done for the year 1999 for the Brahmaputra river. The unavailability of tributary discharge could not made possible to calibrate the model at tributary scale. The different calibration parameters were used in the model. The model was calibrated for monsoon and non–monsoon seasons separately.

TH-1911_10610425

The model validation was performed for the year 2000. It was found that the simulated hydrograph could able to capture the seasonal and as well as flood pulses of different interval. However, the rising and receding phases of the simulated discharge was gradual as compared to observed discharges at Guwahati gauge station. The performance of simulated discharge was found statistically satisfactory with R^2=0.85 and RMSE=1233 m^3/sec. The discharge hydrograph of the main channel of the Brahmaputra river was analyzed and it was found that flood pulses at different locations from upstream to downstream were simulated with their occurrence at different time interval. The tributary wise discharge was also analyzed for the period of 1999 to 2015. It was found that the different tributaries in the Brahmaputra river contribute approximately 9% to 15% of annual flow in the Brahmaputra river. The peak discharge contribution of each tributary was estimated for the year 2004. The mean discharge and its deviation was estimated for each tributaries for the period of 17 years. The peak values for mean discharge vary from 2,700 m^3/sec to 5,000 m^3/sec during the monsoon month. The monthly scale discharge was used in the hydrodynamic modeling of the Brahmaputra river to generate the monthly water surface profiles for the period of 2013 to 2015. The model Hydrological model setup and simulations were discussed in detail in chapter 7.

9.1.7 Hydrodynamic Modeling: Satellite Altimetry and Discharge Data Assimilation

To study the river morphological dynamics, hydrodynamic modeling was performed with varying bed roughness at different reaches of the river. The reach and season wise variations of river bed roughness indicate the morphological phase of the river. The assimilation of altimetery retrieved water level was done to validate and calibrate the hydrodynamic model. The one–dimensional hydrodynamic model was setup for the river reach of about 560 km with 58 cross sections. The input parameters such as discharge variations at different cross sections were provided from hydrological model simulation. The boundary condition was given as water level elevations at upstream and downstream of the river. The estimation of Manning's roughness coefficient was done using altimeter derived hydraulic parameters of the river at different locations. To perform the comparative analysis Manning's roughness coefficients were also estimated using different empirical equations, which used the particle size distributions. The reach wise particle size distribution was used to deriver the longitudinal variations of Manning's roughness coefficient. The model was setup to predict monthly water surface profiles of the river. The hydrodynamic simulations were performed for steady flow at monthly time scale. The Manning's roughness coefficient was found to be higher using empirical equations as compared to altimeter derived values.

TH-1911_10610425

The empirical equation derived Manning's roughness coefficient have the range of about 0.027 to 0.04. The range of altimeter derived Manning's roughness coefficient was 0.009 to 0.015 for both the monsoon and non–monsoons seasons. The Manning's roughness coefficients derived using empirical equation were found to be 2 to 3 times higher than the altimeter derived Manning's roughness coefficient. The velocity variations were also compared for the downstream of the Guwahati. The observed velocities were close to simulated velocity using altimeter derived Manning's roughness coefficient. However, the velocities were under predicted using empirical equations for all the cases. The longitudinal water surface profiles simulated using different empirical equations were compared with water surface profiles simulated using altimeter derived Manning's roughness coefficient for monsoon and non–monsoon seasons. The chapter 8 described in detail about the integration approach of different information to study the river hydrodynamic variations.

9.2 Recommendations for Future Research

This study provide an understanding towards the use of advanced geo–spatial techniques to understand the braided river morphology. To further carry out the research in this direction, it may yield useful results. The scope of future research discussed as follows.

1. Assimilation of multi-satellite altimetry retrieved water levels into the hydrodynamic models.
2. To study the river flood–plain wetland interactions using retrieved water levels over the flood–plains of a river.
3. To interpret long–term morphological changes using intra–seasonal variations from microwave satellite images.
4. Identification of different morphologically active groups using microwave satellite images of multiple wavelength and polarization.
5. Use of 2–D and 3–D hydrodynamic and morphological models to study the bar migration, bar formation and sediment deposition around the sand bars.

TH-1911_10610425

Bibliography

Ashworth, P. J., Best, J. L., Roden, J. E., Bristow, C. S., and Klaassen, G. J. (2000). "Morphological evolution and dynamics of a large, sand braid-bar, Jamuna River, Bangladesh." *Sedimentology*, 47(3), 533–555.

Bamber, J. L. (1994). "A digital elevation model of the Antarctic ice sheet derived from ERS-l altimeter data and comparison with terrestrial measurements." *Annals of Glaciology*, 20(1), 48–54.

Bernini, A., Caleffi, V., and Valiani, A. (2009). "Numerical modelling of alternate bars in shallow channels." *Braided Rivers: Process, Deposits, Ecology and Management (Special Publication 36 of the IAS)*, 21, 153.

Berry, P. (2006). "Two decades of inland water monitoring using satellite radar altimetry.." *In: 15 Years of Progress in Radar Altimetry*, Proc. Symp., Venice Lido, Italy, 13–18.

Berry, P., Garlick, J., Freeman, J., and Mathers, E. (2005). "Global inland water monitoring from multi-mission altimetry." *Geophysical Research Letters*, 32(16).

Bertoldi, W., Ashmore, P., and Tubino, M. (2009). "A method for estimating the mean bed load flux in braided rivers." *Geomorphology*, 103(3), 330–340.

Beven, K. and Kirkby, M. J. (1979). "A physically based, variable contributing area model of basin hydrology/Un modèle à base physique de zone d'appel variable de l'hydrologie du bassin versant." *Hydrological Sciences Journal*, 24(1), 43–69.

Bristow, C. S. (1987). *Brahmaputra River: Channel migration and deposition. In: Etheridge, F.G., Flores, R.M., Harvey, M.D. (Eds.), Recent Developments in Fluvial Sedimentology*, Vol. 39. SEPM (Soc. Sediment. Geol.) Spec. Publ., 63–74.

Calmant, S. and Seyler, F. (2006). "Continental surface waters from satellite altimetry." *Comptes Rendus Geoscience*, 338(14), 1113–1122.

Calmant, S., Seyler, F., and Cretaux, J. F. (2008). "Monitoring continental surface waters by satellite altimetry." *Surveys in geophysics*, 29(4), 247–269.

TH-1911_10610425

Cartwright, D. and Edden, A. (1973). "Corrected tables of tidal harmonics, Geophys." *JR astron. Soc*, 33, 253–264.

Cartwright, D. and Tayler, R. (1971). "New computations of the tide-generating potential." *Geophysical Journal International*, 23(1), 45–73.

Chelton, D. B., Ries, J. C., Haines, B. J., Fu, L.-L., and Callahan, P. S. (2001). *Satellite altimetry. In Satellite Altimetry and Earth Sciences, Fu, L.-L. and Cazenave, A. (eds.)*. Number 1-131. San Diego, CA: Academic.

Coleman, J. M. (1969). "Brahmaputra River: channel processes and sedimentation." *Sedimentary Geology*, 3(2), 129–239.

Coulthard, T., Wiel, M., Van De, J., et al. (2006). "A cellular model of river meandering." *Earth Surface Processes and Landforms*, 31(1), 123–132.

Crétaux, J.-F., Jelinski, W., Calmant, S., Kouraev, A., Vuglinski, V., Bergé-Nguyen, M., Gennero, M.-C., Nino, F., Del Rio, R. A., Cazenave, A., et al. (2011). "Sols: A lake database to monitor in the near real time water level and storage variations from remote sensing data." *Advances in space research*, 47(9), 1497–1507.

Da Silva, J. S., Calmant, S., Seyler, F., Rotunno Filho, O. C., Cochonneau, G., and Mansur, W. J. (2010). "Water levels in the amazon basin derived from the ers 2 and envisat radar altimetry missions." *Remote Sensing of Environment*, 114(10), 2160–2181.

Davis, C. H. (1995). "Growth of the Greenland ice sheet: a performance assessment of altimeter retracking algorithms." *IEEE Transactions on Geoscience and Remote Sensing*, 33(5), 1108–1116.

Davis, C. H. (1997). "A robust threshold retracking algorithm for measuring ice-sheet surface elevation change from satellite radar altimeters." *IEEE Transactions on Geoscience and Remote Sensing*, 35(4), 974–979.

Dutta, S. and Ghosh, S. (2012). "Impact of climate and land use changes on the flood hazard of the middle brahmaputra reach, india." *Journal ref: Journal of Disaster Research*, 7(5), 573–581.

Fairbridge, R. W. (1968). "Braided streams." *Geomorphology*, Springer, 90–93.

Frappart, F., Seyler, F., Martinez, J.-M., Leon, J. G., and Cazenave, A. (2005). "Floodplain water storage in the Negro River basin estimated from microwave remote sensing of inundation area and water levels." *Remote Sensing of Environment*, 99(4), 387–399.

TH-1911_10610425

Ghosh, S. and Dutta, S. (2012). "Impact of climate change on flood characteristics in Brahmaputra basin using a macro-scale distributed hydrological model." *Journal of earth system science*, 121(3), 637–657.

Goswami, D. C. (1985). "Brahmaputra River, Assam, India: Physiography, basin denudation, and channel aggradation." *Water Resources Research*, 21(7), 959–978.

Jarrett, R. D. and Petsch, H. E. (1985). "Computer program NCALC user's manual; verification of Manning's roughness coefficient in channels." *Report No. 85-4317*, US Geological Survey,.

Karmaker, T. and Dutta, S. (2010). "Generation of synthetic seasonal hydrographs for a large river basin." *Journal of hydrology*, 381(3), 287–296.

Karmaker, T. and Dutta, S. (2011). "Erodibility of fine soil from the composite river bank of Brahmaputra in India." *Hydrological Processes*, 25(1), 104–111.

Karmaker, T. and Dutta, S. (2016). "Prediction of Short-Term Morphological Change in Large Braided River Using 2D Numerical Model." *Journal of Hydraulic Engineering*, 04016039.

Karmaker, T., Ramprasad, Y., and Dutta, S. (2010). "Sediment transport in an active erodible channel bend of Brahmaputra river." *Sadhana*, 35(6), 693–706.

Kouraev, A. V., Zakharova, E. A., Samain, O., Mognard, N. M., and Cazenave, A. (2004). "Ob'river discharge from TOPEX/Poseidon satellite altimetry (1992–2002)." *Remote sensing of environment*, 93(1), 238–245.

Lane, E. W. and Carlson, E. (1953). "Some factors affecting the stability of canals constructed in coarse granular materialsl." *Proceedings: Minnesota International Hydraulic Convention*, ASCE, 37–48.

Lee, H. K. (2008). "Radar altimetry methods for solid earth geodynamics studies." Ph.D. thesis, The Ohio State University, The Ohio State University.

Legresy, B. and Remy, F. (1997). "Altimetric observations of surface characteristics of the Antarctic ice sheet." *Journal of Glaciology*, 43(144), 265–275.

Leon, J. G., Calmant, S., Seyler, F., Bonnet, M.-P., Cauhope, M., Frappart, F., Filizola, N., and Fraizy, P. (2006). "Rating curves and estimation of average water depth at the upper Negro River based on satellite altimeter data and modeled discharges." *Journal of hydrology*, 328(3), 481–496.

TH-1911_10610425

Leopold, L. and Wolman, M. (1957). "River channel patters: braided, meandering and straight 282-B." *U.S Geological Survey Professional Paper*, 39–85.

Martin, T. V., Zwally, H. J., Brenner, A. C., and Bindschadler, R. A. (1983). "Analysis and retracking of continental ice sheet radar altimeter waveforms." *Journal of Geophysical Research: Oceans*, 88, 1608–1616.

Meyer-Peter, B. and Muller, T. (1948). "Formulas for bedload transport: Report on Second Meeting of International Association for Hydraulics Research." *Stockholm, Sweden*.

Mishra, S. K., Sarkar, R., Dutta, S., and Panigrahy, S. (2008). "A physically based hydrological model for paddy agriculture dominated hilly watersheds in tropical region." *Journal of hydrology*, 357(3), 389–404.

Mosselman, E. (2009). "Bank protection and river training along the braided Brahmaputra–Jamuna River, Bangladesh." *Braided Rivers: Process, Deposition, Ecology and Management, edited by: Smith, GHS, Best, JL, Bristow, CS, and Petts, GE, Blackwell, Oxford, UK*, 277–287.

Murray, A. B. and Paola, C. (1994). "A cellular model of braided rivers." *Nature*, 371(54-57).

Murray, A. B. and Paola, C. (2003). "Modelling the effect of vegetation on channel pattern in bedload rivers." *Earth Surface Processes and Landforms*, 28(2), 131–143.

Nicholas, A. (2003). "Investigation of spatially distributed braided river flows using a two-dimensional hydraulic model." *Earth Surface Processes and Landforms*, 28(6), 655–674.

Nykanen, D. K., Foufoula-Georgiou, E., and Sapozhnikov, V. B. (1998). "Study of spatial scaling in braided river patterns using synthetic aperture radar imagery." *Water resources research*, 34(7), 1795–1807.

Papa, F., Durand, F., Rossow, W. B., Rahman, A., and Bala, S. K. (2010). "Satellite altimeter derived monthly discharge of the Ganga–Brahmaputra River and its seasonal to interannual variations from 1993 to 2008." *Journal of Geophysical Research: Oceans*, 115.

Philip, J. A. (1996). "Mid-channel bar growth and its relationship to local flow strength and direction." *Earth Surface Processes and Landforms*, 21, 123.

Rajyalakshmi, N. and Dutta, S. (2006). "Regionalization of rainfall–runoff processes in rice agriculture dominated watersheds." *Water science and technology*, 53(10), 131–139.

Richardson, W. R. and Thorne, C. R. (2001). "Multiple thread flow and channel bifurcation in a braided river: Brahmaputra–Jamuna River, Bangladesh." *Geomorphology*, 38(3), 185–196.

TH-1911_10610425

Roux, E., Santos da Silva, J., Cesar Vieira Getirana, A., Bonnet, M.-P., Calmant, S., Martinez, J.-M., and Seyler, F. (2010). "Producing time series of river water height by means of satellite radar altimetry a comparative study." *Hydrological Sciences Journal*, 55(1), 104–120.

Sarkar, R., Dutta, S., and Panigrahy, S. (2008a). "Characterizing overland flow on a preferential infiltration dominated hillslope: Case study." *Journal of Hydrologic Engineering*, 13(7), 563–569.

Sarkar, R., Dutta, S., and Panigrahy, S. (2008b). "Effect of scale on infiltration in a macropore-dominated hillslope.." *Current Science (00113891)*, 94(4).

Sarker, M. H. and Thorne, C. R. (2009). "Morphological response of the Brahmaputra–Padma–Lower Meghna river system to the Assam earthquake of 1950." *Braided Rivers: Process, Deposits, Ecology and Management (Special Publication 36 of the IAS)*, 21, 289.

Sarma, J. (2005). "Fluvial process and morphology of the Brahmaputra River in Assam, India." *Geomorphology*, 70(3), 226–256.

Smith, L. C. (1997). "Satellite remote sensing of river inundation area, stage, and discharge: A review." *Hydrological processes*, 11(10), 1427–1439.

Smith, L. C., Isacks, B. L., Bloom, A. L., and Murray, A. B. (1996). "Estimation of discharge from three braided rivers using synthetic aperture radar satellite imagery: Potential application to ungaged basins." *Water Resources Research*, 32(7), 2021–2034.

Strickler, A. (1923). *Beitrage zur Frage der Geschwindigheitsformel un der Rauhigkeitszahlen fur Strome, Kanaleund Geschlossene Leitungen*. Mitteilungen des Eidgenossischer Amtes fur Wasserwirtschaft, Bern, Switzerland, 16 pp.

Thomas, R. and Nicholas, A. (2002). "Simulation of braided river flow using a new cellular routing scheme." *Geomorphology*, 43(3), 179–195.

Thorne, C. R., Russell, A. P., and Alam, M. K. (1993). "Planform pattern and channel evolution of the Brahmaputra River, Bangladesh." *Geological Society, London, Special Publications*, 75(1), 257–276.

Vignudelli, S., Kostianoy, A. G., Cipollini, P., and Benveniste, J. (2011). *Coastal altimetry*. Springer Science & Business Media.

Wahr, J. M. (1985). "Deformation induced by polar motion." *Journal of Geophysical Research: Solid Earth*, 90, 9363–9368.

TH-1911_10610425

Wingham, D., Rapley, C., and Griffiths, H. (1986). "New techniques in satellite altimeter tracking systems." *ESA Proceedings of the 1986 International Geoscience and Remote Sensing Symposium(IGARSS'86) on Remote Sensing: Today's Solutions for Tomorrow's Information Needs,*, Vol. 3.

Zade, M. and Dutta, S. (2003). "RISE-A Distributed Hydrologic Model For Rice Agriculture: Concept And Evaluation." *Watershed Hydrology*, 6, 240.

Zakharova, E. A., Kouraev, A. V., Cazenave, A., and Seyler, F. (2006). "Amazon River discharge estimated from TOPEX/Poseidon altimetry." *Comptes Rendus Geoscience*, 338(3), 188–196.

Zhang, H., Nakagawa, H., Baba, Y., Kawaike, K., Rahman, M. M., and Uddin, M. N. (2011). "Hydraulic and morphological consequences of bank protection measures along the Jamuna River, Bangladesh." *Annuals of Disas Prev Res Inst Kyoto Univ*, 511–523.

TH-1911_10610425

Appendix A

Hydrological Modeling

A.1 DESCRIPTION OF THE HYDROLOGICAL MODEL

Rice Irrigation System Evaluation (RISE) model (Dutta and Zade 2003) is a distributed physically based hydrological model in which surface and sub-surface hydrologic processes have been conceptualized for a watershed in tropical/sub-tropical regions. This model defines the dominant hydrological processes based on different distinct hydrological similarity classes (HSC). For the present study four distinct HSCs were delineated based on seven distinct type of soil classes and seven land-use/land-cover types. The four delineated classes are i) Macropore dominated vegetated hillslope ii) Paddy cultivation dominated agricultural lands iii) Semi-impervious urban areas and iv) Wet lands and permanent sinks. For each class, runoff generation processes have been conceptualized as depicted in Figure A.1. Macropore dominated processes have been conceptualized for HSC-1 while retention excess flow and Hortonian infiltration excess overland flow have been conceptualized for HSC-2 and HSC-3 respectively. Water budgeting has been done for HSC-4. Subsurface storm flow processes are mathematically inter-coupled with infiltration processes. Lateral flow to the channel segment has been conceptualized following the steepest gradient method while

TH-1911_10610425

the linearized channel routing process follows the kinematic wave approximation approach. The mathematical formulation of each hydrological processes used in the model have been presented in the next section, details of which are available in Mishra et al. (2008).

A.1.1 Infiltration Process

A.1.1.1 Macropore dominated vegetated hillslope

Infiltration process in a vegetated hillslope is controlled by micropore and macropore flow mechanism in its subsoil formations (Sarkar et al., 2008b). But in tropical/subtropical regions, subsurface flow mechanism is governed mainly by both the soil matrix and macropore networks as the monsoon season advances to its peak and generally have concentrated rainfall over short time span; though during the onset of monsoon season soil matrix flow primarily governs the infiltration rate. If the maximum infiltration rate of a vegetated hillslope is f_{max}, due to combined effect of micropores and macropores the resulting overland flow rate (R) can be expressed (Sarkar et al., 2008a) as

$$R = 0 \text{ when } i \leq f_{\max} \tag{A.1}$$

$$R = i - f_{\max} \text{ when } i > f_{\max} \tag{A.2}$$

where i is the rainfall intensity.

A.1.1.2 Paddy cultivation dominated agricultural lands

The hard pan formation below the plow layer, typical in paddy agricultural system, having very low permeability (typically, 2–4 mm/h) inhibits the infiltration of ponded field water. A permeability factor has been introduced for defining this special infiltration behavior. If h is the retaining depth in the paddy field, h_1

TH-1911_10610425

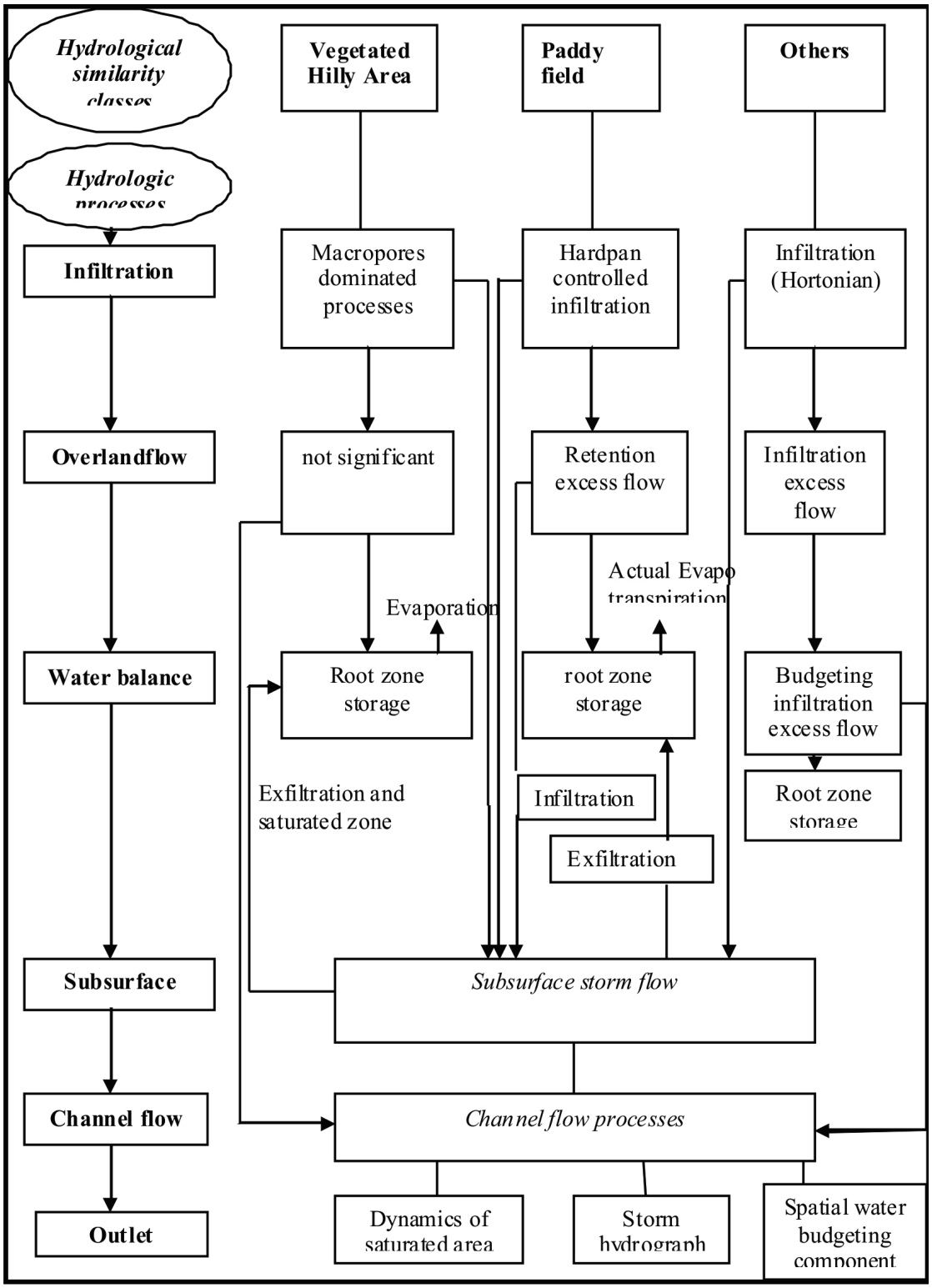

FIGURE A.1: Flow chart of Water budgeting using RISE model.

TH-1911_10610425

and h_2 are the depth of plow layer and the depth of hard pan formation respectively, using the two layer Green-Ampt model, the infiltration rate at the bottom of the lowest layer i.e. the hard pan formation can be formulated as

$$f = \frac{k_1 k_2 \left(h_1 + h_2 + h + \Psi_1\right)}{h_1 k_2 + h_2 k_1} \tag{A.3}$$

where Ψ_1 is the suction pressure of the saturated plow layer; k_1 and k_2 are saturated hydraulic conductivities of plow layer and hard pan formations respectively. Value of k_2 can be obtained from the relation: $k_2 = (k_1/r)$ where r is the degree of soil impermeability (dimensionless) due to the formation of hard pan layer.

A.1.1.3 Semi-impervious urban area

The dominant runoff generation mechanism in this type of area is Hortonian infiltration excess runoff generation process. The infiltration rate for this case can be obtained by the analytical solution of one dimensional Richard's equation for saturated soil horizon. This results in Philip's two-term infiltration equation, given as

$$f_c\left(t\right) = 0.5St^{-0.5} + A_0 \tag{A.4}$$

where $f_c(t)$ is the potential infiltration rate (mm/h), S is the sorptivity, and A_0 is the gravitational infiltration rate (mm/ h).

A.1.2 Water budgeting

A.1.2.1 Macropore dominated vegetated hillslope

Storage of water in the root zone is primarily contributed by the soil matrix as the pore water in the macropore zone has very short resident time. If S_r be

TH-1911_10610425

the subsurface storage at time t, the mass balance equation considering only evapo-transpiration losses in the root zone can be expressed as

$$\frac{ds_r}{dt} = i - ET_{actual} + f_{ex} \text{ when } i \leq f_{\max} \tag{A.5}$$

$$\frac{ds_r}{dt} = f_{\max} - ET_{actual} + f_{ex} \text{ when } i > f_{\max} \tag{A.6}$$

where ET_{actual} is the actual evapo-transpiration rate (mm/h) and exfiltration rate from the soil subsurface is f_{ex} (mm/h). All the rainfall above the maximum storage capacity, S_{max} contributes to subsurface recharge.

A.1.2.2 Paddy cultivation dominated agricultural lands

The retention depth (h) of water in a paddy field can be formulated as

$$\frac{dh}{dt} = (i - f - ET_{actual} - h_{ov} + f_{ex}) \tag{A.7}$$

If h_{ret} is the maximum retention depth of the field the unit discharge of over-spilled water in the field h_{ov} is related to the retention depth (h) as

$$h_{ov} = \frac{h - h_{ret}}{\Delta t} \text{ when h} \leq h_{ret} \tag{A.8}$$

otherwise,

$$h_{ov} = 0 \tag{A.9}$$

where Δt is the simulation time interval. Retention depth (h) at the previous time step has been used in Equation A-8 without any significant error in water budgeting. Thornthwaite's formula has been used to determine potential evapo-transpiration from daily temperature data and subsequently multiplied by a seasonal crop coefficient, which can be taken in the range of 0.9-1 for the region, to obtain the actual evapotranspiration (ET_{actual}) for paddy fields.

TH-1911_10610425

A.1.2.3 Semi-impervious urban areas

Water held in the subsurface layer of this zone has not been considered for water budgeting unless any exfiltration process occurred. This is due to the fact that in this area the water held in subsurface zone is negligible.

A.1.2.4 Wet lands as permanent sinks

During monsoon season, wetlands receive precipitation and lateral subsurface flow. It loses some part of its storage as evaporation. At macro-scale hydrologic condition it works as a locally hydrologic sink.

A.1.2.5 Subsurface flow component

Subsurface flow approximation (Beven and Kirkiby, 1979) has been followed for the model to calculate the dynamics of saturated excess zone and direct subsurface flow contribution to the channel. The soil moisture local deficit at each grid cell can be expressed by the following equation for a spatially averaged recharge rate f,

$$S_i = \overline{S} + m\left[\left(\lambda - \ln\frac{\alpha}{\tan\beta}\right) - (\ln T_0 - \delta)\right] \tag{A.10}$$

Where S_i is the local storage deficit per unit plane area (m), $\bar{S}$ is lumped storage deficit (m), m is a parameter controlling the rate of decline of transmissivity with increasing storage deficit (m), T_0 is the local saturated transmissivity (m^2/s), two topographic constants λ and δ are defined as

$$\lambda = \frac{1}{A}\sum\nolimits_j A_j \ln\left(\frac{\alpha}{\tan\beta}\right) \tag{A.11}$$

$$\delta = \frac{1}{A}\sum\nolimits_j A_j \ln T_0 \tag{A.12}$$

TH-1911_10610425

where A is the total area of the catchment (m^2), and A_j is the area associated with the point j (m^2), $\tan\beta$ represents the local hydraulic gradient, is the area of the hillslope per unit contour length (m). Integration of the equation A.7 over the entire watershed gives the mean soil moisture deficit (St) at time t and can be expressed as

$$\overline{S}_t = \overline{S}_{t-1} + (q_{t-1} - f)\,\Delta t \tag{A.13}$$

where $q_{(t-1)}$ is the runoff per unit catchment area (m/s) at time $(t-1)$, and f is the average recharge from paddy fields and vegetated hillslope (m/s), while Δt is the time interval used for the model simulation. For a particular grid exfiltration (fex) has been considered to be equal to the magnitude of S_i when the local deficit is negative.

The subsurface flow rate qb per unit length (m^2/ s) to the channel is given as

$$q_b = \exp\left(-\left(\lambda - \delta\right)\right)\exp\left(-S_i/m\ \right) \tag{A.14}$$

The mean exfiltration rate (q_0) from saturated area can be obtained from

$$q_0 = (1/At\ )\int_{A_s}\{-S_i - \Delta t\}dA \tag{A.15}$$

where A_s is the saturated area of the catchment (m^2).

A.1.3 Channel routing

A.1.3.1 Lateral flow to the channel segments

The contributing area of each of the delineated channel segment is obtained based on "the steepest gradient" method from a digital elevation dataset. The total runoff generated in the contributing area of each channel segment from the above mentioned three classes reaches in the form of lateral flow to that

TH-1911_10610425

segment. The lateral flow rate is given by

$$q_t = q_b + \frac{1}{A}\left[\int_{A_p} h_{ov}dA + \int_{A_{sm}} \left(-\frac{S_i}{\Delta t} + i\right) dA + \int_{A_{um}} RdA + \int_{A_{sh}} \left(-\frac{S_i}{\Delta t} + i\right) dA\right]$$

$$+\frac{1}{A}\left[\int_{A_{uh}} (i - f)\, dA\right] \tag{A.16}$$

where A_p, A_{sm}, A_{um}, A_{sh}, and A_{oh} are the areas of paddy fields (m^2), area in vegetated hillslopes giving saturation excess overland flow (m^2), infiltration excess overland flow area in vegetated hillslopes (m^2), saturation excess overland flow area in semi-impervious urban clusters (m^2), and infiltration excess overland flow area in semi-impervious clusters (m^2), respectively,

A.1.3.2 Linearized channel routing

Using kinematic wave approximation the continuity and momentum equations for a steep channel can be expressed as a second order partial differential equation, (Rajyalakshmi and Dutta, 2006) with the boundary conditions $Q(0,t) = s(t),\ Q(x,0) = 0$ and $Q(\infty,t) = 0$, as

$$\frac{\partial Q}{\partial t} = D\frac{\partial^2 Q}{\partial X^2} + C\frac{\partial Q}{\partial X} \tag{A.17}$$

where Q is the discharge (m^3/s), D is the diffusion coefficient (m^2/s), C is the kinematic celerity (m/s), t is time (s) and X is the distance from upstream end (m). If a uniformly distributed lateral impulse enters the channel over a reach length $S = [(X = S) - (X = 0)]$, the solution of the Equation A-17 becomes

$$Q_i^{'}(S,t) = \int_0^S \frac{X}{2(\pi D t^3)^{\frac{1}{2}}} \exp\left[-\frac{(X - Ct)^2}{4Dt}\right] dX =$$

TH-1911_10610425

$$\frac{D^{\frac{1}{2}}}{(\pi t)^{\frac{1}{2}}}\left\{\exp\left[\frac{(Ct)^2}{4Dt}\right]-\exp\left[-\frac{(X-Ct)^2}{4Dt}\right]\right\}+\frac{C}{2}\left\{erf\left[\frac{Ct}{2(Dt)^{1/2}}\right]+erf\left[\frac{(S-Ct)}{2(Dt)^{1/2}}\right]\right\} \tag{A.18}$$

where erf represents an error function. The solution of Equation A-18 at distance S, when a uniformly distributed lateral impulse of q_1 enters the channel over a reach length $\Delta X = [(X = X^*) - (X = 0)]$ with $X^* < S$, is obtained directly from

$$Q'_{f(\Delta X)}(S,t) = \frac{ql}{\Delta X}\left[Q'(S,t) - Q'(S-\Delta X,t)\right] \tag{A.19}$$

TH-1911_10610425

TH-1911_10610425

Appendix B

Hydrodynamic Modeling

HEC-RASv-4.1 is a one dimensional hydrodynamic model, often used to simulate steady and unsteady flow simulations for the rivers. It is also used to perform sediment transport computations and water quality analysis. In this study, steady flow analyses are carried out without including the sediment transport and water quality modules. The energy equation is solved to determine the water surface profiles from one cross section to another cross section (Figure B.1). The energy Equation B.1 is given below:

$$Z_2 + Y_2 + \frac{a_2 {V_2}^2}{2g} = Z_1 + Y_1 + \frac{a_1 {V_1}^2}{2g} + h_e \tag{B.1}$$

Where:

Z_1, Z_2 = Elevation above datum

Y_1, Y_2 = Depth of water at cross sections

V_1, V_2= Average velocities

a_1, a_2 = Weights of velocities

g = Gravitational acceleration

h_e = Energy head loss

TH-1911_10610425

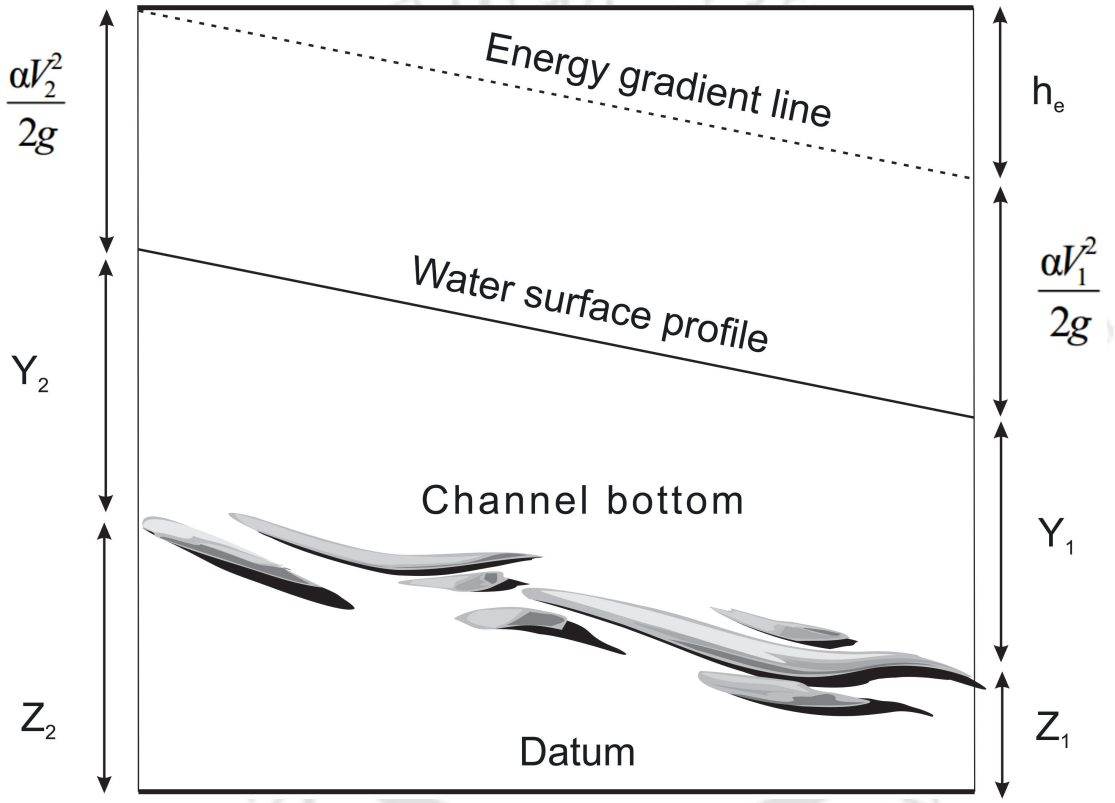

FIGURE B.1: Energy loss in the channel section.

TH-1911_10610425

Publications

Journals

- Dubey, A. K., Gupta, P. K., Dutta, S., and Singh, R. P. (2015). An improved methodology to estimate river stage and discharge using Jason-2 satellite data. Journal of Hydrology, 529, 1776-1787.
- Dubey, A. K., Gupta, P., Dutta, S., and Singh, R. P. (2015). Water level retrieval using SARAL/AltiKa observations in the Braided Brahmaputra river, Eastern India. Marine Geodesy, 38(sup1), 549-567.
- Dubey, A. K., Gupta, P., Dutta, S., and Kumar, B. (2014). Evaluation of satellite-altimetry-derived river stage variation for the braided Brahmaputra River. International Journal of Remote Sensing, 35(23), 7815-7827.
- Gupta, P. K., Dubey, A. K., Dutta, S., Singh, R. P. and Chauhan, P. (2015). Monitoring major inland water bodies of India using SARAL/ALTIKA: some results. NNRMS, (B)-39, 91-96.

In preparation

- Dubey, A. K., Gupta, P., Dutta, S., and Singh, R. P. Morphological dynamics of middle reach of the Brahmaputra river using microwave and optical satellite images.
- Dubey, A. K. and Dutta, S. Integrated Hydrological and Hydrodynamic modeling of the Brahmaputra river using SARAL/Altika retrieved water surface profiles.

Conferences

- Dubey, A. K., Dutta, S., Gupta, P., Kumar, B. (2011). Use of satellite altimetry for the large braided Brahmaputra river. National Conference on Hydraulics and Water Resources (HYDRO -2011), pp 727-734. December 29-30, 2011, SVNIT, Surat, India.
- Dubey, A. K., Verma, R., Dutta, S., Gupta, P., Kumar, B. (2011). Morphological dynamics of Brahmaputra river using satellite altimetry derived river stage records. National Symposium on Empowering Rural India through space Technology pp 291-292. October 9-11, 2011, Bhopal, India.

TH-1911_10610425